RECENT RIVERINE CARBON OF THE YELLOW RIVER: FLUXES, OUTGASSING AND BURIAL

LISHAN RAN

NATIONAL UNIVERSITY OF SINGAPORE

2013

RECENT RIVERINE CARBON OF THE YELLOW RIVER: FLUXES, OUTGASSING AND BURIAL

LISHAN RAN

M.Sc. (*Chinese Academy of Sciences*)

A THESIS SUBMITTED FOR THE DEGREE OF

DOCTOR OF PHILOSOPHY

DEPARTMENT OF GEOGRAPHY

NATIONAL UNIVERSITY OF SINGAPORE

2013

DECLARATION

I hereby declare that this thesis is my original work and it has been written by me in its entirety. I have duly acknowledged all the sources of information which have been used in the thesis.

This thesis has also not been submitted for any degree in any university previously.

_____

Lishan Ran
5 July 2013

Acknowledgements

I would like to express my sincere gratitude to my supervisor, Prof. Lu Xixi, for his guidance and mentorship throughout my four-year doctoral research in Singapore. Prof. Lu has been a superb academic role model. Indeed, he has been in making my academic experience here invaluable. Without his inspirational and constant support, I would never have been able to finish my doctoral research. I am also honored that Prof. David Higgitt and Prof. Alan Ziegler have served on all of my graduate committees from start to finish. I appreciate the time they have taken to guide my work and have enjoyed all of our discussions over the years. My thanks also go to my fellow friends, including Xiankun, Song Liu, Swehlaing, Shaoda, Rui Chen, Yi Liu, Seonyoung, Suraj, Evangeline, Menusha, Nick, Guanie, Orlando, for the camaraderie and friendship over the past few years.

This thesis could not have been conducted without the unflagging and generous support (both material and intellectual) from the staff at the Toudaoguai, Tongguan, and Lijin hydrological gauge stations of the Yellow River Conservancy Committee. I thank Mr. Qihai Yi, Mr. Siyi Liao, Mr. Shuangyin Tian, Mr. Jianming Zhang and many others for their hard work and generous assistance during my field sampling campaigns. And also, I would like to thank Dr. Huiguo Sun and Dr. Jingtai Han at Chinese Academy of Sciences, Dr. Shurong Zhang at Beijing Normal University, and Dr. Zhongbao Xin at Beijing Forestry University for their technical and logistic assistance in running experiments and analyzing samples. I am also indebted to them for the stimulating ideas and fruitful collaborations.

This thesis has been supported by the National University of Singapore PhD scholarship and the Ministry of Education (Singapore). Various necessary computational resources were provided by geography department. Sincere thanks go to Ms Pauline Lee, Mr. Lee Choon Yoong and Ms Wong Lai Wa and other staff in the department for their kind administrative guidance and help.

Finally, I would like to express my deep appreciation for my family and friends for their continuous support during my doctoral years.

Lishan
5 July 2013, Singapore

Table of Contents

Summary

Riverine carbon transport is an important component of global carbon cycling. Understanding its influencing factors and internal dynamics is important in the face of climate change and strong anthropogenic footprints that are now occurring in many landscapes worldwide. However, most prior studies are based on river systems located in tropical environments; comprehensive studies on Chinese river basins remain largely lacking. Focusing on the Yellow River that is characterized by severe soil erosion and strong human impacts, this thesis investigated the delivery processes of riverine carbon, including inorganic and organic, within the temperate river basin. Impacts of the strong human activities on riverine carbon transport were elucidated in an attempt to provide insight into future carbon cycle studies, which is expected to be given more attention with anticipated increasing atmospheric carbon concentration.

Based on sampling at three hydrological stations along the mainstem channel of the Yellow River between July 2011 and July 2012, the water geochemistry characteristics were investigated qualitatively and quantitatively. The Yellow River waters were characterized by significantly high total dissolved solids (TDS) concentrations compared with other large rivers of the world. The strong chemical weathering is the combined result of extensive human activities and severe physical erosion due to highly erodible loess deposits and unique hydrological regimes. Owing to continuous implementation of soil conservation measures and other afforestation/ reforestation activities on the Loess Plateau, its chemical weathering intensity has shown a decreasing trend over the past decades. In addition, due to reductions in water discharge, fluxes of the TDS and the dissolved inorganic carbon (DIC) have decreased sharply. Consumed atmospheric CO_2, estimated from DIC data and mass balance equations, suggests that carbonate weathering provided the major contribution to the total atmospheric CO_2 consumption. Silicate weathering accounted for only about 26%, although all the generated DIC by silicate weathering was derived from the atmosphere.

Both historical records and recent sampling results were used to investigate vertical exchange of CO_2 between the riverine waters and the atmosphere throughout the Yellow River basin. The mean CO_2 partial pressure (pCO_2) of the Yellow River waters was estimated at 2800 μatm. Except in the headwater region where the pCO_2 was lower than the atmospheric equilibrium (i.e., 380 μatm), the riverine pCO_2 was significantly higher than the atmospheric equilibrium. Therefore, the Yellow River basin as a whole acted as a carbon source for the atmosphere, with the headwater

region representing a carbon sink. Based on gas transfer velocity derived from wind speed and water current velocity, CO_2 outgassing flux showed strong spatial and temporal/seasonal variability. An estimated 1.05-4.19 Mt of CO_2 was emitted into the atmosphere annually, accounting for about 0.5-1.8% of the global mean CO_2 efflux from rivers alone (0.23 Gt/yr).

Likewise, organic carbon transport in the Yellow River has been significantly affected by human activities over the past few decades. As a result of continuous dam construction, carbon burial behind dams has become the single largest fate for the eroded organic carbon except decomposition. When other terrestrial carbon burial or stabilization components were included, about half of the eroded organic carbon was sequestered or stabilized on land, with dam trapping being the largest contributor. Given that carbon burial could effectively protect carbon from further decomposition, redistribution of organic carbon among different carbon reservoirs has changed basin-wide carbon cycling. From a temporal perspective, high-frequency sampling indicated that the dissolved organic carbon (DOC) concentration showed strong seasonal variations, with low values occurring in the wet season and high values in the dry season. These seasonal differences suggested the dilution effect of increased water discharge in the wet season. Particulate organic carbon (POC) content of the suspended solids was relatively low and remained largely stable through the study period. Similar to the DIC, the seaward DOC and POC fluxes were greatly reduced relative to historical records.

In conclusion, human activities have substantially changed the transport characteristics of riverine carbon in the Yellow River. In particular, carbon burial with sediment deposition and carbon outgassing into the atmosphere have affected basin-scale carbon cycle. Riverine carbon fluxes, burial, and outgassing in the Yellow River have been systematically studied. Underlying factors, in particular human impacts, have been discussed to elaborate the observed changes. The obtained conclusions will shed light on a deeper understanding of global carbon budget and global climate change.

List of Tables

List of Figures

List of Acronyms and Symbols

CO_2	Carbon Dioxide
CWR	Carbonate Weathering Rate
DAI	Deviation Area Index
DEM	Digital Elevation Model
DIC	Dissolved Inorganic Carbon
DOC	Dissolved Organic Carbon
GIS	Geographic Information Systems
NDAI	Normalized Difference Area Index
OC	Organic Carbon
pCO_2	Partial Pressure of Riverine CO_2
PIC	Particulate Inorganic Carbon
PN	Particulate Nitrogen
POC	Particulate Organic Carbon
Q	Water Discharge
Q_s	Sediment Load
SDR	Sediment Delivery Ratio
SO	Stream Order
SOC	Soil Organic Carbon
SSC	Suspended Sediment Concentration
SWR	Silicate Weathering Rate
TAlk	Total Alkalinity
TDS	Total Dissolved Solids
TE	Trapping Efficiency
TOC	Total Organic Carbon
TSS	Total Suspended Sediment/Solids
USLE	Universal Soil Loss Equation
YRCC	Yellow River Conservancy Commission
$\Delta\tau$	Water Residence Time

Chapter 1 Introduction

1.1 General background

Rivers serve as the major links between terrestrial systems and oceans in terms of material transfer on Earth. They carry water as well as products of erosion and weathering from the continents into the oceans (Berner et al., 1983; Meybeck, 1987; Berner, 1995; Syvitski et al., 2003; Meybeck, 2004; Walling, 2006; Cole et al., 2007; Bass et al., 2011; Melack, 2011a; Berner and Berner, 2012). Rivers dwarf other transport agents, such as wind, in maintaining the mass balance between the terrestrial and oceanic pools. Syvitski et al (2003) estimated approximately 95% of the global sediment entering the ocean is transported through rivers. Their significance ranges from their importance to global denudation cycle, through their role in global biogeochemical cycling, to the functioning of coastal ecosystems and the evolution of coastal landforms (Ludwig et al., 1996; McLaughlin et al., 2003; Beusen et al., 2005; Seitzinger et al., 2010).

Historically, rivers have played an important role in human development because they provide both fresh water supply and allow a comfortable living environment. As a result of human proximity, rivers have been substantially affected by human activities ranging from dam construction, to water extraction for agriculture, and to the input of domestic and industrial effluents. These impacts have considerably changed the transport dynamics of water and associated dissolved and suspended solids. In addition to these changes in physical nature, characteristics of water chemistry have

been significantly altered, causing a number of biogeochemical responses (e.g., Chen et al., 2002; Meybeck 2004; Berner and Berner, 2012).

Whilst most of the solutes in river water are derived from chemical weathering of minerals contained in the rocks within the drainage basin, the suspended fraction originates mainly from physical denudation induced by various driving factors, internal or external. Concentrations of the dissolved elements are a complex admixture of their relative abundance in minerals and of the mode and rate of their chemical weathering processes. In addition to the significance in maintaining mass balance on a global scale, chemical weathering of minerals on land involves a net atmospheric CO_2 drawdown (Berner et al., 1983; Kump and Arthur, 1999; Amiotte-Suchet et al., 2003; Liu et al., 2011; Hartmann et al., 2013). As such, chemical weathering is critical to mitigating rapidly increasing atmospheric CO_2 concentration (e.g., Liu et al., 2011; Berner and Berner, 2012). Accelerated chemical weathering due to orogenesis at geological scale, and thus increased atmospheric CO_2 consumption, has been proposed to explain the lower temperatures that resulted in global cooling and the inception of glaciated environments (Raymo, 1991; Riebe et al., 2001; DeConto and Pollard, 2003; Basak and Martin, 2013). Studying chemical weathering associated CO_2 consumption is thus important for climate change assessments.

In addition to inorganic carbon, rivers also transport organic carbon downstream. Riverine organic carbon initially originates from the atmosphere and represents an

important pathway of the biogeochemical cycling of carbon (Bianchi, 2011). In terrestrial ecosystems, as plants take up atmospheric CO_2 to produce biomass, carbon not released directly back to the atmosphere by plants or soil respiration is stored or becomes incorporated into soil carbon pool through decomposition. As soil carbon would be flushed into rivers by runoff or groundwater, transfer of organic carbon from land to ocean via rivers thus reduces the size of terrestrial carbon pool. Organic carbon transported by rivers can be divided into dissolved and particulate (DOC and POC) fractions. The dissolved fraction is largely derived from rainfall and soil processes, including leaching of plant litter and chemical weathering. The particulate load, on the other hand, dominated by the products of physical denudation, represents erosion and sediment transport from the surface of the soil (Hope et al., 1997; Schlünz and Schneider, 2000). Transport of inorganic and organic carbon from land to ocean constitutes a key component of global carbon cycle (Meybeck, 1987; Schlünz and Schneider, 2000; Berner and Berner, 2012).

The nature of the transported carbon and its fate within a drainage basin are determined by basin physical characteristics and by the complex biogeochemical processes. As stated above, worldwide fluvial transport of elements has been strongly affected by human activity. This is particularly true for the river basins located in developing countries, where extensive human activities are modifying basin landscape at unprecedented rates (Syvitski et al., 2005). During the Anthropocene, the nature of riverine carbon results from both natural and anthropogenic processes. Therefore, it is essential to separate the effects of human activities from those

resulting from natural processes for a better understanding of current and historical human impacts, as well as for predicting future trends.

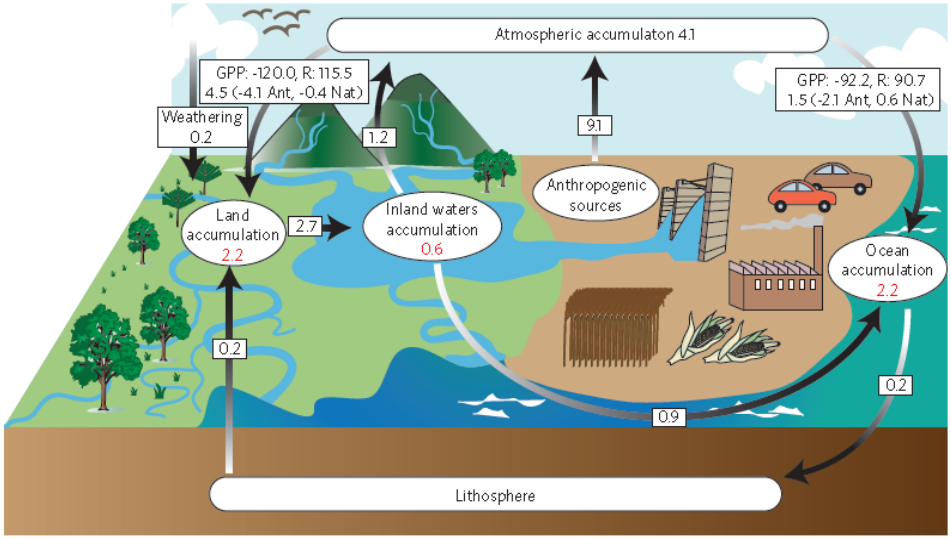

Figure 1.1 Global carbon cycle (adapted from Battin et al., 2009). The schematic highlights flux of carbon drawdown by chemical weathering of rocks, and also the carbon flux through inland waters, mainly rivers. GPP is the gross primary productivity. Inserted values are net fluxes between pools (black) or rates of change within pools (red) in unit of Gt/yr (1G=10^9).

Previously published estimates of atmospheric CO_2 drawdown due to chemical weathering were mostly based on riverine dissolved inorganic carbon (DIC) concentration data and drainage basin lithological distributions (i.e., carbonates and silicates). On the basis of measurements in major rivers of the world, the estimates ranged from 0.20 to 0.25 Gt/yr (Ludwig et al., 1998; Gaillardet et al., 1999; Regnier et al., 2013) (Figure 1.1). The consumed CO_2 is mainly produced by oxidation of soil organic matter (Mortatti and Probst, 2003). Among the major rock types, carbonate weathering consumes the greatest amount of atmospheric CO_2 (58.7% of the total consumption), while silicate weathering accounts for the remaining 41.3% (Gaillardet et al., 1999). As a result of large carbonate outcrops and high drainage intensity, the

highest specific CO_2 consumption fluxes have been observed in south and south-east Asia. In particular, the rivers in the part of Asia between 75°-135° E longitude and 10°-40°N latitude contribute 22.7% of the global total CO_2 consumption (Ludwig et al., 1998). However, these estimates do not take into consideration the consumed CO_2 during weathering of basalts from volcanic arcs and volcanic islands. The total CO_2 consumption rate is therefore about 0.29 Gt/yr if the additional drawdown is included (Gaillardet et al., 1999). Although the total consumed CO_2 by rock weathering is minor in comparison with other fluxes among the atmosphere, ocean, and the biosphere (Figure 1.1), it is of the same magnitude as the land-ocean and land-atmosphere exchanges. From this perspective, chemical weathering induced atmospheric CO_2 uptake potentially plays an important role in modulating climate change by reducing the growth rate of atmospheric CO_2 (Ludwig et al., 1996; Berner and Berner, 2012).

Latest estimates of the quantity of organic carbon fluxes from land to the oceans via rivers vary from 0.33 to 0.49 Gt/yr (Degens et al., 1991; Hedges and Keil, 1995; Ludwig et al., 1996; Aufdenkampe et al., 2011). Spatially, wet tropical rivers, such as the Amazon, Congo, Godavari, and Mekong rivers, deliver the largest quantities of organic carbon to global oceans, whereas contributions of temperate and cold rivers are comparatively minor. In particular, a considerable proportion of the POC fraction is labile - 35% for global rivers on average (Schlünz and Schneider, 2000) - and may become quickly oxidized after reaching river waters. For individual river basins, the oxidization proportion varies widely, depending on both physical and biogeochemical

controlling factors. For instance, previous studies estimated that the oxidized proportion of mobilized POC by soil erosion ranged from 0% to near 100% of the total eroded POC (Smith et al., 2001; Lal, 2003; Renwick et al., 2004). Based on measurements of organic carbon concentration and water and suspended solids fluxes at river mouths, the total estimated carbon fluxes transported by world rivers range from 0.7 to 0.9 Gt/yr (Cole et al., 2007; Aufdenkampe et al., 2011; Figure 1.1).

Furthermore, of particular interest in current scientific debate regarding carbon dynamics is the role of soil erosion in the global carbon budget. There has been no explicit answer to the question of whether soil erosion is a carbon sink or a carbon source (Stallard, 1998; Lal, 2003; Lal, 2004; Van Oost et al., 2007; Lal and Pimentel, 2008; Kuhn et al., 2009; Van Oost et al., 2012). Van Oost et al (2007) presented carbon inventory measurements showing consistent evidence for an erosion-induced sink of atmospheric carbon equivalent to approximately 26% of the total carbon mobilized by erosion. In contrast, Lal et al (2004) identified soil erosion as an important source of atmospheric CO_2. Their assessments assumed that 20% of the carbon displaced by water erosion is released into the atmosphere, which is mostly due to the breakdown of aggregates and subsequent decomposition during transport by overland flow. Consequently, the effect of soil erosion on the global carbon budget is estimated to range from a sink of 1 Gt/yr to a source of the same magnitude (Stallard, 1998; Smith et al., 2001; Van Oost et al., 2007).

Few studies have comprehensively analyzed the fate of mobilized soil organic carbon by erosion at a watershed/continental scale (Smith et al., 2001). Whilst these studies generally assume that carbon storage on land with sediment deposition is a long-term carbon sink, little is known about the residence time of carbon in the deposits. In view of the potential magnitude of carbon sink or source, mobilization of terrestrial carbon by erosion may have a significant effect on the global carbon budget although whether soil erosion induces a carbon sink or a carbon source is still highly uncertain. Resolving these uncertainties and obtaining a better understanding of the fate of erosion-induced carbon and its implications for regional or global carbon cycle require integrated investigations of carbon and sediment fluxes.

Inland water systems have historically been considered as passive pipes in global and regional carbon balance computations, delivering significant amounts of terrestrially-derived carbon from land to ocean (Cole et al., 2007; Regnier et al., 2013) (Figure 1.2a). In such cases, the transported carbon via inland waters does not interact with the atmosphere and/or the geosphere, but rather are conservatively transported downstream into the ocean. As a result, the total carbon amount reaching the inland waters from land (0.9 Gt/yr) equals its export into the ocean (0.9 Gt/yr) (Cole et al., 2007). In recent years, it has been recognized that a significant proportion of the carbon entering inland waters from terrestrial ecosystems does not reach the ocean (Richey et al., 2002; Figure 1.2b). Rivers and streams have been widely recognized to be net sources of atmospheric CO_2, with considerable CO_2 emission into the

atmosphere occurring during the transport of carbon (Richey et al., 1980; Richey et al., 1991; Telmer and Veizer, 1999; Alin et al., 2011).

The magnitude of CO_2 evasion into the atmosphere could even be larger than the lateral fluvial export into the ocean. For example, Richey et al (2002) found the waters of the Amazon exported about 13 times more carbon by CO_2 outgassing than by the export of total organic carbon or of inorganic carbon to the Atlantic Ocean. Annually, at least 0.75 Gt of carbon is transferred from inland waters into the atmosphere (Figure 1.2b). Further, the transported carbon, POC in particular, would also be sequestered within inland waters under favorable conditions such as reservoir sedimentation. Globally about 0.15-0.3 Gt of carbon is stored annually in inland waters with sediment (Cole et al., 2007). Summing these estimates for carbon outgassing and storage shows that global carbon losses during the delivery from land to sea are slightly higher than that exported into the oceans. With respect to individual river basins, the contrast between carbon losses and seaward carbon export is likely to differ due to the differences in both natural processes and human impacts. Particularly, this contrast would be more apparent for rivers greatly disturbed by human activities, for example by reservoir construction, as reservoirs are the largest single component for carbon burial (Cole et al., 2007). At the watershed scale, knowing the carbon dynamics along with its delivery from land to ocean is therefore vital for understanding its fate and potential implications for the carbon cycle.

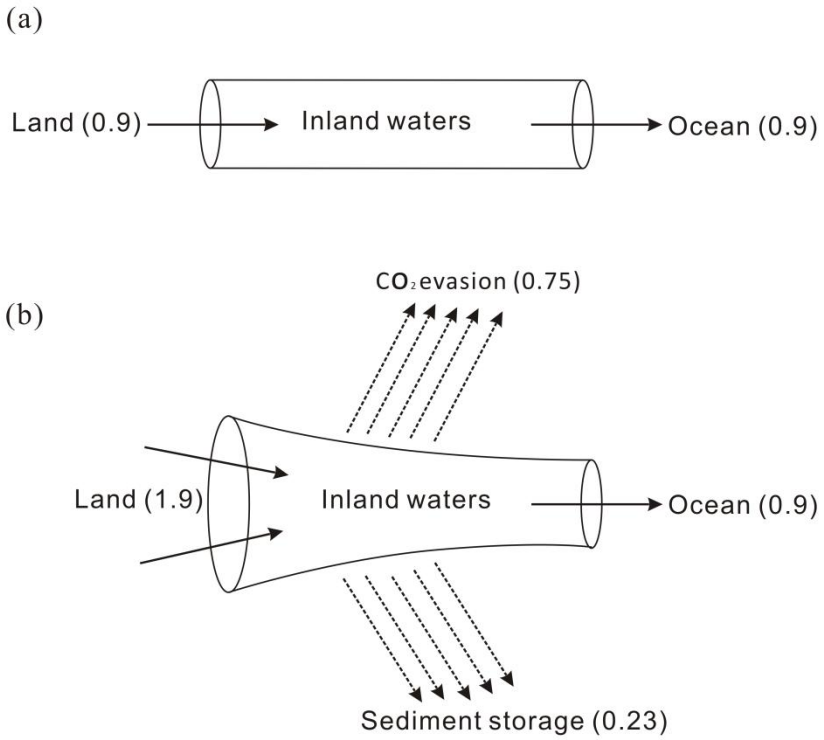

Figure 1.2 Schematic view of the role of inland aquatic systems in global carbon cycle. (a) the conventional view considering the inland waters as a passive pipe that conservatively delivers terrestrially-derived inorganic and organic carbon into the oceans. (b) a recently proposed view that takes the inland waters as an active component in global carbon cycle with carbon storage in sediments and carbon emission into the atmosphere during the transport processes. Twice the amount of carbon is transported into inland waters than is transported to the ocean, indicating that terrestrially-derived carbon is more actively consumed than previously thought. The figures in the brackets indicate the annual fluxes (Gt/yr). Adapted from Cole et al (2007).

As stated above, not all carbon entering river systems is horizontally transported downstream into estuaries or oceans, but rather, quite a large proportion is likely emitted vertically into the atmosphere or stored within the drainage basin, on floodplains, and behind dams (Figure 1.3). As the aqueous CO_2 concentrations in most world rivers are significantly higher than the atmospheric CO_2 equilibrium, CO_2 concentration gradients will result in widespread CO_2 evasion from the water to the

atmosphere. Moreover, deposition of suspended solids, in reservoirs for example, would lead to carbon storage, particularly the POC adsorbed to suspended solids. Approximately, 1-3 Gt of carbon has been sequestered in reservoirs constructed largely within the past 50 years with deposited sediments of more than 100 Gt (Syvitski et al., 2005).

As the largest producer of global fluvial sediment, Asia has seen the largest sediment reduction region in recent decades compared to other continents due to continuous dam construction (Syvitski et al., 2005; Walling, 2012). It is anticipated that the sediment flux to the oceans will be further reduced in future upon completion of more new reservoirs, in which more carbon will be buried (Gao et al., 2002; Cole et al., 2007). Nevertheless, unlike the seaward carbon flux that has been largely quantified based on measurements taken near river mouths, the fluxes of CO_2 evasion into the atmosphere and carbon burial remain poorly constrained (Figures 1.1 and 1.2b).

Further work is required to provide a precise quantitative assessment of the fluxes to reconcile present differences, upon which their implications for global carbon cycle can be defined more accurately. Particular attention must be paid to the temporal perspective and the variations of impact trajectories in different areas of the globe and for river basins of different sizes. Furthermore, different forms of carbon may transform through complex physical and biogeochemical processes, such as microbial utilization, flocculation, photosynthesis, and respiration (Aucour et al., 1999; Cai et al., 2004; Sun et al., 2011) (Figure 1.3). These complicated internal interactions are

the combined results of an array of climatic, hydrological, and biological factors, which collectively determine the direction and magnitude of the transformation.

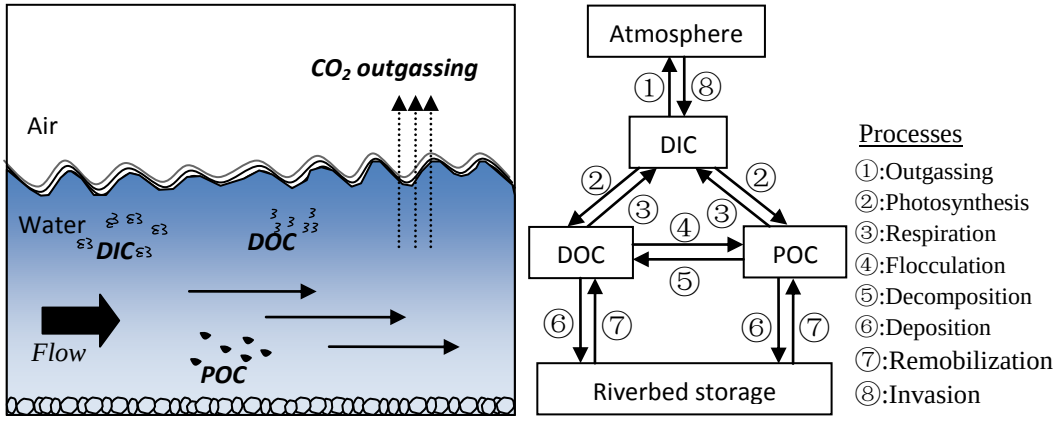

Figure 1.3 Schematic diagram showing aqueous CO_2 evasion from water surface as riverine carbon transports downstream (left), and the internal links among different carbon forms (right). DIC: dissolved inorganic carbon; DOC: dissolved organic carbon; POC: particulate organic carbon.

In summary, numerous attempts so far have been made to elucidate riverine carbon transport processes focusing either on the micro-scale with studies of particular rivers, or on the macro- or global scale with studies of flux estimation and climate change impacts (e.g., Berner et al., 1983; Berner, 1995; Meybeck, 2004; Bass et al., 2011; Melack, 2011a). Despite this rich literature, many uncertainties, such as human impacts on carbon transport, remain to be addressed as to how the driving forces have affected the transport of different forms of carbon and their responses to increasingly strong human activities. As such, an in-depth presentation of comprehensive analysis of riverine carbon dynamics based on typical river systems is needed.

1.2 Justification for the study area

The Yellow River basin is one of the most severely degraded regions in the world suffering from erosion in excess of the soil loss tolerance level (i.e., 1000 t/km^2/yr, see Zhao, 1996) due to its distinct climatic and lithological features. Readily erodible loess deposits are widely distributed in its middle reaches (the Loess Plateau, see Figure 2.1). Affected by heavy rainfall events, the Yellow River is characterized by extraordinarily high soil erosion intensity and sediment yields. As carbon cycle processes are closely correlated with physical erosion, atmospheric CO_2 uptake increases from accelerated chemical weathering; and the mobilized organic carbon from eroding sites is subject to burial with sediment or oxidation into the atmosphere. Given the complicated impacts of soil erosion on the carbon cycle, the Yellow River provides an excellent area to study the correlation between soil erosion and the carbon cycle at the large catchment scale.

The Yellow River basin has been exposed to extensive human impacts during the past few decades. In general, human activities have affected physical and biogeochemical properties from two competing aspects. Soil erosion intensity has been greatly accelerated due largely to strong anthropogenic interventions, such as forest clearance and intensification of land use, during the period 1950s-1970s in particular (Xu, 2003). As a consequence, the sediment transport and carbon cycling have been significantly affected. For example, the mean annual suspended sediment load of the Yellow River during the period is 1.6 Gt (e.g., Shi et al., 2002), based on hydrological records measured at Sanmenxia station where the river flows out of the Loess Plateau

and enters the North China Plain. In some years, the annual sediment load could be as high as 3 Gt as a result of more intensive human activities and higher rainfall (Wang et al., 2007b), in the "Great Leap Forward" period of 1958-1959 for example. In contrast, implementation of widespread soil conservation programmes and dam construction have caused a sharp reduction in sediment load since the 1970s. In particular, a large quantity of sediment has been trapped behind dams, with which it is expected that the buried carbon is considerable. Compared to other large rivers of the world, these human-induced changes are competing and unparalleled and could provide some insights about the extent and magnitude of human impacts on basin-wide carbon cycling.

Furthermore, loess deposits represent a distinctive geomorphological landscape, with wide distribution in Asia, Europe, and North America. Due to their unique chemical properties with carbonates constituting a considerable proportion (Zhang et al., 1995a), loess particles are vulnerable to weathering and soil erosion. Therefore, quantifying the resultant atmospheric CO_2 consumption due to weathering of loess plays a significant role in assessing global carbon cycle changes. As some of the carbon consumed would be emitted into the atmosphere during the delivery process towards the ocean, understanding the mechanisms governing weathering processes and subsequent riverine carbon transport is also of importance.

The Yellow River has been continuously measured from the 1950s through a hydrological network, including about 250 hydrological gauge stations and more than

100 meteorological stations scattered across the entire basin. In addition, supplementary data on basin features, such as geological background, spatial heterogeneity of soil erosion intensity, and human activities (i.e., detailed information on soil conservation programmes and dam construction), are publicly available for use. These datasets, with long-term hydro-chemical records, made it practical to carry out the study on riverine carbon transport within the river basin.

The Yellow River basin is therefore a potentially incomparable experimental area for exploring riverine carbon transport processes as impacted by natural factors and human activities. With the help of long-period, continuous recording of hydro-chemical variables throughout the river basin started before large-scale human activity, the spatial and temporal dynamics of riverine carbon transport could be fully investigated to unravel its controlling mechanisms. In particular, given the magnitude of anthropogenic perturbations, the human impacts on carbon cycle could be effectively assessed.

1.3 Aims and significance

With respect to the Yellow River basin, although numerous efforts have been devoted over the past several decades to investigating water discharge and sediment dynamics, most of the emphasis has been on the physical processes. In contrast, studies on chemical properties and carbon transport received less attention, and the driving factors affecting these processes remain largely unexplored. The physical processes of sediment mobilization, deposition, and transport represent key components of the

biogeochemical carbon cycle through the transfer of sediments from land to oceans (Meybeck, 1993b; Hoffmann et al., 2010; Dürr et al., 2011; Berner and Berner, 2012). Research on carbon cycling at the watershed scale has been given increasingly more attention in recent years, as such studies lay a solid foundation for global-scale assessments. It is critical to recognize that the carbon associated with the sediment and water transported by the Yellow River possibly plays an important role in the global carbon cycle, because the Yellow River accounts for 5-6% of the global annual sediment flux to the oceans (Walling, 2006). Specific research gaps for prior and ongoing studies on riverine carbon transport and associated carbon outgassing within the Yellow River basin are the following:

- Spatial and temporal variability of chemical weathering intensity remains unclear. Impacts of the influencing factors, including natural processes and anthropogenic disturbances, on the chemical weathering processes and associated atmospheric CO_2 consumption remain to be explicitly explored.
- In recent years, significant riverine CO_2 evasion across the water-air interface in tropical rivers has been recognized as a carbon source for the atmosphere. However, corresponding assessments of CO_2 emission from temperate rivers, such as the Yellow River, have not yet been conducted.
- Erosion-induced carbon mobilization has long been controversial regarding its role in the carbon cycle. As for the Yellow River basin, less work has been done with respect to the mobilized carbon compared to the eroded sediment. Although deposition on land has been a major fate for the mobilized soils, quantitative assessment of the associated carbon burial has rarely been reported.

Equally, human-induced carbon burial through sediment trapping has also not yet been evaluated in detail. Given the sedimentation magnitude, the carbon burial would be considerable, even at the global scale.

- Riverine organic carbon transport is controlled by several environmental variables. To what extent these variables could affect its transport varies from one place to another? As for the Yellow River basin with severe soil erosion and strong agricultural activity, few studies have been carried out to elucidate its dynamics.

In view of the above knowledge gaps regarding the Yellow River and its potential significance in the global carbon cycle, the overall aim of the current study was to investigate the transport processes of riverine inorganic and organic carbon within the Yellow River basin, and the interactions between the Yellow River basin and the atmosphere as well as the oceans. Furthermore, using field sampling and historical records, this study also attempted to explore the responses of carbon transport to both natural and human factors. Four specific objectives of this research were to:

- examine spatial and seasonal variations of chemical weathering in the Yellow River basin and the associated atmospheric CO_2 consumption as well as the inorganic carbon export.
- investigate riverine CO_2 exchange with the atmosphere across the water-air interface in the Yellow River network and its future trends.
- quantify the basin-wide organic carbon budget associated with erosion, deposition, and transport processes of sediment during the past few decades.

- analyze the transport processes of organic carbon (DOC and POC) and to quantitatively estimate the riverine organic carbon export fluxes and finally, to explore their spatial and temporal dynamics as affected by various influencing factors.

The results of this present study may contribute to a better understanding of the mechanisms of chemical weathering and associated CO_2 drawdown from the atmosphere and their potential influencing factors at a watershed scale. In addition, the results may provide insights into understanding the riverine organic carbon transport processes in a river system with high sediment concentration and strong influences from human activity. Furthermore, the results may shed light on studies of CO_2 outgassing from a river system completely different from previous study areas that were mostly based on tropical rivers.

It is understood that large-scale field sampling campaigns seem necessary to analyze the spatial and temporal variability of riverine carbon transport and carbon emission. Given that the Yellow River basin is so big (ca.752,000 km^2) and the difficulty in logistical accessibility, widespread field sampling throughout the basin was impractical. Therefore, representative sampling sites were selected to collect samples during the fieldwork. In addition, this study also relied heavily on historical records retrieved from archives.

1.4 Research questions and framework of the methodology

In order to realize the research objectives stated above, several key questions to be resolved have been proposed:

- What are the chemical weathering processes in the Yellow River basin and the implications for atmospheric CO_2 equilibrium? What are their controlling factors?
- What is the spatial and temporal variability of the aqueous CO_2 pressure (pCO_2) level throughout the Yellow River basin? What are the CO_2 outgassing fluxes across the water-air interface from the entire river network and what are their implications?
- What are the major sources of the three different forms of riverine carbon (DIC, DOC, and POC) and are there any spatial and/or temporal differences in quantities and compositions under the combined influences of climatic change and strong human disturbances?
- Reservoirs are an important component in trapping erosion-derived sediment, how much has the POC been buried in reservoirs with sediment during the past decades? And what are its implications for organic carbon cycle within the basin?
- To what extent has the eroded organic carbon from the river basin been decomposed en route to the ocean? What is the organic carbon budget regarding the Yellow River basin and how have human activities during the last few decades changed it?

To address these questions and to achieve the objectives stated in the previous section, the research framework was designed as shown in Figure 1.4. Collection of water chemistry information included two parts. One is retrieval of historical records; the other is recent field sampling. The historical water chemistry datasets were combined with recent field sampling data to explore the spatial and temporal variability characteristics of riverine carbon transport and associated carbon emission and storage. Firstly, chemical weathering in the Yellow River basin was analyzed, upon which the consumed atmospheric CO_2 was estimated. Secondly, pCO_2 in the river waters was investigated over space and time, and total CO_2 evasion into the atmosphere was evaluated through empirical models. Thirdly, recently captured remote sensing imageries were used to delineate reservoirs for precisely estimating the amount of deposited sediment behind dams. Based upon the estimated reservoir sedimentation, a basin-wide organic carbon budget was compiled and discussed. Finally, the organic carbon transport dynamics along the mainstem channel were explored. Specifically, variations in the long-term POC fluxes were analyzed by comparing current calculations with previous sampling results (i.e., in the 1980s). While historical information on DOC transport was not available, study of its spatial and temporal (seasonal) variations were mainly based on recent sampling data. With the quantified lateral and vertical carbon transport fluxes, a simplified carbon transport diagram in the Yellow River was established (in Chapter 9), in which the impacts of human activities were highlighted.

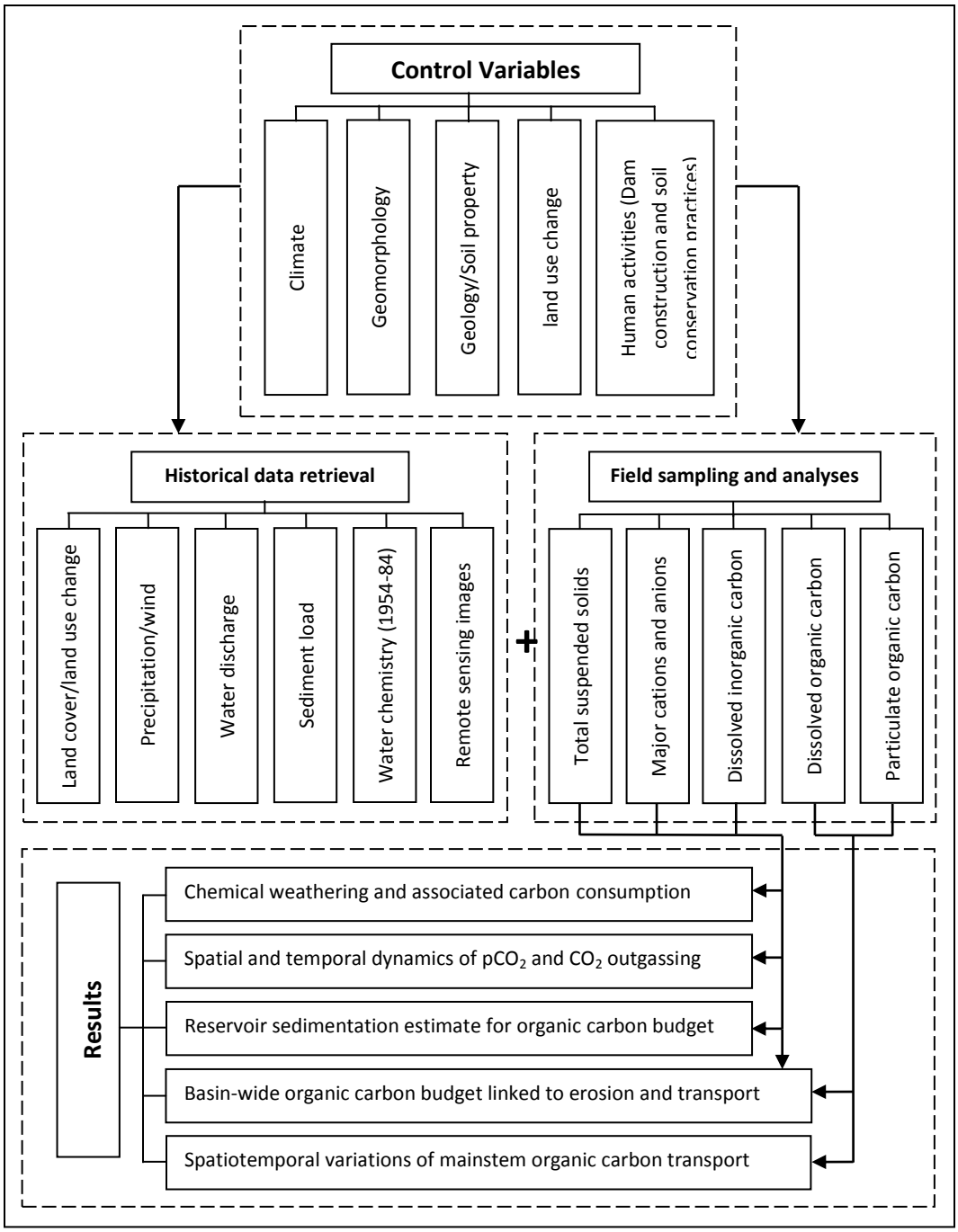

Figure 1.4 Framework of the overall research methodology.

1.5 Arrangement and structure of the dissertation

The structure of this thesis and the main content that each chapter covered are briefly described below. To ensure the content flows logically, separate introductions and literature reviews for each specific research topic are provided at the beginning of each chapter before presenting the results.

Chapter 2 provides an overall description about the background information of the Yellow River drainage basin.

Chapter 3 examines the chemical weathering processes and their spatial and temporal characteristics. More importantly, the associated atmospheric CO_2 consumption was estimated through empirical models, and its implications for global carbon budget were discussed.

Chapter 4 investigates riverine CO_2 exchange across the water-air interface with the atmosphere within the Yellow River network by analyzing historical records of water chemistry and recent sampling results.

Chapters 5 and 6 estimate reservoir sedimentation by analyzing satellite images (for reservoir delineation) and hydrological records of sediment measured at gauge stations (for sediment yield estimates). The estimated reservoir sedimentation amount is then used to assess a basin-wide organic carbon budget.

Chapter 7 explores the organic carbon budget within the drainage basin during 1950-2000 by using budgetary equations which took into account the processes of erosion, transport, and deposition of organic carbon with sediment.

Chapter 8 examines the delivery characteristics of organic carbon along the mainstem channel during the period 2011-2012, and evaluated its spatial and temporal variations with other literature-based datasets.

Chapter 9 summarizes the main findings of the study, and presented existing limitations and corresponding recommendations on how to address them in future work.

Chapter 2 Description of the Yellow River basin

Located in north China, the Yellow River is well-known for its severe soil erosion and high sediment load in the world. In this chapter, a general description of the Yellow River basin was presented from the aspects of geographical characteristics, climate, hydrology, geology, and major human impacts exerted during the past few decades. Because this study attempted to explore the transport dynamics of three different forms of carbon within the Yellow River basin and their external interactions with the atmosphere and the geosphere, it can be found that the research subjects were diverse although closely correlated. As such, datasets from different sources were utilized, and necessary descriptions of these datasets were needed. Therefore, in addition to the brief description presented here, an additional description of corresponding datasets analyzed in individual chapters was also presented, when necessary.

2.1 Geographical background

The Yellow River ranks 26th in the world in terms of drainage basin size and is the second longest river in China, next only to the Yangtze River. Situated from 41^{o}50$^{'}$N-95^{o}53$^{'}$E to 32^{o}10$^{'}$N-119^{o}05$^{'}$E, its drainage area is about 752,000 km^{2}, with a channel length of about 5460 km (Figure 2.1). The river rises on the northern flank of the Bayankela Mountains of Qinghai Province. It stretches from west to east in north China, covering three distinct topographic landscapes, including the Qinghai-Tibetan Plateau, the Loess Plateau, and the North China Plain. It first flows on the Qinghai-

Tibetan Plateau at an elevation of 4500 m, turns towards the east and flows down the plateau near Lanzhou, and then crosses over the Loess Plateau and the great North China Plain before finally emptying into the Bohai Sea. Based on its geographical differences, the river can be divided into three reaches. The upper reaches extend from the river source to Toudaoguai station, draining an area of 386,000 km^2 and a length of 3471 km; the middle reaches stretch 1206 km from Toudaoguai station to Huayuankou station and drain an area of about 343,750 km^2; and lastly the lower reaches extend over a length of 786 km from Huayuankou station to the river mouth and drain an area of 22,730 km^2 (Figure 2.1; Table 2.1). Rapid changes in channel slope near Lanzhou and Huayuankou stations correspond roughly to the boundaries between the Qinghai-Tibetan Plateau (upstream of Lanzhou), the Loess Plateau (Lanzhou-Huayuankou), and the North China Plain of the lower reaches (Figure 2.1). Due to active tectonic uplift, the drainage system is relatively young. The Yellow River is joined by a large number of tributaries. Of these, the largest tributaries, from upstream downward, include Taohe, Huangshui, Wudinghe, Fenhe, Beiluohe, Weihe, Yiluohe, and Qinhe (Figure 2.1). Hydrological characteristics of some major tributaries are summarized in Table 2.1.

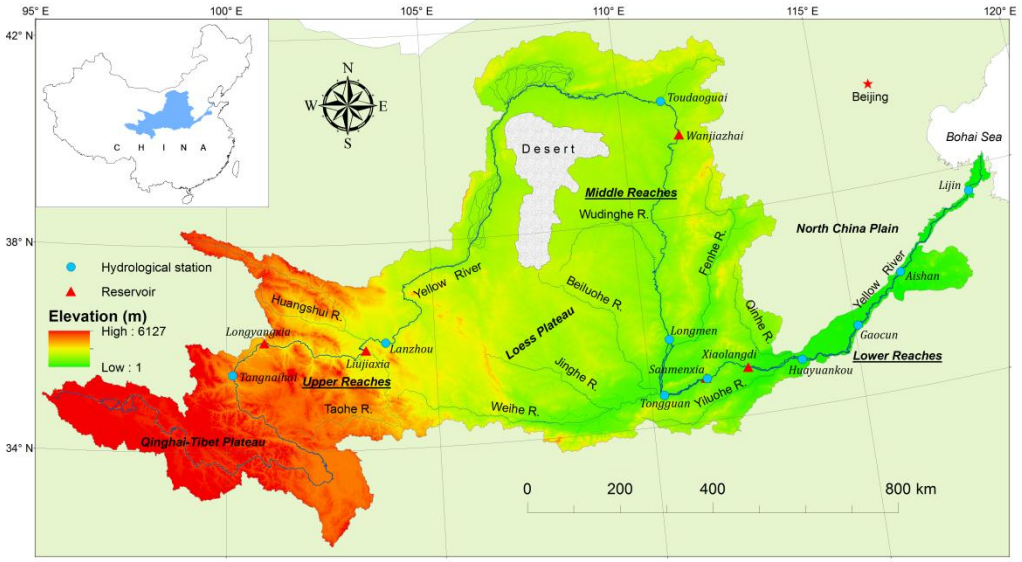

Figure 2.1 Schematic map of the Yellow River basin showing the locations of major tributaries, hydrological gauge stations, and major reservoirs. The Yellow River flows through three different topographic landscapes as characterized by significant elevation differences. Sampling at Toudaoguai, Tongguan, and Lijin stations was conducted during 2011-2012.

2.2 Climate, hydrology, and vegetation

The Yellow River drainage basin is characterized by highly variable hydroclimatic conditions, with strong aridity in the northern parts of the basin, marked precipitation seasonality and, in many areas, a relatively short rainfall period. The annual mean temperature varies from 1-8 ℃ in the upper reaches (upstream of Toudaoguai), 8-14 ℃ in the middle reaches (roughly between Toudaoguai and Huayuankou), and 12-14 ℃ in the lower reaches (downstream of Huayuankou) (Chen et al., 2005). The highest temperature usually occurs in July and the lowest in January. The mean annual precipitation is highly variable across the river basin (Figure 2.2), increasing from 368 mm in the upper reaches, to 530 mm in the middle reaches, and further to 670 mm in the lower reaches (Table 2.1). On average, the multi-annual precipitation is about 400 mm for the entire river basin. With an average of about 1100 mm/yr,

potential evaporation in the river basin is much higher than precipitation and shows considerably strong spatial variability (Table 2.1).

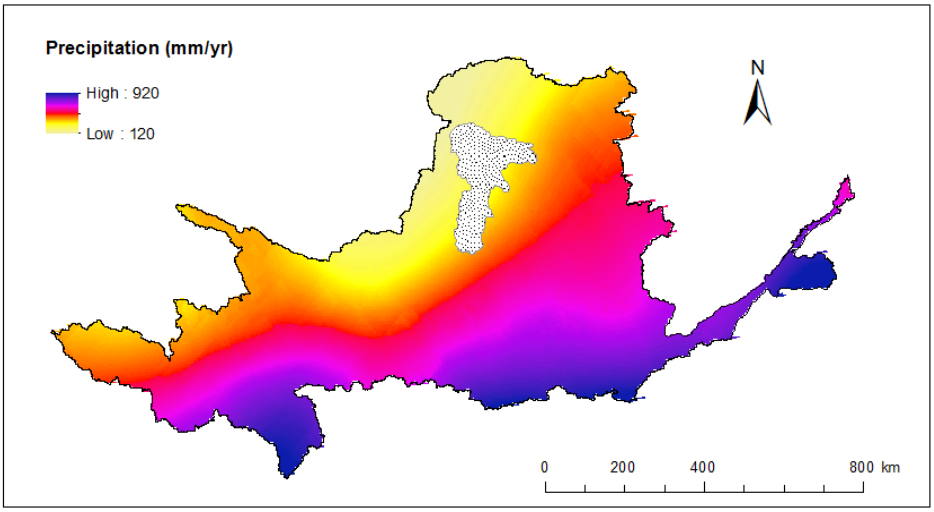

Figure 2.2 Spatial variations of annual mean precipitation in the Yellow River basin showing high precipitation in southeast while low values in northwest. Data from China Meteorological Administration (http://www.cma.gov.cn/).

In general, the potential evaporation in the headwater region is lower compared with the middle and lower reaches due to low temperature and relatively high precipitation. Indeed, in some locations on the eastern flank of the Qinghai-Tibetan Plateau, the annual precipitation could be up to about 900 mm in humid years (Figure 2.2). In contrast, the potential evaporation in the catchments surrounding the desert (Figure 2.1) reaches the peaks of around 1900 mm/yr or even more. For the entire middle and lower reaches, the potential evaporation is largely in the range of 800-1400 mm/yr, although at some tributary catchments it could be significantly higher. Overall, the spatial variability of annual average precipitation and temperature in the river basin suggests that the upper and middle reaches are mostly in arid and semi-arid regions, while the lower reaches are situated in a humid climate. These spatial variations in climate are collectively the result of geological and topographical differences.

Table 2.1 Geographical characteristics of the Yellow River basin.

Item	Mainstem channel			Major tributaries				
	Upper reach Headwater-Toudaoguai	Middle reaches Toudaoguai-Huayuankou	Lower reaches Huayuankou-river mouth (Lijin)	Wudinghe	Beiluohe	Jinghe	Weihe	Fenhe
Length (km)	3471	1206	786	491	447	483	818	710
Drainage area (km^2)	386,000	343,750	22,730	30,260	25,600	45400	106,500	39,800
Altitude (m, asl)	4480-991	991-110	110-0	1350-585	1100-330	1500-360	1500-330	1800-380
P (mm/yr)	368	530	670	300-500	600-900	350-600	400-900	500-600
E (mm/yr)	700-1900	900-1400	800-1200	1000-1400	900-1200	1200-1500	900-1200	900-1000
T (℃)	1-8	8-14	12-14	6-10	12-14	6-13	6-13	6-12
Q_C (km^3/yr)	10.4	5.3	7.3	NA	NA	NA	NA	NA
Gauge station	Toudaoguai	Huayuankou	Lijin	Baijiachuan	Zhuangtou	Zhangjiashan	Huaxian	Hejin
Q (km^3/yr)	21.5	37.6	30.8	1.13	0.8	1.61	6.8	1.02
Q_S (Gt/yr)	0.11	0.89	0.73	0.11	0.08	0.22	0.32	0.022
Q_{TDS} (Mt/yr)	12.06	19.59	15.65	0.6	0.61	1.08	3.7	0.76
D_{50} (mm)	0.016	0.019	0.019	0.032	0.029	0.027	0.017	0.018
SSC (kg/m^3)	4.33	22.6	22.4	84.4	106.7	167.3	50.9	13.4
TDS (mg/l)	561	521	508	529	759	673	544	748

P: annual precipitation; E: potential evaporation; T: temperature; Q_C: annual water consumption; Q: annual water discharge; Q_S: annual suspended sediment load; Q_{TDS}: annual total dissolved solids; D_{50}: median grain size of the suspended sediment; SSC: suspended sediment concentration; TDS: concentration of total dissolved solids. NA indicated the data were not available. Data were retrieved from Chen et al., (2005); Wang et al., (2007b); Wang et al., 2008; Peng et al., (2010), and the Yellow River Sediment Bulletins yearly published by the Yellow River Conservancy Committee during 1950s-2010.

In addition to spatial variability, temporal variations of climate are also distinct. For example, several strong storm events in the wet season from June to September could account for 85% of the annual precipitation in the upper and middle reaches (Zhao, 1996; Wang et al., 2007). While the temperature in summer could be higher than 20 ℃, it decreases to below zero in winter with ice forming on river water surfaces. Accompanying the seasonal variations of temperature, evaporation shows similar seasonal fluctuations. Except for the upstream mountainous areas where snowfall supply can be significant, rainfall is the major source of river runoff for most part of the drainage basin (Chen et al., 2005). As a result, river flows are extremely sensitive to changes in precipitation (Lu, 2004), showing strong inter-annual variability with the annual maximum runoff over the minimum runoff being >11.

Both temperature and precipitation in the Yellow River basin have showed temporal changes over the past decades (Figure 2.3). While the temperature has presented an increasing trend since the 1950s, the annual average precipitation has decreased slightly. In particular, the trends have become increasingly more apparent since the 1990s, resulting in lower runoff. The contrasting temperature and precipitation trends reflect the river basin's responses to global climate change (Lu et al., 2013). For example, the annual mean temperature has increased by 0.85 ℃ post-1990 compared with the pre-1990 period, corresponding to a 12.6% increase. If with continuously increasing temperature in the forthcoming decades as predicted by the IPCC (2007), the precipitation would further decrease, although the magnitude is difficult to quantify.

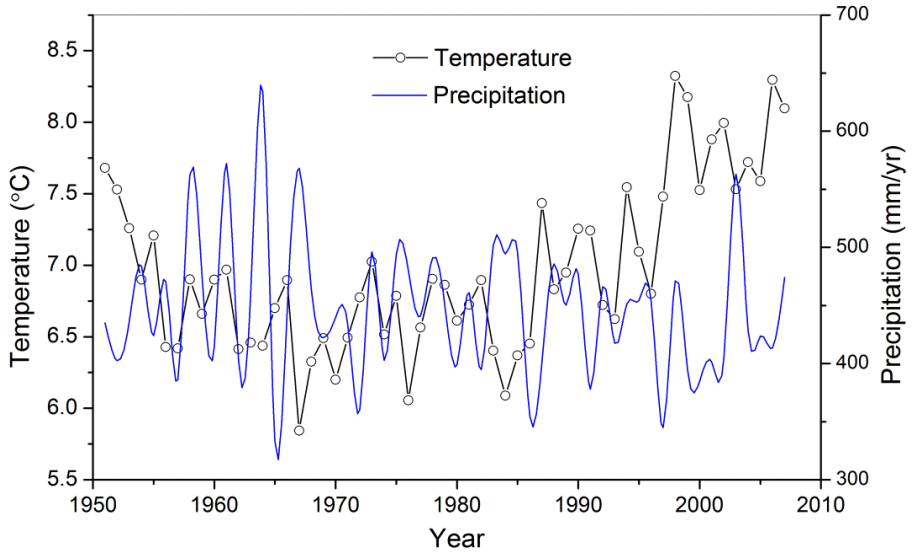

Figure 2.3 Time series of annual mean temperature and precipitation in the Yellow River basin during 1951-2007. The averages were calculated from all meteorological stations in the catchment. Data from China Meteorological Administration (http://www.cma.gov.cn/).

Due to the uneven spatial distribution of precipitation, river runoff in the Yellow River basin is also characterized by strong spatial variations. Whereas more than 57% of the water comes from its upper reaches in the Qinghai-Tibetan Plateau, the middle and lower reaches contribute only 43% (Wang et al., 2003a; Yang et al., 2004b). With a multi-year mean annual runoff depth of 77 mm (Wu et al., 2008a), the annual average water discharge at Lijin station during 1950-2012 is 30.5 km^3/yr. It shows a variability that is relatively lower in the El Niño periods and higher during the La Niña periods (Fu et al., 2004). Well-known for its high sediment yield, the Yellow River used to be the second largest river of the world in terms of sediment discharge, next only to the Ganges-Brahmaputra river system (Milliman and Meade, 1983). For the Loess Plateau with huge amounts of highly erodible soil material, the suspended sediment concentration (SSC) could be in excess of 1000 kg/m^3 in some hyperconcentrated flow events, and its mean annual SSC is 35 kg/m^3 (Zhao, 1996; Xu,

2002). These concentrations are far greater than that for any other large river in the world. Prior to the 1970s, annually about 1.6±0.3 Gt of sediment was discharged downstream through the Sanmenxia station and 1.21 Gt into the Bohai Sea (Figure 2.1).

Similar to the spatial distribution of water resources, sediment yield in the Yellow River basin also has significant spatial variability (Figure 2.4). Most of the suspended sediments (~90%) are derived from the middle reaches where the river drains the extensive loess deposits, which are acknowledged as the most easily erodible material available to moving water (Milliman and Meade, 1983; Huang and Zhang, 2004). In contrast, the upper reaches contribute only about 10% of the total sediment (Figure 2.4). For the lower reaches, due to gentle channel slope and reduced sediment carrying capacity, large amounts of sediment are deposited on the intervening alluvial plains each year, causing the lower mainstem channel to form a unique 'suspended river' where the riverbed is raised over the surrounding grounds by several meters (Wang et al., 2007b).

It can be clearly seen that the sources of water and sediment are quite different. The upper reaches are the major water contributors and the middle reaches the main sediment providers, while the lower reaches act more as a region of sedimentation and human water consumption. In addition, as a result of the 'suspended river', the lower Yellow River channel is extremely vulnerable to avulsion. More than 26 main channel channel course shifts have been recorded in the last 3000 years due to

frequent channel avulsions (Chen et al., 2005). The channel course has not changed since a natural course shift in 1855.

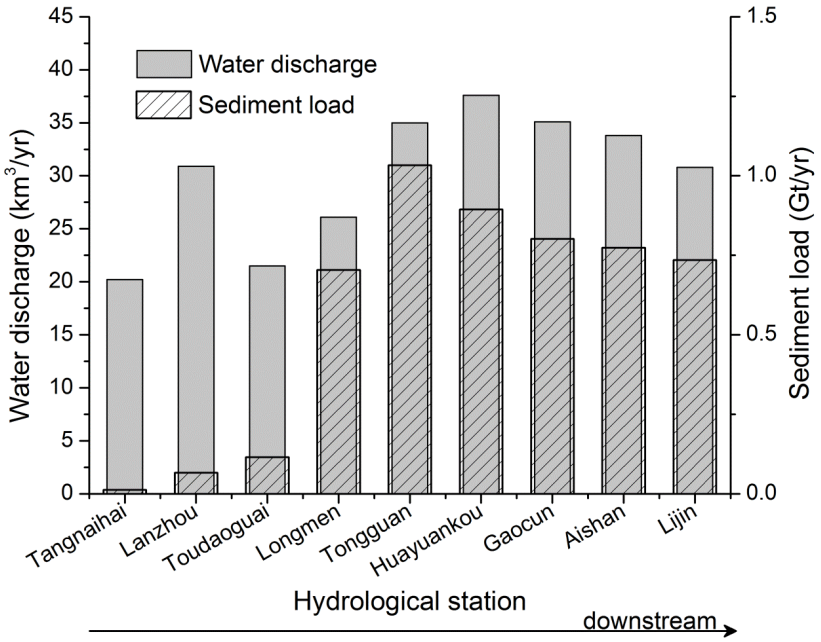

Figure 2.4 Spatial variations of water discharge and sediment load measured at hydrological stations along the mainstem channel. Most of the sediment load originates from the Loess Plateau, in particular the middle reaches downstream of the Toudaoguai station. The annual averages were based on long-term hydrological records measured during the period of 1950s-2010. Refer to Figure 2.1 for locations. Data from Ministry of Water Resources of China, (2010a).

Vegetation growth in the Yellow River basin is controlled by low precipitation and temperature as well as extensive human activities. The headwater region is largely developed with grassland and woodland with minor mountain, glacier, desert, and swampland (Wu et al., 2005). Alpine shrub and meadows are the major vegetation types, with pockets of conifer forests. In recent years, vegetation cover in the headwater region has decreased as a result of degradation of permafrost and subsequent lowering of groundwater table (Wang et al., 2000). In contrast, the wide middle reaches/Loess Plateau are sparsely vegetated and the ecological environments

are very fragile. Located in arid, semi-arid and sub-humid climates with annual precipitation increasing from less than 200 mm in the northwest to more than 700 mm in the southeast (Figure 2.2), natural vegetation cover in the middle reaches varies from arid desert, to steppe, to broad-leaf deciduous forest (Yang and Yuan, 1991).

Although extensive efforts have been devoted to restoring vegetation since the 1960s, significant increase in vegetation cover started only in recent years, in particular after the implementation of the Grain-for-Green Project in the late 1990s (Chen et al., 2007a). By analyzing the Normalized Difference Vegetation Index (NDVI) variations over 1981-2006, Xin et al (2008) found that the vegetation restoration in the Yellow River basin showed strong spatial differences. Increased vegetation cover was found in the northern part of the river basin, whereas the hilly and gully areas in the Loess Plateau and the southern part of the basin showed decreasing trends. As large-scale vegetation restoration programs are being conducted across the river basin, vegetation cover is expected to increase in the near future.

2.3 Geological characteristics

The Yellow River basin is developed mainly on the Sino-Korean Shield, which was formed during the Archean and Proterozoic (Zhang et al., 1995a; Chen et al., 2005). On average, the headwater region on the Qinghai-Tibetan Plateau has an elevation of >2000 m, the middle reaches on the Loess Plateau are in the range of 500-2000 m in elevation, and the lower reaches on the northern China Plain are below 500 m. The mean local relief (the maximum-minimum elevation within each 10-min grid cell) of

the entire drainage basin is about 461 m (Summerfield and Hulton, 1994).The rock outcrop in the drainage basin ages from Precambrian to Quaternary, with the geology encompassing a broad range of tectonic zones (Zhang et al., 1990).

The headwater region of the Yellow River, draining the western Bayan Har fold belt of the Indosinian (Late Triassic) age, is mainly composed of sandstone, dolomitic limestone, and minor volcanic rocks (Yang et al., 1986; Wu et al., 2005). The middle reaches, mainly the Loess Plateau, are dominated by Quaternary loess and loess-like deposits (Figure 2.5). With a typical accumulation thickness of 130-180 m and could be up to 250 m in some localities (Liu et al., 1991), the loess is formed primarily from dust falling as a result of major climatic changes in the early Pleistocene (ca. 2.4-2.6 Ma) and quasi-continuous accumulation throughout the entire Quaternary period (Liu and Zhang, 1988). The thick loess-paleosol sequence has recorded probably the most complete terrestrial record of environmental changes during the Quaternary (Liu and Zhang, 1988; Chen et al., 2005). Typically, based on the research results of Liu and Zhang (1988), from the surface layer downward, there are three different strata, including Malan loess (Late Pleistocene), Lishi loess (Middle Pleistocene) and Wucheng loess (Early Pleistocene) which overlies the red clay formation (4.5-7.2 Ma) of the Pliocene and late Tertiary. In addition, the Paleosol layers are frequently present within or between these loess strata. Approximately, the Quaternary loess and loess-like deposits cover an area of 0.33×10^6 km^2, accounting for about 44% of the total drainage area (Chen et al., 2005). From northwest to southeast of the whole basin, their particle size becomes increasingly finer (Xu, 2005).

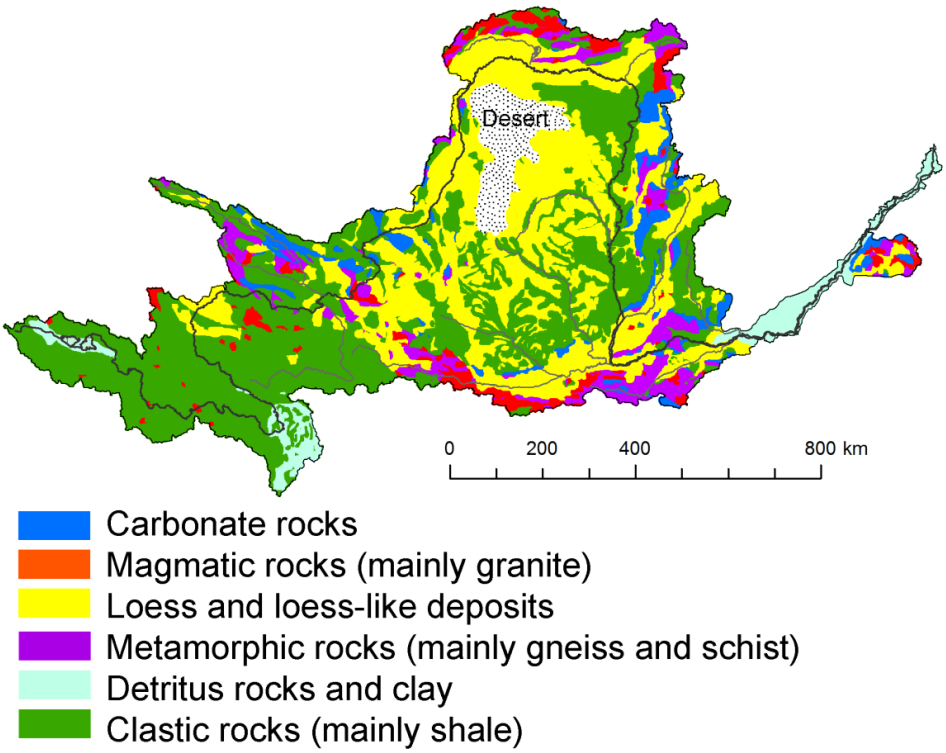

Figure 2.5 Lithological map of the Yellow River basin showing distribution of major rocks. Adapted from Chen et al (2005).

In addition to loess deposits, outcrops of Archean to Tertiary granites and metamorphic rocks, mainly gneiss and schist, can be found in areas near the northern and southern boundaries of the drainage basin as well as the headwater region (Yang et al., 1986; Zheng, 1997; Wu et al., 2005), as shown in Figure 2.5. Furthermore, carbonates, coal series, and clastic rocks from Paleozoic to Mesozoic age are scattered in highlands and deep valleys along the river course, and red clastic rocks of Cretaceous and Tertiary age with gypsum beds can be found in the upper and middle reaches (Zhang et al., 1995a). These strata play a critical role in determining the chemical compositions of the Yellow River waters. Because weathering of these rocks will result in consumption of atmospheric CO_2, estimating the magnitude of

consumption and studying its influencing factors are critical for understanding the basin carbon cycle.

2.4 Major human impacts

Human activities in the Yellow River basin have a long history. At present, the Yellow River is the water source for more than 140 million people and at least 50 large and medium-sized cities (Chen et al., 2005). While the upper Yellow River basin is sparsely populated (i.e., <100 person/km^2), the middle and lower reaches are characterized by quite high population density, usually >200 person/km^2 (Chen et al., 2005). To utilize the spatially unevenly distributed water resources, large-scale water withdrawal projects for agriculture, industry, and domestic use have been constructed. In addition, a large amount of effort has been devoted to controlling soil erosion on the Loess Plateau.

2.4.1 Water withdrawal for irrigation

Under the arid and semiarid conditions of northern China, most of the Yellow River basin is short of usable water. To develop agriculture, large volumes of river water are withdrawn from the main channel every year (Figure 2.6). Irrigation has long been critical to agriculture in the Yellow River basin for more than 2000 years (Chen et al., 2005). Many irrigation zones have been developed along the river since 1950 (Figure 2.7). Two major irrigation zones are the Ning-Meng irrigation zone in the upper Yellow River basin and the North China Plain irrigation zone along the lower Yellow River.

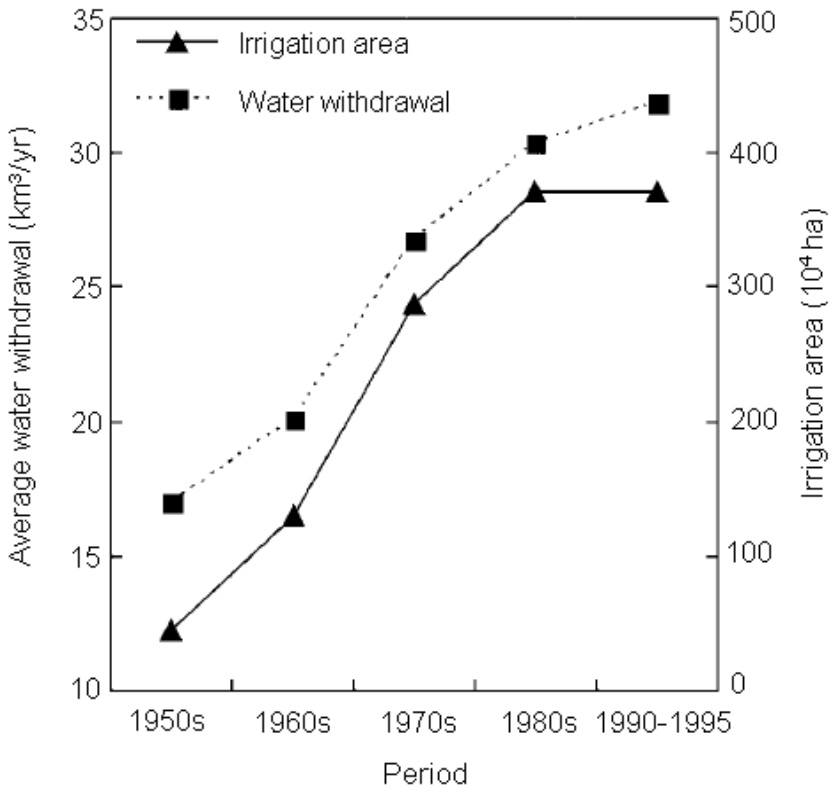

Figure 2.6 Temporal changes in irrigation water withdrawal and irrigation area in the Yellow River basin during 1950-1995. Data from Chen et al (2003).

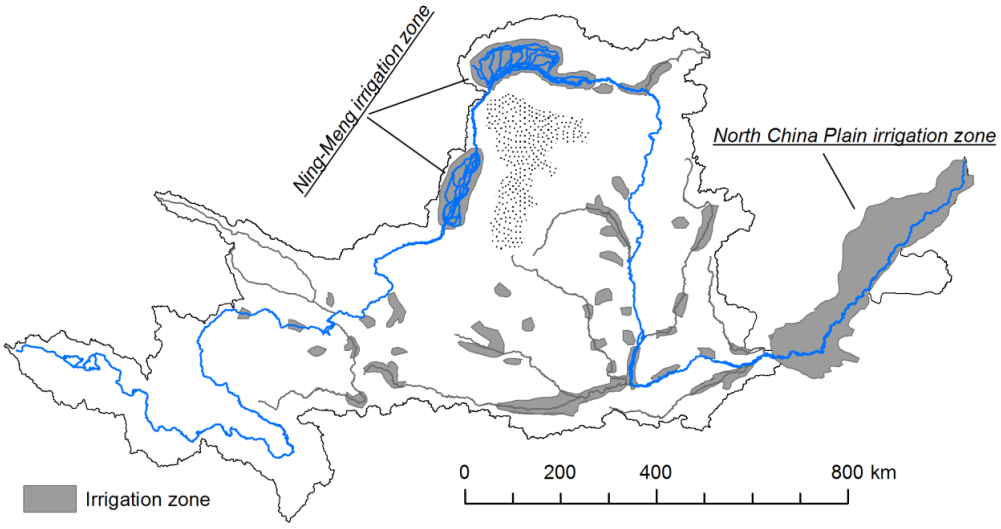

Figure 2.7 Major irrigation zones in the Yellow River basin. Large volumes of water are diverted every year from the Yellow River for agricultural production, in particular the Ning-Meng and North China Plain irrigation zones as shown in the figure. Adapted from Yang et al (2004a).

Over the past 60 years, the water amount withdrawn from the Yellow River has increased dramatically due to growing demand within the basin and the surrounding regions (Zhao, 1996). Nevertheless, modern irrigated agriculture is the largest water consumer in the river basin. For example, during the period 1988-1992, the irrigation water withdrawn from surface water accounted for 92% of the total surface water withdrawal, and the irrigation water withdrawn from groundwater accounted for 61% of the total groundwater withdrawal (Chen et al., 2003). Of the 113,000 km^2 cultivated land in the Yellow River basin in 1997, approximately 75,000 km^2 were irrigated (Chen et al., 2003). According to Pang and Jiang (2003), the amount of water withdrawn from the Yellow River for irrigation has doubled from 12.5 km^3 in 1950-1959 to more than 30 km^3 during the period of 1990-1999. Decadal increases in water withdrawal can be clearly seen from Figure 2.6. As a result, the frequency of zero-flow in the lower Yellow River has increased, and its duration has also lengthened such that during 1997 no water discharged into the ocean for 330 days (Grafton et al., 2013).

Massive water withdrawal has triggered an array of environmental problems. Rapid expansion of irrigated agriculture and agricultural intensification is an important factor for water quality degradation. For example, due to extensive construction of flood irrigation systems without proper drainage canals, widespread water logging and soil salinization occurred in the North China Plain irrigation zone during 1958-1964 (Chen et al., 2003). Moreover, Chen et al (2005) attributed the observed increase in the concentration of major ions of the Yellow River waters to the impacts

of intensified irrigated agriculture over the studied four decades (1958-2000). Furthermore, excessive water withdrawal from the main channel has resulted in longitudinally reduced water discharge in the river (see Figure 2.4). For instance, due to water withdrawal during the stretch between Lanzhou and Toudaoguai stations, mainly the Ning-Meng irrigation zone, the multiannual mean water discharge at Lanzhou station (30.9 km^3/yr) is 30% higher than at Toudaoguai station (21.5 km^3/yr). In the lower Yellow River, the annual water discharge decreases gradually from Huayuankou station downstream until the river mouth, as shown at Gaocun, Aishan, and Lijin stations in Figure 2.4, which is also largely due to water withdrawal along the channel course (Figure 2.7). The greatly reduced flow has caused a deleterious impact on riverine habitats and ecosystem health for the delta wetlands (Peng et al., 2010), despite recent increases in flow as a result of adoption of more environment-friendly practices that attempted to restore the ecological integrity of the damaged riverine ecosystems.

2.4.2 Dam and reservoir construction

In recent years, impacts of dams/reservoirs on river systems have received considerable attention worldwide (e.g., Vörösmarty and Sahagian, 2000; Nilsson et al., 2005; Syvitski et al., 2005; Yang et al., 2006). Several studies have included the Yellow River when attempting to explore the global impacts of dams/reservoirs on river water and sediment transport into the oceans (e.g., Walling and Fang, 2003; Syvitski et al., 2005; 2009). The Yellow River has become a highly fragmented and regulated river due to continuous dam construction within the river basin for various

purposes since the 1950s. By 2010, more than 3000 reservoirs had been built in the river basin with a total storage capacity of about 72 km^3. The storage capacity is significantly larger than the annual water discharge (Wang et al., 2007). Located mainly in the upper and middle Yellow River basin, these reservoirs could effectively intercept water and trap sediment from flowing downstream, resulting in rapid reductions in the seaward fluxes. Particularly, reservoirs constructed on the mainstem channel have played an important role in affecting water and sediment delivery as a result of their large storage capacity (Figure 2.8; Table 2.2). Up to 2007, there have been 24 large reservoirs with individual storage capacities exceeding 0.1 km^3 within the river basin.

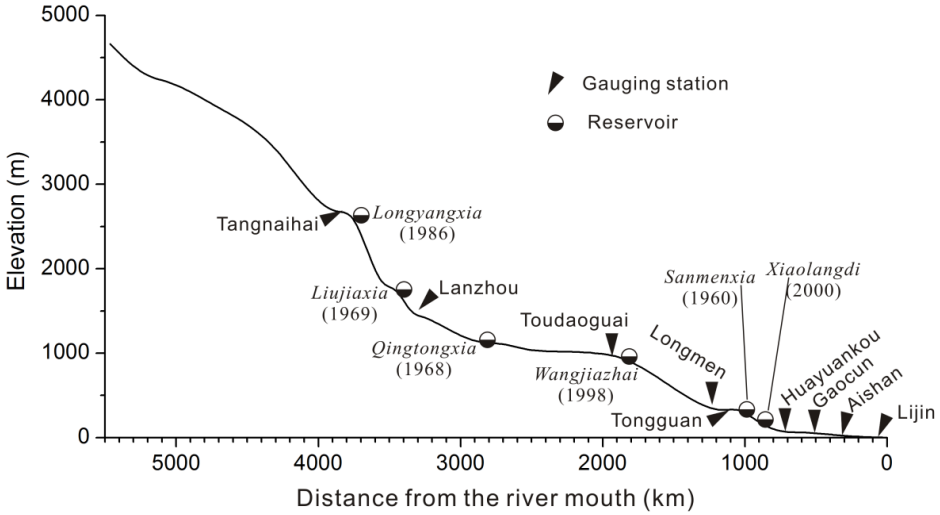

Figure 2.8 Longitudinal profile of the mainstem channel of the Yellow River showing the locations of large reservoirs constructed during the past decades. The figures in the brackets denoted the year of completion.

In addition to economic benefits, such as energy generation (Table 2.2), operation of these reservoirs has also caused severe environmental and ecological problems. For example, with the operation of the four most important reservoirs, namely the Sanmenxia since 1960, Liujiaxia since 1969, Longyangxia since 1986, and

Xiaolangdi since 2000, transport dynamics of the water and sediment in the Yellow River have been significantly changed, compared with the pre-dam period (i.e., the 1950s) (Figure 2.9). Both water discharge and sediment load have showed stepwise reductions during the past 60 years (Wang et al., 2007b; Peng et al., 2010). From a spatial perspective, significant water reductions started from 1987 when the Longyangxia Reservoir was put into operation (Figure 2.9a). Joint operation of the Longyangxia and Liujiaxia reservoirs in the upper reaches stored water in the flooding season for irrigation diversion, resulting in direct water reductions in the downstream channel. Because the Loess Plateau is the major sediment source, considerable sediment reductions were observed downstream of the Loess Plateau (Figure 2.9b). As indicated in Figure 2.9b, the sediment fluxes from Longmen to Lijin stations showed remarkable decreases after the completion of each major dam.

Table 2.2 General information of the major reservoirs constructed in the Yellow River basin*.

Reservoir	Drainage area	Height	Top water level (a.s.l.)	Storage capacity	Installed capacity	Electricity generation	Year of completion
	10^4 km^2	m	m	km^3	10^4 kW	10^8 kW.h/yr	
Longyangxia	13.1	178	2600	24.7	128	59.4	1986
Lijiaxia	13.7	165	2180	1.65	200	59	1997
Liujiaxia	18.2	147	1735	5.7	116	55.8	1968
Yanguoxia	18.3	55	1619	0.22	39.6	21.7	1962
Bapanxia	21.6	33	1578	0.049	18	9.5	1970
Daxia	22.8	71	1480	0.09	30	14.7	1996
Qingtongxia	27.5	42.7	1156	0.62	27.2	10.4	1967
Sanshenggong	31.4	9	1055	0.08	/	/	1961
Wanjiazhai	39.5	90	980	0.898	108	27.5	1998
Tianqiao	40.4	47	834	0.068	12.8	6.1	1977
Sanmenxia	68.8	106	335	9.75	40	13	1960
Xiaolangdi	69.4	173	275	12.65	180	58.4	2000

*Data from Zhao (1996); Wang et al (2007b); and the Hydrological Yearbooks of the Yellow River yearly published by the Yellow River Conservancy Commission (YRCC).

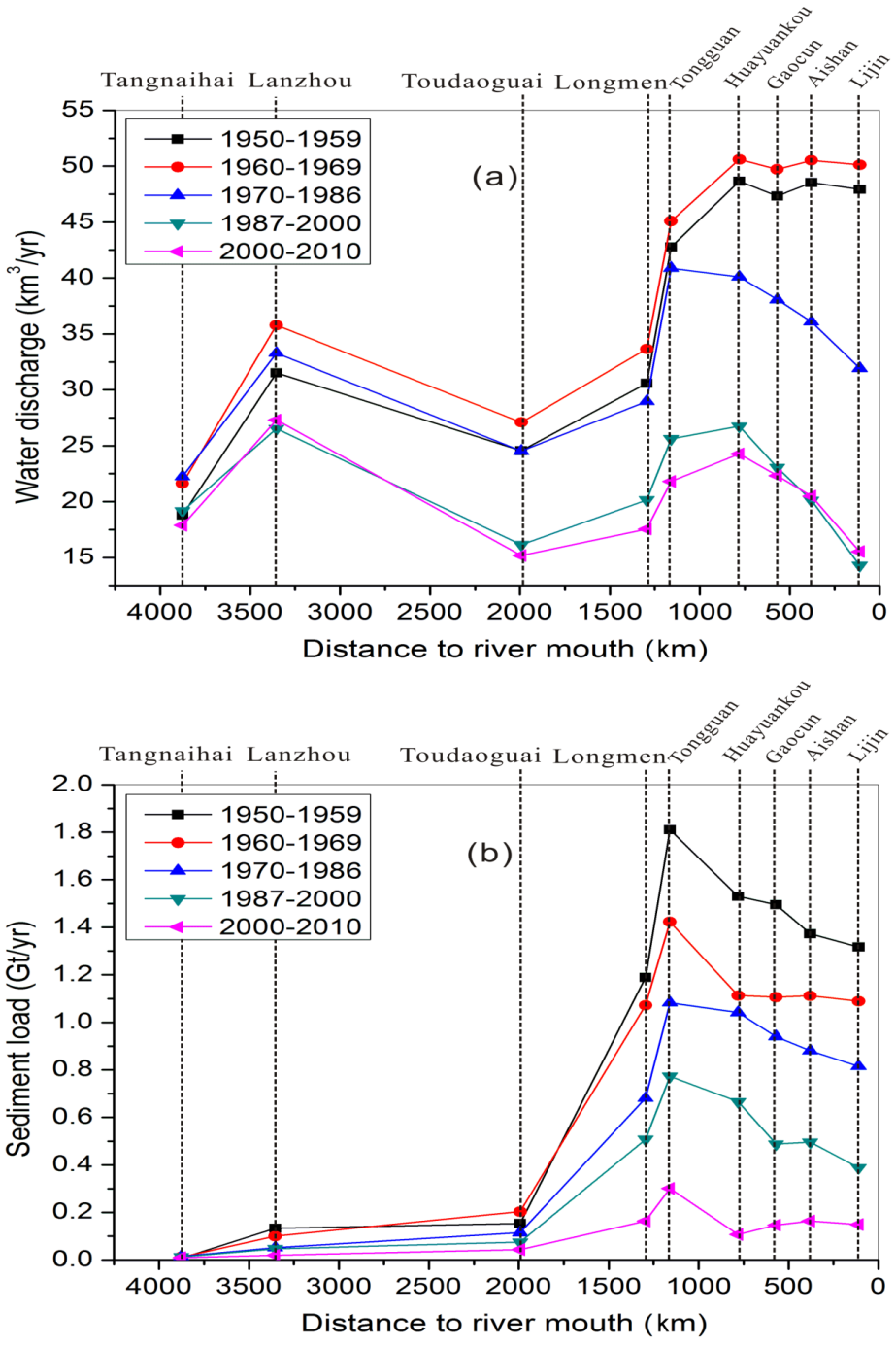

Figure 2.9 Downstream variations of water discharge (a) and sediment load (b) as affected by reservoir operation during the period of 1950-2010. Key reservoirs built on the Yellow River mainstem channel that are able to significantly regulate water and sediment transport include the Sanmenxia Reservoir (1960), Liujiaxia Reservoir (1969), Longyanxia Reservoir (1986), and the Xiaolangdi Reservoir (2000). Data from Ministry of Water Resources of China (2010a), see Appendix.

Reservoir sedimentation has been a severe problem for almost all the reservoirs constructed in the Yellow River basin, in particular those on the Loess Plateau. One example is the Sanmenxia Reservoir. During the period 1960-1973, the total sediment deposited in the reservoir amounted to 7.91 Gt, accounting for 83% of the sedimentation accumulated from 1960 to 2007 (Table 2.3). In fact, the sediment trapping reached 6.22 Gt in just four years from 1960 to 1964. Another example is the Xiaolangdi Reservoir. Located downstream of the Sanmenxia Reservoir, sedimentation in the reservoir has been periodically measured (Table 2.3). Approximately, 3.24 Gt of sediment has been trapped during the period 1997-2007 with a mean trapping rate of 0.294 Gt/yr. Although the sedimentation magnitude varies between different reservoirs, sediment trapping in reservoirs has been an important fate for sediment transported by the river.

Table 2.3 Sediment trapping by the Sanmenxia and Xiaolangdi reservoirs. The two reservoirs are located immediately downstream of the Loess Plateau. Refer to Figure 2.1 for location. Negative values denote scour. Data from Peng et al (2010).

Reservoir	Time periods					
Sanmenxia	1960-1964	1965-1973	1974-1985	1986-1999	2000-2007	1960-2007
Trapping (Gt)	6.219	1.691	0.161	1.751	-0.268	9.554
Average (Gt/yr)	1.244	0.188	0.013	0.125	-0.034	0.201
Xiaolangdi				1997-1999	2000-2007	1997-2007
Trapping (Gt)				0.085	3.152	3.237
Average (Gt/yr)				0.028	0.394	0.294

2.4.3 Soil conservation and sediment control practices

The Loess Plateau covers a total area of 640,000 km^2, about 330,000 km^2 of which within the Yellow River basin supplies approximately 90% of the total suspended solids (Zhao, 1996; Peng et al., 2010). Due to strong soil erosion associated with distinct rainfall regime characterized by intensive rainfalls, sediments from tributaries

in the middle reaches have larger median grain size (D_{50}) than those in the mainstem channel (Table 2.1). The most severe soil erosion mainly occurs in the reaches between Toudaoguai and Longmen stations (Figure 2.10), particularly the Wudinghe, Beiluohe, and Jinghe tributaries. To mitigate soil erosion effectively and maintain the productivity of land, a number of soil conservation practices and watershed management projects have been implemented throughout the basin since the late 1950s. Generally, these practices include terrace construction, silt check dams, reforestation, and planting of grass, with the former two usually called engineering measures and the latter two vegetation restoration measures (Figure 2.11). Terraces are usually constructed on slopelands with slopes less than 25°, while reforestation and grass planting are conducted on slopelands with slopes larger than 25°.

Figure 2.10 Severe soil erosion occurring frequently on the Loess Plateau, resulting in serious land degradation and nutrient losses.

In attempting to increase moisture retention and storage and to reduce the on-site impacts of soil erosion linked to reduced soil productivity and crop yields, these practices have been remarkably effective in reducing sediment yields since the late 1970s (Xu, 2002; Peng et al., 2010). Furthermore, comprehensive sediment control programmes, such as construction of silt check dams, have also addressed the off-site

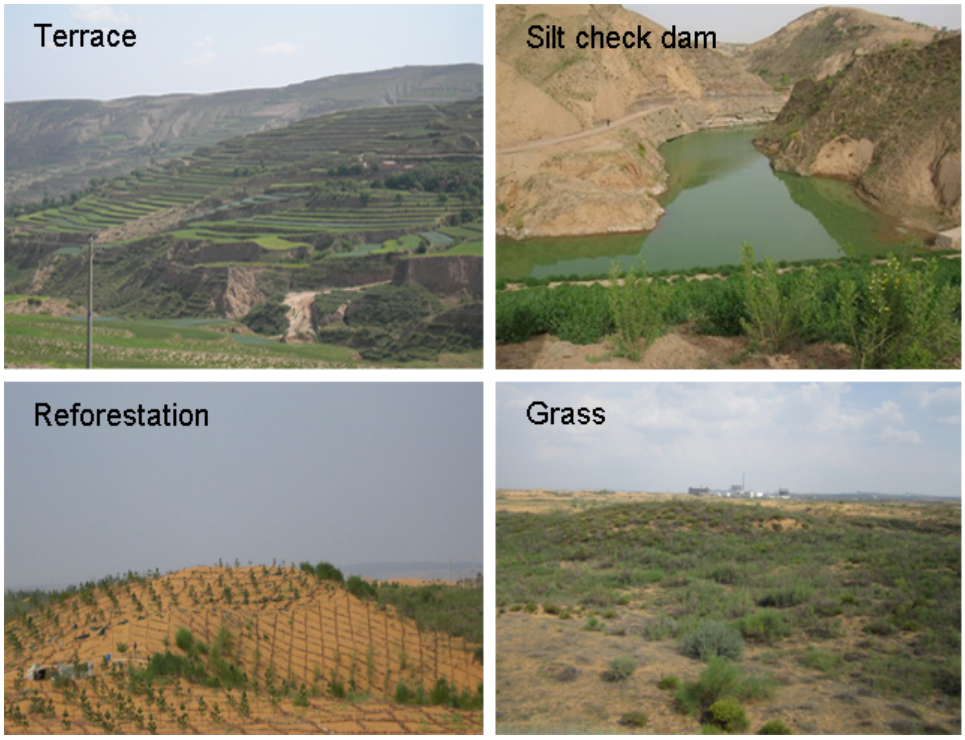

Figure 2.11 Major soil conservation measures widely implemented within the Yellow River basin in the past few decades. Terraces and silt check dams are usually called engineering measures, and reforestation and grass plantation are called vegetation restoration measures.

impacts of soil erosion and sediment mobilization. By the end of 2000, soil conservation practices had been applied to 158,000 km^2 in the middle reaches, including 46,000 km^2 of terraces, 88,000 km^2 of reforestation, and 24,000 km^2 of grass planting. In addition, more than 110,000 silt check dams have been completed to exclusively trap sediment (Yellow River Conservancy Committee, 2000-2007). On average, sediment yield from the middle reaches has been reduced by 0.25-0.3 Gt/yr in the past four decades due to the implementation of widespread soil conservation practices (Zhao, 1996; Walling and Fang, 2003; Huang and Zhang, 2004; Peng et al., 2010). Along with water withdrawal for agricultural irrigation and flow regulation by dams, soil conservation practices have been widely regarded as an important human

activity in affecting water discharge and sediment load in the Yellow River basin. In addition, soil conservation practices have been found to play a more significant role than dams in reducing seaward sediment fluxes. For example, based on comprehensive analyses of long-term water and sediment records, Wang et al (2007) and Peng et al (2010) ascribed 40% of the reduced sediment load at Huayuankou station to soil conservation practices. In comparison, sediment retention within reservoirs accounted for 30% of the total reduced sediment load; and decreased precipitation due to climate change was responsible for the remaining 30%.

Chapter 3 Chemical weathering and atmospheric CO_2 consumption

3.1 Introduction

Chemical weathering of rocks is one of the most important processes regulating the level of atmospheric CO_2 (e.g., Loughnan, 1969; Kempe, 1979; Berner et al., 1983; Kump et al., 2000; Lenton and Britton, 2006; Hartmann et al., 2012; Basak and Martin, 2013; Regnier et al., 2013). In general, the rocks on Earth's surface exposed to weathering agents can be classified into three types: carbonates (e.g., limestone and dolomite), silicates (e.g., sandstone, shale, and basalt), and evaporates (e.g., halite and gypsum/anhydrite). Several typical rock weathering reactions commonly observed in the field are presented in Table 3.1. Chemical weathering reactions of most silicates in soils proceed incongruently (White and Brantley, 1995; Kump et al., 2000). Briefly, the mobile elements, such as Ca and Na, tend to be removed in dissolved form by soil solutions, whereas the immobile elements are incorporated into stable secondary soil minerals, such as clays and metallic oxy-hydroxides which accumulate in soil horizons (Viers et al., 2007). For example, in the weathering process of K-feldspar (Table 3.1), K and silica (dissolved Si) will be exported by waters out of the weathering site while Al and some Si accumulate in the weathering site to form montmorillonite ($Al_2Si_4O_{10}(OH)_2$). In contrast, the dissolution of carbonates is congruent. All the products of the dissolution are aqueous species, and thus could be transported downstream by flowing waters. For example, the weathering products of calcite are Ca^{2+} and HCO_3^-. In addition, dissolution of evaporites usually does not need the involvement of acid, such as carbonic acid (H_2CO_3) or sulfuric acid (H_2SO_4).

The consumed carbonic acid during the chemical weathering processes is mainly derived from oxidation of organic matter in soils, which can be expressed as:

$CH_2O+O_2 \rightarrow CO_2+H_2O \rightarrow H_2CO_3$ (Equation 3.1)

Table 3.1 Major chemical weathering reactions widely occurring in the Yellow River basin (Zhang et al., 1995a, and references therein).

Rock type	Mineral	Reaction equation
Silicates	Na-feldspar into kaolinite	$2NaAlSi_3O_8+2CO_2+11H_2O \rightarrow 4H_4SiO_4+2HCO_3^- +2Na^+ +Al_2Si_2O_5(OH)_4$
	K-feldspar into montmorillonite	$2KAlSi_3O_8+2CO_2+6H_2O \rightarrow 2\ H_4SiO_4+2HCO_3^-+2K^+ + Al_2Si_4O_{10}(OH)_2$
	Plagioclase into kaolinite	$2NaCaAl_3Si_5O_{16}+6H_2CO_3+11H_2O \rightarrow 4H_4SiO_4+6HCO_3^- +2Na^+ +2Ca^{2+}+3Al_2Si_2O_5(OH)_4$
	Illite into kaolinite	$2KAl_3Si_3O_{10}(OH)_2+2CO_2+5H_2O \rightarrow 3Al_2Si_2O_5(OH)_4+ 2HCO_3^-+2K^+$
	K-feldspar into kaolinite	$2KAlSi_3O_8+2CO_2+11H_2O \rightarrow Al_2Si_2O_5(OH)_4+2HCO_3^- +4H_4SiO_4+2K^+$
Carbonates	Calcite	$CaCO_3+ H_2O+ CO_2 \rightarrow Ca2^+ +2HCO_3^-$
	Dolomite	$CaMg(CO_3)_2+2\ H_2O+2\ CO_2 \rightarrow Ca^{2+}+Mg^{2+}+4HCO_3^-$
Evaporites	Gypsum	$CaSO_4.2H_2O+ H_2O \rightarrow Ca^{2+}+SO_4^{2-}+3H_2O$
	Halite	$NaCl \rightarrow Na^+ +Cl^-$

Examination of the chemical reactions in Table 3.1 suggests that dissolution of evaporites does not consume atmospheric CO_2, whereas dissolution of carbonates and silicates exerts a net effect on the balance of CO_2 in the atmospheric system. In particular, for the generated HCO_3^- due to carbonate weathering, only half of the carbon comes from the atmosphere (CO_2) while the other half comes from the carbonates themselves. In addition, because the residence time of HCO_3^- in the oceans is about one million years, carbonate dissolution would have a net effect on the CO_2 balance of the atmosphere only on a timescale that is similar or shorter than the residence time of HCO_3^- (White and Blum, 1995; Berner and Berner, 2012). Therefore, on a longer timescale, the consumed atmospheric CO_2 through carbonate weathering will be released back to the atmosphere with the precipitation of carbonates in the oceans.

In contrast, as far as the silicate weathering is concerned, all the carbon in the generated HCO_3^- comes from the atmosphere. More importantly, silicate weathering represents a net consumption of atmospheric CO_2. For example, the dissolution of 1 mol of anorthite ($CaAl_2Si_2O_8$) will consume 2 mol of atmospheric CO_2 (Table 3.1). If the dissolved Ca^{2+} is then precipitated as limestone in the oceans, only 1 mol of carbon in the generated HCO_3^- could be returned to the atmosphere. As such, weathering of silicates plays an important role in controlling the CO_2 balance of the atmosphere over a longer timescale. Atmospheric CO_2 consumption by global rock weathering is estimated at 0.2-0.288 Gt/yr at present (Berner et al., 1983; Ludwig et al., 1998; Gaillardet et al., 1999; Battin et al., 2009). Of this atmospheric carbon, carbonate weathering accounts for about 40% of the worldwide atmospheric CO_2 uptake for all weathering, although carbonates cover only 13% of the total continental area (Suchet et al., 2003). The remaining 60% of CO_2 uptake is attributed to weathering of silicates that represent 84% of the total continental area. Recorded rapid increase in atmospheric CO_2 concentration started only about 250 years ago from the beginning of the industrial revolution (Canadell et al., 2007), which is negligible compared with the length of the geological timescale. Therefore, although carbonate weathering has no net effect on CO_2 balance of the atmosphere on a geological timescale of 1 million years, its significance in affecting atmospheric CO_2 balance at a short timescale cannot be ignored.

Studies of chemical weathering and associated atmospheric CO_2 consumption have been carried out worldwide using increasingly more systematic and holistic

approaches, including in the Amazon (Richey et al., 1991; Amiotte-Suchet and Probst, 1993; Mortatti and Probst, 2003), Ganges-Brahmaputra (Galy and France-Lanord, 1999; Hren et al., 2007; Vance et al., 2009), Yangtze (Li and Zhang, 2005; Chetelat et al., 2008; Wu et al., 2008b), Congo (Probst et al., 1992; Amiotte-Suchet and Probst, 1993), Pearl (Wu et al., 2008b; Gao et al., 2009), and Mississippi (Meybeck and Ragu, 1997; Cai et al., 2008).

With respect to the Yellow River, similar studies focusing on water chemistry started from the 1980s. Hu et al (1982) appear to be the first researchers introducing the water chemistry characteristics of major Chinese rivers in the western literature. By analyzing the elemental geochemistry characteristics through sampling in the estuary and southern Bohai Sea in May 1985, Zhang et al (1990) concluded that intense weathering of carbonates and evaporites is the main source of major dissolved solutes. Furthermore, Zhang et al (1995a) collected water samples along the mainstem channel and major tributaries in August 1986. They examined the spatial variations in concentrations of major elements, and again discovered that chemical weathering is of primary importance in affecting river chemistry; while atmospheric input is very limited. Based on water chemistry records measured monthly at 100 hydrological gauge stations during the period of 1958-2000, Chen et al (2005) investigated the spatial and temporal variability of the major solute chemistry. The concentrations of some ions, such as Na^++K^+, Cl^-, and SO_4^{2-}, were found to be 10-20 times higher than other world large rivers. In addition, the concentrations of all the major ions except HCO_3^- showed a persistent increasing trend during the period. While these studies

have improved the understanding about the water chemistry characteristics of the Yellow River, the results are based on single expeditions and are outdated as huge changes have occurred in the drainage basin in the past decades. In addition, previous studies did not discuss the associated atmospheric CO_2 drawdown, which is expected to be important in the global carbon budget given the size of the catchment.

In this chapter, the chemical weathering processes of the Yellow River basin were first analyzed by sampling at three hydrological gauge stations along the mainstem channel. With identified ion sources, the associated atmospheric CO_2 uptake due to weathering of carbonates and silicates was then evaluated. The major dissolved constituents examined in this study are Ca^{2+}, Mg^{2+}, Na^{+}, K^{+}, Cl^{-}, SO_4^{2-}, HCO_3^{-}, and dissolved silica (SiO_2). The objectives are threefold: 1) to examine the spatial and seasonal variations of the major ion concentrations along the mainstem channel of the Yellow River, 2) to investigate possible sources for the dissolved solutes and analyze the chemical weathering characteristics, and 3) to assess the associated atmospheric CO_2 consumption and its implications in global carbon budget.

3.2 Materials and methods

3.2.1 Field sampling and *in situ* measurements

Water samples were collected at three mainstem hydrological gauge stations, namely Toudaoguai, Tongguan, and Lijin, during the period between July 2011 and July 2012. The locations of the sampling stations are indicated in Figure 3.1a. In general, a weekly sampling frequency was employed. More samples, for example on a daily

basis, were collected during flooding periods in order to explore the responses of dissolved loading transport to high flows. The stations were selected to assess spatial variation in the river system across the basin. In particular, Toudaoguai and Tongguan stations are located near the boundaries of the upper-middle and the middle-lower reaches, respectively. Comparison of the two stations could reveal the differences in the nature of water and associated dissolved species from the Loess Plateau. Located about 110 km upstream of the river mouth and free of tidal influences, Lijin station measurements represent dissolved loading delivery to the Bohai Sea.

Water column samples were collected ~0.5 m below the surface water from 3-5 points across the cross-section using acid-washed but carefully neutralized 5-L high density polyethylene (HDPE) containers (Figure 3.1b). The samples were fully combined to create one sample representing the entire cross-sectional profile. The container was rinsed with sample water several times before filling. *In situ* temperature and pH were synchronously measured using a portable pH meter (Hanna HI9125). Records of daily water discharge and total suspended solids (TSS) were available at the hydrological gauge stations. During the sampling, 161 water samples were collected from the three stations for the purpose of analyzing the water chemistry characteristics.

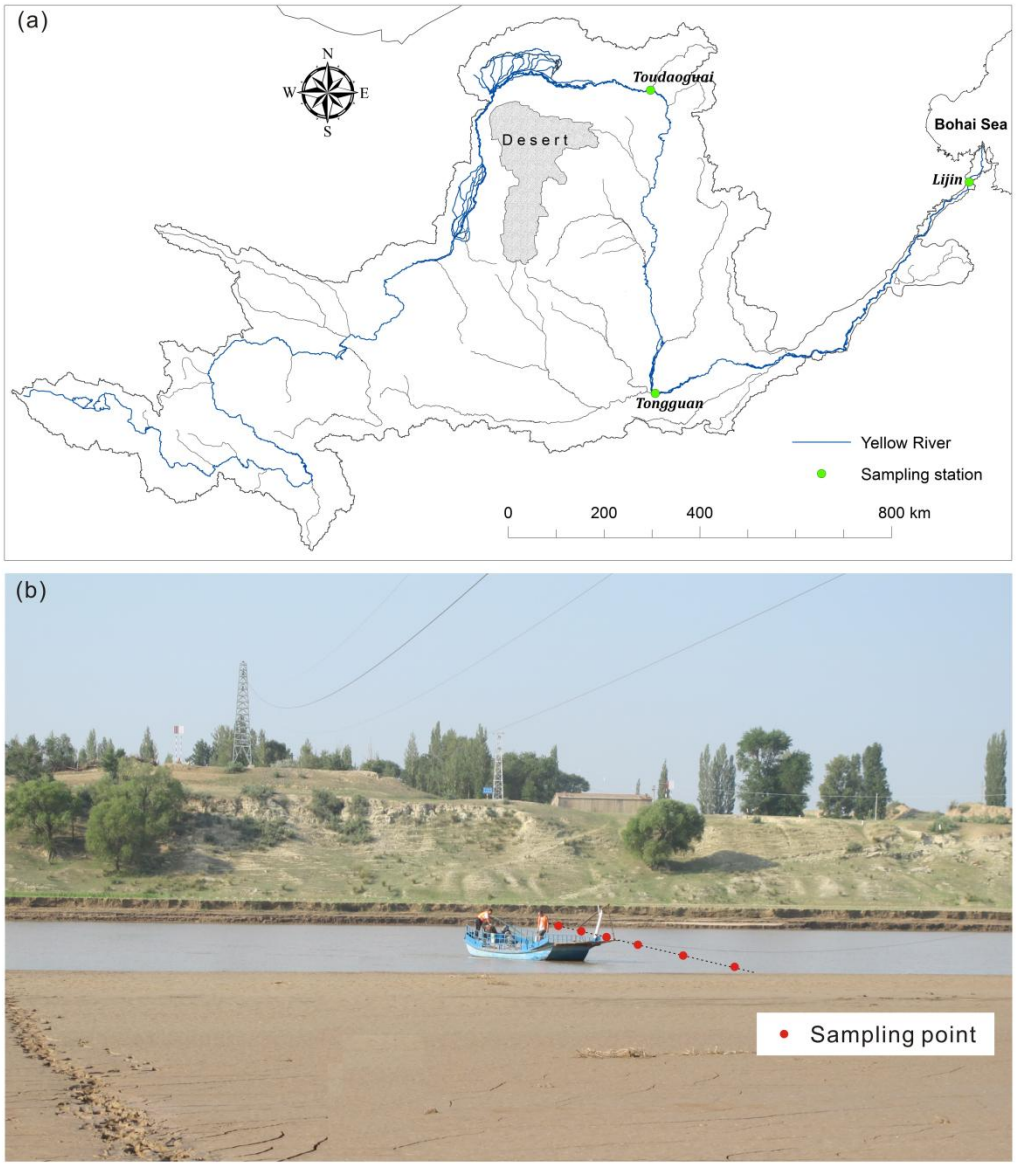

Figure 3.1 Locations of the sampling sites along the Yellow River (a) and sampling strategy (b). Water samples collected from 3-5 sampling points across a cross-section were mixed up to represent the entire cross-sectional profile. Panel b shows a sampling campaign at Toudaoguai station.

3.2.2 Laboratory analyses

The total alkalinity, referring to the buffering capacity of the carbonate system in water, was determined by titration with 0.02 M HCl within 5 h following sampling. Methyl orange was used to indicate the fixed endpoint of the reaction at pH=4.5 (see

a detailed description also in Chapter 4). Given the pH range measured in the Yellow River (~7 to 8.5), the total alkalinity is largely equal to the total dissolved inorganic carbon (DIC) that is the sum of all carbon present in HCO_3^-, CO_3^{2-}, H_2CO_3, and aqueous CO_2 (Stumm and Morgan, 1970). HCO_3^- accounted for >95% of the DIC species. Therefore, the concentration of HCO_3^- was assumed to be equal to that of the titrated total alkalinity in this study.

Samples for determining cation concentrations were first acidified to let the pH<2 by adding concentrated HNO_3 (10 M). Concentrations of the major cations (Ca^{2+}, Mg^{2+}, Na^+, and K^+) and anions (Cl^- and SO_4^{2-}) were determined by an Ion Chromatography (Dionex DX-500, Dionex, U.S.A.) in CNNC Beijing Research Institute of Uranium Geology, China. Dissolved silica was determined by a High Resolution-Inductively Coupled Plasma-Mass Spectrometry (HR-ICP-MS, Element I, Finnigan Mat, Germany), also in CNNC Beijing Research Institute of Uranium Geology, China. The analysis errors (1 σ) of these measurements were below 2% (Zhang, 2008).

One method to assess the data quality is the charge balance (in meq=10^{-3} equivalents per liter) between total dissolved cations ($TZ^+=Na^++K^++2Mg^{2+}+2Ca^{2+}$) and total dissolved anions ($TZ^-=Cl^-+HCO_3^-+2SO_4^{2-}$). The normalized inorganic charge balance (NICB) is defined as $(TZ^+-TZ^-)/(TZ^++TZ^-)$. On average, the NICB for the sampled waters is less than 8%, which is generally within the combined analytical uncertainty for all measurements (Jacobson et al., 2003; Chen et al., 2005).

3.3 Results and discussion

3.3.1 Hydrological characteristics and major ion compositions

River waters showed neutral to alkaline pH values, varying from 7.03 to 8.53 (Table 3.2). The waters were usually more alkaline during summer than winter. The pH range indicated that the riverine total alkalinity was mainly determined by the bicarbonate alkalinity. The water temperatures ranged from 0 (winter) to 29 ℃ (summer) and showed a clear seasonal variation. Compared with Toudaoguai station in the upper river basin, both the water discharge and TSS concentration increased significantly at Tongguan station in the middle reaches, which reflected the great contribution of the reaches Tongguan station controls, mainly the Loess Plateau, to the Yellow River. According to long-term observations, approximately 90% of the sediment of the Yellow River is supplied from the Loess Plateau (Zhao, 1996; Xu, 2003). Downstream of Tongguan, the water discharge reduced gradually along the river course due to water withdrawal for irrigation and industrial uses (see Figures 2.4 and 2.6), resulting in lower measurements at Lijin. In contrast with water discharge, the TSS concentrations did not show significant reductions between Tongguan and Lijin stations, which are largely due to the impacts of reservoir regulation for purposes of sediment flushing, usually during June and July in every year to mitigate sedimentation.

Table 3.2 Hydrological characteristics for the three stations studied during 2011-2012 (Q: water discharge; TSS: total suspended solids).

Item	Toudaoguai (n=46)			Tongguan (n=57)			Lijin (n=58)		
	min	max	mean	min	max	mean	min	max	mean
T (℃)	0	24.7	13.75	0.2	29	14.42	2.8	28.2	18.83
pH	7.62	8.47	8.14	7.03	8.31	7.80	7.07	8.53	8.11
Q (m^3/s)	126	1430	564	290	5260	1094	164	3260	881
TSS (kg/m^3)	0.216	6.57	1.97	0.469	29.6	4.55	0.565	29.5	4.31

Ternary diagrams, also known as Piper diagrams (Piper, 1953), were employed to demonstrate the dominant ions in the sampled riverine waters (Figure 3.2). Specifically, the proportions (in meq) of the major cations (Ca^{2+}, Mg^{2+}, and the sum of Na^{+} and K^{+}) were plotted in Figure 3.2a; and the proportions (in meq) of the major anions (Cl^{-}, SO_4^{2-}, and HCO_3^{-}) were plotted in Figure 3.2b. In addition, the proportion of dissolved Si, HCO_3^{-}, and the sum of Cl^{-} and SO_4^{2-} were plotted in Figure 3.2c to analyze silicate weathering and its contribution to water chemistry.

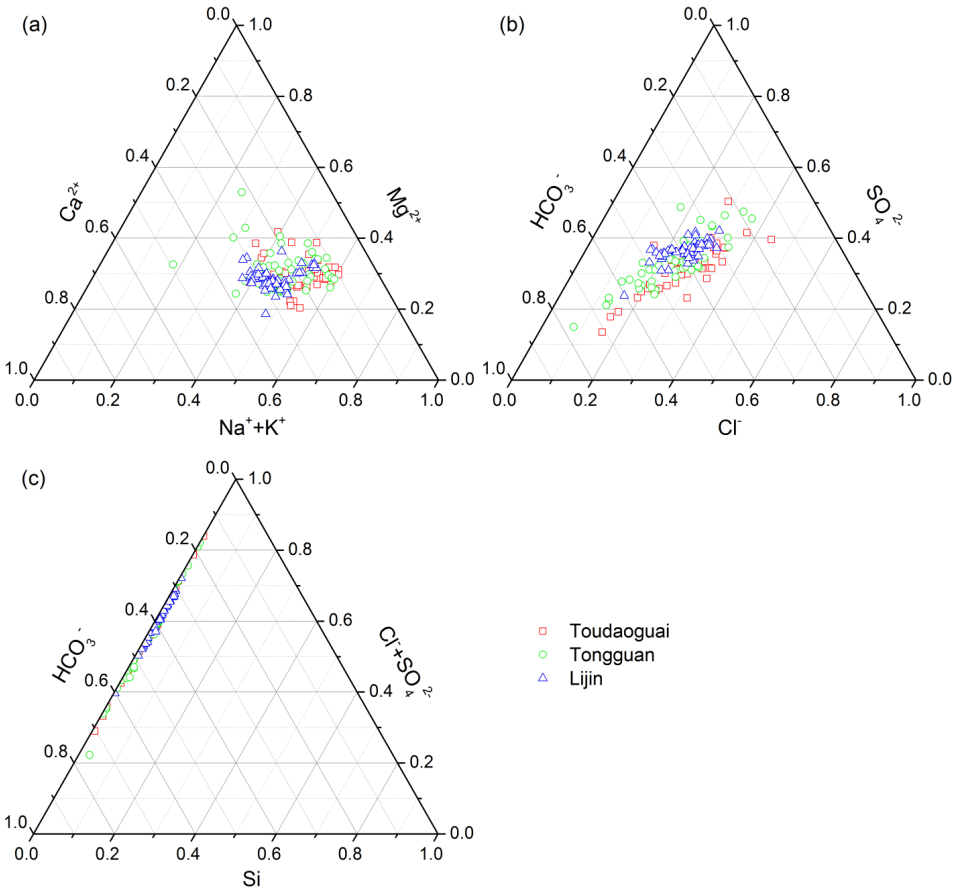

Figure 3.2 Ternary diagrams showing the relevant dominance (in meq) of (a) major cations (Ca^{2+}, Mg^{2+}, Na^{+}+K^{+}), (b) major anions (HCO_3^{-}, SO_4^{2-}, Cl^{-}), and (c) ion comparison (Si, Cl^{-}+SO_4^{2-}, HCO_3^{-}).

With respect to the cations, most of the data points clustered relatively closer towards the Na^{+}+K^{+} apex for all the three stations (Figure 3.2a). Based on molar concentration,

Na^+ is the most abundant cation in stream waters at the three stations, in the order $Na^+ > Mg^{2+} > Ca^{2+} > K^+$. On average, they accounted for 63%, 20%, 15%, and 2%, respectively, of the total cations. That is, Na^+, Mg^{2+}, Ca^{2+}, and K^+ provided 47%, 30%, 22%, and 1% of the total cationic charge, respectively. As for the anions, they scattered more widely in comparison with the cations (Figure 3.2b). Most of the data points clustered closer towards the HCO_3^- apex for the three stations. Similarly, based on molar concentration, HCO_3^- is the most abundant anion, in the order $HCO_3^- > Cl^- > SO_4^{2-}$. They represented about 48%, 31%, and 21%, respectively, of the total anions. That is, HCO_3^-, Cl^-, and SO_4^{2-} provided 39%, 26%, and 35% of the total anionic charge, respectively. From the concentration order, it is clear that the dominant ion pairs are Ca^{2+}-HCO_3^- and Na^+-Cl^- during the study period. These characteristics indicated that water chemistry in the Yellow River was mainly controlled by intense weathering of carbonates and evaporites in the watershed (Zhang et al., 1995a; Chen et al., 2005).

Based on prior research (e.g., Zhang et al., 1990; Zhang et al., 1995a; Chen et al., 2005), the impact of atmospheric deposition of cyclic salts is insignificant and was not taken into account in this study. Therefore, the measured ion concentrations were regarded as the products of chemical weathering of rocks occurring in the drainage basin. Dissolved Si in the Yellow River is mainly supplied from weathering of silicates with clay minerals as by-products (Zhang et al., 1995a). In Figure 3.2c, the dissolved Si represented quite a small proportion of the total ($Si+Cl^-+SO_4^{2-}+HCO_3^-$). On average, HCO_3^- and the sum of Cl^- and SO_4^{2-} accounted for about 47% and 52% of

the total equivalents, respectively. In comparison, the dissolved Si accounted for only 1%. The extremely low percentage for dissolved Si suggested that carbonate weathering is the major source for water chemistry. Silicate weathering is comparatively weak, which is consistent with the lithological composition of the basin. Even so, the effects of silicate weathering on CO_2 uptake could be significant. This will be discussed later.

3.3.2 Spatial and seasonal variations

Transport of dissolved loads by rivers is strongly controlled by the hydrological regime of accompanying water discharge and sediment (Chen et al., 2005; Gao et al., 2009). Weekly based concentrations of the major ions for the Yellow River waters were characterized by different seasonal variations (Figure 3.3). Despite with several exceptionally high values, Cl^-, SO_4^{2-}, Na^+, K^+, and Mg^{2+} at all the three stations remained largely stable throughout the sampling period. The exceptionally high points may be due to anthropogenic pollution, in particular for the two values in December 2011 at Tongguan station, which is located about 150 km downstream of the Xi'an metropolitan area. High pollutant inputs may have elevated the TDS concentrations.

In contrast, there are significant seasonal changes in HCO_3^-, Ca^{2+}, and dissolved Si. HCO_3^- is higher in winter than in summer on average with the peaks occurring in the coldest months. In addition, HCO_3^- is substantially higher at Tonguan than at the upstream Toudaoguai and downstream Lijin stations. This is particularly true for the

winter months. In comparison, the Ca^{2+} concentration showed completely different seasonal changes among the three stations. This cation fluctuated narrowly (0.5-0.8 mmol/l) before increasing to around 1.1 mmol/l in June at Toudaoguai. The Ca^{2+} concentration at Tongguan and Lijin showed an upward trend from December to January before decreasing steadily until the end of the sampling campaign. As a result, the Ca^{2+} concentration at Tongguan and Lijin was significantly higher than that at Toudaoguai (Figure 3.3). Dissolved Si at Toudaoguai station remained low until June 2012, but then increased sharply, similar to the Ca^{2+} concentration. On the contrary, an earlier and more rapid increase (7-fold) of dissolved Si in January was observed at Tongguan station. Finally, the dissolved Si presented a gradual increase at Lijin until June before decreasing. Obviously, the substantial discrepancies in dissolved Si concentration over space and time indicated the differences in silicate weathering rate in the upper, middle, and the lower reaches of the river basin.

To better understand the seasonal variability of major ions at the three stations, monthly averages of the sampling results are tabulated in Table 3.3 (see Appendix), showing considerable differences among different months or stations. Concentrations of the major ions at Tongguan were higher than that at Toudaoguai or at Lijin on average, demonstrating the combined effects of drainage characteristics and human activities. For example, the TDS concentration at Tongguan is 1.2- and 1.1-fold of that at Toudaoguai and Lijin, respectively. Furthermore, the monthly averages are plotted with water discharge (Figure 3.4). For Toudaoguai station, the concentrations of SO_4^{2-}, Ca^{2+}, and Mg^{2+} were relatively low and did not show significant changes

through the period (Figure 3.4a). In contrast, the concentrations of Cl^- and Na^++K^+ varied widely between different months. Likewise, despite far narrower fluctuations, the HCO_3^- concentration also showed a slight seasonal variation. Higher concentrations were observed in the winter months from November to February. Due to the high weight percentage of Cl^-, Na^++K^+, and HCO_3^- in the TDS, the resulting TDS concentration is highly dependent on the seasonal variations of these solutes. Indeed, its seasonal trend is approximately parallel to that of Cl^- and Na^++K^+.

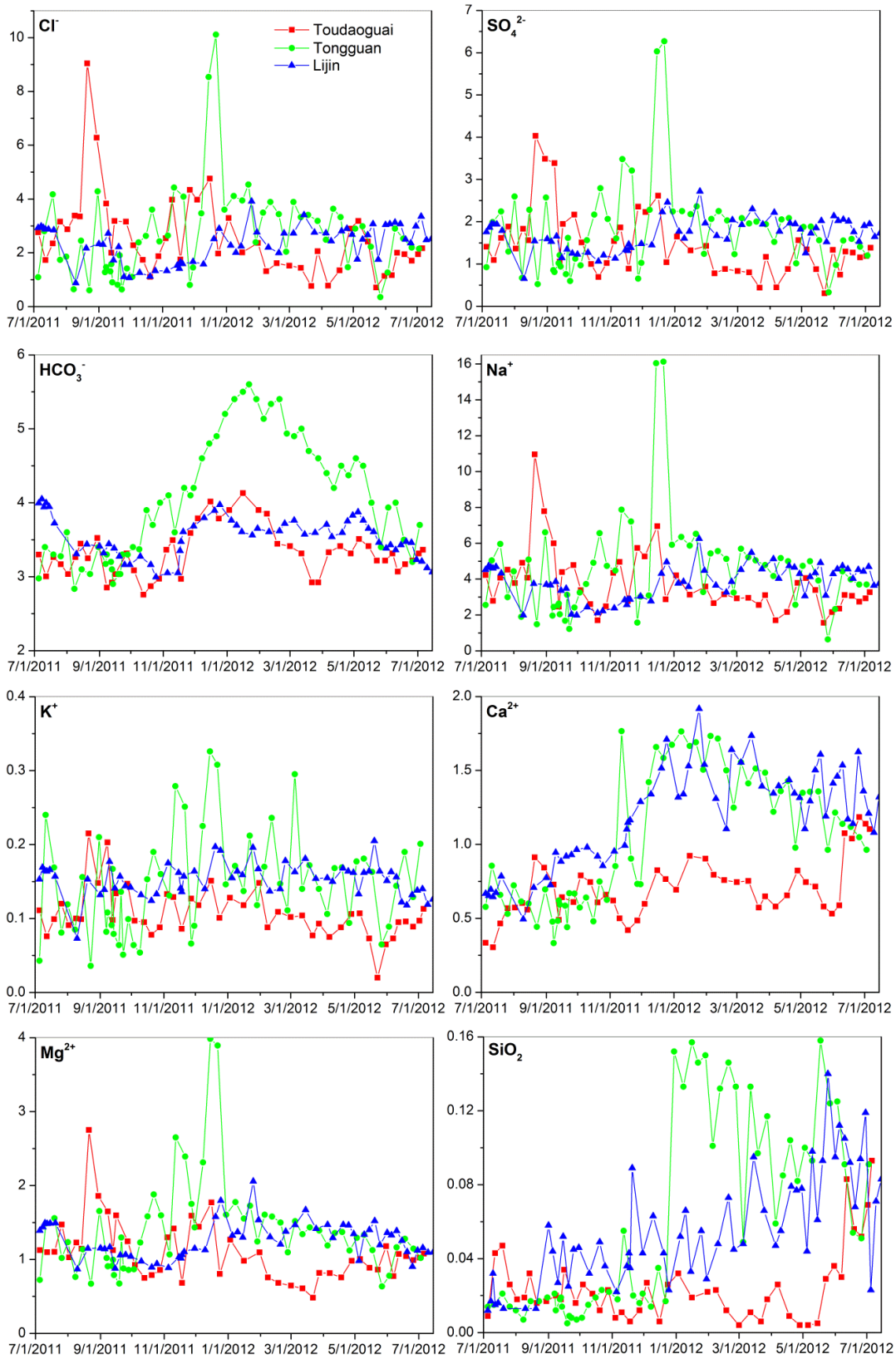

Figure 3.3 Weekly time series of major ions (mmol/l) at the three sampling sites.

Table 3.3 Monthly averages of the water chemistry results at the three sampling stations during 2011-2012.

Month	pH	T	HCO_3^-	SO_4^{2-}	Cl^-	Ca^{2+}	Mg^{2+}	Na^+	K^+	SiO_2	TDS
		℃	mmol/l	mmol/l	mmol/l	mmol/l	mmol/l	mmol/l	mmol/l	mmol/l	mg/l
						Toudaoguai					
July	8.20	23.45	3.24±0.13	1.43±0.29	2.35±0.53	0.65±0.38	1.15±0.16	3.64±0.73	0.10±0.02	0.05±0.03	562.3
August	8.30	22.76	3.31±0.19	2.46±1.22	4.99±2.64	0.70±0.17	1.60±0.72	6.30±3.04	0.13±0.05	0.02±0.01	832
September	8.05	16.93	3.03±0.20	2.14±0.96	3.04±0.76	0.62±0.10	1.40±0.26	4.41±1.47	0.15±0.04	0.02±0.01	665
October	8.22	12.6	2.92±0.14	1.06±0.34	1.75±0.49	0.70±0.08	0.83±0.08	2.55±0.69	0.09±0.01	0.02±0.01	452.9
November	8.18	8.68	3.36±0.27	1.66±0.61	3.15±1.22	0.51±0.08	1.25±0.40	4.46±1.25	0.12±0.02	0.01±0.01	633.9
December	8.01	0.33	3.86±3.86	1.96±1.96	3.57±3.57	0.73±0.73	1.34±1.34	5.03±5.03	0.12±0.12	0.02±0.02	733.6
January	8.18	0.30	3.98±0.13	1.47±0.16	2.56±0.66	0.84±0.13	1.12±0.14	3.64±0.54	0.13±0.02	0.02±0.01	624.9
February	8.22	0.35	3.65±0.29	0.83±0.07	1.46±0.21	0.78±0.03	0.72±0.05	2.91±0.34	0.10±0.01	0.02±0.01	474.2
March	7.86	5.70	3.14±0.26	0.81±0.30	1.45±0.53	0.68±0.09	0.64±0.14	2.89±0.23	0.09±0.01	0.01±0.01	434.1
April	8.11	12.70	3.35±0.05	0.96±0.56	1.68±1.10	0.69±0.12	0.85±0.12	2.55±1.09	0.09±0.02	0.01±0.01	467.2
May	8.14	19.28	3.34±0.15	0.97±0.49	1.86±1.14	0.64±0.10	0.98±0.14	2.79±1.13	0.07±0.04	0.02±0.02	479.7
June	8.17	21.18	3.19±0.10	1.12±0.25	1.71±0.38	0.97±0.26	0.97±0.14	2.82±0.35	0.09±0.01	0.06±0.02	496.2
						Tongguan					
July	8.08	25.6	3.33±0.26	1.53±0.56	2.39±1.17	0.72±0.19	1.16±0.35	4.05±1.42	0.15±0.08	0.03±0.03	592
August	7.99	24.74	3.19±0.30	1.73±1.04	1.97±1.52	0.62±0.11	1.09±0.39	3.90±2.17	0.12±0.07	0.01±0.01	576.7
September	7.88	17.87	3.15±0.14	0.99±0.30	1.25±0.40	0.54±0.11	0.93±0.17	2.23±0.57	0.1±0.040	0.01±0.01	431.5
October	7.77	15.22	3.67±0.28	1.91±0.68	2.43±0.89	0.61±0.10	1.43±0.39	4.64±1.28	0.12±0.06	0.02±0.01	665.2
November	7.49	10.02	4.04±0.25	2.00±1.28	2.68±1.58	1.00±0.44	1.86±0.66	4.83±2.69	0.16±0.10	0.03±0.02	736.6
December	7.56	2.58	4.88±0.25	4.21±2.25	6.43±3.40	1.58±0.12	2.95±1.18	10.29±6.79	0.25±0.08	0.06±0.07	1313.3
January	7.82	0.90	5.48±0.10	2.01±0.52	3.75±0.94	1.66±0.11	1.57±0.24	5.51±1.51	0.16±0.04	0.15±0.01	905.3
February	7.75	1.38	5.20±0.21	1.89±0.45	3.21±0.81	1.55±0.23	1.45±0.24	4.85±1.08	0.17±0.05	0.13±0.02	835.4
March	7.90	6.58	4.80±0.18	2.00±0.06	3.45±0.31	1.49±0.06	1.42±0.07	5.19±0.38	0.19±0.07	0.10±0.04	833
April	7.96	14.45	4.37±0.12	1.67±0.51	2.73±0.97	1.25±0.20	1.26±0.12	4.23±1.19	0.13±0.04	0.08±0.02	710.8
May	7.58	21.20	4.13±0.55	1.41±0.74	2.12±1.23	1.26±0.20	1.10±0.32	3.58±2.01	0.15±0.05	0.12±0.03	634
June	7.64	23.75	3.66±0.38	1.38±0.28	2.22±0.70	1.13±0.07	1.09±0.22	3.61±0.91	0.14±0.04	0.08±0.03	599.3
						Lijin					
July	7.64	26.82	3.67±0.42	1.84±0.11	2.87±0.26	0.86±0.27	1.35±0.18	4.40±0.42	0.15±0.02	0.03±0.03	678.1
August	7.31	26.85	3.38±0.09	1.10±0.63	1.52±0.92	0.60±0.15	1.01±0.20	2.87±1.24	0.11±0.06	0.01±0.01	484.9
September	8.21	23.47	3.31±0.11	1.39±0.20	1.93±0.64	0.88±0.09	1.07±0.10	3.15±0.80	0.15±0.02	0.04±0.01	545.6
October	8.06	20.23	3.15±0.14	1.18±0.11	1.24±0.10	0.92±0.06	0.94±0.04	2.26±0.16	0.13±0.01	0.04±0.01	467.7
November	8.41	13.35	3.37±0.27	1.35±0.13	1.53±0.14	1.11±0.12	1.04±0.09	2.76±0.24	0.16±0.01	0.05±0.02	531.4
December	8.46	7.43	3.89±0.09	2.05±0.53	2.33±0.68	1.52±0.19	1.50±0.34	4.02±1.12	0.18±0.03	0.04±0.02	715.1
January	8.31	3.42	3.66±0.08	1.97±0.44	2.64±0.76	1.53±0.24	1.52±0.32	4.39±1.10	0.17±0.02	0.05±0.02	713.5
February	8.36	4.20	3.65±0.06	1.76±0.24	2.31±0.38	1.35±0.27	1.30±0.09	3.59±0.30	0.15±0.02	0.06±0.02	650.9
March	8.07	9.07	3.64±0.10	2.06±0.21	2.96±0.38	1.56±0.17	1.52±0.13	4.86±0.54	0.17±0.01	0.07±0.02	746.1
April	8.15	17.84	3.69±0.12	1.95±0.17	2.71±0.18	1.37±0.05	1.41±0.08	4.57±0.42	0.16±0.01	0.07±0.02	711.8
May	8.33	25.74	3.67±0.16	1.68±0.30	2.35±0.58	1.34±0.21	1.29±0.21	3.91±0.81	0.17±0.03	0.09±0.04	654.4
June	8.40	27.70	3.40±0.08	1.92±0.21	2.88±0.31	1.39±0.18	1.21±0.18	4.45±0.23	0.14±0.02	0.10±0.02	691.5

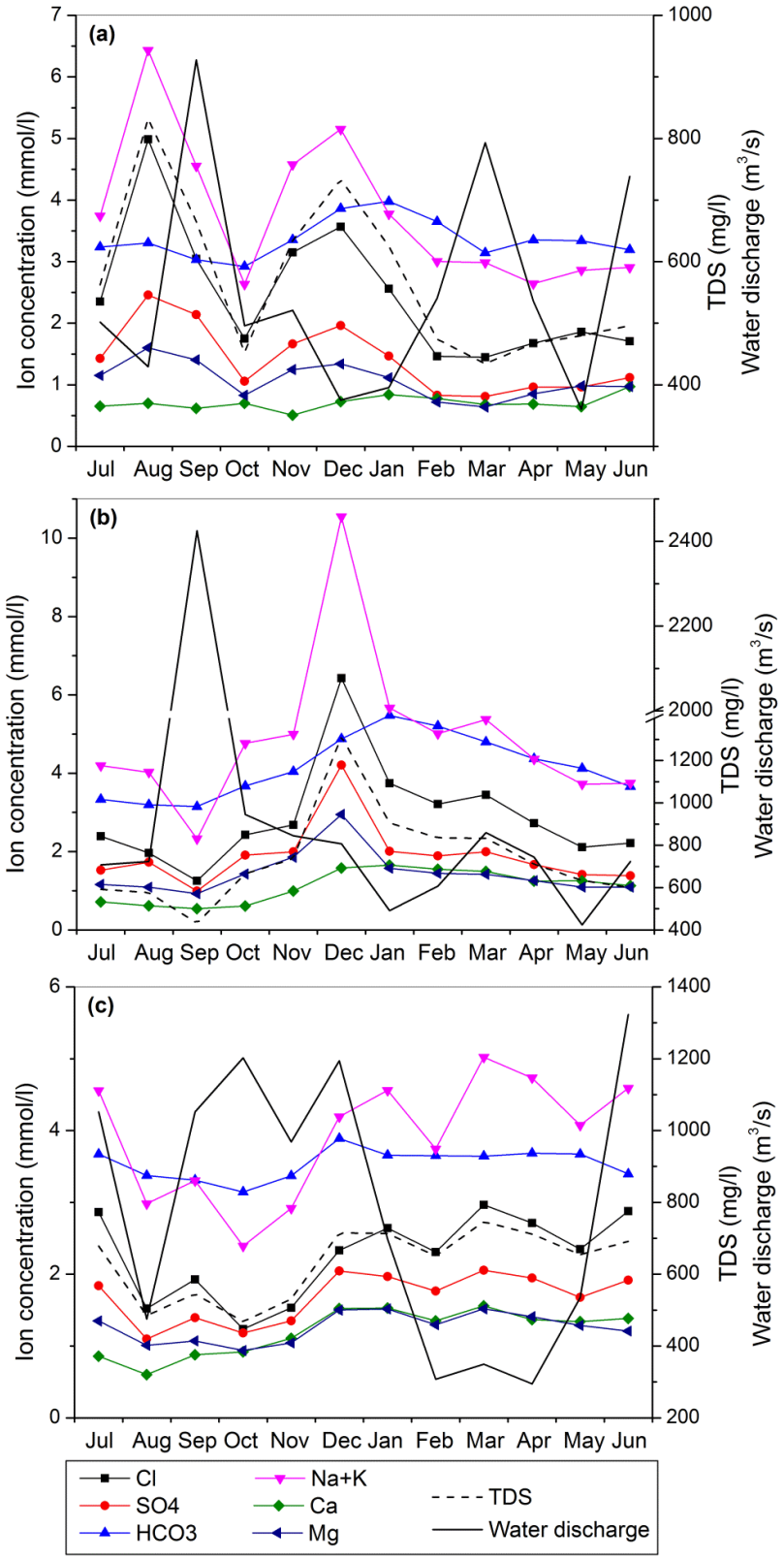

Figure 3.4 Seasonal variations in concentration of major ions and water discharge at (a) Toudaoguai, (b) Tongguan, and (c) Lijin. Data from Table 3.3.

Seasonal variations at Tongguan station were different from Toudaoguai (Figure 3.4b). Unlike the seasonal pattern of water discharge with the highest value recorded in September, the concentrations of all ions reached peaks in December before decreasing until the onset of the wet season starting from June and ending in September. Except for Ca^{2+}, which remained largely stable during the study period, the other ions presented strong seasonal changes, in particular the Cl^- and the sum of Na^+ and K^+. On the basis of monthly average, the maximum over the minimum concentration ratios of Cl^- and Na^++K^+ were 5.1 and 4.5, respectively. Because all the ions showed same seasonal patterns, the TDS concentration peaked in December; and the lowest TDS concentration occurred in September. As for the lowermost Lijin station, except the sum of Na^+ and K^+ showing a relatively strong seasonal variation ranging from 2.4 mmol/l in October to around 5 mmol/l in March, the other ions showed slight seasonal fluctuations. However, it is important to emphasize that all ion concentrations showed gradual increasing trends from August 2011 onwards. The highest concentrations were usually measured in June and July, coinciding with the sediment flushing period (Figure 3.4c). In this period, huge amounts of water stored in the reservoir cascades during the dry season were released downstream, usually starting from mid-June, to generate man-made high flows. As a result, the water discharge increased sharply and was much higher than the natural floods that usually occur in September (Figure 3.4c). In addition, due to limited runoff supply in the lower Yellow River reaches, the TDS concentration at Lijin decreased slightly in comparison with that at Tongguan.

Overall, the seasonal patterns of different ion concentrations are diverse. Spatially, the concentration changes are also different among the three stations. These differences in ion concentrations probably revealed the susceptibility of chemical weathering of various rocks, and the influence of its driving factors, such as precipitation and temperature, on controlling chemical reaction rates. Furthermore, hydrological processes of water discharge are also important for solute delivery in river waters, and thus should be taken into account.

3.3.3 Relationships between major ions and water discharge

Using the accompanying measurements of water discharge and TSS concentration at the three sampling stations, the relationships of all dissolved constituents with water discharge and TSS were investigated in an attempt to elucidate the coupling effects. Usually, the standard rating relationship between dissolved species and water discharge can be expressed as a power equation (Walling and Webb, 1986; Jarvie et al., 1997; Zhang et al., 2007):

$$C=aQ^b \quad \text{(Equation 3.2)}$$

where, C is the concentration of major ions or TDS (mg/l), Q is the corresponding water discharge (m^3/s), a is the regression constant, and b is the regression exponent to be determined. In addition to water discharge, the empirical relationship was also applied to total suspended solids (TSS, in kg/m^3). The formula was expressed as:

$$C=aTSS^b \quad \text{(Equation 3.3)}$$

The regression results of the power relationships between the concentrations of dissolved ions as well as TDS and water discharge as well as TSS are summarized in

Table 3.4. In common with many studies, these results demonstrated a rating relationship in which most of the dissolved species, except Si at Toudaoguai station, showed a negative relationship with water discharge changes. This is particularly true for Ca^{2+} and Si at Tongguan, and Na^{+} and Mg^{2+} at Lijin. In addition, the Cl^{-} had a relatively steep slope at all three stations. When related to the TSS concentration, the dissolved constituents showed much more complex relationships (Table 3.4). While all the dissolved species showed negative relationships with TSS at Tongguan (Figure 3.5), some of them were positively correlated with TSS delivery, such as Ca^{2+}, Mg^{2+}, and Si at Toudaoguai, and Cl^{-}, SO_4^{2-}, HCO_3^{-}, and Na^{+} at Lijin.

Table 3.4 Exponent b in power relationships $C=aQ^b$ between major ion concentrations (C, in mg/l) and water discharge (Q, in m^3/s), and $C=aTSS^b$ between major ion concentrations and total suspended solids (TSS, in kg/m^3).

Item	Toudaoguai		Tongguan		Lijin	
	Q	TSS	Q	TSS	Q	TSS
Cl^{-}	-0.262	-0.073	-0.401	-0.254	-0.065	0.033
SO_4^{2-}	-0.127	-0.006	-0.268	-0.16	-0.043	0.009
HCO_3^{-}	-0.058	-0.048	-0.162	-0.09	-0.028	0.001
Na^{+}	-0.162	-0.057	-0.335	-0.194	-0.065	0.017
K^{+}	-0.029	-0.046	-0.265	-0.179	-0.039	-0.015
Ca^{+}	-0.007	0.029	-0.407	-0.25	-0.036	-0.077
Mg^{2+}	-0.057	0.041	-0.168	-0.095	-0.069	-0.012
SiO_2	0.439	0.273	-0.979	-0.59	-0.034	-0.056
TDS	-0.106	-0.031	-0.228	-0.11	-0.041	0.004

Differences in the resulting exponents revealed the differing responses of the studied dissolved species to water discharge and TSS during the delivery processes (see Figure 3.5 for example). The form of the rating relationship for individual ion parameters indicated the sources of runoff and the location and solubility of the components (Edwards, 1973; Jarvie et al., 1997).

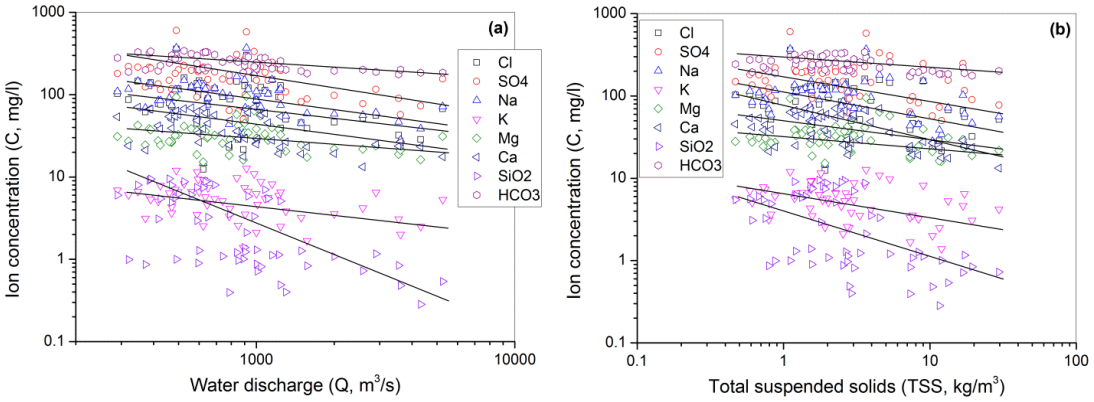

Figure 3.5 Plots of the relationships between (a) concentrations of major ions and water discharge (Q) and (b) between concentrations of major ions and total suspended solids (TSS). Only measurements at Tongguan station were presented as an example.

TDS showed negative relationships with both water discharge and TSS at Toudaoguai and Tongguan (see Figure 3.6 for example). In general, most major ion concentrations are higher under low flow than storm flow conditions. This trend reflects a dilution effect by surface runoff during the flooding season (Gao et al., 2009). In contrast, while correlated negatively with water discharge, the TDS at Lijin showed a slight positive relationship with TSS. These strong contrasts among the three stations may largely result from the impacts of human activities. Due to flow regulation by upstream reservoir cascades, the seasonal differences of the TSS concentration at Lijin were significantly altered, although the annual mean value only decreased slightly compared with Tongguan (Table 3.2). High TSS concentrations occurred in the low flow period, coinciding with the high TDS concentration episodes. As a result, the TDS concentrations showed a weak positive relationship with increasing TSS concentrations.

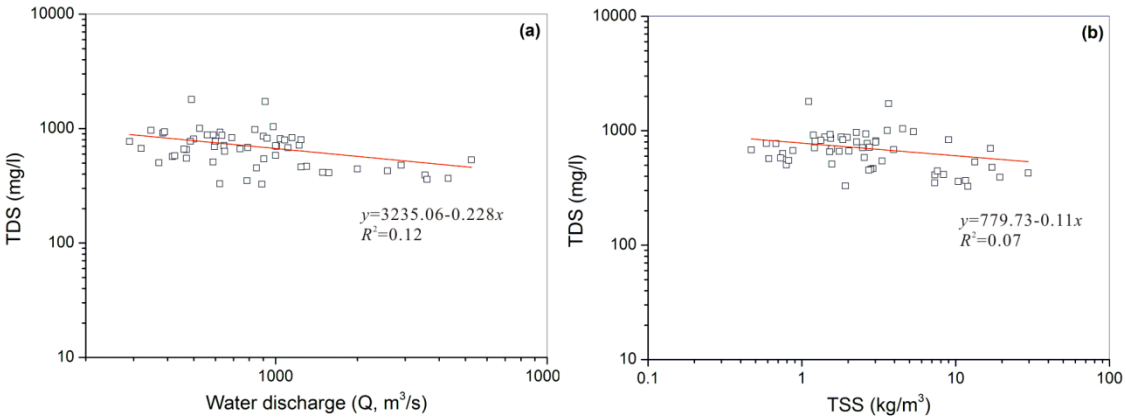

Figure 3.6 Plots of the relationships between (a) total dissolved solids (TDS) and water discharge (Q) and (b) TDS and total suspended solids (TSS). Only measurements at Tongguan station are presented as an example.

Figure 3.7 showed that the TDS flux (TDS concentration×water discharge, in kg/s) was positively correlated with the TSS flux (TSS concentration×water discharge, in kg/s). From the figure, it can be seen that the TSS flux increased much faster than the TDS flux (~2.3 times faster). As TSS is the product of physical erosion and TDS is controlled by chemical weathering of rocks, higher TSS flux relative to the TDS flux is consistent with the extremely strong soil erosion intensity within the drainage basin (Zhao, 1996; Wei et al., 2006). High physical erosion due to highly erodible loess deposits widely occurs in the drainage basin. For example, according to the estimates made in the 1980s, while the TSS load is about 1.1×10^{12} kg/yr, the corresponding TDS flux is only 20×10^{9} kg/yr on average, with the former being 50-100 times the latter (Zhang et al., 1995a). Also, the measurements at Tongguan were scattered more widely than that at the other two stations away from the regression line, which is likely due to the complexity in the Loess Plateau in terms of physical erosion and chemical weathering.

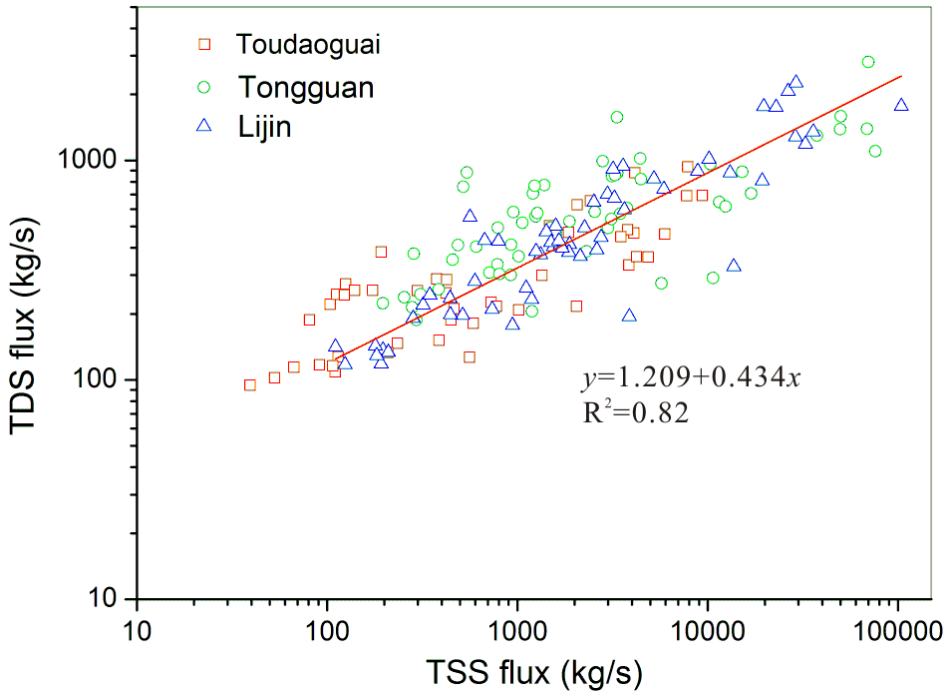

Figure 3.7 Relationship between TSS flux and TDS flux. The regression line was fitted based on all the measurements at the three sampling sites.

3.3.4 Sources of major ions

Several attempts have been made previously to classify rivers in terms of water chemistry to determine which of a number of environmental factors that affect river water chemistry characteristics are more important (Meybeck, 1987; Berner, 1995; Roy et al., 1999; Berner and Berner, 2012). Based on concentration changes of the major dissolved species that characterize the end-members of the world's surface water chemistry, Gibbs (1970) proposed a diagrammatic representation of the mechanisms responsible for controlling the chemical compositions of various waters on the earth surface (Figure 3.8). According to the classification, the major natural mechanisms controlling world surface-water chemistry can be defined as (1) atmospheric precipitation, both composition and amount; (2) chemical weathering of

rocks; and (3) evaporation and fractional crystallization. Rivers are dominated by each of these mechanisms, depending on drainage characteristics.

While atmospheric precipitation-controlled rivers are usually located in areas of high rainfall and low relief where the rate of supply of dissolved solutes to the rivers is very low, rock weathering-dominated rivers are in areas of intermediate rainfall and runoff, and evaporation-crystallization-controlled saline rivers are in arid regions (Berner and Berner, 2012). However, Gibbs's classification has proved to be controversial by many subsequent studies. Feth (1971) pointed out that the evaporation-crystallization process is not the major mechanism for the composition and concentration for Gibbs's two examples. Furthermore, based on sampling data in the Amazon River basin, Stallard (1980) concluded that high Na/Ca and high TDS rivers are primarily the result of chemical weathering of rock salt rather than the evaporative evolution of typical rock weathering river water (see also Berner and Berner, 2012). Also, for several Amazon tributaries which are rainfall-controlled rivers according to the Gibbs diagram, Stallard and Edmond (1983) found that sea salt made only a very small change to the river composition.

Despite the controversies, it is useful for identifying the sources of chemical compositions for rivers under the cluster of rock weathering with intermediate TDS (Zhang, 2008). With respect to the Yellow River, the TDS concentration ranged between 327 and 1800 mg/l, falling into the cluster of rock weathering as illustrated by plotting the weight ratio $Cl^-/(Cl^-+HCO_3^-)$ on the *x*-axis and the variations in TDS

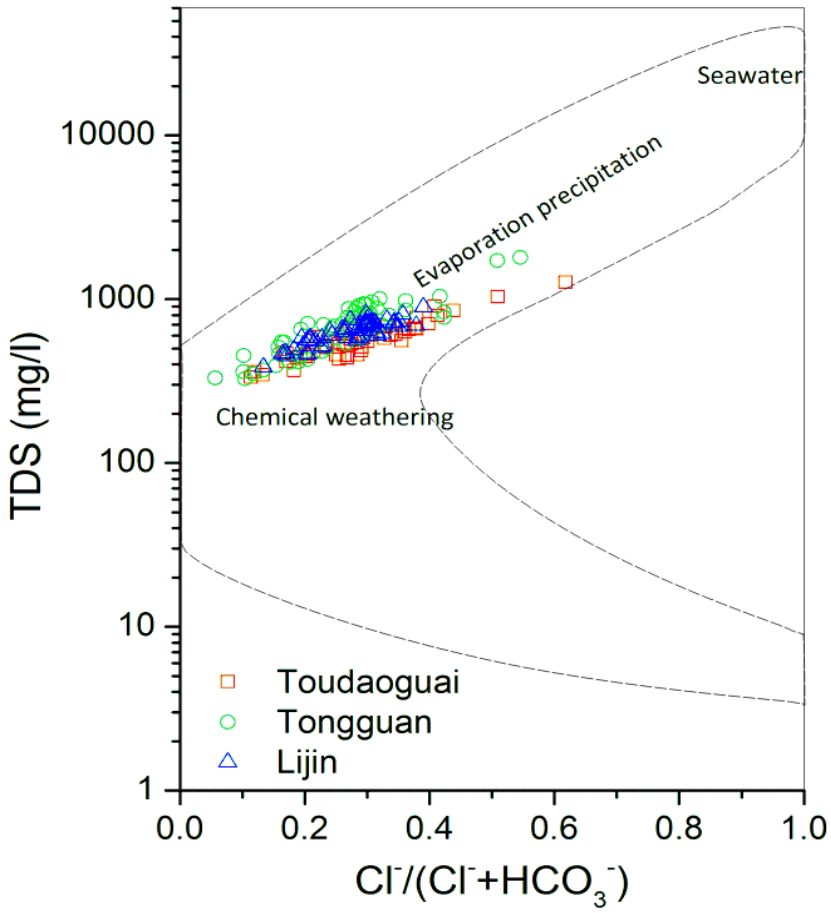

Figure 3.8 A Gibbs plot showing the variation of the weight ratio of Cl/(Cl+HCO_3) as a function of the total dissolved solids (TDS). The dashed line represents the range of the global waters (Gibbs, 1970).

on the *y*-axis (Figure 3.8). Contributions of evaporation precipitation also contributed to the river water chemistry, in particular for Toudaoguai and Tongguan stations. As the data points were situated far away from the seawater input end-member, it appears that the effects of cyclic salt input on the Yellow water chemistry are limited as indicated earlier. In addition, the weight ratios for Toudaoguai and Tongguan stations were more widely ranged than for Lijin station, in particular in the direction where the $Cl^-/(Cl^-+HCO_3^-)$ ratios were higher than 0.4. Apparently, this suggested the contribution of evaporite weathering (Gibbs, 1970; Berner and Berner, 2012).

Evaporite minerals in the Yellow River basin are mainly distributed in its upper and middle reaches under semi-arid climate (Zhang et al., 1995a; Chen et al., 2005). Furthermore, extensive irrigation activities in these regions in recent decades may have enhanced the natural evaporation/crystallization processes. As the irrigation water would selectively precipitate Ca- and Mg- carbonates, resulting in return water to the river being more concentrated in other ions (Chen et al., 2005).

As demonstrated in Figure 3.8, chemical weathering of rocks within the watershed is the primary mechanism controlling the water chemistry of the Yellow River. However, knowing that is far from enough for understanding the influences of different rock types (i.e., carbonates, silicates, and evaporites) on the delivery of dissolved species. More importantly, the associated effects on atmospheric CO_2 balance can be quantified only after the contributions from weathering of the three rocks are explicitly determined. Stoichiometric analysis would provide some qualitative information for tracing sources of major dissolved species in rock weathering-dominated river waters (Stallard and Edmond, 1983; Baron, 1990; Zhang et al., 1995b; Zhang et al., 2007; Gao et al., 2009).

Plots of major ions are presented in Figure 3.9. The sum of Na^+ and K^+ showed a linear relationship with Cl^- parallel to the 1:1 trend line (Figure 3.9a), indicating that a considerable amount of dissolved ions came from evaporite weathering (halite). This is consistent with the widespread presence of evaporite outcrops in the river basin (Chen et al., 2005). It should be pointed out that, except for one data point, all the

others are located above the 1:1 trend line indicative of a pure evaporite source. This indicated additional sources of Na^+ and K^+ from weathering of silicates, such as Na- and K-aluminosilicates, or from anthropogenic pollution inputs besides evaporite dissolution. The plot of SO_4^{2-} versus (Ca^{2+}+Mg^{2+}) in Figure 3.9b indicates the control of evaporite sulfate dissolution (i.e., gypsum/anhydrite) and sulfide weathering on the concentrations of Ca^{2+} and Mg^{2+} (Zhang, 2008). Similarly, most data points are above the 1:1 trend line, reflecting the involvement of carbonic acid during the weathering processes of carbonates and silicates. Therefore, it is evident that atmospheric CO_2 drawdown occurred during the chemical weathering processes in the drainage basin. In addition, the data points at Toudaoguai and Tongguan stations were more scattered than at Lijin station. Because the former two stations are located much closer to the weathering sites (the Loess Plateau), distribution of the data points thus directly indicated the differences of weathering products. In contrast, as Lijin station is near the river mouth, the weathering products are subject to various in-channel biogeochemical processes in the lower Yellow River before being measured.

As for the plot of HCO_3^- against the sum of Ca^{2+} and Mg^{2+}, while the trend line deviated significantly from the 1:1 trend line, most of the data points were scattered near the 1:1 trend line (Figure 3.9c), which is characteristic of carbonate dissolution in water chemistry. Some data points for Toudaoguai and Tongguan are below the 1:1 trend line, demonstrating the importance of weathering of Na- and K-aluminosilicates in providing the extra HCO_3^-. By contrast, almost all the data points for Lijin measurements are above the 1:1 trend line. The extra Ca^{2+} and Mg^{2+} may come from

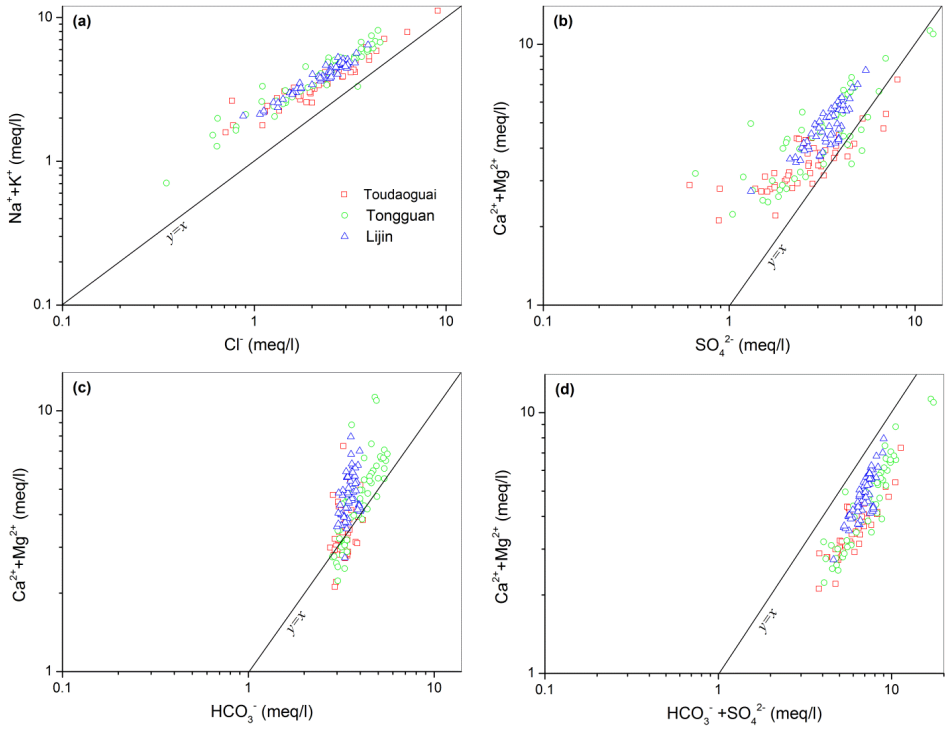

Figure 3.9 Concentration comparisons of (a) Cl^- and Na^++K^+, (b) SO_4^{2-} and Ca^{2+}+Mg^{2+}, (c) HCO_3^- and Ca^{2+}+Mg^{2+}, and (d) HCO_3^-+SO_4^{2-} and Ca^{2+}+Mg^{2+} at the three stations. The solid line represents the 1:1 trend line.

dissolution of sulfates, such as $CaSO_4$. Furthermore, the riverine HCO_3^- might have been transformed into aqueous CO_2 and released during the delivery processes due to anthropogenic input of acid. Both are possible in the Yellow River basin due to reported distribution of gypsum and intense population density (Zhang et al., 1995a; Chen et al., 2005). The plot of (HCO_3^-+SO_4^{2-}) versus (Ca^{2+}+Mg^{2+}) is different from the above three plots, all the data points are far below the 1:1 trend line with roughly a parallel trend (Figure 3.9d). Relatively, the measurements at Lijin are closer to the 1:1 trend line, in particular for these with higher (HCO_3^-+SO_4^{2-}) concentrations. The phenomenon of data much closer to the 1:1 trend line when the (HCO_3^-+SO_4^{2-}) concentration is higher also hold true for the other two stations (Figure 3.9d). Higher concentration of (HCO_3^-+SO_4^{2-}) relative to (Ca^{2+}+Mg^{2+}) indicated that there are

additional sources of HCO_3^- and SO_4^{2-} in addition to carbonates. That is, weathering of Na- and K-aluminosilicates likely played an important role in controlling the chemical compositions of the Yellow River waters given the deviation from the 1:1 trend line.

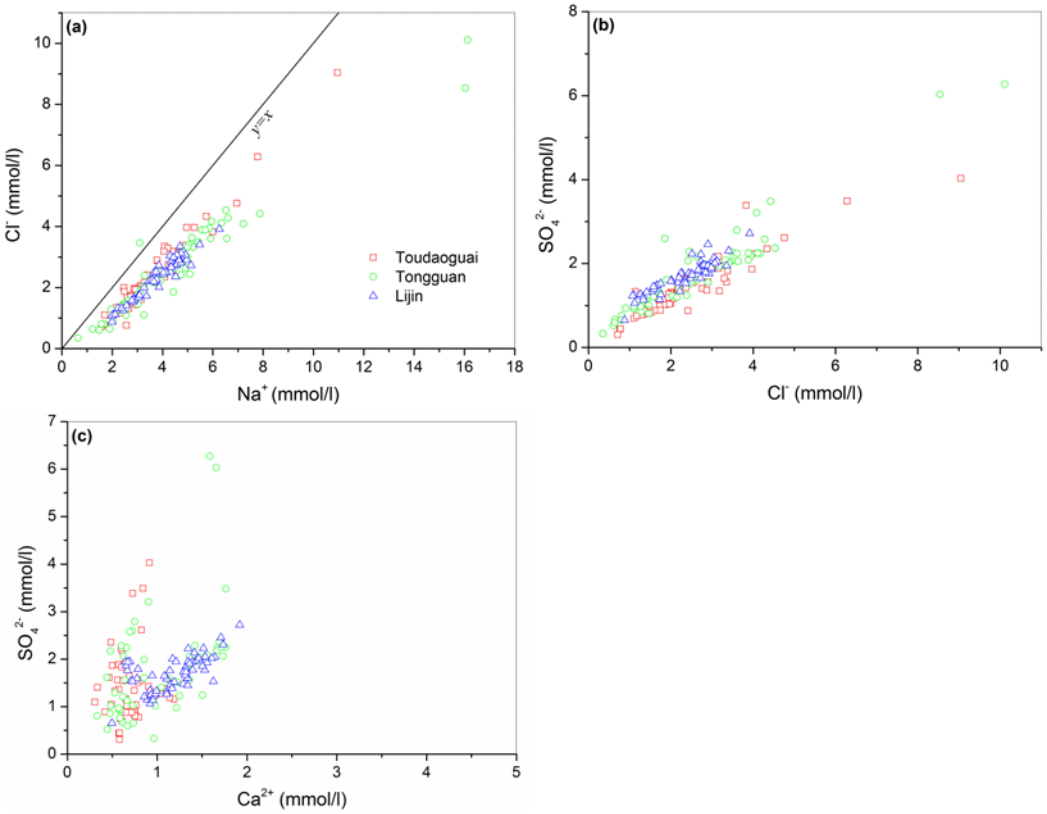

Figure 3.10 Comparisons between (a) Na^+ and Cl^-, (b) Cl^- and SO_4^{2-}, and (c) Ca^{2+} and SO_4^{2-}. Higher Na^+ relative to Cl^- highlighted weathering of Na-silicates, in addition to the contribution of evaporite dissolution.

Considering the widespread outcrop of evaporites in the Yellow River basin (Chen et al., 2005), concentrations of Cl^- and Na^+ are plotted to differentiate the contribution from halite (NaCl) to the total water chemistry (Figure 3.10a). As can be seen, all the data points, except one measured at Tongguan, are below the 1:1 trend line. In particular, the Na^+ concentration is linearly correlated with the Cl^- concentration, which suggests a rock weathering source for Cl^- and indicates that the atmospheric

input contribution is minor. The mean Na/Cl molar ratio at Toudaoguai, Tongguan, and Lijin is 1.59, 1.75, and 1.67, respectively. These ratios are significantly higher than the Na/Cl molar ratio of 0.86 for seawater (Turner et al., 2010; Berner and Berner, 2012). This demonstrated that weathering of Na-feldspars or Na-silicate clays in sandstone, shales, and other detrital sediment rocks is a significant source for the extra Na^+ in excess of Cl^-. From Figure 3.10b, a linear relationship between Cl^- and SO_4^{2-} can be clearly found for data points of all the three stations, suggestting the contribution of gypsum/anhydrite dissolution. Because gypsum and anhydrite are generally related to NaCl in its source formation although they do not necessarily form in proportion (Huh et al., 1998), the linear relationship observed here indicated that dissolution of gypsum occurs in the drainage basin, as also demonstrated in Figure 3.10c.

Figure 3.11 shows the comparison of Na normalized molar ratios between Ca^{2+} and HCO_3^- and between Ca^{2+} and Mg^{2+}. These correlations suggest the mixture of the three major rock types. Specifically, most of the data points are located between the end-members of silicates and evaporites, which have lower Ca/Na ratios (Figure 3.11a). With respect to the Na normalized Ca-Mg relationship, the data points are situated much closer to the end-member of the silicate reservoir (Figure 3.11b), stressing the importance of silicate weathering in supplying Ca and Mg ions. Overall, the Na normalized molar ratios are in a narrow variation range. For example, the Ca/Na ranged from 0.1 to 0.5, Mg/Na from 0.2 to 0.5, and HCO_3/Na from 0.6 to 2.

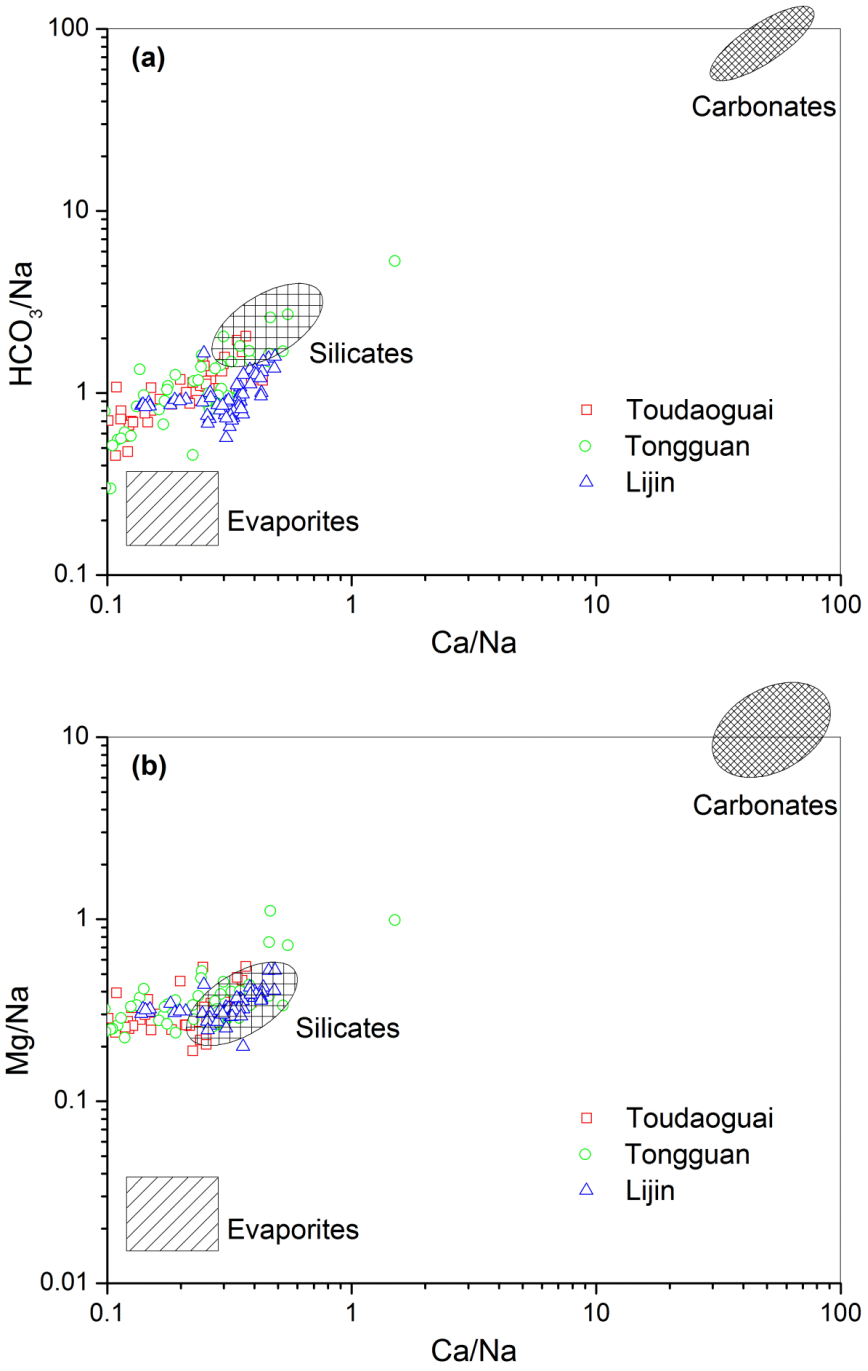

Figure 3.11 Mixing diagrams using Na-normalized molar ratios at the three stations: (a) HCO_3/Na vs Ca/Na, (b) Mg/Na vs Ca/Na. End member reservoirs were adopted from Gaillardet et al (1999), which were estimated by using data on small rivers draining homogenous lithology, such as carbonates, silicates, and evaporites. The rainwater (marine) end-member was not represented due to its very different chemical signatures.

3.3.5 Chemical weathering rate and atmospheric CO_2 consumption

Because carbonate dissolution is not a geological long-term carbon sink as stated above, accurate understanding of silicate to carbonate weathering proportion is essential when discussing CO_2 as an important driving force for climate change (Lenton and Britton, 2006; Battin et al., 2009). For example, climate models usually use a silicate to carbonate proportion for estimating the potential long-term CO_2 drawdown resulted from chemical weathering (Munhoven, 2002; Lerman et al., 2007; Hartmann et al., 2009).

Generally, there are two approaches in quantitatively analyzing the sources of riverine solutes by calculating mass balance, from which the consumed atmospheric CO_2 could be estimated. One is the direct or forward method, which contains a series of mass balance equations that relate the assumed ratios of dissolved concentrations derived from the weathering products of carbonates, silicates, and evaporites as well as atmospheric deposition input (Garrels and Mackenzie, 1967; Berner et al., 1983; Meybeck, 1987; Amiotte-Suchet and Probst, 1993; Benedetti et al., 2003; Moon et al., 2007; Gao et al., 2009; Hartmann et al., 2009; Berner and Berner, 2012). The other is the indirect or inverse method, which uses water chemistry data to recalculate rock weathering products under the assumption that weathering products are characterized by specific geochemical end-members representing different lithologies (Allègre and Lewin, 1989; Negrel et al., 1993; Gaillardet et al., 1999; Roy et al., 1999; Wu et al., 2005; Moon et al., 2007; Hartmann et al., 2009). One disadvantage of the inverse method is that it does not allow for a spatial resolution of CO_2 consumption beyond the resolution of the catchment areas of applied river sampling locations (Hartmann et

al., 2009). The forward method was employed in this study to decipher the relative contributions of carbonate, silicate, and evaporite weathering to the Yellow River waters.

The forward method is a simple budget to allocate the dissolved load (in molar concentration) to the corresponding source minerals (Meybeck, 1987). Soluble elements in rivers are a mixture of atmospheric input and weathering of silicate, carbonate, sulfide and evaporite minerals. For any element X in the dissolved load, its mass balance equation can be expressed as follows:

$$[X]_{riv}=[X]_{cyc}+[X]_{eva}+[X]_{carb}+[X]_{sil}+[X]_{sul}+[X]_{anth} \quad \text{(Equation 3.4)}$$

where, the subscript riv=river; cyc=cyclic source; eva=evaporite source; carb=carbonate source; sil=silicate sources; sul=sulfide source (only for SO_4^{2-}); anth=anthropogenic source. The brace [] denotes molar concentration.

To quantify the major ion fluxes supplied by chemical weathering of rocks, corrections should be made to exclude the contributions made by atmospheric inputs (cyclic inputs) and anthropogenic influences. For sites where evaporite dissolution is not strong, the input of chloride (Cl) concentration through precipitation is generally used as a parameter for evaluating atmospheric contribution (Ryu et al., 2008; Gao et al., 2009; Berner and Berner, 2012). As far as the Yellow River basin is concerned, contribution from cyclic salts into dissolved solids in river waters is small (Chen et al., 2005). There are at least three reasons for this argument. Firstly, most of the Yellow River basin (>98%) is situated in inland China characteristic of arid-semiarid climate with precipitation significantly lower than evaporation (400 mm/yr vs. 1100 mm/yr).

Secondly, although the basin is in the continental monsoon climate region, southeastern wind coming from the oceans could only affect the lower reaches in the short summer months, whereas northwesterly wind prevails in the upper and middle reaches (the Loess Plateau) during most of a year. Finally, all the three sampling stations are free of tidal influence, so the collected samples reflected only the dissolved composition of upstream waters. Particularly, by analyzing the concentration characteristics of major ions along the Yellow River mainstem, Zhang et al (1995a) concluded that atmospheric deposition of cyclic salts to the river waters is very limited, but rather, chemical weathering and physical erosion are the primary factors affecting river chemistry. This can also be seen from the contribution diagram of different sources in which minor contribution for the Yellow River is made by cyclic salts (Gaillardet et al., 1999). Therefore, the contribution of cyclic input was not taken into account in this study. Another simplification in this method has been made by assuming that generally there is only a small anthropogenic source in the river waters because of the difficulty in quantifying its effects. Based on the above assumptions, the mass balance equation could be simplified as:

$$[X]_{riv}^{*}=[X]_{eva}+[X]_{carb}+[X]_{sil}+[X]_{sul} \qquad \text{(Equation 3.5)}$$

Equation (3.5) can be further simplified based on following straightforward assumptions. First, all Cl is only derived from evaporites (e.g., halite), and it is inert in natural environments and therefore behaves as a conservative element during surface processes (Feth, 1981). Second, the dissolution of carbonates does not contribute to the dissolved Na and K. Third, sulfate is entirely derived from sulfide oxidation, which to a certain extent would underestimate the sulfate contribution from

evaporites (e.g., gypsum and anhydrite) and thus the Ca existing in evaporites accompanying the dissolution processes. Finally, Equations (3.10) and (3.11) are difficult to solve because of the uncertainty about silicate versus carbonate contributions. To facilitate the calculation of the two equations, the ionic ratios Ca/Na=0.2 and Mg/Na= 0.2 for silicate fraction as assign by Gaillardet et al (1999) were adopted in this study. According to the chemical reactions releasing dissolved ions shown in Table 3.1 and the interrelationships between different dissolved ions (Zhang et al., 2008) as well as the assumptions made above, Equation (3.5) can be further constricted for different elements as follows:

$[Cl]_{riv}^{*}=[Cl]_{eva}$ (Equation 3.6)

$[Na]_{riv}^{*}= [Cl]_{eva}+[Na]_{sil}$ (Equation 3.7)

$[SO_4]_{riv}^{*}=[SO_4]_{sul}$ (Equation 3.8)

$[K]_{riv}^{*}=[K]_{sil}$ (Equation 3.9)

$[Ca]_{riv}^{*}=[Ca]_{carb}+[Ca]_{sil}$ (Equation 3.10)

$[Mg]_{riv}^{*}=[Mg]_{carb}+[Mg]_{sil}$ (Equation 3.11)

$[HCO_3]_{riv}^{*}=[HCO_3]_{carb}+[HCO_3]_{sil}$ (Equation 3.12)

$[HCO_3]_{carb}=2[Ca]_{carb}+2[Mg]_{carb}$ (Equation 3.13)

$[HCO_3]_{sil}=2[Ca]_{sil}+2[Mg]_{sil}+[Na]_{sil}+[K]_{sil}-2[SO_4]_{sul}$ (Equation 3.14)

After the contributions of parent rocks to the major ions in the river were determined, the silicate and carbonate weathering rates for a given basin can be calculated by using cation components supplied from silicate and carbonate minerals, dissolved Si, in combination with information on drainage area and water discharge, Q (Roy et al., 1999).

The silicate weathering rate (SWR) is calculated as:

$SWR= ([Ca]_{sil}+[Mg]_{sil}+[Na]_{sil}+[K]_{sil}+[SiO_2]) \times Q/\text{drainage area}$ (Equation 3.15)

The carbonate weathering rate (CWR) is calculated as:

$$CWR = ([Ca]_{carb} + [Mg]_{carb} + 0.5 \times [HCO_3]_{carb}) \times Q/\text{drainage area} \quad \text{(Equation 3.16)}$$

On the basis of the assumptions made above and the established mass balance equations, the chemical weathering rates of various rocks are presented in Table 3.5. The chemical weathering rates of all the four rock types are characterized by considerable uncertainties as illustrated by the differences between the minimum and the maximum, stressing the differences in dissolved ion transport between different seasons. For example, the maximum/minimum ratios for weathering of carbonates, silicates, evaporites, and sulfides at Toudaoguai station are 5.7, 4, 12.7, and 13, respectively. As a result, the maximum/minimum ratio for its TDS is 9.1. Similar, if not higher, ratios are characteristic of the Tongguan and Lijin measurements. Spatially, the weathering rates for all items presented a rapid increase from Toudaoguai to Tongguan, and then decreased slightly at Lijin, which again indicated the great contribution of the Loess Plateau to the dissolved load of the Yellow River, similar to its role in sediment supply. Approximately, 13.7 ± 11.3 Mt of TDS deriving from rocks is delivered into the Bohai Sea per year, accounting for around 10% of the corresponding seaward TSS flux observed at Lijin station. As regards the consumed atmospheric CO_2, huge differences also exist in both carbonate weathering and silicate weathering at the three stations. The Loess Plateau plays an important role in CO_2 consumption at the watershed scale.

Table 3.5 Rates of chemical weathering and atmospheric CO_2 consumption in the Yellow River basin estimated from mass balance models.

	Carbonate weathering		Silicate weathering		Evaporite weathering	Sulfide weathering	Total rock weathering	
	TDS (10^6 t/yr)	CO_2 (10^6 t/yr)	TDS (10^6 t/yr)	CO_2 (10^6 t/yr)	TDS (10^6 t/yr)	TDS (10^6 t/yr)	TDS (10^6 t/yr)	CO_2 (10^6 t/yr)
				Toudaoguai (drainage area: 367,572 km^2)				
min	0.822	0.108	0.351	0.029	0.718	0.51	2.401	0.316
max	4.688	0.402	1.411	0.391	9.149	6.694	21.942	0.561
mean	2.243	0.267	0.792	0.165	2.577	2.407	8.019	0.432
				Tongguan (drainage area: 724,878 km^2)				
min	1.889	0.258	0.534	0.01	0.553	0.857	3.833	0.541
max	9.484	0.858	2.913	0.588	16.013	16.295	44.715	0.96
mean	4.656	0.505	1.617	0.232	4.284	4.695	15.252	0.737
				Lijin (drainage area: 752,146 km^2)				
min	2.318	0.312	0.945	0.018	1.291	1.584	6.138	0.497
max	7.589	0.554	2.248	0.377	5.769	6.574	22.18	0.751
mean	4.629	0.463	1.496	0.165	3.472	4.132	13.729	0.628

Particularly, the contributions of different ion sources, namely carbonates, silicates, evaporites, and sulfides, to the TDS and their corresponding CO_2 consumption contributions are presented in Table 3.6 for comparison. The calculated results were based on the averages shown in Table 3.5. Although the dissolved ions are indicative of silicate weathering mechanism as illustrated in Figure 3.11, the contribution of silicate weathering to the TDS is small, accounting for only 9.9-10.9% at the three stations. In contrast, carbonate weathering is the primary source of riverine TDS, representing 28%-33.7%. Furthermore, the contribution of weathering of evaporites and sulfides could not be ignored. The two items collectively contributed 55.4-62.1% of the TDS, which is larger than the combined contribution of carbonate and silicate weathering. Spatially, while the contributions of carbonate weathering and silicate weathering to the TDS increased from the upstream Toudaoguai to the downstream Lijin, the contribution of evaporite weathering decreased accordingly. In general, carbonate weathering is a major contributor to the water chemistry, while the

contribution from weathering of silicates is relatively minor. This can also be validated from the high inorganic carbon composition in the suspended solids (Wang et al., 2012). Dissolution of evaporites, in particular in the upper reaches above Toudaoguai station, played an important role in supplying dissolved solids.

Table 3.6 Contributions of different sources of dissolved ions, expressed as % of the total.

Station	Carbonates		Silicates		Evaporites	Sulfides
	TDS	CO_2	TDS	CO_2	TDS	TDS
Toudaoguai	28	61.8	9.9	38.2	32.1	30
Tongguan	30.5	68.5	10.6	31.5	28.1	30.8
Lijin	33.7	73.7	10.9	26.3	25.3	30.1

Based on the chemical reaction equations involving CO_2 (shown in Table 3.1), the consumed atmospheric CO_2 by rock weathering ($[\Phi CO_2]$) can be calculated using the following equations:

For the CO_2 consumed by silicate weathering:

$$[\Phi CO_2]_{sil}= \Phi[TZ^+]_{sil}=2[Ca]_{sil}+2[Mg]_{sil}+[Na]_{sil}+[K]_{sil}-2[SO_4]_{sul} \quad \text{(Equation 3.17)}$$

For the CO_2 consumed by carbonate weathering:

$$[\Phi CO_2]_{carb}= \Phi[TZ^+]_{carb}=[Ca]_{carb}+ [Mg]_{carb} \quad \text{(Equation 3.18)}$$

The consumed atmospheric CO_2 as a result of chemical weathering is tabulated in Table 3.5. Comparing the two weathering processes showed that the consumed atmospheric CO_2 in the Yellow River basin was mainly due to carbonate weathering, whereas only 26.3-38.2% was a result of silicate weathering (Table 3.6). Particularly, the proportion of silicate weathering to the total CO_2 consumed decreased from Toudaoguai through Tongguan to Lijin. For the entire drainage basin as measured at Lijin, the mean specific CO_2 consumption rate by carbonate weathering and silicate

weathering is 0.513×10^5 mol/km^2/yr and 0.183×10^5 mol/km^2/yr, respectively. This huge difference is largely the result of weathering susceptibility of carbonate minerals. Carbonates are much more susceptible to chemical weathering than most silicate minerals (Liu and Zhang, 1988; Chen et al., 2007c). Relating to the sub-basins the three stations individually control, it is clear that chemical weathering in the middle reaches plays a more critical role relative to the upper or the lower reaches, which also coincided with the spatial distribution of physical erosion. Compared with Tongguan, the reduced CO_2 consumption flux at Lijin may suggest CO_2 outgassing across the water-air interface during the delivery processes towards the river mouth. This will be discussed in detail in Chapter 4.

It should be pointed out that the calculations were based on the assumption that the observed sulfate is entirely derived from sulfide oxidation, which did not take into account the impacts of gypsum/anhydrite dissolution. Sulfide weathering in the Yellow River basin due to acid rain came primarily from SO_2 from coal power plants and coal combustion in small furnaces and household stoves (Terada et al., 2002; Xu et al., 2009). In addition, pyrite oxidation would also form sulfuric acid (H_2SO_4) that further attack carbonates and silicates (Moon et al., 2007; Berner and Berner, 2012). As a consequence, the amount of atmospheric CO_2 during chemical weathering is reduced when sulfuric acid is involved. As mentioned earlier, however, there is gypsum/anhydrite outcrop in the drainage basin, in particular in the tributaries of the upper reaches (Chen et al., 2005). This can also be seen from the significant relationship between $Ca^{2+}+Mg^{2+}$ and SO_4^{2-} in Figure 3.9b, which indicated that not all

the measured SO_4^{2-} was derived from sulfide weathering alone, but rather, dissolution of gypsum/anhydrite also contributed to the chemical compositions. In this study, because the dissolved carbonates or silicates attacked by sulfuric acid should have involved CO_2 uptake, the consumed atmospheric CO_2 might have been underestimated. Therefore, the calculated chemical weathering rate and atmospheric CO_2 uptake are conservative.

Combining the rock weathering products and the generated HCO_3^- derived from the atmosphere showed that the mean TDS concentration at Lijin was 639±103 mg/l during 2011-2012, which was more than 6 times that of the world water discharge-weighted average of 97 mg/l (Meybeck, 2004). In comparison, the mean TDS concentration of the Yellow River during 1958-2000 was 452 mg/l at Luokou (Chen et al., 2005), about 150 km upstream of Lijin, thus corresponding to approximately a 40% increase over the years. Extensive irrigation in the river basin has been considered the major reason as it enhanced the natural evaporation/crystallization processes (Chen et al., 2003). Meanwhile, a huge amount of irrigation water is withdrawn each year for desalination of soils prior to agriculture, which promotes the solute-enriched leachates from the irrigated lands to river water. In addition, application of chemical fertilizers and dumping of domestic/industrial wastewater may have also contributed to the elevated TDS concentrations. Furthermore, greatly increased residence time due to flow regulation by reservoirs would promote evaporation, thus increasing the concentrations of dissolved solutes. Overall, the total TDS load was about 14.4±2.6 Mt/yr during 2011-2012. That is, the specific chemical

weathering rate was 19.1±3.4 t/km^2/yr, which was negligible compared to the physical erosion rate (>1000 t/km^2/yr, see Chapter 6) over the same period. Moreover, it must be noted that the chemical weathering rate may have been overestimated because non-weathering products mentioned above were included.

Comparison between physical erosion rate and chemical denudation rate of major world rivers presents strong spatial differences, suggesting differences in driving forces of the two natural processes in controlling the riverine export (Figure 3.12). As a result of intensive chemical weathering and physical erosion, most of the large rivers in the world are scattered within the zone between the lines of $y=x$ and $y=0.1x$. This indicates that mostly the chemical weathering rate accounts for 10%-100% of the physical erosion rate. In particular, the large and turbid rivers originating from the Qinghai-Tibetan Plateau, such as the Salween, Yangtze, Indus, and Ganges with considerable mass supply from the Himalayan highlands, are characterized by high rates of both physical erosion of suspended sediments and chemical denudation of dissolved solids. In this region under active tectonic activity with steep gradient and monsoonal climate, it is evident that physical erosion is likely to be more dominant than chemical weathering (below the $y=x$ line) (Dalai et al., 2002). In contrast, European rivers, such as Weser, Danube, Elbe, Seine, and Po, and North American rivers, such as St. Lawrence and Columbia, generally showed higher chemical weathering rate over the physical erosion rate, which is probably due to significant anthropogenic pollution inputs as they drain densely populated, industrialized, and

cultivated areas (Gaillardet et al., 1999; Roy et al., 1999). Furthermore, good vegetation protection and gentler slopes helped to reduce physical erosion.

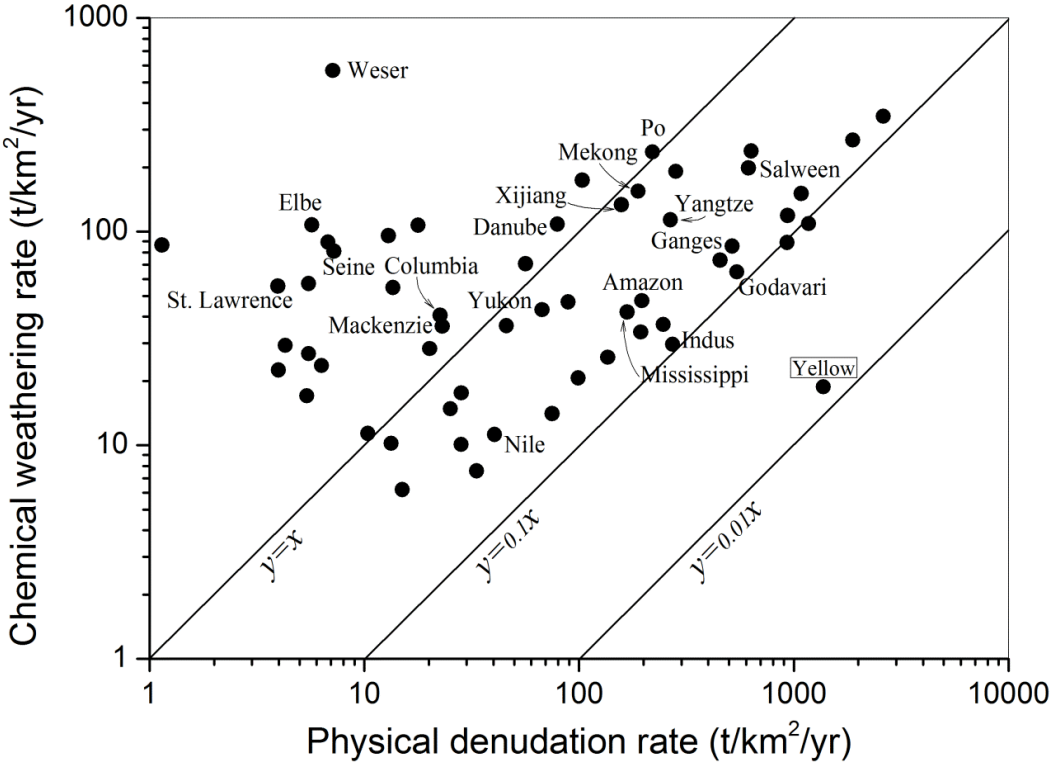

Figure 3.12 Comparison between physical denudation rate and chemical weathering rate of some large world rivers. All data were from the compilation of Gaillardet et al (1999), except the physical denudation in Salween (Bird et al., 2008). The Yellow measured at Lijin was from this study.

Although the relationships between chemical weathering and physical erosion have remained poorly quantified as long-term chemical weathering rates have been difficult to measure, physical erosion and chemical weathering appear to be closely interrelated (Stallard and Edmond, 1983; Edmond and Huh, 1997; Riebe et al., 2001; Gabet and Mudd, 2009). While chemical weathering disintegrates the bedrock and transforms it into secondary products available for physical removal, physical erosion removes material from the top of the regolith surface, thus exposing fresh minerals to chemical weathering. The increased supply of fresh minerals drives higher chemical

weathering rates, thus resulting in more atmospheric CO_2 uptake (Raymo and Ruddiman, 1992; Berner and Berner, 2012). However, such a positive relationship does not hold true in all situations. If the physical erosion is significantly faster than chemical weathering, the so-called weathering-limited regime (Stallard and Edmond, 1983), chemical weathering will be limited by the kinetics of chemical reactions. Indeed, at the highest physical erosion rates, chemical weathering rates may decline, because the potential increases in chemical weathering rate from the exposure of fresh materials are offset by a decrease in the total volume of minerals exposed as a result of thinner regolith (West et al., 2005; Gabet and Mudd, 2009).

According to Gabet and Mudd (2009), the relationship between physical erosion rate (E) and chemical weathering rate (W) can be simply expressed as: $W \propto E^{\lambda}$, where λ is a dimensionless constant. Obviously, if $\lambda \approx 1$, increases in physical erosion will be matched by similar increases in chemical weathering. If $\lambda < 1$, large increases in physical erosion would result in progressively smaller increases in chemical weathering (Millot et al., 2002; West et al., 2005). The Yellow River is well-known for its severe physical erosion, with extreme soil erosion rates up to >50,000 t/km^2/yr (Zhao, 1996). Substituting the physical erosion and chemical weathering rates of the Yellow River into the empirical relationship shows that λ is only about 0.47. The small λ demonstrates the dominance of physical erosion over chemical weathering in the river basin (Figure 3.12), and is consistent with the discussion above.

3.3.6 Temporal changes of TDS and implications for atmospheric CO_2 balance

Recording of TDS transport in the Yellow River basin began in the 1960s (Zhang et al., 1990; Zhang et al., 1995a; Meybeck and Ragu, 1997; Chen et al., 2005). Owing to rapid reductions of water discharge, the seaward TDS flux as measured usually at the lowermost Luokou or Lijin stations has decreased sharply over the past decades (Figure 3.13a), although the concentrations of TDS and major ions throughout the river have been increasing (Chen et al., 2005). The TDS flux into the Bohai Sea decreased from more than 20 Mt/yr in the pre-regulated 1960s to less than 10 Mt/yr in the 1990s when the lower reaches suffered from continuing periods of interrupted water flow (Ran and Lu, 2013). During this period of about 40 years, the Yellow River annually delivered around 11 Mt of dissolved solids to the ocean (Gaillardet et al., 1999). In recent years, in particular after the operation of the Xiaolangdi Reservoir in 2002, water discharge into the Bohai Sea has been greatly restored, leading to increased water discharge and thus the TDS flux. Regarding the dominant ion in the Yellow River waters, HCO_3^- accounted for 42% (mass ratio) of the total dissolved flux during the period 1963-1998 (Chen et al., 2005). It decreased slightly to represent about 34% during 2011-2012. The reduced HCO_3^- proportion indicated increased concentrations of other ions, which is largely the result of strong water regulation activities in recent years in the watershed (Chen et al., 2005).

The dramatic reductions of the seaward fluxes of water discharge and TDS will have profound physical and biogeochemical impacts in the lower reaches of the Yellow River, the estuary, and the open sea. For example, precipitation of calcite on the riverbed as a result of interrupted water flow may harden the bed and prevent

undercutting in the next flood, thus raising the riverbed level and posing a risk of channel avulsion for the riparian residents (Chen et al., 2005). Solutes are important nutrient sources for aquatic ecosystems. Thus, reductions in these solute fluxes would definitely affect those aquatic biota that heavily rely on nutrient supply via rivers. Regulation of rivers by damming and eutrophication in river basins have substantially reduced dissolved silicon loads into the Black Sea and the Baltic Sea (Humborg et al., 2000). The resulting changes in the nutrient composition of river discharges have been invoked to explain the dramatic shifts in phytoplankton species composition. Generally, the effects on riverine and coastal environments could be far-reaching. More efforts are needed to elucidate the impacts regarding the dramatic reductions of major solutes and suspended sediment in the Yellow River.

Based on available historical records, comparison between annual TDS and TSS fluxes are plotted in Figure 3.13b. Although the data points scattered widely, it is clear that the annual TDS fluxes are positively correlated with the annual TSS fluxes, similar to the relationship based on individual samplings as shown in Figure 3.7. As the TSS fluxes represent the intensity of physical erosion as discussed earlier, the positive correlation is consistent with the coupling between physical erosion and chemical denudation (Oliva et al., 2003; Gabet et al., 2010). Because the soil erosion intensity and thus the TSS fluxes in the river basin are expected to further decrease with implementation of soil conservation programmes and continuous dam construction, the chemical weathering rate and therefore the TDS concentration will

be progressively reduced. In addition, with decreasing water discharge (Figure 3.13a), the TDS fluxes reaching the Bohai Sea will see further reductions.

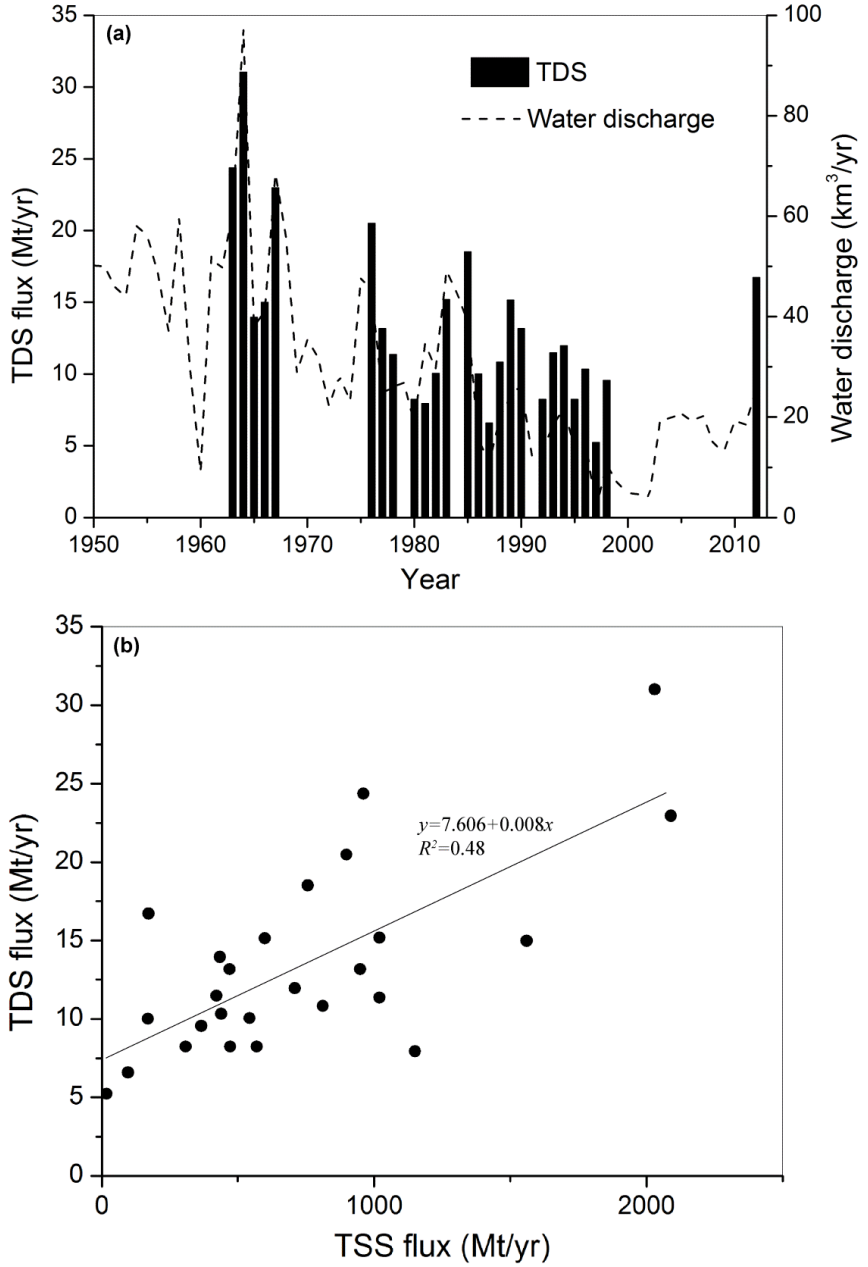

Figure 3.13 Temporal variations of annual TDS fluxes of the Yellow River into the Bohai Sea (a) and comparison between annual TDS and TSS fluxes showing positive correlation (b). Note that the data measured before 2000 were based on Luokou station (about 150 km upstream of Lijin) and adapted from Chen et al., 2005. Given that no considerable water input or output occurred in the stretch between the two stations, the obtained TDS fluxes at the two stations can be taken as seaward export and are comparable.

In association with the chemical weathering of rocks in the entire Yellow River basin, annually 0.63 ± 0.18 Mt of CO_2 is consumed on average. As stated earlier, globally the mean atmospheric CO_2 uptake rate by chemical weathering was estimated at 0.2-0.288 Gt/yr. Therefore, the annual CO_2 uptake in the Yellow River basin accounted for 0.22-0.32% of the global total uptake rate. Of the mean 0.63 Mt of CO_2 consumed each year, approximately 74% is due to carbonate weathering and 26% is from silicate weathering. If using 0.288 Gt/yr as the annual global CO_2 consumption rate (Gaillardet et al., 1999), weathering induced atmospheric CO_2 uptake in the Yellow River basin represented about 0.31% of the annual global CO_2 consumption by carbonate weathering (0.148 Gt/yr) and 0.12% of that by silicate weathering (0.14 Gt/yr), respectively. Higher carbonate weathering contribution is consistent with the predominance of carbonate outcrop in the drainage basin.

When normalized to the drainage area (~752,000 km^2), the mean uptake rate of atmospheric CO_2 caused by chemical weathering is about $(0.7 \pm 0.2) \times 10^5$ mol/km^2/yr. Apparently, this uptake rate is low compared to other river basins. For example, the uptake rate of atmospheric CO_2 in the Yamuna drainage basin, located at the south slope of the Himalaya, is $2\text{-}4 \times 10^5$ mol/km^2/yr (Singh et al., 2005). In the semi-arid to monsoonal Godavari river basin in India, the CO_2 uptake rate is about 8.06×10^5 mol/km^2/yr (Jha et al., 2009). Under humid climate, the uptake rate can be even higher (i.e., $>10 \times 10^5$ mol/km^2/yr). For example, the mean CO_2 uptake rate in the Pearl River basin in south China is 11.9×10^5 mol/km^2/yr (Gao et al., 2009). For basalt watersheds throughout the volcanic island of Dominica in the Lesser Antilles, the

CO_2 uptake rate by chemical weathering can be as high as 15.75×10^5 mol/km^2/yr (Goldsmith et al., 2010). Much less precipitation and lower atmospheric temperature can be employed to explain the lower atmospheric CO_2 consumption rate.

Particularly, the CO_2 consumption rate due to silicate weathering in the Yellow River basin (0.183×10^5 mol/km^2/yr) was significantly lower than its fractional area of continental drainage which has an average CO_2 uptake rate of 0.876×10^5 mol/km^2/yr (Gaillardet et al., 1999). This lower value may be due to additional contributions from the easily weatherable and widely distributed carbonates in the river system. Furthermore, low temperature and precipitation may have also restrained the weathering rate as discussed above. In response to global warming, the rates of chemical weathering will be increased due to the positive feedback between chemical weathering and temperature (Brady and Carroll, 1994; Berner, 1995; Chen and Brantley, 1997; Kump et al., 2000; Berner and Berner, 2012). As a result, the carbon sink potential through chemical weathering processes will be enhanced. With respect to the Yellow River basin characterized by wide carbonate outcrops, the rates of chemical weathering are greatly accelerated. Therefore, the significance of chemical weathering induced atmospheric CO_2 drawdown cannot be neglected in global carbon budget studies.

3.4 Summary and conclusions

By analyzing water samples collected at three mainstem hydrological gauge stations based on a weekly sampling frequency, this chapter investigated the chemical

weathering processes in the Yellow River basin during the period of July 2011-July 2012. Specifically, the weathering rates of rocks in the drainage basin were estimated by using a forward model, and the associated atmospheric CO_2 consumption flux was assessed through mass balance equations. Furthermore, the implications of chemical weathering and associated atmospheric CO_2 consumption were evaluated in the context of the global carbon cycle.

The Yellow River mainstem waters showed neutral to alkaline pH values with a range from 7.03 to 8.53, revealing the dominance of bicarbonate in riverine total alkalinity. Riverine electrical charges were balanced. Concentrations of the major ions were characterized by varying seasonal variations. At the three stations, Na^+ is the most abundant cation in stream waters, in the order $Na^+ > Mg^{2+} > Ca^{2+} > K^+$. For the anions, HCO_3^- is the most abundant anion, in the order $HCO_3^- > Cl^- > SO_4^{2-}$. In general, the dominant ion pairs are Ca^{2+}-HCO_3^- and Na^+-Cl^-. Because atmospheric cyclic input to the river chemistry is very limited, chemical weathering is of first importance affecting the chemical compositions of the Yellow River waters. Furthermore, with much of the river basin draining loess deposits and clastic rocks, these characteristics indicated that water chemistry was mainly controlled by intense carbonate weathering and dissolution of evaporites.

The concentration variations of the major ions responded to the dilution effect of the water discharge, with the exception of dissolved silica at Toudaoguai station. Based on mass balance models, the weathering characteristics of various rock types were

identified, and their chemical weathering rates were calculated. Due to the wide outcrop of carbonates and evaporties in the drainage basin, contributions from weathering of the two rocks were much larger than that from silicates. In addition, although the contribution of sulfide weathering may have been overestimated, its contribution should not be ignored. From a spatial perspective, the middle reaches (the Loess Plateau) contributed much more dissolved solids than the upper or the lower reaches, suggesting a positive feedback between chemical weathering and physical erosion.

Taking Lijin as the control station of the entire river basin, the mean TDS concentration of the Yellow River is 639 mg/l on average, which is more than 6 times the world water discharge-weighted average of 97 mg/l. During the study period of 2011-2012, the mean seaward TDS load was about 14.4 ± 2.6 Mt/yr, corresponding to a specific chemical weathering rate of about 19.1 ± 3.4 t/km^2/yr. Compared with the historical water chemistry records for the period 1958-2000, the TDS concentration showed a 40% increase, which is likely due to intensive agricultural pollution and dam construction in the catchment. In spite of the increased TDS concentration, the annual TDS flux into the Bohai Sea has a downward trend as a result of rapid reductions in the seaward water discharge. The sharply reduced dissolved solids would trigger profound impacts on the physical and biogeochemical cycles in the lower reaches, the estuary, and even the open sea, thus deserving extra attention for a better understanding.

In association with the chemical weathering processes, 0.63 ± 0.18 Mt of atmospheric CO_2 was annually consumed during the study period, of which 74% was by carbonate weathering and 26% was by silicate weathering. With a drainage area of about 752,000 km^2, the mean uptake rate of atmospheric CO_2 caused by chemical weathering was estimated at $(0.7 \pm 0.2) \times 10^5$ mol/km^2/yr, which is significantly lower than in most other river basins. Overall, the annual CO_2 uptake in the Yellow River basin represented 0.22-0.32% of the global total uptake rate. Because all the SO_4^{2-} was assumed to be of sulfide weathering origin and gypsum and anhydrite's contribution was not taken into account, the obtained CO_2 consumption rate may have been slightly underestimated. Given the reports on outcrop of gypsum and anhydrite in the watershed (Zhang et al., 1995a; Chen et al., 2005), the total CO_2 uptake rate should be higher than estimated here. More efforts are needed in the future to investigate the dissolution of gypsum and anhydrite and its effects on estimates of chemical weathering rate and atmospheric CO_2 drawdown. In addition, input of human pollutants was simplified in this study. Future work is also needed to determine its impacts on the water chemistry characteristics and the associated CO_2 consumption.

Chapter 4 Riverine pCO_2 dynamics and estimate of CO_2 outgassing

4.1 Introduction

River systems play a substantial role in global carbon budget studies, because they can modulate and adjust the carbon dynamics not only of their watersheds but also of the coastal systems into which the fluvial waters are discharged (Berner and Berner, 2012; Richey et al., 2002). Thus, fluvial exports of carbon, including both inorganic and organic, into oceans represent an important pathway of the global carbon cycle. Annually, about 0.9 Gt of carbon is delivered into the oceans via inland waters that also include wetlands, lakes, estuaries, and reservoirs (Cole et al., 2007; Battin et al., 2009). However, rivers are not passive conduits and do not simply shuttle terrestrial material to the sea. Evidence is accruing to demonstrate that only a small portion of the carbon that enters a river network reaches the ocean (Cole et al., 2007). A considerable fraction is buried in sedimentary deposits or returned to the atmosphere en route (Richey et al., 2002; Yao et al., 2007). Consequently, rivers are now viewed as net sources of atmospheric CO_2. Recent estimates have shown that global rivers could transfer 0.23-56 Gt C/yr to the atmosphere across the water-air interface (Cole et al., 2007; Tranvik et al., 2009; Aufdenkampe et al., 2011). Comparative studies with seaward carbon export have highlighted the significance of CO_2 outgassing from inland waters in assessing the global carbon budget (e.g., Richey et al., 2002; Battin et al., 2009; Butman and Raymond, 2011). With such a huge release, the terrestrial CO_2 sink may prove smaller than previously thought (Melack, 2011b).

Aqueous CO_2 originates largely from terrestrial ecosystem respiration, *in situ* decomposition of autochthonous organic matter, and the precipitation of carbonates. Partial pressure of riverine CO_2 (pCO_2) reveals the intensity of gas exchange at the water-air interface with the atmosphere. Although with pronounced spatial and seasonal variations due to impacts from various natural and anthropogenic disturbances, riverine pCO_2 in most world rivers was found substantially higher than the atmospheric equilibrium (i.e., 380 μatm), indicating a net emission (Cole et al., 2007). While studies on riverine CO_2 outgassing from mainstem channels or estuary waters, have been done for rivers such as the Amazon (Richey et al., 2002); Yangtze (Zhai et al., 2007), Pearl (Yao et al., 2007), and Mekong (Li and Lu, 2012), estimates of CO_2 outgassing from river network systems are rare. This is largely caused by two reasons. One is the difficulty of quantifying the areal extent of stream and river waters using traditional mapping techniques. The other is the constraints of time and logistics to conduct large-scale spatial sampling that covers not only the mainstem channels but the tributaries and streams, particularly for large river basins.

Because tributaries and streams usually have stronger turbulence and more rapid mixing with the atmosphere than the mainstem channels, they could be more biogeochemically active in terms of contribution to atmospheric CO_2 (Alin et al., 2011; Butman and Raymond, 2011; Benstead and Leigh, 2012). For example, Aufdenkampe et al (2011) found that the CO_2 outgassing fluxes from small streams could be up to 2-3 times higher than that from larger river channels. Estimates of CO_2 emission focusing only on the mainstem channels might therefore have substantially

underestimated the role of a particular river system in carbon cycling. High frequency sampling at both space and time scales is thus needed for better understanding the role played by streams and rivers in biogeochemical cycles of carbon.

The Yellow River basin is characterized by high transport of sediment and total dissolved solids (TDS) among the large rivers of the world (Chapter 3). Its long-term mean TDS concentration of 452 mg/l is about four times the world median value (Chen et al., 2005). Based on selected hydrological stations or river reaches, previous studies have largely analyzed the chemical weathering processes and associated CO_2 consumption (e.g., Hu, 1982; Zhang et al., 1995a; Chen et al., 2005; Wu et al., 2008, and see more descriptions in Chapter 3). Nevertheless, few studies have examined the consequent carbon dynamics in riverine waters. In addition, studies on ecosystem respiration in the river basin were mainly focused on degradation of organic matter and carbon losses on sloping lands and the effects of land use changes, such as vegetation restoration and changes of tilling practices (Zhao et al., 2008; Li et al., 2010). It remains largely unknown about the fate of the lost carbon that enters the river network.

With historical records measured throughout the Yellow River network during the 1950s-1984 and recent sampling along the mainstem during 2011-2012, this study sought to assess the spatial and temporal variations of pCO_2. Furthermore, a new method based on the entire river network was developed to estimate the total water surface area, with which the basin-wide CO_2 outgassing fluxes across the water-air

interface were estimated. Application of this work is expected to facilitate similar studies on CO_2 emission from a complete river network system that includes small headwater streams, large tributaries, and the mainstem channel.

4.2 Materials and methods

4.2.1 Historical records of water chemistry and wind

Historical data of major ions and dissolved silica measured from a network of hydrological stations throughout the basin were extracted from the Yellow River Hydrological Yearbooks, which are produced each year by the Yellow River Conservancy Commission (YRCC). Other variables concurrently measured at each sampling event, including pH, water temperature (*T*), water discharge, and flow velocity, were also extracted from the yearbooks. Over the period from the 1950s to 1984, the sampling frequency ranged from 1 to 5 times per month, depending on hydrological regime. During the period of 1966-1975, sampling at some stations was suspended or stopped completely due to political instability. Post-1984 records are not in the public domain. Given the discontinuity, only the sampling stations with at least 2-year-long records were used, and finally 129 stations were eligible for the present study as shown in Figure 4.1.

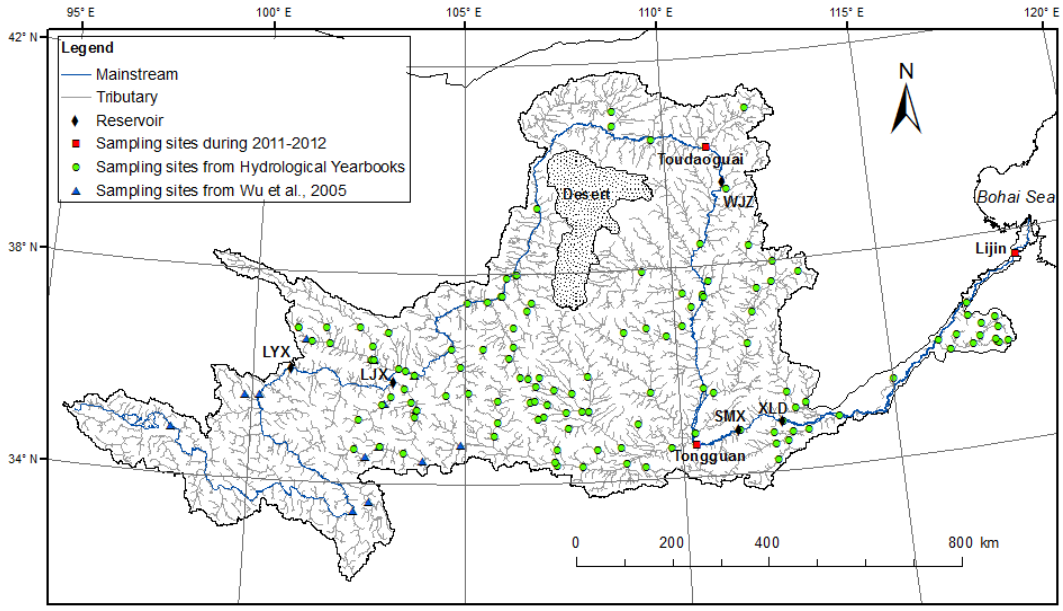

Figure 4.1 Location map of the sampling sites used to calculate pCO_2 and CO_2 outgassing from streams and rivers of the Yellow River basin. Acronyms for the mainstem reservoirs: LYX-Longyangxia; LJX-Liujiaxia; WJZ-Wanjiazhai; SMX-Sanmenxia; and XLD-Xiaolangdi.

Chemical analyses of the collected water samples were performed in the laboratory under the authority of the YRCC following the standard procedures and methods described by Alekin et al (1973) and the American Public Health Association (1985). Detailed description of sample analysis can be found in Chen et al (2002b). Particularly, the pH and temperature were measured in the field, and the total alkalinity (TAlk) was determined using a fixed end-point titration on filtered samples.

Use of historical records always raises the issue of data reliability. No detailed information on quality assurance and quality control for the monitored variables is available in the yearly hydrological reports. On the other hand, however, extensive efforts have been made to assess the quality by analyzing the differences of variables measured at the same station over the same period but from different sources. The

Luokou station located on the lower Yellow River mainstem channel has also been monitored under the United Nations Global Environment Monitoring System (GEMS) Water Programme since 1980 (available at http://www.unep.org/gemswater/). As pCO_2 is considerably sensitive to pH changes (Li et al., 2012), the pH values from the two sources were compared (Table 4.1). The comparison indicated that the dataset from the Hydrological Yearbooks agreed well with that from the GEMS/Water Programme, with differences of <2%. The high data quality of the Hydrological Yearbooks can also be verified through the comparison of concentration of major ions at the station from the two datasets (Chen et al., 2005). Similar data consistency can also be found for the Yangtze and Pearl rivers which were monitored using the same analytical methods (Chen et al., 2002b; Zhang et al., 2007).

Table 4.1 Comparison of the pH values at Luokou station during 1980-1984 from different data sources (arithmetic mean ± standard deviation).

Data source	Year				
	1980	1981	1982	1983	1984
GEMS/Water Programme	8.27±0.11	8.21±0.21	8.10±0.20	8.14±0.10	8.25±0.09
This study	8.11±0.13	8.14±0.07	8.13±0.07	8.10±0.03	8.09±0.05
% of variation	1.93	0.85	-0.37	0.49	1.94

In addition to available databases, the analyses presented here were dependent upon literature citations. Considering the data paucity of the Hydrological Yearbooks regarding the upper Yellow River, data collected from 17 sites in the upper Yellow River basin were retrieved from Wu et al (2005) (Figure 4.1). During 1999-2000, they measured the pH and temperature at the time of sampling, and determined the TAlk through Gran titration. Comparison with previous sampling results (Zhang et al., 1995) shows their data agreed well.

To estimate the gas transfer velocity of CO_2, compiled wind information for the Yellow River basin and adjacent regions was collected from the China Meteorological Administration (http://www.cma.gov.cn/). Daily mean wind speed measured at 10 m height above the ground at 148 meteorological observation stations during the same period was used.

4.2.2 Recent field sampling and analyses

Between July 2011 and July 2012, weekly sampling on the mainstem channel was undertaken at Toudaoguai (5 July 2011-6 July 2012), Tongguan (5 July 2011-3 July 2012), and Lijin stations (5 July 2011-15 July 2012) (Figure 4.1). The frequency increased to daily sampling when large flood events occurred. In each sampling event, water column samples were collected ~0.5 m below the surface water from 3-5 points across the cross-section. The samples were combined in acid-washed, but carefully neutralized, 5-L high density polyethylene (HDPE) containers (see the sampling description in Chapter 3). Determination of pH and water temperature was performed *in situ* using a Hanna HI9125 pH/Temp meter, which was calibrated prior to each measurement against pH7.01 and pH10.01 buffers. Replicate measurements showed the precision for pH and temperature were ±0.04 units and ±0.1 ℃, respectively. The TAlk was determined by titrating 50-ml of water with 0.02 M hydrochloric acid (HCl) within 5 hours after sampling. Three parallel titration results showed the analytical error was below 3%. The parallel alkalinity concentrations were then averaged. Corresponding auxiliary data, including water discharge and suspended sediment concentration, at the three stations were measured daily by the station staff. Generally,

the Toudaoguai and Tongguan sampling results reflected the TAlk and pCO_2 changes from the Loess Plateau, while the Lijin sampling results could represent the seaward export, because it is located only about 110 km upstream of the river mouth and is free of tidal influences.

4.2.3 Calculation of pCO_2 and CO_2 outgassing flux

With the available data of TAlk, pH, and water temperature, the dissolved inorganic carbon (DIC) species, including HCO_3^-, CO_3^{2-}, H_2CO_3, and aqueous CO_2, can be determined, from which the pCO_2 can be calculated using the CO2SYS program (Lewis and Wallace, 1998).

The CO_2 outgassing flux across the water-air interface can be calculated according to

$$F_{CO_2} = k \times K_H \times (pCO_{2w} - pCO_{2a}) \quad \text{(Equation 4.1)}$$

where, F_{CO_2} is the CO_2 flux across the air-water interface (mmol/m^2/d); k is the gas transfer velocity of CO_2 (cm/h); K_H is Henry's constant for CO_2 at a given temperature (Weiss, 1974); pCO_{2w} and pCO_{2a} are the partial pressure of CO_2 in the water and water in equilibrium with the atmosphere, respectively.

A positive F_{CO_2} indicates that a net CO_2 outgassing occurs from the waters to the atmosphere, and a negative F_{CO_2} represents CO_2 invasion from the atmosphere to the water body. Although *in-situ* gas transfer values were not available, they can be estimated by incorporating major forcing factors, such as boundary layer stability, current velocity, wind speed, and slope. Several empirical relationships have been

made to estimate the gas transfer velocity (e.g., Wanninkhof, 1992; Abril et al., 2000; Raymond and Cole, 2001; Borges et al., 2004; Butman and Raymond, 2011). To determine the variations in *k* values derived from this simple parameterization methodology, quantification of the gas transfer velocity in this study was based on two empirical functions.

First, the relationship fitted by Raymond and Cole (2001) was used because it provided a reasonable estimate for the neighbouring Yangtze River (Zhai et al., 2007). The formula can be expressed as follows:

$$k = 1.91 \times e^{0.35u} \times (Sc/600)^{-1/2} \quad \text{(Equation 4.2)}$$

where, u is the wind speed measured at 10 m height (m/s) and Sc is the Schmidt number of CO_2 for temperature. The Schmidt number for 20 ℃ in freshwater is 600 (Wanninkhof, 1992).

Field chamber measurements of *k* indicated that small rivers and streams (channels <100 m wide) had a significantly higher *k* than large rivers with channel width >100 m (Alin et al., 2011). More importantly, small rivers and streams could account for >80% of the total outgassing fluxes (Rasera et al., 2008). Given the differences in *k* and the importance of small rivers and streams, the relationships developed by Alin et al. (2011) were then employed to estimate the CO_2 outgassing. For rivers with channel width >100 m, the *k* value is a function of wind speed.

$$k = 4.46 + 7.11 \times u \quad \text{(Equation 4.3)}$$

For small rivers and streams, the best parameterized statistical relationship suggested that *k* is highly dependent on flow velocity (*w*, in units of cm/s).

$$k = 13.82 + 0.35 \times w \quad \text{(Equation 4.4)}$$

As the meteorological observation stations are not exactly situated at the same locations as the hydrological stations, the ordinary Kriging interpolation method was used to estimate the on-site wind speed in ESRI ArcGIS 9.3 (Luo et al., 2008).

4.2.4 Water surface area

Another important factor affecting CO_2 outgassing is the areal extent of the water-air interface. Due to incomplete understanding of the distribution and areal extent of river networks, the significance of rivers in the global carbon cycle dynamics remains poorly constrained. For example, a percentage of the drainage area is usually assumed to estimate the water surface area (e.g., Cole and Caraco, 2001; Wang et al., 2007; Li et al., 2012). However, the percentage could be highly variable, depending on the drainage density that is further controlled by a number of factors, such as climate, geological structure, and geomorphological development. Using an arbitrarily assumed percentage without careful consideration would thus misestimate the areal extent and the subsequent CO_2 outgassing flux.

The water surface area of streams and rivers has often been underestimated by traditional mapping techniques, which typically depend on low-resolution aerial photographs. In comparison, a digital elevation model (DEM) is able to provide a reasonably accurate picture of the areal extent (Benstead and Leigh, 2012). To

estimate the basin-wide water surface area of the Yellow River basin, ESRI ArcGIS 9.3 was utilized to delineate the stream channel geometry from a 90×90 m resolution SRTM DEM dataset (USGS: http://www.usgs.gov/). The stream network was first delineated with a threshold value of 100 cells assuming a stream channel starts to form within the cells. The stream order (SO) for each extracted stream channel was then identified using the Strahler stream order classification method, and its length was quantified. Five stream orders were identified, with the mainstem channel being the 6th order and the smallest detectable streams the 2nd order (Figure 4.2). However, the smallest streams (1st order) failed to be included due to resolution limitation of the DEM images.

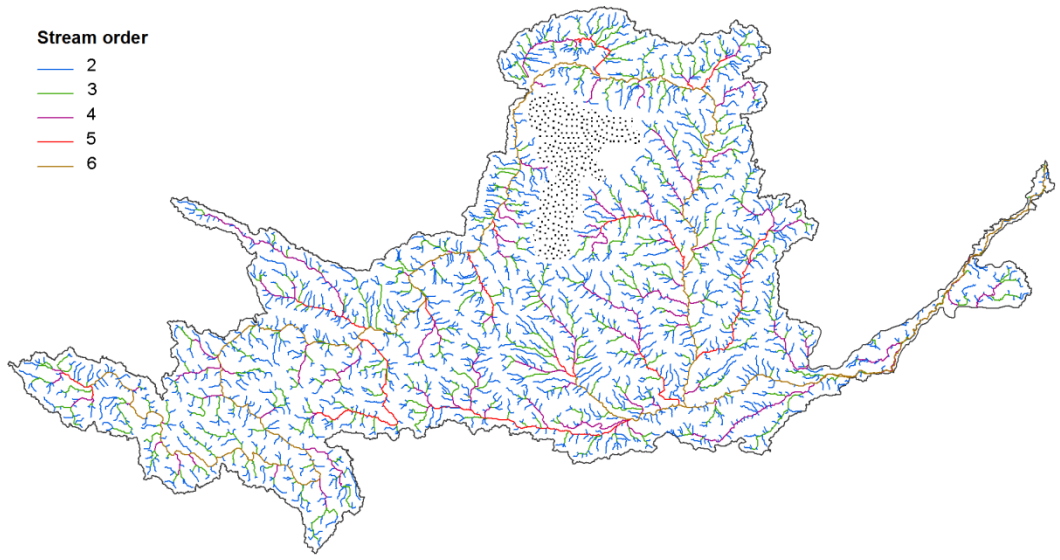

Figure 4.2 Drainage networks of the Yellow River derived from SRTM DEM dataset (source: US Geological Survey: http://www.usgs.gov/).

Since the 1st order streams play an important role in CO_2 emission, their surface area needs to be quantified to accurately estimate the total CO_2 efflux. According to the Horton's law on stream morphometry, there exist geometric relationships between the number and mean length of streams of a given order and the corresponding order

(Horton, 1945). The empirical relationships between stream order and stream number as well as stream channel length based on the delineated 5 stream orders were established to characterize the first order streams. By assigning the stream order in the relationships to 1, the stream number and channel length of the first order streams can be estimated. As for the channel width (here, the channel width was referred to as the width of the channel with water cover), it is closely related to water discharge as illustrated in hydraulic geometry (Leopold and Maddock, 1953). Moreover, because water discharge is positively related to drainage area, and drainage area is correlated with stream order (Horton, 1945), channel width could thus be roughly estimated by relating it to stream order. Based on field measurements of cross-sections and delineations from high-resolution Landsat images (also from the USGS), the mean channel widths of the stream orders 2-6 in both the dry and wet seasons were compiled (the widths in different seasons actually did not change significantly, see Chapter 5 on water surface changes). With the obtained channel width information, Horton's law was extended to calculate the channel width of the first order streams. Once the geometrical features of streams of different orders are parameterized, the total water surface area of the Yellow river network can be calculated.

4.3 Results

4.3.1 Characteristics of hydro-chemical variables

To better describe the spatial changes, the river basin was divided into seven sub-basins, including the headwater region (HR), Huang-Tao tributaries (HT), Qing-Zuli tributaries (QZ), Ning-Meng reaches (NM), the middle reaches of the Yellow River

(MY), Wei-Yiluo tributaries (WY), and the lower reaches of the Yellow River (LY), as shown in Figure 4.3. Overall, the Yellow River waters were characterized by strong alkalinity (Figure 4.3a). The pH values displayed significant spatial variations, with the higher values usually in the headwater region where the highest was measured at 9.1. For the waters sampled from the Loess Plateau in the middle reaches (mainly between Toudaoguai and Tongguan stations; Figure 4.1), the pH was generally in the range of 7.71-8.47. At some tributary sampling sites (i.e., the QZ), the waters were more acidic, and the pH could be as low as 6.4. Towards the river mouth, the pH showed a downward trend in the lower reaches (LY). With one exception at the Lijin station (Figure 4.1), the pH values were all below 8.13 and even below 7 at some tributary sampling sites. In addition to spatial variations, the pH also showed seasonal changes. In general, the waters were more alkaline during the dry season (October-May) than during the wet season (June-September), with greater seasonal differences in the tributaries than in the mainstem.

Ranging from 855 μmol/l to 8633 μmol/l, the TAlk also had complex spatial variability. While the HR and LY sub-basins showed the lowest TAlk level (<2600 μmol/l), the TAlk in the sub-basins on the Loess Plateau was high, which had a mean TAlk of about 3800 μmol/l. The highest TAlk was measured in the QZ sub-basin. It is evident that the TAlk and pH showed similar spatial variations, but in completely opposite directions, with high TAlk coinciding with low pH. Based on all sampling results, about 58% of the TAlk values fell into the range of 3000-4000 μmol/l and 92% in the range of 2000-5000 μmol/l. The mean TAlk for the Yellow River waters was 3560 μmol/l.

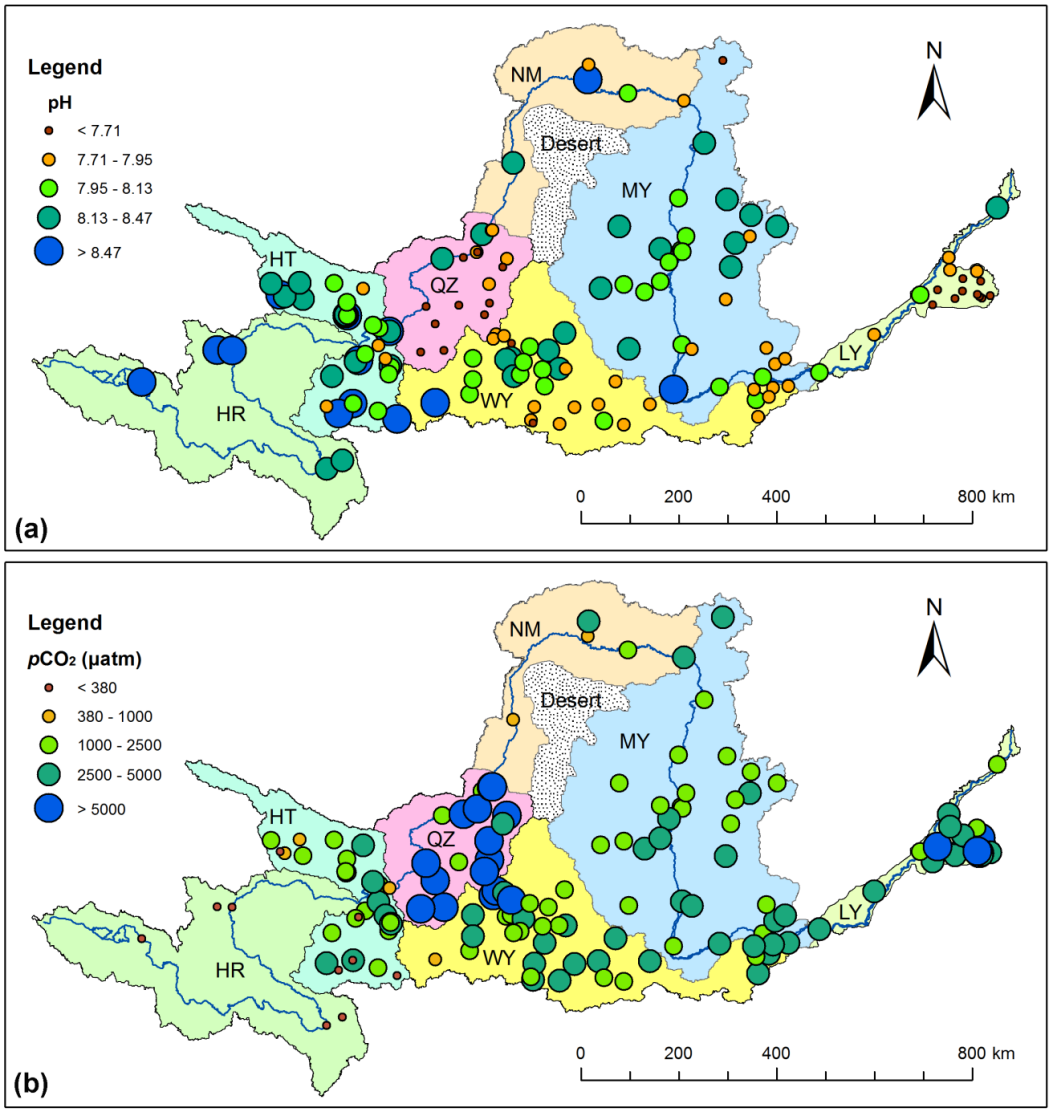

Figure 4.3 Spatial variations of (a) pH and (b) CO_2 partial pressure (pCO_2) across the Yellow River basin. The basin was divided into seven sub-basins according to variations in pCO_2 and wind speed. Acronyms are: HR: headwater region; HT: Huang-Tao tributaries; QZ: Qing-Zuli tributaries; NM: Ning-Meng reaches; MY: middle Yellow River; WY:Wei-Yiluo tributaries; LY: lower Yellow River.

The TAlk concentrations across the river basin remained largely stable during the sampling period. Figure 4.4 shows an example of the TAlk variations at Luokou station in the lower Yellow River. In spite of the discontinuous measurements from 1968 to 1974, it is clear that the annual mean TAlk concentration did not change significantly over time. Plotting the TAlk with corresponding water discharge showed

that they are negatively correlated (Figure 4.5). The TAlk concentration decreased slightly with sharply increasing water discharge during the flooding season.

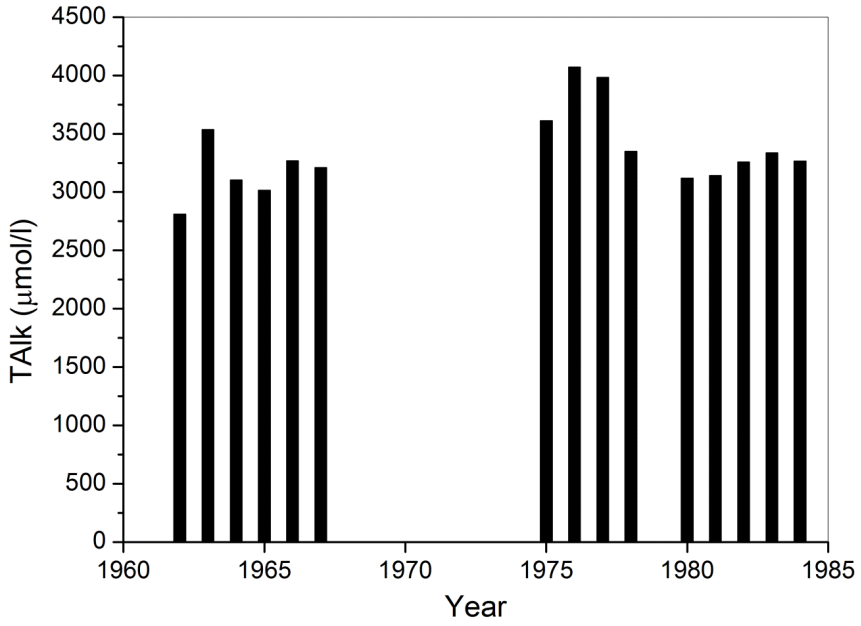

Figure 4.4 Temporal trend of the total alkalinity (TAlk) concentration of the Yellow River at Luokou station showing insignificant temporal variations.

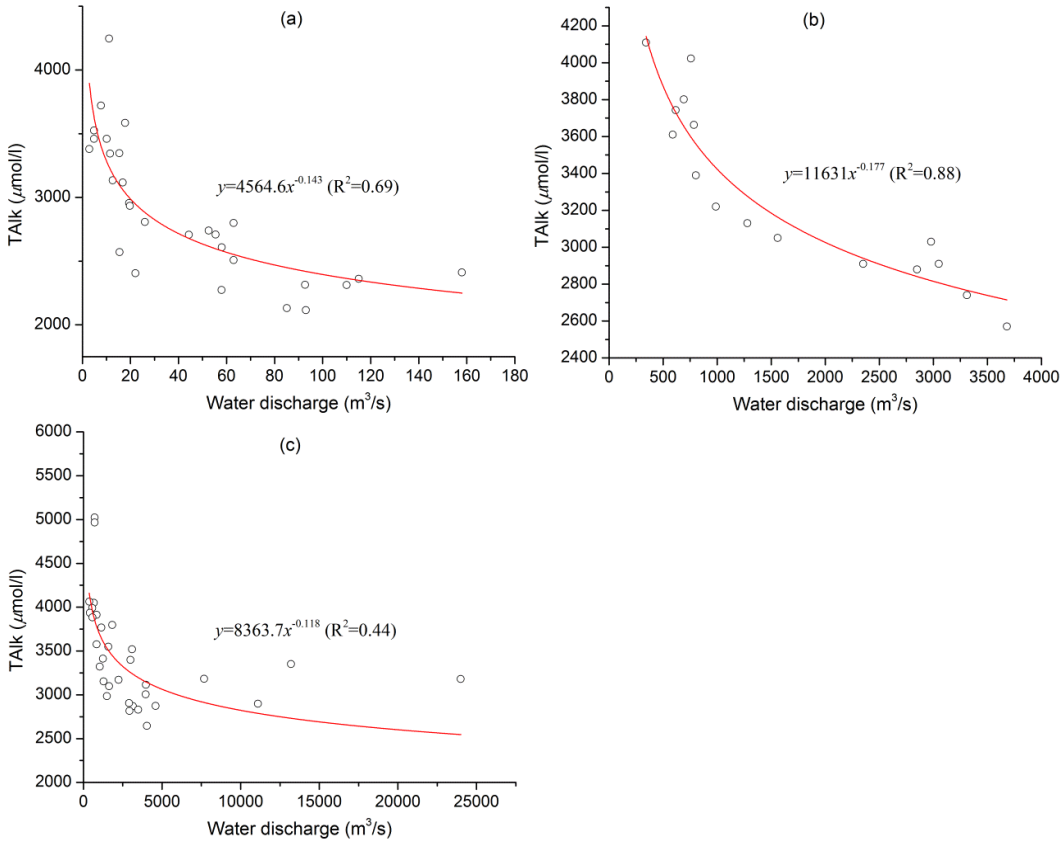

Figure 4.5 Dependence of total alkalinity (TAlk) on water discharge at typical sampling sites. a is from a tributary (in QZ sub-basin); b and c are from the mainstem channel.

4.3.2 Spatial and temporal variations of pCO_2

The pCO_2 varied significantly throughout the river basin from about 200 μatm to more than 30,000 μatm. Spatially, except the headwater region with pCO_2 lower than the atmospheric CO_2 concentration of 380 μatm, the remaining basin had a considerably high pCO_2 (Figure 4.3b). The highest pCO_2 was calculated to be 36,790 μatm at a tributary sampling site in the QZ sub-basin as a result of low pH. For the middle Yellow River reaches, including the MY and WY sub-basins, the waters were considerably supersaturated with respect to the atmospheric equilibrium, with the pCO_2 mostly in the range of 1000-5000 μatm (Figure 4.3b). In comparison, the pCO_2 level in the lower Yellow River reaches was much higher, and could exceed 10,000 μatm at some sampling sites. Overall, tributaries usually showed higher pCO_2 levels than the mainstem and exhibited larger spatial variations. On average, the pCO_2 in the Yellow River basin was 2800 μatm during the sampling period, which is about 7-fold the atmospheric CO_2 equilibrium, indicating an absolute outgassing trend from the waters to the atmosphere.

The pCO_2 level at most sampling sites also showed strong seasonal variations. High pCO_2 usually occurred in the months before the start of the flooding season (June-September). During the flooding season, the pCO_2 decreased to a relatively low level before it increased from October onwards. The seasonal ratio of pCO_2, expressed as the ratio of pCO_2 in the dry season over that in the flooding season, ranged from 0.8

to 2.35, with >60% ratios in the range of 1.05-1.8. The magnitude of pCO_2 variations differed spatially, with the waters sampled from the middle reaches having larger seasonal differences. In contrast, the upper and lower reaches were characterized by comparatively weak seasonal variations. There was no statistically significant difference in the pCO_2 values between the dry season and the flooding season (p>0.05 by paired t-test).

4.3.3 Estimate of historical CO_2 outgassing fluxes

Based on Horton's law, the empirical relationships between stream order and stream number as well as channel length are shown in Figures 4.6a and 4.6b, respectively. With a higher correlation coefficient (R^2), the relationship between SO and stream number is stronger than that between SO and mean stream channel length. When the SO (x in the equations) was set to 1, the number and the mean channel length of the first order streams could be obtained. There are 14454 first order streams with a mean channel length of about 2570 m (Table 4.2). Comparing the channel widths of typical cross-sections delineated from Landsat images with field measurements indicated a difference of <10% for stream orders 4, 5, and 6. As such, a geometric relationship between channel width and corresponding stream order was fitted to characterize the first order streams (Figure 4.6c). The average channel width for the first order streams is 3.44 m (Table 4.2).

Table 4.2 Hydraulic geometry of stream networks in the Yellow River basin.

Stream order	No	Mean length	Mean width	Surface area	% of total
		m	m	km^2	
1	14454	2570	3.44	128	4.2
2	2062	14283	6.6	194	6.4
3	291	42267	24.9	306	10
4	94	91352	65.9	566	18.6
5	15	279574	86.2	362	11.9
6	1	4920988	303	1491	48.9
Total				3047	100

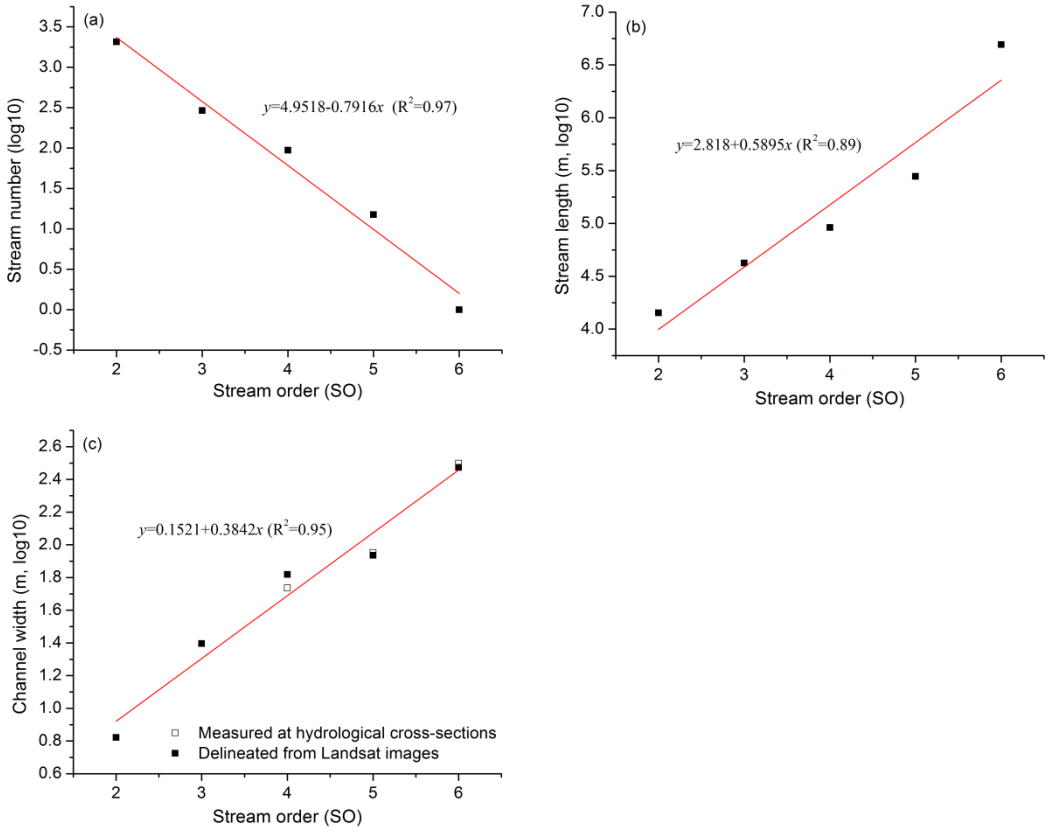

Figure 4.6 Empirical relationships between stream order (SO) and (a) stream number, (b) channel length, and (c) channel width. Note the log transformation on the *y*-axes.

When the stream number, length, and width for each stream order were determined, the total water surface area was quantified per stream order by multiplying the mean channel width per stream order by the summed length of the corresponding stream

order. The total water surface area of the Yellow River basin was estimated at 3047 km^2 (Table 4.2), accounting for around 0.41% of the drainage area. In particular, the mainstem channel (the 6^{th} order) accounts for nearly half of the total water surface area, whereas the smallest streams (the first order) represent only 4.2%. In addition, the number of stream order in the Yellow River basin is relatively small, indicating a lower development level of drainage density.

Interpolation of wind speed indicated significant spatial variability throughout the river basin (Figure 4.7). The headwater catchments, the tributaries near the desert in the NM sub-basin, and the LY sub-basin generally had higher wind speed. The highest wind speed of 6.81 m/s occurred in the LY sub-basin near the estuary. In comparison, wind speed in the middle reaches was relatively low, mostly in the range of 1.3-2.8 m/s. On average, the wind speed is 2.4 m/s for the entire river basin. Since the water sampling sites did not coincide exactly with the meteorological stations, wind speed for the sampling sites was determined from the generated wind speed raster map in Figure 4.7. Then, the obtained wind speed was applied to calculate the gas transfer velocity using Equations 4.2 and 4.3. In addition, ranging from 0.4 to 2.6 m/s, water current velocity concurrently measured at the hydrological stations was put into Equation 4.4 to estimate the gas transfer velocity for the small rivers and streams.

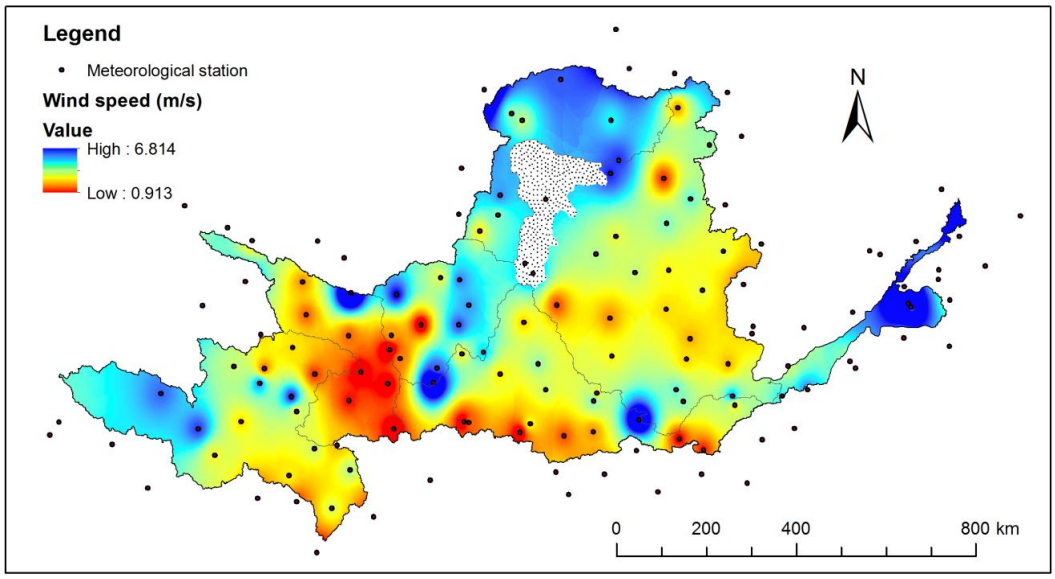

Figure 4.7 Spatial variability of wind speed determined using the ordinary Kriging interpolation method based on 148 meteorological stations (88 stations are within the river basin and 60 stations are around the river basin).

Due to low CO_2 partial pressure (i.e., <380 μatm), waters in the headwater region played a net carbon sink role across the water-air interface, leading to a drawdown of atmospheric CO_2 (Table 4.3; Figure 4.8). The mean CO_2 outgassing flux ranged from -6.3 to -24.5 mmol/m^2/d, depending on the empirical equations used for calculating the gas transfer velocity. With the highest pCO_2, the QZ sub-basin exhibited the highest CO_2 outgassing flux (Figure 4.8), despite its gas transfer velocity being moderate (Table 4.3). In view of individual sampling results, the highest CO_2 outgassing flux of 396.3 mmol/m^2/d (or 1246.4 mmol/m^2/d if using the methods in Alin et al (2011)) was also in the QZ sub-basin. The CO_2 outgassing flux in the Ning-Meng sub-basin (NM) was slightly higher than in the middle Yellow sub-basin (MY), as both the wind speed and TAlk concentration of the former were higher than the latter. In addition, due to the highest gas transfer velocity as a result of high wind speed (Figure 4.7), the CO_2 outgassing fluxes in the lower Yellow reaches (LY) were

significantly high, second only to the QZ sub-basin (Table 4.3; Figure 4.8). The Raymond and Cole (2001) model provides the minimum estimate of the CO_2 outgassing flux. Meanwhile, the Alin et al. (2011) model provides the maximum estimate. Thus, the average gas transfer velocity was 3.82-13.46 cm/h for the entire river basin. This is largely consistent with the widely assumed or measured *k* values in other rivers of 8-15 cm/h (Yang et al., 1996; Richey et al., 2002; Yao et al., 2007; Li et al., 2012). Accordingly, the annual CO_2 outgassing fluxes from the water surface of the Yellow River network system were estimated at $0.98\text{-}3.49\times10^{11}$ mol (or 1.18-4.19 Mt) (Table 4.3). That is, the Yellow River waters acted as an atmospheric CO_2 source with a specific CO_2 outgassing flux of 32.2-114.6 mol/m^2/yr.

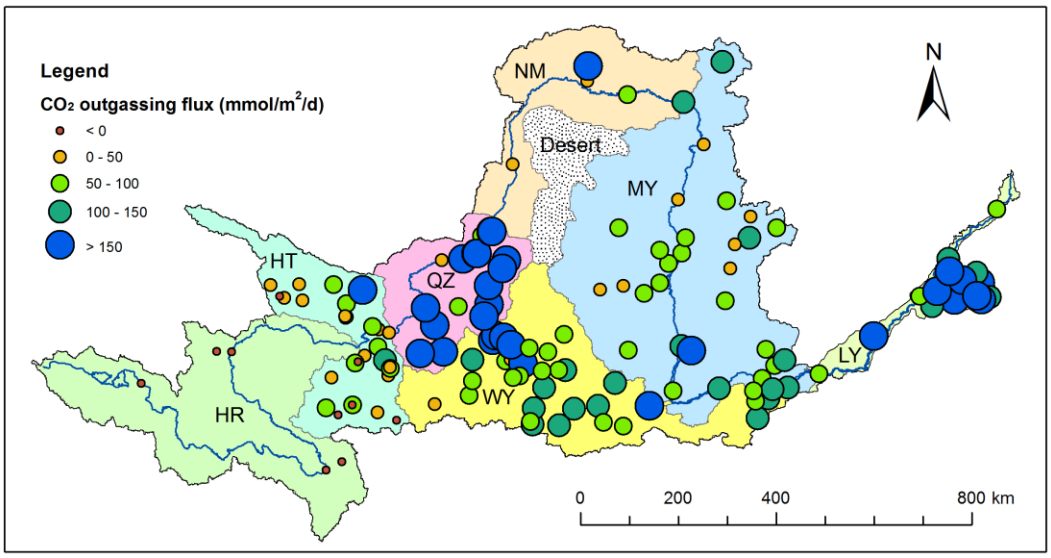

Figure 4.8 Spatial variations of the estimated CO_2 outgassing flux based on the Raymond and Cole (2001) method.

Table 4.3 Sub-basin summary of hydrological characteristics and the estimated CO_2 outgassing flux from the Yellow River basin.

Sub-basin	Drainage area	Water area	*T*	Annual precipitation	Wind speed	*k* (cm/h)		TAlk	CO_2 emission flux (mmol/m^2/d)		Annual CO_2 emission (10^{11} mol/yr)	
	km^2	km^2	℃	mm	m/s	R&C01	Alin11	μmol/l	R&C01	Alin11	R&C01	Alin11
Headwater/HR	143422	695	8.5	510	2.4	3.22	12.51	2013	-6.3	-24.48	-0.016	-0.062
Huang-Tao/HT	73490	180	10.5	415	1.66	2.65	7.88	3231	40.3	119.84	0.026	0.079
Qing-Zuli/QZ	65626	320	11.3	325	2.58	3.76	14.45	4255	252.4	969.99	0.295	1.133
Ning-Meng/NM	85034	442	12.4	273	2.88	4.29	13.91	4478	83.9	272.04	0.135	0.439
Middle Yellow /MY	233435	767	13.6	510	2.21	3.62	12.39	4010	76	260.12	0.213	0.728
Wei-Yiluo/WY	123871	362	14.2	573	2.12	3.48	9.94	3669	99.5	284.2	0.132	0.376
Lower Yellow /LY	27268	281	17	679	3.31	5.71	23.11	2782	192.3	778.29	0.197	0.798
Total/Mean	752146	3047	12.3	496	2.4	3.82	13.46	3491	105.4	380	0.982	3.491

Note: *T* is temperature; *k* is gas transfer velocity; TAlk is total alkalinity; R&C01 and Alin11 represent the two methods proposed by Raymond and Cole (2001) and Alin et al (2011), respectively, in calculating the gas transfer velocity.

4.3.4 pCO_2 and CO_2 outgassing fluxes during 2011-2012

Figure 4.9 shows the weekly results sampled at the Toudaoguai, Tongguan, and Lijin stations during the hydrological year of July 2011- July 2012. Both the TAlk and pCO_2 showed large spatial differences among the three stations. The mean TAlk at Toudaoguai station (4075 μmol/l) was significantly higher than that at Tongguan and Lijin stations (3664 μmol/l and 3580 μmol/l, respectively). Similarly, the mean pCO_2 at Tongguan station (4770 μatm) was also significantly higher than that at Toudaoguai and Lijin stations (1624 μatm and 1347 μatm, respectively). The highest pCO_2 (26,318 μatm) was measured at Tongguan in early May. Furthermore, high sampling frequency made it possible to explore the seasonal variations of TAlk and associated changes in pCO_2 and CO_2 outgassing fluxes. The TAlk was higher in the dry season than in the flooding season at the three stations (Figure 4.9). In particular, the Tongguan station, located immediately downstream of the Loess Plateau, showed the highest difference between the two seasons relative to the other two stations (Table 4.4 and Figure 4.1).

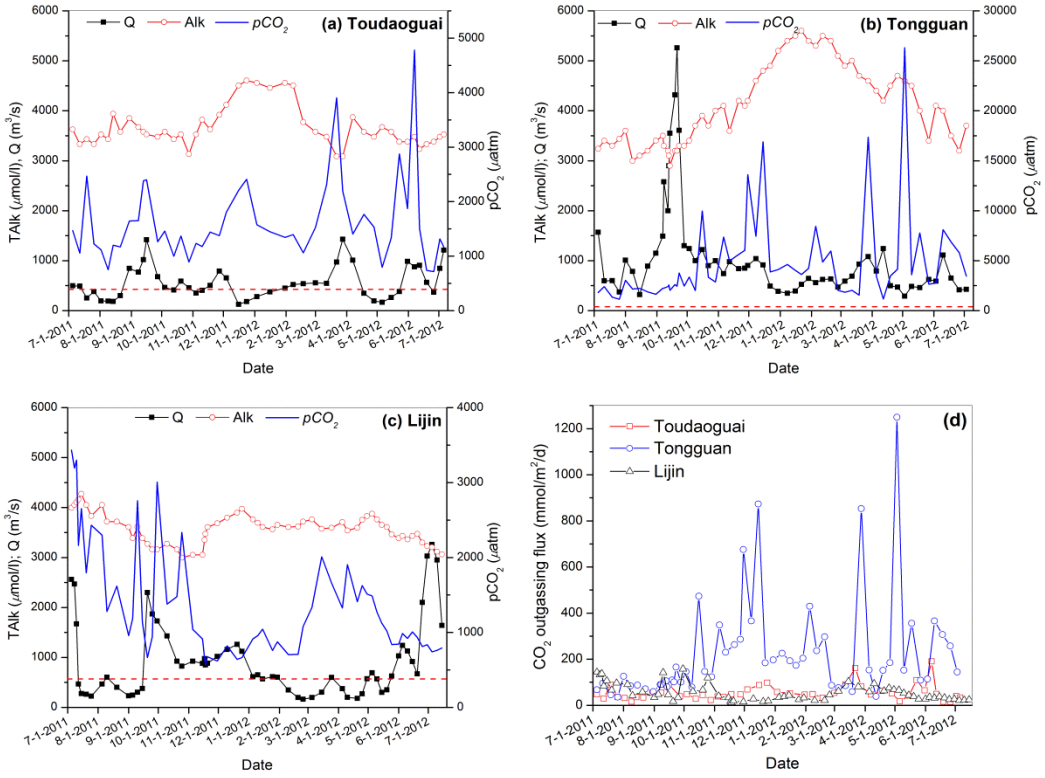

Figure 4.9 Seasonal variations in water discharge (Q), TAlk, *pCO₂*, and CO_2 outgassing flux at the three mainstem stations during July 2011-July 2012. The dotted line denotes the atmospheric CO_2 concentration of 380 µatm. Refer to Figure 4.1 for location.

Likewise, the *pCO₂* showed similar seasonal variations. With a much lower pH (7.72), the *pCO₂* at Tongguan station in the dry season was high at 6016 µatm, which is 2 fold the value in the wet season. In comparison, the difference at Toudaoguai station is much smaller. It is clear that both the TAlk and *pCO₂* increased substantially as waters from the Loess Plateau entered the mainstem channel. However, they decreased along the channel course towards the ocean, as revealed at Lijin station (Table 4.4). In addition, the *pCO₂* showed complex relations with water discharge (Q). While the *pCO₂* changed positively with water discharge at Toudaoguai station, it presented decreasing trends with increasing water discharge in the wet season at Tongguan and Lijin stations (Figure 4.9). As suspend sediment concentration (SSC)

is correlated positively with water discharge, the relationship between pCO_2 and SSC showed trends similar to the pCO_2-Q responses (Figure 4.10). Unlike the positive correlation at Toudaoguai (Figure 4.10a), the pCO_2 decreased quickly with increasing SSC at the two downstream stations (Figures 4.10b and 4.10c). In general, the pCO_2 at all three stations was significantly higher than the atmospheric CO_2 concentration, although the pCO_2 differences between water and the atmosphere varied substantially among different stations or different seasons (Figure 4.9a-c).

Table 4.4 Historical and seasonal differences of pCO_2 and CO_2 outgassing at the three stations.

Station	Item	Historical records		2011-2012	
		Wet season	Dry season	Wet season	Dry season
Toudaoguai	pH	7.89	8.01	8.19	8.11
	TAlk (μmol/l)	3595	4091	3513	3771
	pCO_2 (μatm)	3716	2708	1580	1655
	CO_2 outgassing flux (mmol/m^2/d)	145.1-703.4	108.8-527.6	52-252.1	58.8-285.2
Tongguan	pH	/	/	7.91	7.72
	TAlk (μmol/l)	/	/	3356	4562
	pCO_2 (μatm)	/	/	2927	6016
	CO_2 outgassing flux (mmol/m^2/d)	/	/	121.9-582.5	285.5-1020.1
Lijin	pH	8.18	8.19	8.23	8.28
	TAlk (μmol/l)	2942	3789	3576	3584
	pCO_2 (μatm)	1344	1349	1609	1132
	CO_2 outgassing flux (mmol/m^2/d)	57.4-259.5	62.1-280.8	64-330.4	46.7-211.3

As the CO_2 outgassing flux is heavily dependent on pCO_2 and gas transfer velocity, the computed CO_2 outgassing flux also presented seasonal trends similar to the pCO_2. Specifically, the CO_2 outgassing flux at Tongguan station showed much stronger seasonal variations, whereas it remained largely stable throughout the study period at Toudaoguai and Lijin stations (Figure 4.9d). Despite the low wind speed at Tongguan

station (<3.5 m/s in most time of the year), its CO_2 outgassing fluxes exceeded 1000 mmol/m^2/d, and the average was about 219.5-1049.2 mmol/m^2/d based on the two gas transfer velocity models. In comparison, the averaged CO_2 outgassing fluxes at Toudaoguai and Lijin stations were 56-271 mmol/m^2/d and 54.5-264.9 mmol/m^2/d, respectively, which are roughly a quarter of the Tongguan outgassing flux.

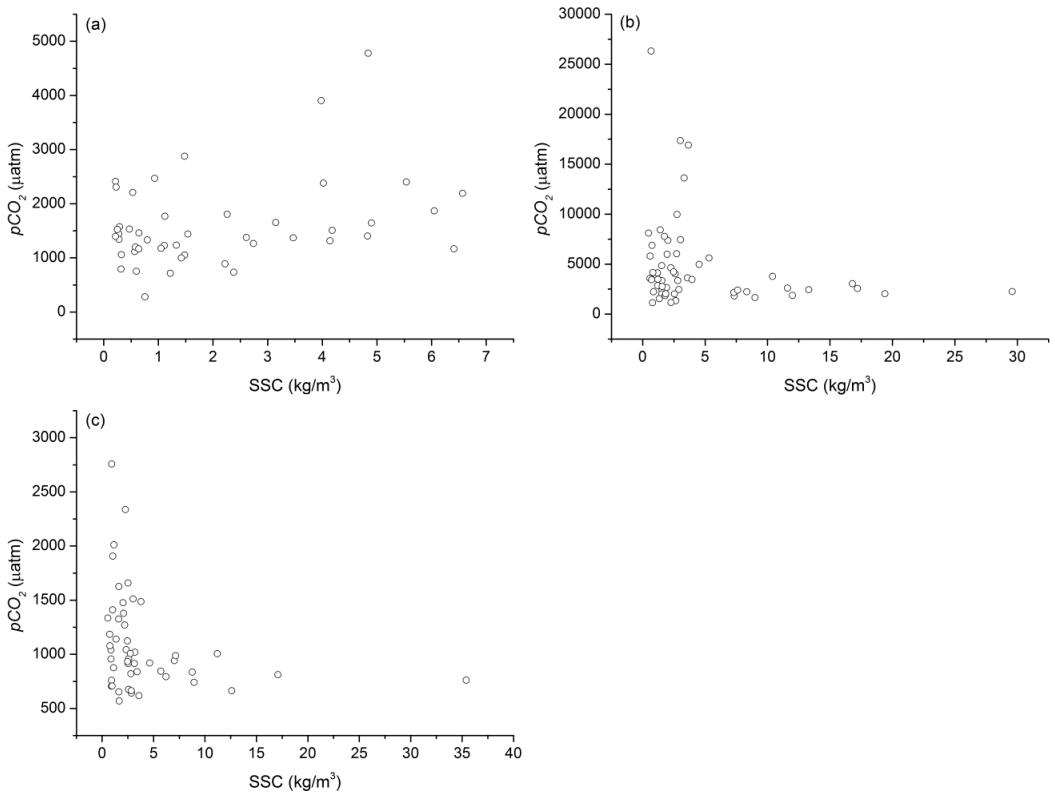

Figure 4.10 Relationship between *pCO_2* and suspended sediment concentration (SSC) at (a) Toudaoguai, (b) Tongguan, and (c) Lijin.

There are also historical hydro-chemical records for comparison at the Toudaoguai and Lijin stations (Table 4.4). It is clear that the pH has increased at both stations over the period. For both the wet and dry seasons, while the *pCO_2* at Toudaoguai station has decreased remarkably over the period, it remained largely unchanged at Lijin station. For the Lijin station, however, although historically the *pCO_2* level was approximately equal between the two seasons, recent field sampling results showed

that it was higher in the wet season than in the dry season. As a result, the CO_2 outgassing fluxes presented a similar change in trend. Overall, compared with the historical records, the CO_2 outgassing flux has decreased by half at Toudaoguai station in both the dry and wet seasons, while it showed a slight increase in the wet season and a 25% decrease in the dry season at Lijin station.

Results of the DIC species calculations for the three stations suggested that HCO_3^- was the dominant component, accounting for 98.4% of the TAlk on average. Taking the Lijin station as the control cross-section for seaward delivery, the total DIC loading discharged into the Bohai Sea during 2011-2012 was computed based on daily water discharge by using Beale's stratified ratio estimator (Parks and Baker, 1997). Approximately, 1.09 Mt of DIC was transported into the ocean during the survey period. In comparison, the average DIC export flux was 2.45 Mt/yr during the 1960s estimated from the historical records, and 1.67 Mt/yr in the early 1980s (Kempe, 1982).

4.4 Discussion

4.4.1 Temporal variability of TAlk and pCO_2

The TAlk concentration of river waters reveals the buffering capacity of waters in a carbonate system to neutralize acids and bases. Due to abundant outcrops of carbonates, groundwater in the Yellow River basin was highly alkaline (Chen et al., 2002a), which directly resulted in the higher TAlk concentration in the dry season when baseflow accounted for 90% of the river runoff. High TAlk concentration in the

Loess Plateau was probably the result of chemical weathering processes. Accelerated by physical erosion, chemical weathering of rocks and soils in the loess deposits is strong. As a result, waters from the Loess Plateau are characterized by exceptionally high dissolved solids with HCO_3^- being the dominant ion (Zhang et al., 1995a; Chen et al., 2005).

The long-term stable TAlk concentration in Figure 4.4 is in contrast with other dissolved solutes that showed persistent increasing trends, as indicated by Chen et al (2005). Although human activities have been proposed as the major reason for the increasing concentrations of other dissolved solutes (Chen et al., 2005), it seems that the TAlk concentration was not significantly affected. Natural weathering processes may have played a much more important role relative to humans in determining the trend in TAlk. As for the relationship between TAlk and water discharge, the TAlk concentration did not decrease at the same rate as the water during the flooding period. Rather, it decreased slightly as indicated by the exponent in the equation (see Figure 4.5). A narrower range of the TAlk concentration changes suggested the coupling results of enhanced export of alkalinity during the flooding season and the dilution effect of water discharge (Piňol and Avila, 1992; Raymond and Cole, 2003).

Riverine pCO_2 is an indicator of the internal carbon dynamics and external biogeochemical processes of the terrestrial ecosystems for a drainage basin (Jones et al., 2003). Four main processes determining the pCO_2 of river waters are: (i) production and transport of soil CO_2; (ii) *in situ* respiration and decomposition of

organic matter; (iii) aquatic photosynthesis; and (iv) CO_2 emission across the water-air interface (Richey, 2003; Yao et al., 2007). Whereas the first two processes are able to increase the pCO_2 level of the water column, the other two processes tend to reduce the pCO_2. Whether the river waters are supersaturated with CO_2 depends on the balance between these processes, which further have different environmental controls.

Carbon in river waters is largely derived from biogeochemical processes occurring in terrestrial ecosystems (Finlay, 2003). Thus, changes in terrestrial ecosystems involving carbon dynamics will likely affect riverine carbon transport. Soil CO_2 content responds positively to seasonal variations of climate variables such as temperature (Epron et al., 1999; Hope et al., 2004). The significant seasonal variations of pCO_2, with the maxima occurring in the dry season and the minima in the wet season, at most tributary stations in the Yellow River basin were likely due, in part, to varying soil CO_2. In addition, riverine pCO_2 could be affected by precipitation intensity and flow regimes (Finlay, 2003; Yao et al., 2007). The Yellow River basin is characterized by high-intensity rainfalls, and several storms could account for >70% of the annual precipitation (Zhao, 1996). Without sufficient time to infiltrate into deep soil horizons, the overland runoff generated by high-intensity rainfalls would have diluted the TAlk and reduced the riverine pCO_2. This could explain the relatively low TAlk and pCO_2 in the flooding period, despite the strong chemical weathering.

The mainstem stations exhibited more complex seasonal patterns than the tributary sampling sites (Figure 4.9). The highest pCO_2 at Toudaoguai and Tongguan stations

occurred in March through May before the flooding season, which is probably due to ice-melt floods during the period. In the winter months with temperature below zero, the river water surface in the upper Yellow River reaches will be frozen until early spring. Due to ice protection at the water-air interface, aqueous CO_2 could not be efficiently released into the atmosphere. As a result, CO_2 typically accumulates in the river waters below the ice cover. With increasing temperature in early spring, the ice begins to thaw and the high-pCO_2 river waters are exported downstream towards the sampling stations, causing the pCO_2 to increase sharply. Below Tongguan station, the river waters are heavily regulated by a cascade of reservoirs, such as the Sanmenxia and Xiaolangdi reservoirs (Figure 4.1). These reservoirs usually store water until late June to create man-made flows for sediment flushing in the lower Yellow River mainstem channel. Consequently, the pCO_2 at Lijin showed a completely different seasonal pattern from the upstream two stations. These significant differences in hydrological regime may have also caused the different relationships between pCO_2 and SSC as shown in Figure 4.10.

Due to trapping of water and suspended solids within the reservoirs, the river-borne carbon dynamics are altered (Cole et al., 2007), depending on the regulation magnitude of the reservoirs on water delivery. Firstly, respiration and degradation of organic matter would be accelerated in static reservoir waters with extended residence time, thereby increasing the riverine pCO_2. Although photosynthesis of aquatic plants tend to represent CO_2 uptake in general, aqueous photosynthesis in the Yellow River appears to be at a low level given the highly turbid environments and thus light

limitation (Chen et al., 2005). Secondly, reduced turbulence would lower the gas transfer velocity across the aqueous boundary layer (Raymond and Cole, 2001; Teodoru et al., 2009), restraining the aqueous CO_2 evasion into the atmosphere and thus a high TAlk and pCO_2 in the waters. Starting from late June, when man-made flows were released from the reservoir sluice gates, the deep water with supersaturated CO_2 is first discharged downstream (Wang et al., 2011a; Ran et al., 2013a), resulting in the high riverine pCO_2 at Lijin station (Figure 4.9c). The duration of high pCO_2 at Lijin coincided with the sediment flushing period, highlighting the impacts of flow regulation on pCO_2 dynamics.

Differences in the hydro-chemical variables between the historical records and recent sampling results revealed temporal changes over the period. Significant increase in pH at Toudaoguai station was largely caused by widespread salinization of agricultural soils. There are two large irrigation zones upstream of Toudaoguai, and large quantities of water are diverted from the river for desalination and irrigation every year (Chen et al., 2005). In the recent decades, the diverted water volume has increased gradually due to growing demand (Ran et al., 2013a). As a result, when washed out from the irrigated farmlands, the return water characterized by high pH has resulted in increased riverine pH. This has further led to greatly reduced riverine pCO_2 and CO_2 outgassing flux, despite the roughly stable TAlk through the period. In addition, the magnitude of reduction was much higher in the wet season when the high-pH return water reached the mainstem with floods (Table 4.4).

In contrast, gentler changes at Lijin station suggested strong buffering capacity of the sub-basin downstream of Toudaoguai in mediating the hydro-chemical concentrations. While reservoir operation was responsible for the observed seasonal differences as discussed earlier, it has also affected the inter-annual variations. Large-scale joint operation of reservoir cascades since 2000 has altered the hydrological regime in the middle and lower Yellow River, resulting in higher TAlk delivery in the wet season. Accordingly, the pCO_2 and CO_2 outgassing fluxes were elevated compared with the 1960s-1984 baseline period (Table 4.4). Furthermore, soil conservation and vegetation restoration widely carried out on the Loess Plateau may have also contributed to the inter-annual changes. More organic carbon has been sequestrated as a result of these aggressive land management practices (Chen et al., 2007b). Given the strong flushing and leaching effects of intensive rainfalls, it is expected that the riverine carbon export has been increased during the wet season. Consequently, decomposition of organic carbon has increased the riverine TAlk concentration and promoted CO_2 emission.

It can be concluded that the observed temporal changes of the TAlk concentration and riverine pCO_2 in the Yellow River waters were caused by natural processes and human activities. In particular, human activities have changed the seasonal patterns by altering the hydrological regime and carbon delivery processes. With continuously enhanced human impacts during the past three decades, the TAlk and associated pCO_2 dynamics have been significantly altered. These changes will be more obvious

in future with stronger anthropogenic perturbations which are certain to occur given the present economic development within the basin.

4.4.2 Spatial patterns of TAlk and pCO_2

The pCO_2 in the headwater region was below the atmospheric CO_2 equilibrium, indicating a net atmospheric CO_2 drawdown. As such, the headwater region acted as a carbon sink with negative CO_2 outgassing fluxes (Table 4.3). The lower pCO_2 was mainly caused by comparatively low TAlk and high pH. Statistical analyses showed that the TAlk in the headwater region is 25% lower than the basin average, while the pH is around 7% higher. With a mean elevation of >3000 m, temperature in this sub-basin is quite low (Table 4.3). It decreases to below zero during the long winter months from October to March. Ground vegetation is characterized by an alpine meadow ecosystem without strong impacts from human activity except grazing. Due to the low temperature, decomposition of organic matter by microbial activities and ecosystem respiration was kinetically inhibited (Kato et al., 2004). Furthermore, the low temperature may have also restricted chemical weathering, although the major rock outcrops in the sub-basin are shales, granites, and limestone (Wu et al., 2005). Collectively, these processes have resulted in the low TAlk in the riverine waters.

However, it should be noted that, unlike the historical records that were sampled monthly, field sampling in the headwater region by Wu et al (2005) was conducted during the late May and June when the flooding season had barely started. Given the enhanced flushing effect of soils by infiltrating rainfall and snowmelt flows in the

beginning period of the wet season (Clow and Drever, 1996; Melack, 2011b), the resultant riverine TAlk and pCO_2 are expected to be close to the peak. With the potentially highest pCO_2, the CO_2 exchange flux appears to be the minimum. In other words, the TAlk and pCO_2 in other seasons would be much lower, suggesting a greater pCO_2 difference across the water-air interface and thereby a stronger CO_2 drawdown.

High TAlk in the QZ sub-basin was primarily determined by its geological features. Carbonates, detritus, and red-beds are common in the tributary catchments (Zhang et al., 1995a), which are susceptible to weathering. As a result, its mean TDS concentration was 8-14 times that of the Yellow River basin average (Chen et al., 2005). Some streams in the sub-basin are nicknamed as “bitter streams” due to the extraordinarily high concentrations of dissolved solids. Furthermore, the sub-basin is characterized by a high drought index with the annual evaporation up to >8 times the annual precipitation (Chen et al., 2005). Such strong evaporation would result in not only the precipitation of minerals with low solubility, such as gypsum and halite, but also the elevated concentrations of the solutes not removed during the crystallization process. Another possible reason is the lack of vegetation protection, which could indirectly enhance chemical weathering by accelerating physical erosion. As a result, the DIC species in the riverine waters were highly condensed, leading to high pCO_2 and CO_2 outgassing fluxes (Figures 4.3b and 4.8) coupled to strong wind turbulence (Figure 4.7).

Downstream variations of the TAlk and pCO_2 along the mainstem stations indicated that the waters from the Loess Plateau had higher TAlk and were more supersaturated with CO_2 than the upper and the lower Yellow River waters (Figure 4.11). As stated earlier, the Loess Plateau is characterized by severe physical erosion. Physical erosion accelerates chemical weathering by increasing the exposure surface of fresh minerals to atmosphere (Millot et al., 2002; Gabet et al., 2010). In addition, dry climate allows the soil horizons to adequately interact with the atmosphere. Consequently, chemical weathering of loess deposits, which are abundant in carbonates, is strong, generating huge quantities of HCO_3^- into the stream and river waters.

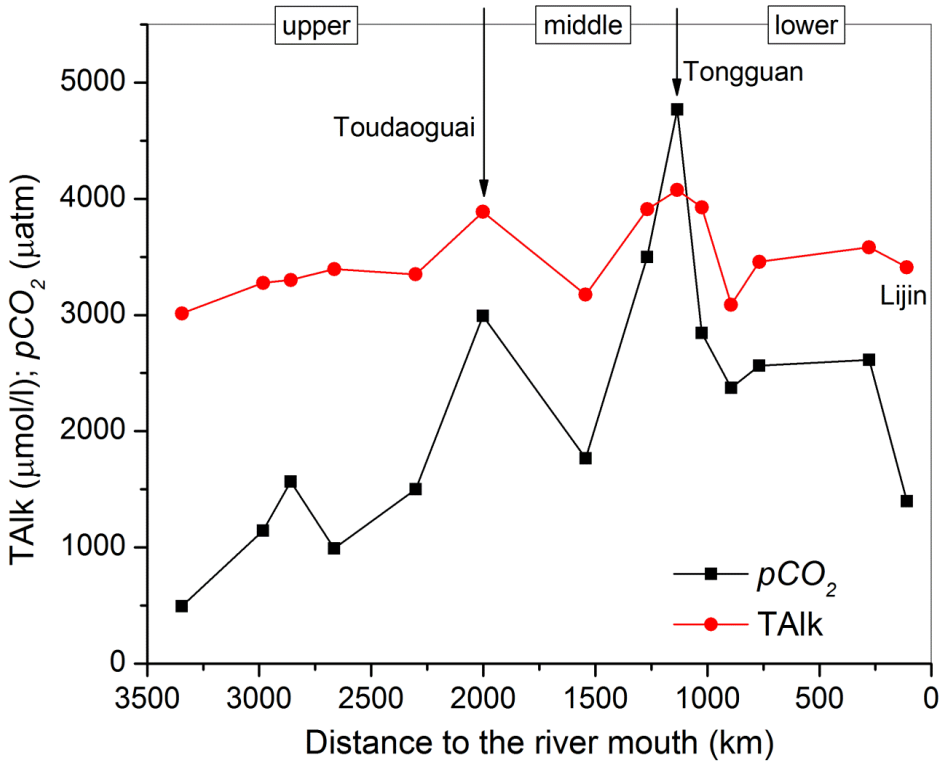

Figure 4.11 Downstream variations of historical TAlk and pCO_2 along the mainstem channel. The stretches between Toudaoguai and Tongguan stations approximately represent the Loess Plateau region. Note that waters in the lower Yellow River were not regulated by reservoirs until 2002 after the Xiaolangdi Reservoir was completed.

As for the human impacts, agriculture in the middle Yellow River basin has been conducted for more than 2000 years (Chen et al., 2005). Tilling practices can not only increase the exposure area of soil materials, but also alter the hydrology regime of surficial soils, increasing the contact rate between water and minerals and the alkalinity export as a result (Raymond and Cole, 2003). Dissolution of soil CO_2 and oxidation of organic matter in agricultural fields are also likely to boost alkalinity production. Furthermore, due to anthropogenically induced rainfall acidification, significantly decreased pH in Chinese croplands (e.g., the middle and lower reaches for the Yellow River basin) has been widely detected (Guo et al., 2010). The decreased pH may also explain the elevated pCO_2 in these regions compared with the headwater sub-basin's higher pH (Figure 4.4).

Increasing pCO_2 until the Tongguan station suggested the responses of pCO_2 to the factors discussed above. Because no large tributary occurs in the lower Yellow River basin, the decreasing TAlk concentration and pCO_2 revealed the reduced TAlk supply and continuous CO_2 evasion (Figure 4.11). In addition, the gas transfer velocity was gradually elevated due to increased wind speed towards the river mouth (Figure 4.7), which contributed to a certain extent to the sharply reduced pCO_2 at the lowermost Lijin station. In brief, the spatial variations of the TAlk and pCO_2 along the Yellow River mainstem channel were the combined results of the differences in soil properties, climate characteristics, geomorphological development, and human impacts.

4.4.3 CO_2 outgassing and lateral DIC export

In estimating the CO_2 outgassing fluxes, one of the greatest uncertainties is in assessing the gas transfer velocity. Except wind speed and flow velocity considered here, gas transfer velocity could also be affected by other factors as mentioned earlier. Indeed, daily wind speed tends to be highly variable, and wind direction is also variable. The inherent variations could influence the gas transfer velocity (Wanninkhof, 1992). Therefore, the used gas transfer velocity derived from mean wind speed may have resulted in errors in estimating the actual CO_2 outgassing. However, as the obtained *k* values, 3.82-13.46 cm/h on average, are comparable with the widely found *k* in other rivers, the resultant CO_2 emission fluxes are reasonable.

Although the smallest streams represent a very small proportion of the estimated total water surface area, their significance in CO_2 degassing cannot be overlooked (Rasera et al., 2008; Davidson et al., 2010). Also, a considerable fraction of aqueous CO_2 in groundwater would have evaded into the atmosphere in a very short distance after emerging from springs or seeps into streams. For example, the first- or second-order streams are usually observed to have higher gas transfer velocity than the large rivers (Alin et al., 2011). The calculated CO_2 outgassing flux in this study is probably conservative, as the sampling stations are all located on higher stream order channels while monitoring CO_2 emission near the springs of groundwater is lacking. Furthermore, some small streams are intermittent and ephemeral with water flowing only in the wet period, thus their water surface area can be extremely variable.

Considering their small proportion accounting for the total area (Table 4.2), however, the effects of surface area changes on total CO_2 outgassing estimation are limited.

In a drainage basin, wetlands and inundated floodplains are another significant carbon sources for the atmosphere, and are sometimes more important than the stream and river waters. For the rivers draining tropical environments for example, because wetlands are well developed and floodplains are inundated during the wet season, their contribution to total CO_2 emission from inland waters could be high (Richey et al., 2002; Cole et al., 2007). Incorporating the CO_2 outgassing from these additional sources would definitely increase the total CO_2 emission flux. With respect to the Yellow River basin, wetlands are poorly developed except in the headwater areas and near the river mouth due to dry climate and low precipitation. Their area is negligible as compared to the delineated water surface area of streams and channels. Furthermore, the mainstem channel, which contributes to about 50% of the total water surface area (Table 4.2), is mostly confined by artificial levees. Hence, unlike (sub)tropical rivers located in humid environments with high precipitation, the total water surface area of the Yellow River basin does not change significantly between the dry and wet seasons. The impacts of not taking wetlands and floodplains into account in the CO_2 outgassing estimate are minor. Overall, the outgassing flux of 0.98×10^{11} mol/yr may represent the minimum estimate, and the flux of 3.49×10^{11} mol/yr could be regarded as the maximum based on available datasets, although the estimate is still conservative and warrants further research.

The seaward DIC export from the Yellow River has experienced a stepwise decrease. Based on the 1960s' DIC export level, it has decreased by 56% to present 1.09 Mt C/yr with a mean reduction rate of 0.03 Mt/yr. If compared to the DIC export level of the early 1980s, the reduction rate is 0.02 Mt/yr. Lower reduction rate in the recent 30 years indicated that the DIC export decreased more rapidly during the period 1960s-1980s. The remarkable decrease in DIC flux is consistent with the reduced water discharge, which has decreased from about 55 km^3/yr in the 1960s to 30 km^3/yr in the early 1980s, and further to the present of 19 km^3/yr (see Chapters 2 and 3). These rapid reductions were largely caused by widespread human activities. Since the 1970s, large-scale soil conservation and water diversion programmes have been carried out in the basin, resulting in decreased mainstem flow and DIC export.

4.4.4 Implications of CO_2 outgassing from the Yellow River

With a global average of 3230 μatm, the riverine pCO_2 showed significant spatial variations worldwide (Table 4.5). Tropical rivers generally have higher pCO_2 compared with temperate rivers. This is likely due to the high temperature and precipitation of tropical environments, which are able to enhance soil CO_2 content, and consequently raise the riverine pCO_2 level via baseflow and interflow (Hope et al., 2004; Liu et al., 2010). *In situ* oxidation of organic materials that are abundantly supplied in tropical river basins could also contribute to the higher pCO_2 (Li et al., 2012). Located in an arid-semiarid climate zone with low temperature and precipitation, the Yellow River waters are more oversaturated with CO_2 than most world rivers. Its relatively high pCO_2 is mostly the result of strong chemical

weathering as revealed by the extremely high TDS concentration and the predominance of HCO_3^- in the dissolved constituents. Other contributors, extensive land use changes for example, could have also enhanced the riverine pCO_2 by facilitating the delivery of weathering products into the river network.

The ratio of CO_2 emission into the atmosphere relative to fluvial export of DIC to the ocean reflects the re-distribution of carbon supplied from upstream drainage systems. For example, in the Amazonian river system, the CO_2 efflux to the atmosphere is about 13-fold the fluvial export of DIC to the Atlantic ocean (Richey et al., 2002). Similarly, for the subtropical Yangtze River basin during the period of the 1960s-1970s, its waters exported about 1.8-2.9 times more carbon by CO_2 emission to the atmosphere than by seaward DIC transport (Wang et al., 2007a). In comparison, the total CO_2 evasion from the temperate Yellow River accounts for around 171% of the seaward DIC flux of the 1960s, or 251% of the early 1980s level, if the maximum of 4.19 Mt/yr is used. In addition, the minimum outgassing flux (1.18 Mt/yr) is approximately equal to the present seaward DIC flux (1.09 Mt C/yr). The magnitude of CO_2 efflux over seaward DIC flux is dependent on the climatic and geomorphological differences existing among different river drainage basins. These characteristics are likely to restrain CO_2 emission, resulting in lower percentages. Another extreme example is the further north Ottawa River, where the CO_2 evasion to the atmosphere represents only 30% of the seaward DIC flux (Telmer and Veizer, 1999).

From a global perspective, the contribution of CO_2 emission from the Yellow River network to the global total CO_2 efflux from rivers (0.23 Gt C/yr, see Cole et al., 2007) is great, accounting for about 0.5-1.8%. Given that the smallest stream channels were not effectively measured and that the river network delineated from the DEM dataset might have underestimated the actual water surface area, the obtained CO_2 outgassing fluxes should be regarded as conservative. If field sampling on the smallest streams is conducted in future, combined with more accurate estimate of water surface area from higher resolution images, present uncertainties could be better constrained and a higher basin-wide CO_2 outgassing flux is anticipated. Overall, the conclusion that the Yellow River network system is an atmospheric CO_2 source can be explicitly made.

Table 4.5 Comparison of pCO_2 and CO_2 outgassing flux of world rivers.

River	Country	Climate	pCO_2	CO_2 outgassing flux	Reference
			μatm	$mol/m^2/yr$	
Amazon	Brazil	Tropics	4350±1900	69	Richey et al., 2002
Ottawa	Canada	Temperate	1200	14.2	Telmer and Veizer, 1999
St. Lawrence	Canada	Temperate	576 (Spring) 207(Autumn)	8.7-30.4 (Spring) -3.4--11.8 (Autumn)	Yang et al., 1996
Hudson	USA	Temperate	1125±403	5.8-13.5	Raymond et al., 1997
York River estuary	USA	Temperate	1070±867	6.3 (Dec 1996-Dec 1997)	Raymond et al., 2000
Elbe inner estuary	Germany	Temperate	580-1100 (April)	65.7	Frankignoulle et al., 1998
Thames inner estuary	UK	Temperate	505-5200 (Nov) 465-4600(Sept)	105.9 (Nov) 76.7 (Sept)	Frankignoulle et al., 1998
Yangtze (Datong)	China	Subtropics	1297	14.2-54.4	Wang et al., 2007
Yangtze estuary	China	Subtropics	650-1440	15.5-34.2	Zhai et al., 2007
Xijiang (Pearl)	China	Subtropical monsoon	2600	69.2-130	Yao et al., 2007
Lower Mekong	(SE Asia)	Tropical monsoon	1100	28	Li and Lu, 2013
Godavari estuary	India	Tropical monsoon	<500-33000	52.6	Sarma et al., 2011
World rivers	/	/	3230	33.9	Cole and Caraco, 2001
Yellow	China	Temperate (arid)	2800±1900	32.2-114.6*	This study

*It is the averages based on all sampling stations in Figure 4.1, not on the sub-basins as shown in Table 4.3.

4.5 Summary and conclusions

Although lateral carbon delivery by rivers has been fairly well documented, CO_2 outgassing from river waters was only recently recognized in evaluating carbon cycling. In this chapter, the dynamics of riverine pCO_2 throughout the Yellow River network was investigated using historical records of water chemistry (1950s-1984) and recent sampling at three hydrological stations along the mainstem channel. The pCO_2 values at all stations but the headwater region were well above the atmospheric CO_2 equilibrium (i.e., 380 μatm) during the survey period, with an average pCO_2 of 2800 ± 1900 μatm. Generally, the Yellow River basin acted as an atmospheric CO_2 source except for the headwater region that was a carbon sink. The pCO_2 levels presented significant spatial variations, with the middle reaches (the Loess Plateau) showing higher pCO_2 than the upper and lower reaches. In addition, tributary waters usually showed higher pCO_2 levels than the mainstem waters. From a seasonal perspective, the pCO_2 varied from about 200 μatm to >30,000 μatm with high pCO_2 occurring in dry seasons. Specifically, high pCO_2 usually occurred from March through May before the flooding season, suggesting a pCO_2 response to ice-melt floods. The spatial and temporal variability of pCO_2 was the result of a myriad of factors, including terrestrial ecosystem, soil properties, and hydrology regime. Human activities, flow regulation by reservoir operation in particular, could also significantly alter its seasonal patterns.

As a result of the uncertainties in gas transfer velocity, the riverine CO_2 outgassing fluxes were estimated in the range of -24.5 and 970 mmol/m^2/d (based on the Alin et

al (2011) model), with the lowest in the headwater region and the highest in the Qing-Zuli tributaries. Based on two gas transfer velocity models, the mean CO_2 outgassing fluxes of the Yellow River waters were estimated at 32.2-114.6 mol/m^2/yr. Consequently, the total CO_2 outgassing fluxes were 0.98-3.49$\times10^{11}$ mol/yr, or 1.18-4.19 Mt/yr. Such a large range suggests that alternative methods like direct measurements of pCO_2 and carbon outgassing are urgently needed. However, given the range of the estimated k values, the present CO_2 outgassing fluxes are acceptable. From a global perspective, the contribution of CO_2 emission from the Yellow River accounted for about 0.5-1.8% of the global total CO_2 efflux of 0.23 Gt/yr from rivers.

Considering the uncertainties in the gas transfer velocity and the possibly underestimated water surface area, the obtained CO_2 outgassing fluxes may have been underestimated. In future with more accurate quantification of gas transfer velocity and the areal extent of water surface, the CO_2 outgassing flux would be increased. It is evident that the weight of the Yellow River in global CO_2 emission from rivers will increase as a consequence. In addition, although with several limitations, using remote sensing images to delineate water surface area is an effective and efficient approach for CO_2 outgassing studies. This is particularly helpful for large river basins like the Yellow River where large-scale field observations are difficult to conduct. It is expected that, with the availability of higher-resolution images, the size of the smallest and most dynamic streams could be better determined. Taking into account the smallest streams in assessing watershed carbon budget could reveal a greater role for river networks in global biogeochemical cycling.

Chapter 5 Delineation of reservoirs and their storage capacity estimate

Sediment trapping by constructed dams in the Yellow River basin is a major reason for the observed reductions in seaward sediment and carbon export (Wang et al., 2007b; Peng et al., 2010). To fully evaluate the impact of soil erosion on the basin-wide organic carbon cycle, it is critical to first quantify the amount of sediment deposition behind dams. By using remote sensing images and hydrological records measured at gauge stations, the completed reservoirs were delineated and their storage capacities were estimated, from which the deposited sediment was estimated (Chapter 6) for assessments of associated organic carbon burial.

5.1 Introduction

Due to the non-conformity of human requirements for water and water resources distribution, a large number of reservoirs are constructed along rivers around the world to meet humans' various demands. By altering the spatial and temporal distribution of water, reservoirs provide a regulated water supply to meet a range of social, economic and environmental needs, including power generation, agricultural irrigation, domestic consumption, and flooding prevention (Lehner and Döll, 2004), which greatly reduce the reliance on the natural availability of water. Driven by rapid economic development and higher requirements for living standards, recent statistics show that globally about 70% of rivers are intercepted by large reservoirs (Nilsson et al., 2005). Currently, more than 45,000 dams over 15 m high are put in operation by dam builders worldwide, which represent nearly an order of magnitude greater

number than in 1950 (World Commission on Dams, 2000). Because of water impoundment, these completed reservoirs have even reduced the magnitude of global sea level rise by 0.55 mm/yr (Chao et al., 2008). In recent decades, more dams have been constructed in countries with rapidly developing economies, such as China, to meet the needs of growing populations (McNally et al., 2009; Kummu et al., 2010). According to Zhang et al. (2008b), owing to the high temporal and spatial variability of climate, more than 85,000 reservoirs have been constructed in China to tap the available water resources to serve various conservation purposes and to control flooding. In view of the limited availability of good storage sites, it is important to preserve the live storage capacity of constructed reservoirs. Therefore, there is a great need to continuously evaluate the quantity of actual storage loss resulting from sedimentation and update control measures at the reservoir and basin levels.

Traditionally, reservoir distribution and storage capacity estimation are evaluated by measurements of topographic maps based on *in situ* hydrographic survey with electronic planimeter, which consists of both overwater and underwater topographic surveys (Butcher et al., 1993; Onikienko, 1995; Peng et al., 2006). Most often, an acoustic detector is used for an underwater topographic survey while overwater topographic survey could only be completed through field or aerophotogrammetrical surveys. Consequently, the traditional approach is usually laborious, costly and time-consuming, and even could not meet the general requirements for secure operation. For example, using the traditional approaches the storage measurement of the Longyangxia Reservoir in China cost 2 million Yuan (320,000 USD) and required 8

years, but the investigation results were still unsatisfactory (Zhang et al., 1999). In addition, due to the complexities of terrain variability and the discrepancies of different devices adopted, precise estimates for reservoirs constructed in larger basins are usually hard to achieve. Furthermore, a long-lasting hydrographic survey would influence a reservoir's normal operation. All these shortcomings indicate that a new method is urgently needed to conduct large-scale reservoir investigation.

With the advent of remote sensing technology supported by cyclic satellites, monitoring reservoirs by means of satellite images has become convenient and far less expensive (Wang and Li, 1998; Goel et al., 2002; Marcus and Fonstad, 2008). Meanwhile, the real-time technology allows for large-scale observation and calculation at different spatial scales. Spatial, spectral, and temporal attributes of remote sensing data provide invaluable and timely information for reservoir operation and management (Sebastian et al., 1995; Goel et al., 2002; Liebe et al., 2003; Mialhe et al., 2008; Rodrigues and Liebe, 2013). However, although the new technology has been widely used in water resource management and environment pollution monitoring (Verdin, 1985; Wang et al., 2004), it has neither been devoted to reservoir delineation and spatial distribution, nor to quantitative estimation of water volume stored in reservoirs and its residence time (Liu and Dai, 1996; Zhou et al., 1998; Goel et al., 2002; Propastin, 2008). The available few studies were mainly focused on individual reservoirs or conducted in quite small watersheds. As a result, only some tentative applications have been reported (Gupta and Bodechtel, 1982; Duane Nellis et al., 1998; Magome et al., 2002). In contrast, applications to a cluster of reservoirs

or in large-scale basins like the Yellow River are rare. More importantly, the residence time analysis of reservoir waters through satellite images will be an important innovation for the traditional analysis strategies.

In order to fully utilize the water resources for multiple purposes, a great number of dams have been built in the Yellow River basin since the 1960s (Waterpub, 2007). Of these, 171 are large- and medium-sized (particularly, 23 large reservoirs). The total water volume stored in the 171 reservoirs is around 33.6 km^3 (YRCC, 2007), representing approximately 54% of the annual water discharge of the entire river basin (based on the reconstructed natural water discharge by Li and Yang, 2004). The total storage capacity of all the registered reservoirs has been estimated to be about 72 km^3, which is ~116% of the natural annual water discharge. However, most of these reservoirs have not been registered on a map for management and research purposes. Considering the basin's distinctive characteristics that annually large amounts of sediment and organic carbon is carried into channels, reservoir sedimentation and the resulting storage capacity losses have significantly affected water availability and the basin-wide organic carbon cycle. With attempts to better understand riverine carbon transport within the basin and analyze associated hydrological processes, an accurate assessment of reservoir spatial distribution and storage volume is needed.

The objectives of this chapter, therefore, are (1) to identify the artificial reservoirs constructed in the Yellow River basin and their spatial distribution using remote sensing images; (2) to quantify the actual storage capacity of the reservoirs through

establishing empirical relationships; and (3) to analyze the impacts of reservoir operation on flow regulation in combination with natural water discharge and the recently measured dataset. Finally, the applicability and limitations of remote sensing in reservoir management were evaluated.

5.2 Runoff characteristics of the Yellow River

As a result of low annual precipitation, water discharge of the Yellow River is low. Although its drainage basin area accounts for about 8% of the total land area of China, runoff in the basin represents only 2% of the total runoff (Fu et al., 2004). Moreover, the amount of water resource present in the watershed per capita is only ¼ of the average in China and about 1/16 of the global average. As discussed in Chapter 2, spatially uneven distribution of precipitation has resulted in serious water-related problems (Xin et al., 2011).

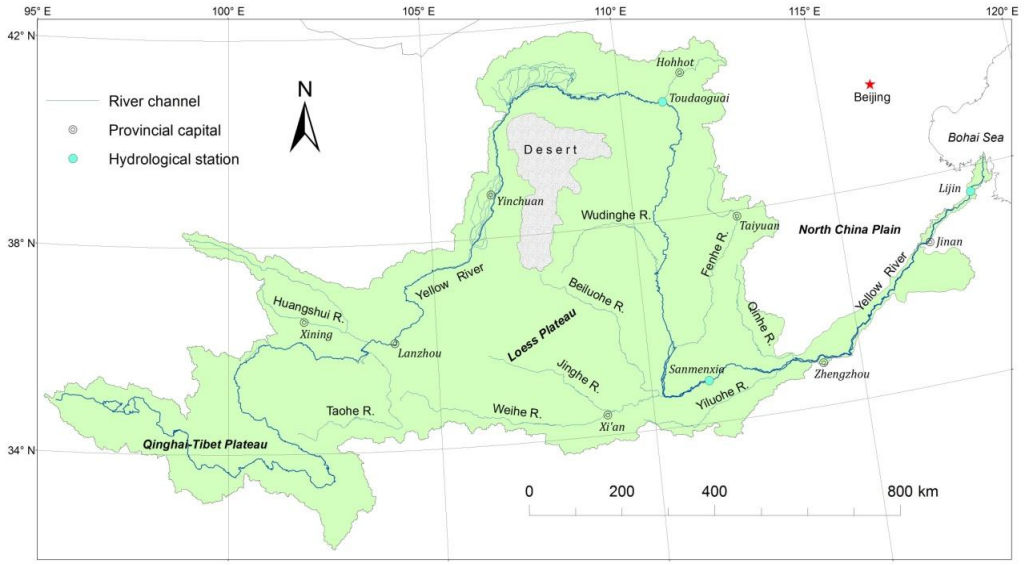

Figure 5.1 Sketch map of the Yellow River basin and the locations of major tributaries and cities.

The water discharge has decreased sharply in recent decades, apparently in response to climate change and anthropogenic influences (Peng et al., 2010). For the whole basin, while the mean annual water discharge at Lijin station during the period 1950-1959 was about 47.4 km^3, it has declined to only 14.1 km^3 in the past decade (2000-2009). In order to examine the impact of human activities on water resources and hydrological cycle, several studies have been reported regarding the reconstruction of natural water discharge (e.g., Zhao, 1996; Li et al., 2001; Mu et al., 2003; Li and Yang, 2004). According to Li and Yang (2004), the mean annual water discharge at Toudaoguai station was 35.77 km^3 (the upper reaches). For the whole basin, it was 62.23 km^3 as reconstructed at Lijin station. Based on recent hydrological records since 2000, the annual water discharge at the two stations has decreased by 58% and 77%, respectively. The higher reduction at Lijin station indicates the magnitude of water withdrawal from the lower Yellow River, which is consistent with the distribution of major irrigation zones (see Figure 2.6).

Almost all the large and medium reservoirs have been constructed in the upper basin above Lanzhou or in the middle basin. In addition, to mitigate sediment deposition in the lower Yellow River channel that imposes great risks on the people living alongside, a large number of small reservoirs have been constructed in the upper and the middle basins, on the Loess Plateau in particular, to retain sediment.

5.3 Materials and methods

5.3.1 Data source

The data used in this study were from the Landsat imagery database (http://edcsns17.cr.usgs.gov/EarthExplorer). Landsat 5 was launched in 1984 by NASA, USA, with a revisiting time of 16-18 days. The Thematic Mapper (TM) sensor uses 7 spectral bands to absorb energy reflected by various surface features. Therefore, expected surface feature interpretation and analysis could be achieved through calibration of different energy levels reflected to the sensor. The coverage of an individual Landsat TM image is 185×185 km^2. The resolution for bands 1-5 and 7 is 30 m, and 120 m for band 6.

In total, 74 images with close-captured date covering the whole basin were downloaded for reservoir identification and analysis (Table 5.1). To reduce disturbances from clouds, only the images with cloud cover less than 5% were selected. The overpass dates of all the images extended from May 2006 to October 2009, and almost all the images were taken during the flood season (93%), extending from June to September, to avoid various undesirable errors caused by adopting images taken in different seasons. For example, reservoir water surface area will be considerably different between dry season and flood season, especially in arid areas where seasonal variation of precipitation is strong, such as in the Yellow River basin. Although reservoirs are at their fullest at the end of the flood season, the water surface area does not change significantly. Comparison of the water surface size of a reservoir in July, September and October indicates that the water surface area in October is about 1.8% larger than in July while only 0.6% larger than in September. It

is believed that the downloaded satellite images could capture a reservoir's largest water surface area in general.

Short of satellite images covering the whole river basin taken in the same year, the reservoir storage volume estimate and the following water retention time analysis were based on the assumption that no new reservoir was completed during the period 2006-2009. The final estimates thus were assumed to represent the actual situation in 2006 or in 2009.

5.3.2 Methods

The infrared, visible red and near-infrared bands in the Landsat images were used to distinguish between land and water and map the extent of open water surface (Töyrä et al., 2002; Liebe et al., 2005; Annor et al., 2009). In the near-infrared and mid-infrared wavelength regions, water, when not turbulent, increasingly absorbs energy making it appear darker in the satellite images while vegetation appears to be bright spots or stripes. This is dependent upon water depth and wavelength. For the visible spectra, generally water bodies have low reflectance depending on the extent of turbidity. For example, clearer water tends to have less reflectance than turbid water.

In this study, the combination of bands 7, 4 and 3 was used to separate water bodies from surrounding surface features. Specifically, band 3 (0.63-0.69 μm in wavelength) senses in a strong chlorophyll absorption region and strong reflectance region for most soils. Band 4 (0.76-0.90 μm in wavelength) operates in the best spectral region

Table 5.1 Summary of the processed Landsat images taken during the period 2006-2009.

Path	Row (Acquired date: dd/mm/yy)							
	31	32	33	34	35	36	37	38
121				(14/05/07)[a]				
122			(21/07/06)	(07/09/07)[a]	(31/07/07)	(22/07/07)[b]		
123				(12/06/07)	(31/07/07)[b]	(22/07/07)		
124			(19/06/07)[a]	(19/06/07)	(23/08/07)	(22/07/07)		
125			(14/08/07)	(12/09/06)	(15/09/07)	(14/08/07)	(14/10/06)	(11/08/06)[a]
126	(17/06/07)[a]	(20/07/07)[b]	(02/06/07)	(17/05/07)	(23/08/07)	(22/09/07)	(12/06/06)	
127	(11/07/07)	(09/08/06)	(10/09/06)	(24/07/07)	(25/06/07)[a]	(24/07/06)	(12/08/07)	
128	(31/05/07)	(03/08/07)	(20/09/07)	(03/08/07)	(03/08/07)	(20/09/07)	(20/09/07)	
129	(22/05/07)[a]	(07/08/06)[a]	(07/08/06)	(08/09/06)	(07/08/06)	(07/08/06)		
130	(19/06/09)	(15/09/06)	(14/08/06)	(06/08/09)[a]	(06/08/09)[b]	(06/08/09)	(18/09/07)	
131			(05/08/06)	(05/08/06)	(21/08/06)	(21/08/06)	(05/08/06)	(05/08/06)[a]
132				(17/07/09)	(16/09/07)[a]	(27/07/06)	(27/07/06)	
133				(18/05/07)	(03/08/06)	(03/08/06)	(03/08/06)	
134					(10/08/06)[a]	(23/06/06)[b]	(10/08/06)	
135					(17/08/06)[b]	(02/09/06)	(02/09/06)[b]	
136					(01/09/09)[a]	(01/09/09)[a]		

[a] indicates cloud cover of 5%.

[b] indicates cloud cover of 2%.

The other images are free of cloud shadow.

to distinguish water bodies as water is a strong near infrared light absorber. Band 7 (2.08-2.35 μm in wavelength) can also separate land and water sharply as it has a strong water absorption region and a strong reflectance region for soil and rock. Before discerning the water bodies from other surface feature classes, the images were preprocessed, including radiance and atmospheric corrections. All the information extraction steps were conducted on the ENVI 4.5.

As mentioned earlier, the cloud shadow makes it difficult to distinguish water bodies (Figure 5.2). Although only very few images had a cloud cover percentage less than 5%, its influence on unsupervised classification methods cannot be ignored. Therefore, supervised classification was used instead. As the surface features of the Yellow River basin are comparatively simple, usually five to six surface feature classes are sufficient to define the surface cover, including water body, bare land, shadow, grassland, city and sometimes cropland, if necessary.

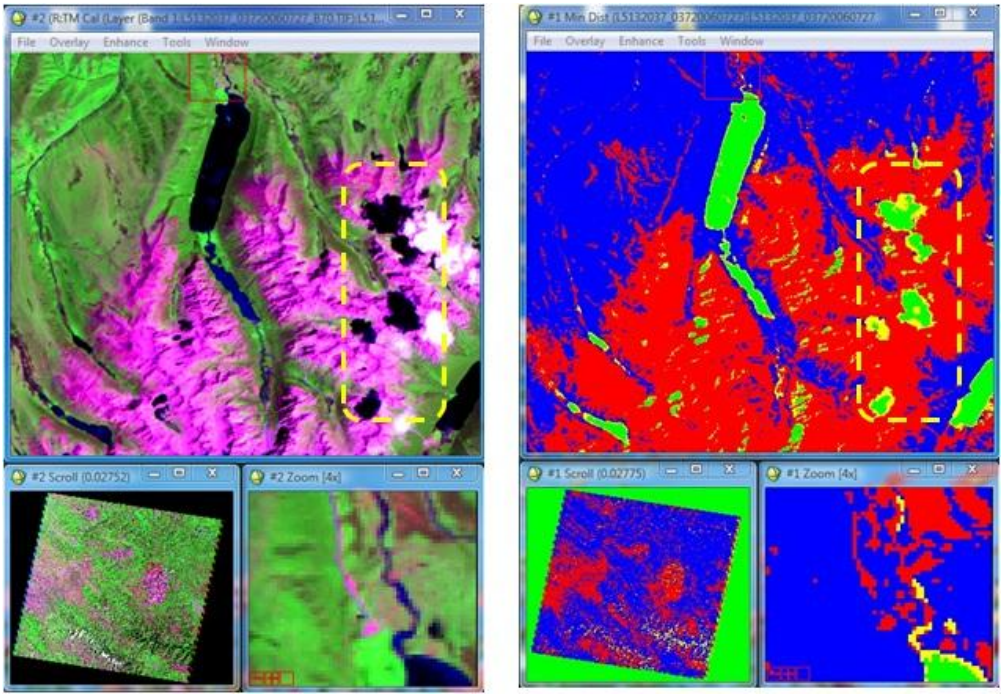

Figure 5.2 An example showing erroneous interpretation of clouds in the yellow dashed rectangle as water bodies.

Although the surface feature can be simply divided into five or six classes, there are considerable complexities. One example is bare land, in the upper basin, especially for the sub-basin upstream of Lanzhou (Figure 5.1). Most of the bare land could be defined as surfaces with rock outcrops and sometimes sparse vegetation. In the Ningxia-Inner Mongolian reach (Yinchuan-Hohhot, Figure 5.1), bare land was mostly defined as desert. In the middle basin, bare land was mainly composed of loess cover. Therefore, the definition of surface feature classes was often different in different regions. However, water bodies were exclusively reservoirs, natural lakes and other water cover features including river channels and paddy fields. As artificial reservoirs are the major concern of this study, visually discernable natural lakes were thus removed manually, such as the two large lakes close to the headwaters (Figure 5.1). Due to the fact that most natural lakes are situated in the sub-basin near the headwaters (Qinghai-Tibetan Plateau), reservoir construction there is limited. Manual detection and removal was reasonable and likely did not substantially affect the accuracy of extraction. In addition, as a result of climate constraints, rice production in the river basin is principally confined to the delta wetlands where reservoir construction was unnecessary. Paddy fields were therefore removed manually.

In order to conduct the supervised classification, usually 15-20 training samples for each defined surface feature class, representing the diversities within the same surface feature, were selected to train the classification algorithm. The sample size depends

on the degree of diversity. However, it does not mean that more samples improved accuracy. Using more samples may increase the risk of obscuring the differences between surface feature classes. After defining the surface feature classes, the minimum distance method was employed to process the images (Foody, 1998; Petit and Lambin, 2001), as it can efficiently discern the surface signatures featured with narrow shape and small number of pixels like reservoirs and lakes with long tail-ends.

For images without cloud cover, inland water bodies were easily discerned and automatically extracted from other surface features with high reliability (Figure 5.3). However, for images with cloud cover presence, the identification of water bodies was somewhat complicated by cloud shadows. Because the software was likely to misinterpret the cloud shadows as water bodies and thus increase the reservoir number and area (Figure 5.2), causing certain difficulties for estimating reservoir storage capacity and water retention time. Since only a few images processed had low cloud cover (<5%), the misinterpretation caused by cloud shadows has been eliminated manually.

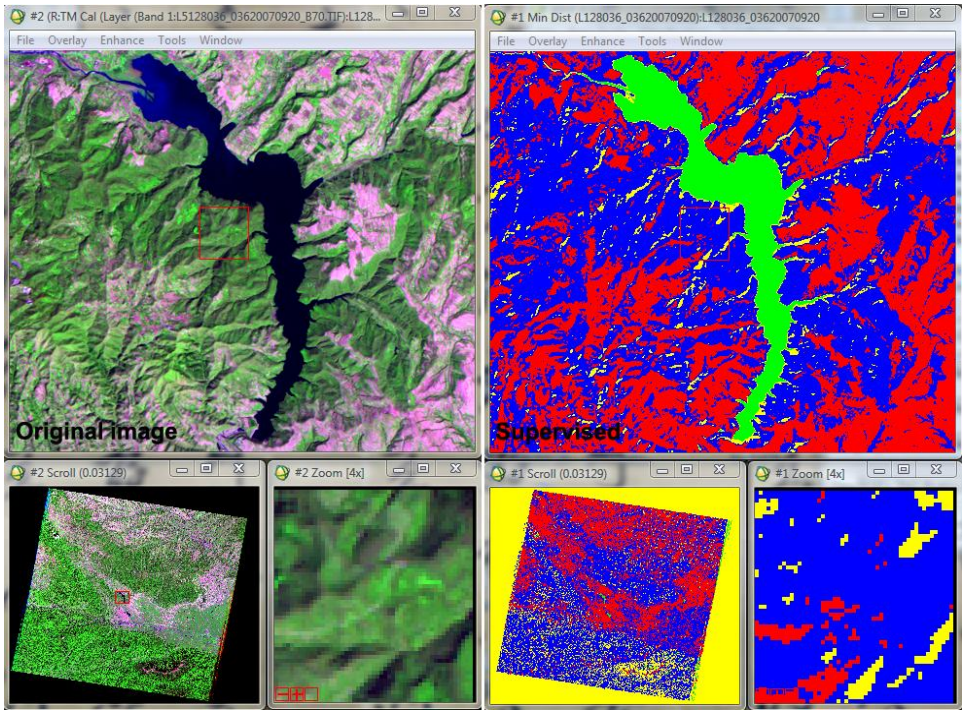

Figure 5.3 Supervised classification using minimum distance, the green color in the top right image is successfully identified as a reservoir shown in the top left image.

After water bodies, now including reservoirs and connected river channels only, were identified from the Landsat images, the next step is to pick out the reservoirs while removing channels. Limited by image quality in spatial resolution, reservoirs constructed on small tributaries could be easily excluded as channel detection failure. In contrast, for the reservoirs built on the mainstem and major tributary channels, the separation of a reservoir's backwater zone from initial river channel background presented a challenge. As far as this basin is concerned, more than 97% of the reservoirs had a clear tail-end. In such cases, the boundary outline could be delineated by cutting the upstream channel above the tail-end on the ArcGIS 9.3 software platform. An example is shown in Figure 5.4. For the reservoirs not having a clear tail-end 'point' (<3% in number), uncertainties arose in the boundary outline

delineation. This is especially true for deep-valley reservoirs, where the post-dam water surface width does not change significantly to be identifiably different from that in the pre-dam period. To reduce the possible errors of tail-ends generated by the software to a minimum, these reservoirs were corrected through available inventory information of reservoir backwater zone (Zhao, 1996; WaterPub, 2007; YRCC, 2007).

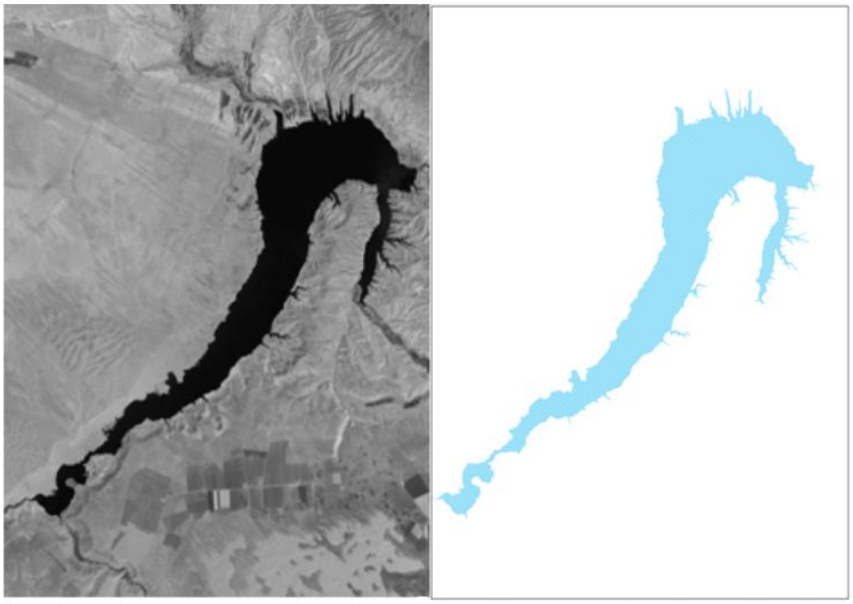

Figure 5.4 Comparison of the Longyangxia Reservoir between the original satellite image (left) and the delineated surface area (right). Located on the uppermost mainstem channel, it ranks first in terms of storage capacity.

After the boundaries of all reservoirs were determined, they were loaded into ArcGIS 9.3 to filter out the speckle noise for the purpose of contiguity. Finally, the surface area of the extracted reservoir polygons was calculated to determine their corresponding storage capacity through developing empirical relationships.

5.4 Results and discussion

5.4.1 Reservoir extraction and correction

In total, 2816 reservoirs were extracted from the Landsat images, with a total water surface area of about 2380.65 km^2 (Table 5.2; Figure 5.5). Comparing with the reservoir inventory indicates that the extracted number is very close to the registered total (3147), accounting for about 89.5%. Small reservoirs on the Loess Plateau that are usually less than 30 m in width were not captured in the 30×30 m^2 resolution of the images. In addition, to combat the severe soil erosion occurring in the basin, in particular in the loess region representing around 37% of the entire basin (Xu and Yan, 2005), many reservoirs were built for sediment retention. These reservoirs would have been filled partially, if not completely, with sediment in a few years and therefore were not detectable. For example, Figure 5.6 shows two disappearing reservoirs on the Loess Plateau with their water surface area having respectively lost 40% (A) and 60% (B) to sedimentation. Consequently, the total number of reservoirs in operation at the time when the images were taken would in fact be less than the number in the inventory. Especially in the remote areas, this is especially true as the local authorities are unable to accurately count the actual reservoir number, owing to outdated monitoring systems and the lack of efficient communication devices.

Table 5.2 Reservoir area statistics based on remote sensing images.

Reservoir area(km^2)	Number	Total surface area(km^2)	Percent of total area (%)
Area<1	2488	188.61	7.94
1≤Area<100	323	1014.06	42.59
Area>100	5	1177.98	49.48
Total	2816	2380.65	100

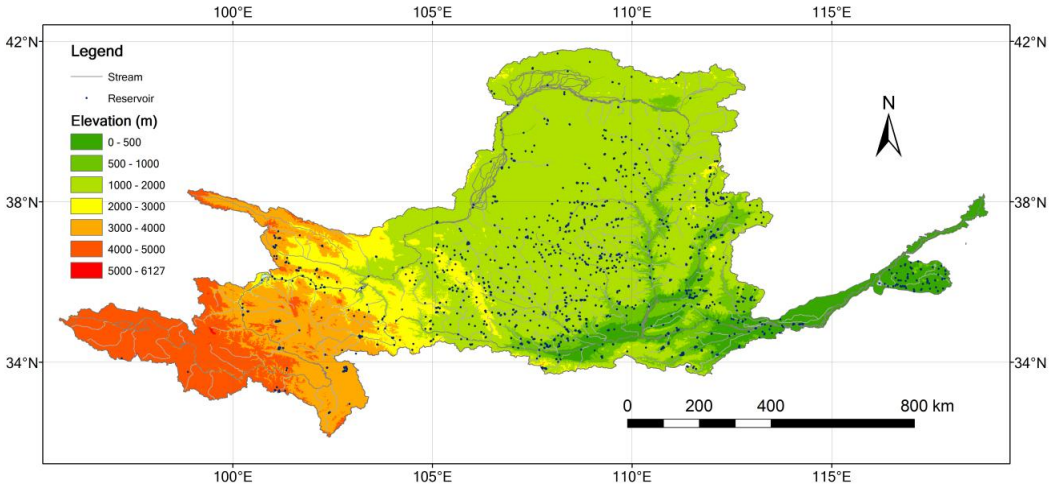

Figure 5.5 Spatial distribution of reservoirs in the Yellow River basin overlapped with elevation change.

Figure 5.6 Two examples showing disappearing reservoir surface area due to sediment deposition.

According to Nilsson et al. (2005), the Yellow River has the same fragmentation magnitude as the Colorado and Nile rivers (fragmentation index: main channel: 3; tributary: 2). Fragmentation describes the longest portion of the mainstem channel left without dams in relation to the entire mainstem channel. However, for the Yellow

River, the longest undammed mainstem channel used in their assessment is the stretch from the headwaters to the Longyangxia Reservoir (see Figure 5.7 below), whose contribution to the whole basin is relatively small. For example, only 1% of the sediment comes from the sub-basin above the reservoir (Gao and Feng, 2002). In contrast, a number of large reservoirs were built in the downstream reaches which receive large quantities of water, sediment, and organic carbon. Therefore, the fragmentation magnitude should be much higher than was assumed. The Yellow River is probably the most strongly fragmented large river system in the world.

Large reservoirs with water surface area >100 km^2 represent nearly half the total water surface area. Reservoirs with water surface area <1 km^2, although having the largest number, represent only 7.9% of the total area (Table 5.2). All the reservoirs with surface area larger than 1 km^2 constitute approximately 92.1% of the total area, but only 11.6% in number, suggesting the significance of large reservoirs in storing water and intercepting sediment and organic carbon from erosion.

With the rapid development of satellite technology, Google Earth can now provide a 15 m resolution for satellite images covering the entire river basin (Yamagishi et al., 2006), which is roughly 2 times higher than the resolution of the images processed in this study. In addition, the accuracy of GPS widely applied in similar field ground truthings is usually 10-20 m (e.g., Zhang et al., 1999; Peng et al., 2006; Annor et al., 2009). Thus, Google Earth, in combination with field work, can be used to verify the image classification results.

The images displayed by Google Earth for the Yellow River basin were mostly taken during the period from August 2006 to September 2008. More than 80% of the images were taken during the flood season, coinciding with the capture time of the analyzed images. Therefore, by means of Google Earth Pro. (http://www.google.com/earth/index.html), 24 representative reservoirs distributed in the upper, middle, and lower reaches of the basin, ranging from large, medium to small in size, were delineated (Figure 5.7). In addition, their respective surface area was calibrated using the built-in polygon area calculation tool (Table 5.3). To correct the acquired surface area results extracted from the remote sensing images ($Area_{sat}$), normalized difference area index (NDAI) and deviation area index (DAI), utilized respectively by Liebe et al. (2005) and Sawunyama et al. (2006), were calculated by comparing with the higher-resolution Google Earth ($Area_{ge}$). NDAI and DAI are defined as follows:

$$NDAI = (Area_{ge} - Area_{sat})/(Area_{ge} + Area_{sat}) \quad \text{(Equation 5.1)}$$

$$DAI = (Area_{ge} - Area_{sat})/Area_{ge} \quad \text{(Equation 5.2)}$$

The NDAI value falls within the range between -1 and 1 with values close to 0 giving the best linear fit between the surface areas obtained from the Google Earth and remote sensing, respectively. Values increasing to both extremes indicate increasing deviation between $Area_{ge}$ and $Area_{sat}$. A negative value implies that $Area_{ge} < Area_{sat}$ and vice versa. Similarly, the DAI values also lie between -1 and 1, with values close to 0 meaning the best linear fit; whereas values increasing to both extremes indicate increasing deviation between $Area_{ge}$ and $Area_{sat}$ (Table 5.3).

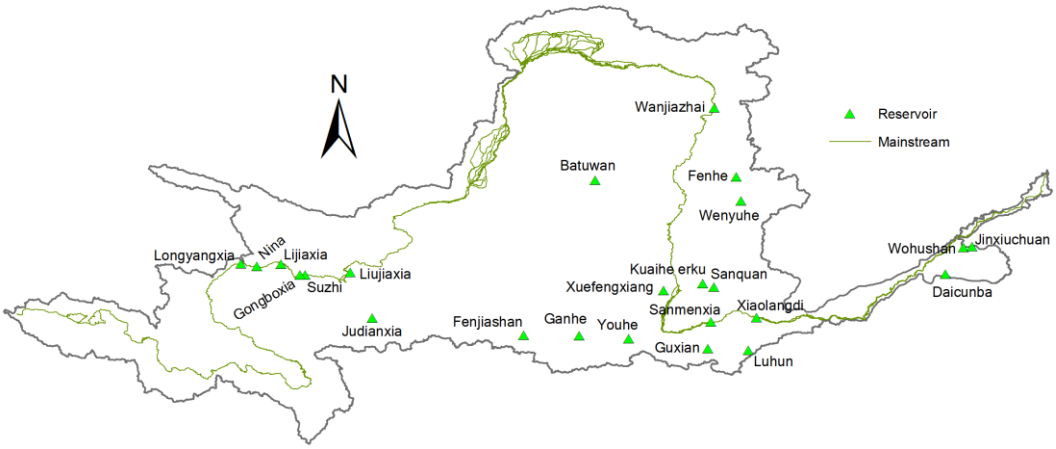

Figure 5.7 Map showing the locations of reservoirs outlined from Google Earth.

Table 5.3 Comparison of water surface area of reservoirs measured from Google Earth and remote sensing images.

Reservoir	Coordinates		$Area_{ge}$	$Area_{sat}$	DAI	NDAI	Storage
	Longitude	Latitude	km^2	km^2			10^8 m^3
Longyangxia	100 °54'57"	36 °7'15"	331.39	353.2	-0.07	-0.03	247
Nina	101 °15'58"	36 °3'46"	2.57	2.51	0.02	0.01	
Lijiaxia	101 °48'26"	36 °7'3"	30.93	31.5	-0.02	-0.01	16.3
Liujiaxia	103 °20'41"	35 °55'56"	101.21	112.78	-0.11	-0.05	57
Xiaolangdi	112 °21'37"	34 °55'26"	251.93	262.59	-0.04	-0.02	126.5
Wanjiazhai	111 °25'42"	39 °34'45"	21.7	19.49	0.1	0.05	8.98
Suzhi	102 °20'13"	35 °52'15"	3.62	3.18	0.12	0.06	0.445
Sanmenxia	111 °20'41"	34 °49'47"	114.89	119.83	-0.04	-0.02	96.4
Gongboxia	102 °13'38"	35 °52'35"	19.18	20.04	-0.04	-0.02	6.2
Youhe	109 °31'10"	34 °27'34"	1.37	1.09	0.2	0.11	
Wenyuhe	112 °1'16"	37 °30'47"	1.88	1.44	0.23	0.13	0.243
Luhun	112 °10'43"	34 °11'58"	30.64	35.16	-0.15	-0.07	11.8
Guxian	111 °16'42"	34 °14'10"	12.62	11.68	0.07	0.04	
Sanquan	111 °9'46"	35 °41'1"	0.35	0.39	-0.11	-0.05	0.0195
Kuaihe erku	111 °24'55"	35 °36'13"	1.13	1.24	-0.1	-0.05	
Ganhe	108 °25'40"	34 °31'25"	2.68	2.5	0.07	0.03	
Fengjiashan	107 °11'20"	34 °31'58"	12.56	14.25	-0.13	-0.06	3.89
Fenhe	111 °55'1"	38 °3'9"	8.55	7.79	0.09	0.05	1.33
Xuefengxiang	110 °17'43"	35 °31'45"	1.53	1.71	-0.12	-0.06	0.436
Wohushan	116 °57'39"	36 °29'26"	4.8	4.93	-0.03	-0.01	1.1
Batuwan	108 °46'53"	37 °58'27"	8.57	7.48	0.13	0.07	1
Jiudianxia	103 °50'0"	34 °54'57"	14.51	15.87	-0.09	-0.04	8.67
Daicunba	116 °33'9"	35 °53'34"	3.98	4.36	-0.1	-0.05	
Jinxiuchuan	117 °8'48"	36 °30'20"	2.06	1.97	0.04	0.02	0.415

The NDAI and DAI results showed that there is a very good linear fit between the two data sets with t-test significance P<0.001 (Figure 5.8). The linear correlation

function of surface areas from Google Earth and the remote sensing images can be expressed as:

$Area_{ge}=0.9426Area_{sat}+0.2974$ ($R^2=0.99$) (Equation 5.3)

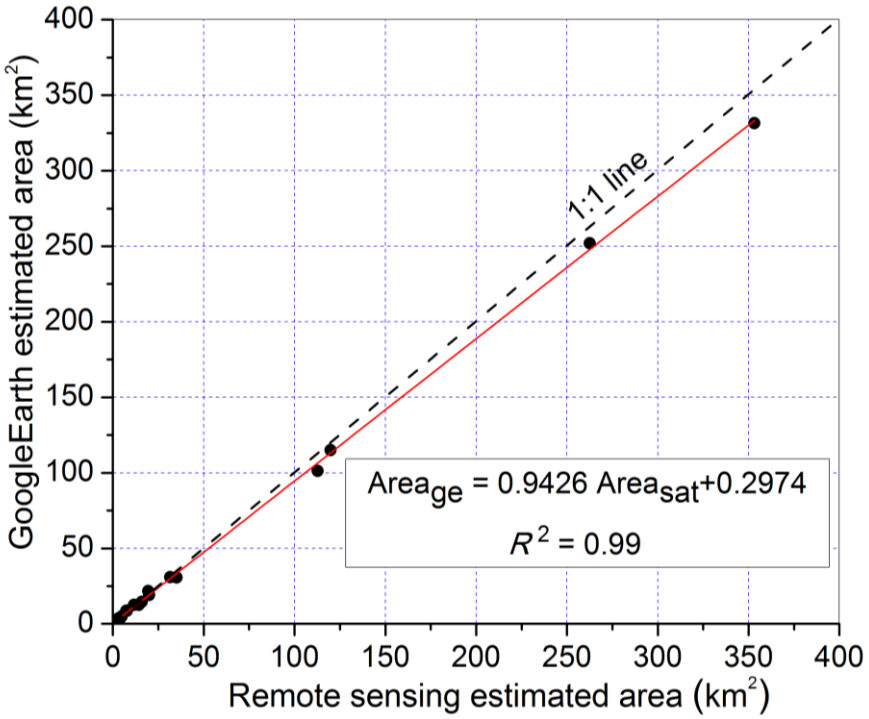

Figure 5.8 Correlation of the estimated area from Landsat images by Google Earth-delineated reservoir polygons.

If the $Area_{ge}$ results are considered the water surface reality, then Equation 5.3 implied that the water surface size extracted from the Landsat images has overestimated the actual size by around 5.7%. On average, the accuracy decreases gradually with increasing water surface area. Probably, the overestimation would be caused by the lower resolution of the Landsat images by which the surrounding non-water features would have been misinterpreted as water, overestimating the actual water surface area (Annor et al., 2009). Notably, for the reservoirs surrounded with flat and smooth bottomlands, various aquatic vegetation, such as reeds growing at the tail-ends or at the edges in wet season in particular, would cause the identifying

programmes considerable difficuly in distinguishing them from waters accurately. An example showing the overclassified water boundary is shown in Figure 5.9, the shaded area is the actual water surface. While the area enclosed within the white polygon was delineated from Google Earth, the red polygon was extracted from the Landsat images. Obviously, the red polygon has overestimated the actual water surface by misidentifying the tail-end vegetation.

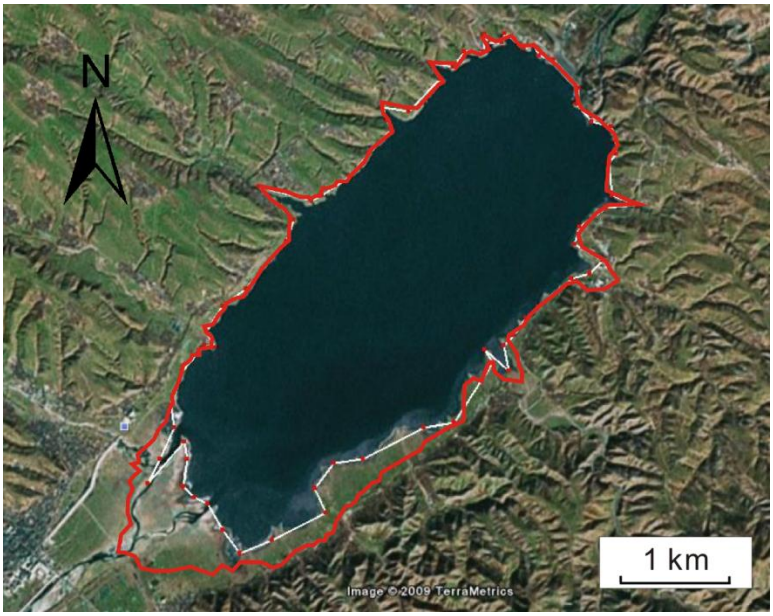

Figure 5.9 Over-classified Luhun Reservoir located in the lowland Yiluohe River basin. Refer to Figure 5.1 for its location.

5.4.2 Estimation of reservoir storage volume

If reservoirs with three-dimensional irregularities can be assumed to approximate the shape of a square pyramid diagonally cut in half (Meigh, 1995; Liebe et al., 2005; Sawunyama et al., 2006), the empirical relationship between reservoir storage capacity and surface area can be expressed as:

$$C = a \times Area_{sat}^{\ b} \qquad \text{(Equation 5.4)}$$

Where, C is the reservoir's storage capacity, $Area_{sat}$ is its water surface area, and a and b are the parameters to be determined. If reservoirs are indeed exactly half

pyramids, then b=1.5, while b>1.5 if the slopes are more convex (rare), in most cases of concave slopes, b<1.5. Particularly, within geomorphologically similar regions the parameters a and b are surprisingly constant (Annor et al., 2009). The correlation is robust and can be reproduced over time and space (Liebe et al., 2005; Annor et al., 2009). However, it must be noted that the parameters would differ in regions with geomorphologic heterogeneities, thus considerable caution is needed when using the relationship (Table 5.4).

Table 5.4 Parameter variations in different study areas.

Equation	Units		Source
	C	*Area*	
$C=7.381\times Area^{1.251}$	10^3 m^3	ha	Meigh, 1995
$C=0.00875\times Area^{1.44}$	m^3	m^2	Liebe et al., 2005
$C=2.646\times Area^{1.5}$	10^3 m^3	ha	Mitchell, 1976
$C=0.77\times Area^{1.299}$	m^3	ha	Mazvimazvi et at., 2004
$C=0.215\times Area^{0.7401}$	10^3 m^3	m^2	Sugunan, 1997
$C=0.0231\times Area^{1.3272}$	m^3	m^2	Sawunyama et al., 2006

Taking into account these differences, the storage capacity information of 18 reservoirs were collected from literature sources or officially published water resources bulletins (An, 1992; Zhao, 1996; Wang et al., 2007; WaterPub, 2007; YRCC, 2007, see Table 5.3). Representing the variations in storage capacity, they were employed to develop the relationship between water surface area and storage volume (Equation 5.4), and the correlation is significant with a correlation coefficient (R^2) of 0.97 (Figure 5.10).

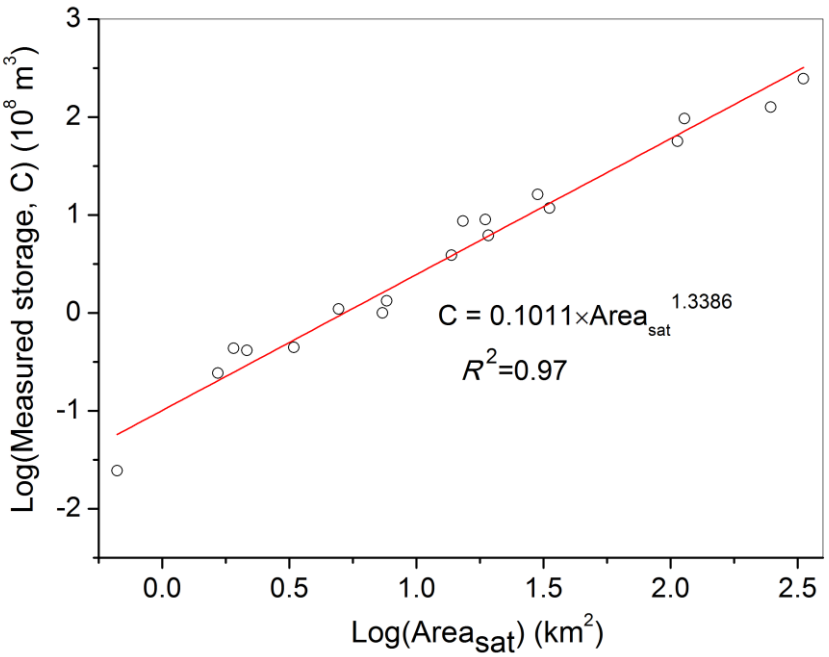

Figure 5.10 Relationship between the surface area ($Area_{sat}$) estimated from Landsat images and the compiled reservoir storage (C).

The empirical equation $C=0.1011\times Area_{sat}^{1.3386}$ was used to estimate the storage capacity (Figure 5.11). The total storage capacity of the reservoirs in the basin is 667.1×10^8 m^3 (or 66.71 km^3) (Table 5.5), which is 92.7% of the published value (72 km^3) (the Ministry of Water Resources of China; http://www.mwr.gov.cn).

In such a large river basin, for different reservoirs, huge spatial heterogeneities exist in geometric shape and water input characteristics. The reservoirs located on valley channels are usually cuneiform-shaped while they tend to be wide and shallow on the flat areas. Each different geometric shape requires a unique parameterization to precisely calculate its storage capacity (Strebelle and Journel, 2001). Also, operation schemes play an important role in affecting storage capacity estimate error. One example is the Longyangxia Reservoir, although having the largest storage capacity of 247×10^8 m^3, it has never reached its normal water level since its completion in

1986 owing to reduced runoff inputs and excessive downstream releases (Wang et al., 2003c). Another possible reason for the estimate error is the misestimate of reservoir water surface area. Therefore, in view of the small difference between the published inventory and the estimate based on actual operation scheme at the given point in time, the estimated accuracy is considered high and can be regarded as optimistic (van de Giesen, personal communication). Furthermore, it can be concluded that all the large- and medium-sized reservoirs were successfully extracted; while some small-sized reservoirs were not captured due to the reasons discussed earlier. In particular, with total storage capacity greater than 0.5 km^3, the extracted 9 large reservoirs constructed on the mainstem channel are shown in Figure 5.11.

Table 5.5 Statistics of reservoir storage estimation. Reservoirs in China are classified into five categories based on storage capacity.

Capacity class	Number	Total capacity(km^3)	Percentage (%)	Standard (10^8 m^3)
Large (I)	5	50.68	75.97	Capacity ≥10
Large (II)*	18	8.629	12.94	1-10
Medium	148	4.363	6.54	0.1-1
Small (I)	256	2.002	3.00	0.01-0.1
Small (II)	2389	1.036	1.55	Capacity ≤ 0.01
Total	2816	66.71	100	

*According to the criteria of large reservoir made by Vörösmarty et al (2003), there are 12 large reservoirs with the maximum storage capacity greater than 0.5 km^3.

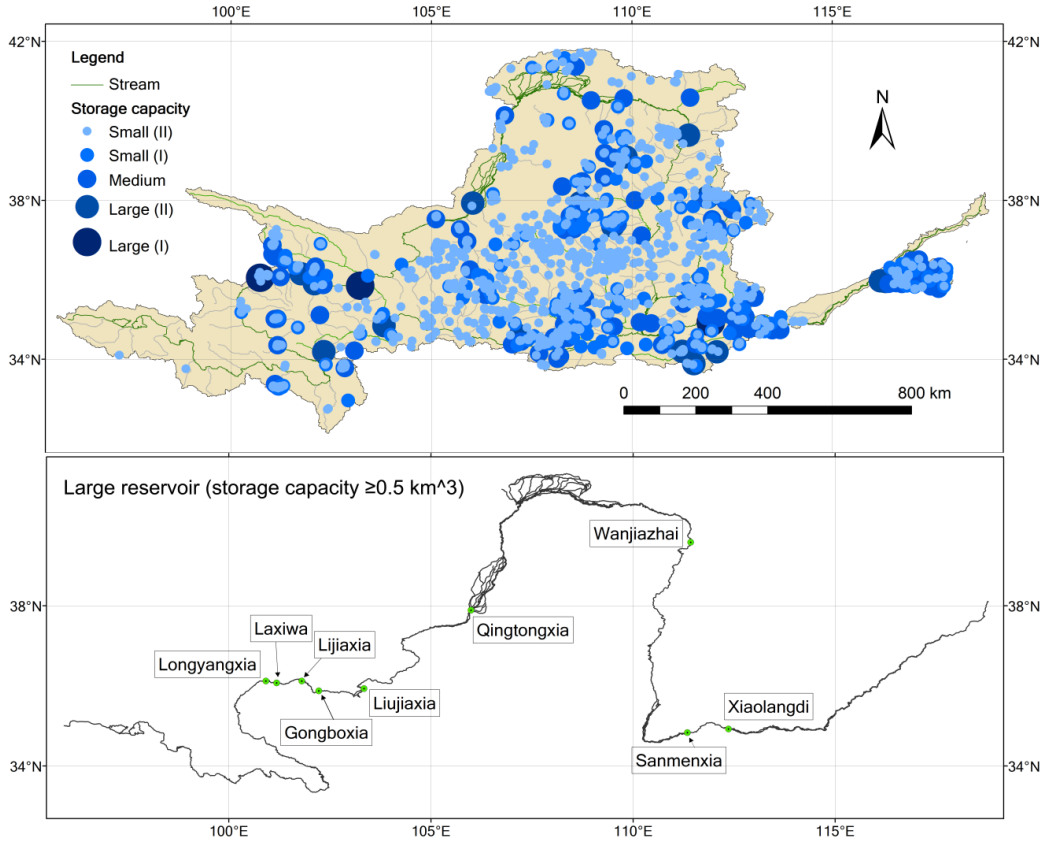

Figure 5.11 Spatial variation of the estimated reservoir storage capacity within the basin (top), and major large reservoirs, with the total storage capacity ≥ 0.5 km^3, constructed on the mainstem channel (bottom).

To investigate the basin-wide reservoir distribution, a density map of the storage capacity was generated by interpolating the individual reservoir points within the basin (Figure 5.12). From the standpoint of geomorphologic characteristics, two stretches in the basin are suitable for reservoir construction. One is the channels above Lanzhou; the other is the middle reaches. The two areas are characterized by narrow channels with steep slope changes. However, constrained by underdeveloped economy and complex geological conditions because of active tectonics, reservoir construction in the reaches upstream of Lanzhou is chiefly limited to the mainstem channel. In contrast, the situation is much better for the middle reaches where the economic requirement is relatively high and is with advanced transportation systems.

Spatially, most reservoirs are located in the middle reaches (~77%), the upper reaches accounts for just 19%. For the lower reaches, owing to long-term levee construction, excessive sediment deposits have raised the riverbed several meters above the adjacent ground (Wang et al., 2007b). The channel is strictly confined to a levee-lined course and only a few small tributaries join the mainstem and, as a consequence, only 113 reservoirs were built in this reach (4%).

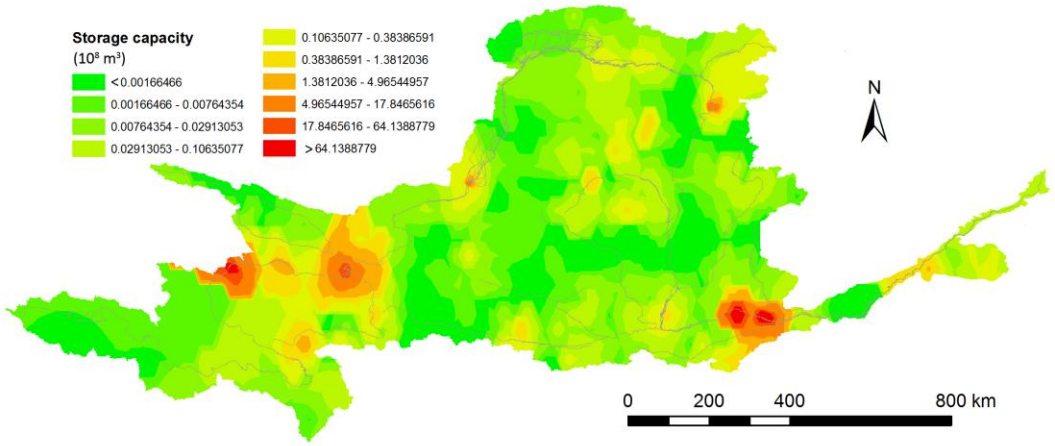

Figure 5.12 Density map of reservoir storage capacity in the Yellow River basin.

5.4.3 Residence time changes

As a reservoir is put into operation, incoming water discharge will be intercepted and the released flow will be reduced to varying extents, depending on the operation schemes. While various human requirements are realized through water interception, reservoir operation also causes a substantial distortion of freshwater runoff from the continents, raising the residence time of water passage along river channels to the oceans (Wisser et al., 2010). Vörösmarty et al (1997) introduced the concept of river water aging to illustrate the impact of the construction of artificial impoundments on flow regime and water cycle. The average length of time water remains within the boundary of a reservoir is one of the key parameters determining a number of direct

and indirect changes in physical, biogeochemical, geomorphological, and hydrological behavior, such as hydrograph distortion, nutrient exchange, microbial development, sediment trapping, and carbon cycle (Ritchie, 1989; Rueda et al., 2006; Cole et al., 2007; Wang et al., 2007a; Wisser et al., 2010).

Further studies on these secondary effects need first a better understanding of water transport and mixing as these processes are closely correlated. To what extent the reservoirs would affect flow distribution and transport varies from place to place due to the differences in natural conditions and social requirements. The time scale, which is generally referred to as the residence time, therefore provides a first order description of the multiple and complex processes occurring within the waters of the reservoir considered. For all the reservoirs located in a given basin, the average residence time ($\Delta\tau$) is defined as follows (Vörösmarty and Sahagian, 2000; Vörösmarty et al., 2003):

$$\Delta\tau = \frac{\sum_{i=1}^{n} V_i}{Q} \qquad \text{(Equation 5.5)}$$

where, V_i is the estimated storage of reservoir *i* (km^3), Q is the annual discharge at the mouth of the regulated sub-basin (km^3/yr), and *n* is the number of reservoirs in each regulated sub-basin.

To get an in-depth understanding of the impacts resulting from reservoir operation on flow regulation, the Yellow River basin was further divided into ten sub-basins (Figure 5.13). The mainstem was divided into four stretch segments: the reaches

upstream of Lanzhou (UL), Lanzhou-Toudaoguai (LT), Toudaoguai-Huayuankou (TH) and the reaches downstream of Huayuankou (DH). Six major tributaries located in the high sediment yielding loess region were extracted for individual consideration. In addition, four mainstem accumulative basins including the basins upstream of Toudaoguai, Sanmenxia, Huayuankou, and Lijin were delineated as well, but not highlighted (Figure 5.1; Figure 5.13).

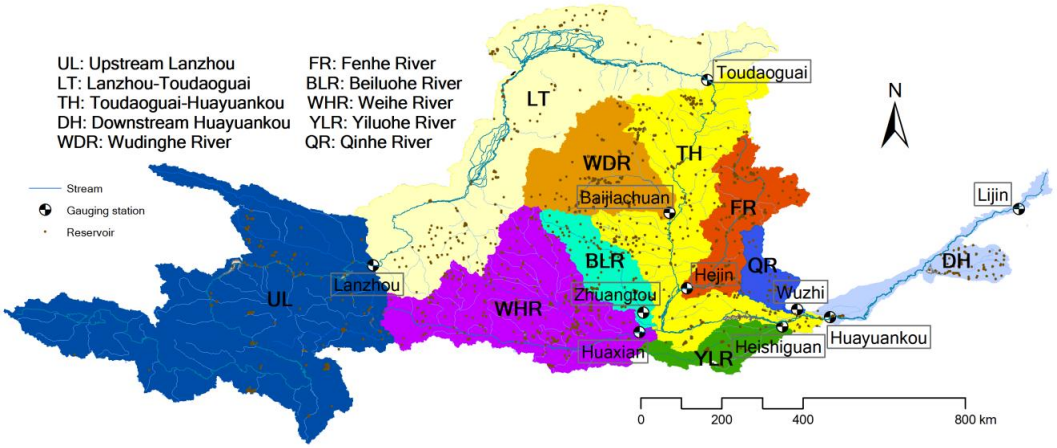

Figure 5.13 Sub-basin division of the Yellow River basin. The extracted reservoirs are overlapped as a reference to sub-basin topographic characteristics.

With efforts to objectively assess the length of the residence time, in this study the restored natural water discharge, which was assumed to be affected by climate changes alone, was used. Li and Yang (2004) have reconstructed the natural water discharge of the main gauging stations, including the mainstem and its major tributaries, by integrating together the losses of agricultural diversion, domestic use, and reservoir storage. The results are tabulated in Table 5.6.

Table 5.6 Summary of reservoir storage capacity and residence time in the sub-basins.

Sub-basin	Controlling station	Reservoir number	Storage	Natural annual discharge	$\Delta\tau(yr)$		*Ratio*[d]
			km^3	km^3/yr	Natural	2006-2009	
Mainstem stretch:							
Lanzhou-Toudaoguai (LT)	Toudaoguai	301	0.605	1.527	0.396	-	
Toudaoguai-Huayuankou (TH)	Huayuankou	743	25.224	6.011	4.196	-	
Downstream Huayuankou (DH)	Lijin	113	0.881	2.649	0.333	-	
Tributary:							
Wudinghe River (WDR)	Baijiachuan	196	1.196	1.541[a]	0.776	1.618	2.1
Beiluohe River (BLR)	Zhuangtou	345	0.103	0.890	0.116	0.219	1.9
Weihe River (WHR)	Huaxian	563	1.042	8.929	0.117	0.253	2.2
Yiluohe River (YLR)	Heishiguan	59	1.058	3.153	0.336	0.750	2.2
Qinhe River (QR)	Wuzhi	38	0.129	1.186	0.109	0.394	3.6
Fenhe River (FR)	Hejin	223	0.56	2.103	0.266	1.429	5.4
Mainstem accumulative basin:							
Upstream of Lanzhou (UL)	Lanzhou	235	35.912	34.244	1.049	1.201	1.1
Upstream of Toudaoguai	Toudaoguai	536	36.517	35.771	1.021	2.144	2.1
Upstream of Sanmenxia[b]	Sanmenxia	2581	53.825	54.13	0.994	2.385	2.4
Upstream of Huayuankou	Huayuankou	2703	65.108	59.584	1.093	2.557	2.3
Upstream of Lijin (whole basin)	Lijin	2816	66.71	62.233	1.072[c]	3.966	3.7

[a] The natural annual discharge of Wudinghe River was averaged based on measured data during 1956-1969 provided by Yellow River Sediment Bulletin (1950-2009), this time period was usually assumed without strong human impacts and flow varied under "natural" conditions (Xu, 2004). Data for the other tributaries and the mainstem were from Li and Yang (2004).

[b] The location of Sanmenxia referred to Figure 5.1.

[c] The basin-wide mean residence time (1.072 yr) was subbasin-based discharge-weighted.

[d] $Ratio=\Delta\tau_{(2006\text{-}2009)}/\Delta\tau_{(Natural)}$.

In the tributary basins, most reservoirs have low residence times (<0.35 yr), indicating a capability to store all the water inputs for around four months without releasing. Particularly, for the Beiluohe, Weihe, and Qinhe rivers, the water exchange rate was relatively faster, implying that the reservoirs exerted a weak effect on the water cycle. In contrast, with a residence time of 0.78 yr, the Wudinghe River showed an exceptionally strong influence on water exchange. Approximately, on an annual scale, 78% of water discharge could be stored by reservoirs and less than one quarter could reach the Yellow River mainstem. Due to concentrated rainfall regime, porous soil structure, and degraded vegetation, the Wudinghe River is one of the tributaries suffering from the severest soil erosion and has been listed as a key area for soil conservation since 1982 (Xu, 2004). Consequently, a large number of reservoirs have been constructed in the basin (see Figure 5.11), resulting in high residence time and greatly reduced exchange rate as the major function of these reservoirs is for sediment trapping.

For the sub-basin upstream of Lanzhou, a number of large- and medium-sized reservoirs have been built. For example, the Longyangxia Reservoir, in combination with other cascade reservoirs like the Liujiaxia (storage capacity: 57×10^8 m^3), has the ability to store more than 85% of the annual discharge of the sub-basin (Zhao, 1996). Similarly, the reservoirs in the Toudaoguai-Huayuankou stretch, including the Sanmenxia and the Xiaolangdi with a storage capacity of 96×10^8 m^3 and 127×10^8 m^3, respectively (Wang et al., 2007; Figure 5.11), result in the highest residence time (4.2 yr). The reservoirs could intercept all the water supplied from the stretch for more

than four years without releasing any downstream, indicating that the water discharge is severely controlled. The other two mainstem stretches (Lanzhou-Toudaoguai and downstream of Huayuankou) have a relatively low residence time (0.4 yr and 0.33 yr, respectively), which is in general accordance with the small-scale reservoir construction limited by arid climate and unsuitable topography.

However, reservoirs located on the mainstem channel regulate not only the water generated in the considered stretch alone; they also manipulate the water supplied from the upstream tributaries. Therefore, the accumulative reservoir storage based on longitudinal stations along the channel course could better reflect the residence time changes. The residence time is high for all five accumulative basins (Table 5.6), illustrating relatively long disturbances from the artificial impoundments. The result is much higher than the estimate made by Nilsson et al (2005), probably because some new reservoirs were constructed and also the inclusion of the small-sized reservoirs in this study.

Overall, under natural conditions, the residence time for the Yellow River as a whole (1.07 yr) is much longer than other large rivers, such as the Nile, or the continental averages (Vörösmarty and Sahagian, 2000; Vörösmarty et al., 2003; Wisser et al., 2010). A striking contrast is that the mean residence time of rivers entering the Pacific Ocean is only 8 days and the global average is only 19 days (Wisser et al., 2010). As the obtained total storage capacity has already underestimated the actual situation, it is expected that the actual residence time will be longer than the estimated.

5.4.4 Impacts on flow regulation

The residence time, from another perspective, indicates the degree to which the river flow regime has been altered by reservoirs (Wisser et al., 2010). The impacts of these impoundments vary depending on their number, size, and the location in the river basin as well as their storage capacity. In order to evaluate the scope and magnitude of flow regulation resulting from reservoir operation in recent years, the residence time for the period 2006-2009 was calibrated. Undoubtedly, the differences between it and the initial value under natural conditions were able to provide insight into flow regulation. The calculated average residence time results are also included in Table 5.6, and the residence time comparison is shown in Figure 5.14.

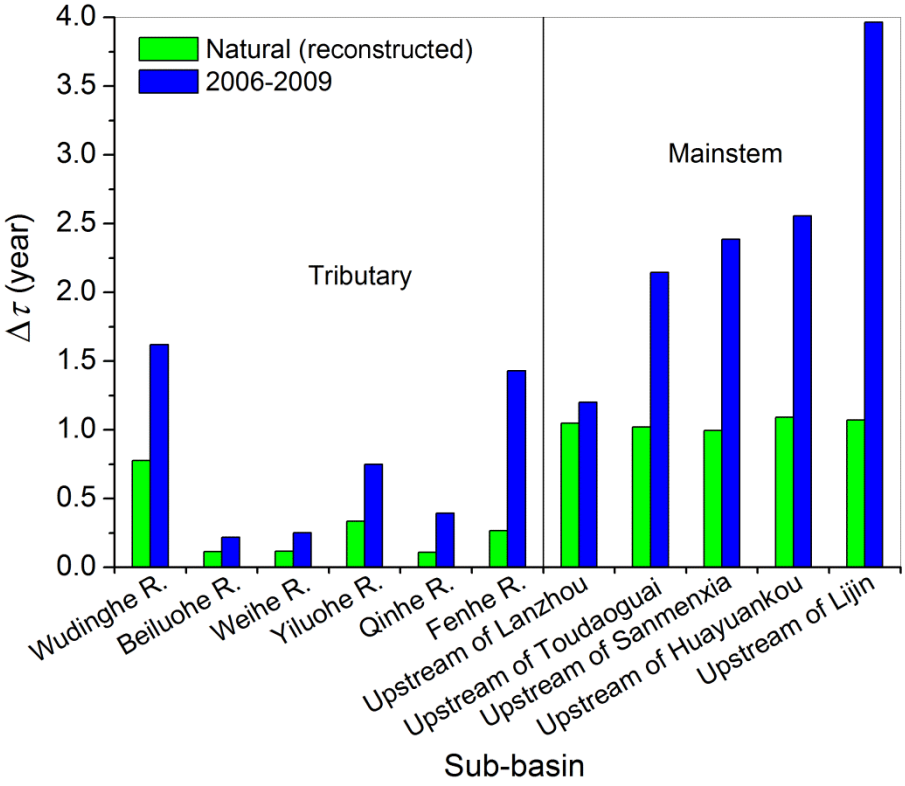

Figure 5.14 Comparison of residence time in the sub-basins computed based on the reconstructed natural annual water discharge and the observed values at hydrological stations, respectively.

In the tributaries of Wudinghe, Weihe, and Yiluohe rivers, the residence time has doubled if the average water discharge from 2006-2009 is used; while in the Qinhe and Fenhe rivers, the residence time was 3.6 and 5.4 times the initial value, respectively. Even for the Beiluohe River with the lowest water discharge and reservoir storage capacity, the residence time has also nearly doubled (1.9 times). Substantially extended residence time has resulted in alterations to the water flow regime, reflecting the strong regulation impacts on water flow due to damming. In view of the present trend of reservoir construction and continuous water reduction, it is expected that such phenomena will become increasingly common. On the other hand, for the five mainstem accumulative basins, the residence time under natural conditions was comparatively low and did not show significant spatial variability, indicating approximately equal flow regulation magnitude. In contrast, it has changed greatly when the water discharge measured during 2006-2009 is used. The amplitude variation became increasingly large in the downstream direction. Specifically, the residence time in the sub-basin upstream of Lanzhou remained roughly stable with a little increase, which is largely because its water discharge has not been significantly affected by water withdrawal. While for the three accumulative basins (upstream of Toudaoguai, Sanmenxia, and Huayuankou), the residence time has doubled and steadily increased, coinciding with the huge water withdrawal along the channel. The sequentially increased residence time highlighted the increasingly enhanced flow regulation.

As far as the whole river basin upstream of Lijin station is concerned, the residence time has sharply increased from 1.07 to 3.97 years (~3.7 times). The extremely long

residence time is consistent with the reports of strong flow regulation (Vörösmarty and Sahagian, 2000; Nilsson et al., 2005). Vörösmarty and Sahagian (2000) claimed that the Nile and Colorado rivers are the most influenced large river basins in the world in terms of residence time (>1 yr) and flow regulation. However, their work has severely underestimated the residence times as only large reservoirs were taken into account. Thus, it can be concluded that the Yellow River is at least among the top three, if not the first ranked.

Limited by lack of time series data of the total storage capacity, a yearly magnitude analysis of flow regulation could not be elucidated. Alternatively, comparison between annual water discharge and the estimated total storage capacity of 2006-2009 is plotted in Figure 5.15. Although the comparison between the two variables can only be regarded as a reference to historical variations, it could serve as a benchmark for predicting future flow regulation and assessing relevant biogeochemical carbon impacts.

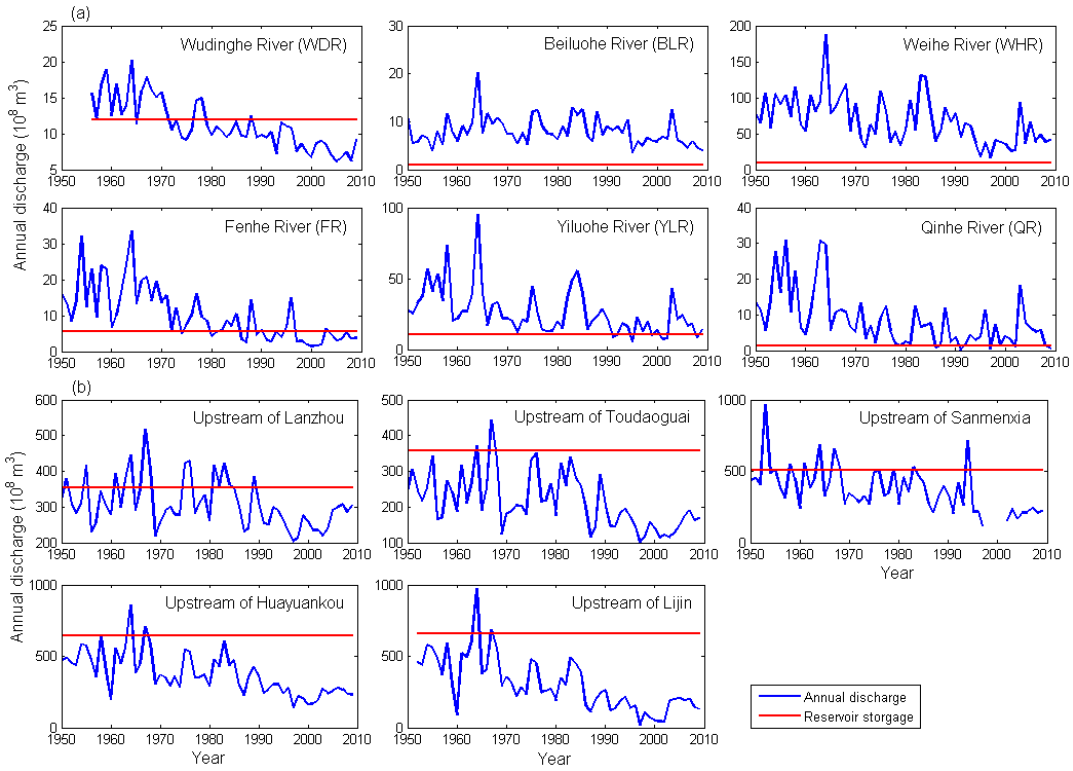

Figure 5.15 Diagrams showing comparison between annual water discharge and the estimated total storage capacity of the reservoirs built within the individual sub-basins. (a): Tributaries; (b): Mainstem accumulative basins.

In all the tributaries, owing to climate change and water consumption/diversion, the annual water discharge has decreased sharply since the 1960s (Xu and Yan, 2005; Wang et al., 2007b). In the meantime, large-scale reservoir construction has been conducted and as a result, the flow regulation magnitude has been enhanced gradually. In particular, for the Wudinghe and Fenhe rivers in the past two decades, their reservoirs' storage capacity has exceeded their respective annual water discharge, and much stronger flow regulation is thus expected (Figure 5.15a). For the rest of the tributaries, considering the declining water discharge and newly operated reservoirs, it is anticipated that the flow regulation magnitude will become far stronger in future. However, to what extent the enhanced flow regulation would influence other biogeochemical behavior remains to be determined.

Irrigation has long been crucial for agricultural productivity in the basin (Zheng, 1984), and the irrigation water consumption has experienced a sharp increase over the past decades (see Figure 2.6). Together with other irretrievable water losses like evaporation from the irrigated farmland, the observed water discharge showed an abnormal downward trend when flowing through the agricultural areas. For example, for the period 1950-2009, the mean annual water discharge at Toudaoguai (215×10^8 m^3) was far less than the upstream Lanzhou (308×10^8 m^3), as was the case between the lowermost Lijin and its closest upstream Huayuankou, with a mean annual water discharge of 303×10^8 m^3 and 377×10^8 m^3, respectively.

In response to the decreasing water discharge and the increasing reservoir storage capacity, the flow regulation magnitude in the mainstem basins has also been enhanced (Figure 5.15b). Temporarily, the total storage capacity during the study period has exceeded the annual water yield since the early 1990s. With respect to the whole river basin (upstream of Lijin), the estimated reservoir storage capacity was approximately equal to the annual water discharge before 1970. After that, due to widespread soil conservation practices and water consumption, coupled with precipitation variations driven by climate change, the annual water discharge has declined abruptly. One direct result is that the potential flow regulation has become more apparent than ever before. The flow regulation would be further enhanced in future, in common with most large Asian rivers (c.f., Lu and Siew, 2006; Zhang et al., 2008a; Kummu et al., 2010). It is worth noting that the estimated flow regulation reflects only the water cycle under ideal conditions; in reality it depends on several

other factors, such as reservoir position and operation scheme. However, this method makes it possible to analyze flow regulation at larger spatial scales, providing a new perspective to assess global water dynamics and biogeochemical carbon cycles.

5.5 Summary and conclusions

Compared with the conventional methods, such as hydrographic surveys which are costly, time-consuming and laborious, the remote sensing technique is a rapid and cost-effective approach in information acquisition with short time intervals at a large spatial scale. Using Landsat images covering the Yellow River basin and relevant computer software, the completed reservoirs in the basin up to 2009 were extracted and their storage capacity was estimated. In addition, the average residence time of water in the reservoirs was assessed. The following specific conclusions can be drawn based on this study:

In total, 2816 reservoirs in the basin were extracted from the remote sensing images, which explains about 89.5% of the registered number (3147 in all), indicating that the application of remote sensing images in reservoir extraction is efficient. Furthermore, while all the large- and medium-sized reservoirs were successfully delineated, about 330 small reservoirs were missing. Cloud cover is an unavoidable interference to precise identification of small reservoirs because sometimes the cloud shadows have been misinterpreted as water bodies. Other kinds of weather-independent satellite images should be sought to serve as an alternative for Landsat images in future, if possible.

The outlined reservoirs from higher-resolution Google Earth images were used as a reference to verify the delineated results from the Landsat images. A good linear correlation was established between the water surface areas of reservoirs from the two sources, suggesting the feasibility of resorting to Google Earth when ground truthing is difficult to conduct. Finally, using the water surface area based empirical equation, the storage volume of all the delineated reservoirs in the basin was calculated (66.71 km^3), accounting for about 92.7% of the authorized total storage capacity, highlighting again the necessity of using other kinds of satellite images to figure out the difference.

Residence time analyses based on sub-basins reveal strong flow regulation by reservoir operation. To what extent the constructed reservoirs impact water exchange varies greatly from one another. Compared with the reconstructed natural water discharge, the obtained residence time (3.97 yr) using recently measured water discharge showed a strong flow regulation regime, ranking the Yellow River in the top three of the list in terms of residence time and flow regulation among large river systems in the world. Decreasing water discharge, coupled with increasing storage capacity resulting from continuing reservoir construction and other human activities, is likely to further extend the residence time in future and thus affect water and carbon cycles within the basin.

The obtained estimate is in good agreement with the published inventory statistics in term of the reservoir number and the total storage capacity. Therefore, the application

of remote sensing technology has provided new insights into future reservoir monitoring and management. In particular, thanks to the unavoidable challenges faced by conventional methods, remote sensing has great potential and the advantages will become far more manifest as satellite images with higher spatial resolution are now becoming available. Estimate of sediment trapping efficiency resulting from reservoir construction, analysis of their spatial and temporal variations, and evaluation of their impacts on sediment and organic carbon fluxes into the ocean, will be presented in the following chapters.

Chapter 6 Estimation of basin-wide reservoir sedimentation

6.1 Introduction

Reservoirs, as an effective way to manipulate continental runoff, are globally essential to river development and have been widely constructed in the world (Nilsson et al., 2005). Currently, although the construction speed in the developed world has been substantially reduced, reservoir projects are greatly supported in the developing countries to fight flooding and droughts and to meet growing energy demands. However, along with the benefits a number of problems are also introduced as a result of dam construction. The modified flow dynamics have changed sediment transport processes to varying extents depending on the water and sediment delivery features, and the operating schedules of reservoirs. As a consequence, reservoir sedimentation and the consequent long-term loss of storage capacity have been a severe problem. On the other hand, the consequent carbon burial has been an important component in assessing catchment carbon cycles (Syvitski et al., 2005).

According to a report of the WCD (World Commission on Dams, 2000), the world's reservoirs are currently losing their storage capacity to sedimentation at an estimated rate of 0.5-1% per year. This implies that, without necessary measures to reduce sediment deposition, around 25% of the world's current water storage capacity may be lost in the coming 25 to 50 years. In China, most reservoirs have lost about 19% of their storage capacity to sedimentation in less than 20 years after operation (Wang et al., 2011c). With sediment filling a reservoir, its usable capacity will be reduced,

which could in turn affect outlet works and turbine operation as well as upstream backwater flooding (Butcher et al., 1993; Morris and Fan, 1998; Wang et al., 2005).

Reservoir sedimentation can disrupt the flow and sediment delivery system. Release of sediment-starved water can commonly result in bed incision and bank collapse in the downstream channels, which can further adversely impact riparian infrastructure and riverine ecosystem, and cause drawdown of the alluvial water table (Vörösmarty et al., 2003; Syvitski et al., 2005; Fu et al., 2008; Schmidt and Wilcock, 2008; Minear and Kondolf, 2009). Deposited sediments in reservoirs also represent an important global sink for carbon and other greenhouse gases (the GHGs), such as methane and N_2O (Dean and Gorham, 1998; Stallard, 1998; McCarty and Ritchie, 2002; Cole et al., 2007; Jacinthe et al., 2012). Despite the area of reservoirs being a very small percentage of Earth's surface, the sediments of these reservoirs can accumulate organic carbon at an estimated rate of about 160 Tg/yr (Dean and Gorham, 1998). While the impoundment of sediment could be a carbon sequestration mechanism, it could also be a possible emission source of GHGs which may evolve in anoxic conditions (Battin et al., 2009; Jacinthe et al., 2012). Such contrasting carbon sink and source potentials have further confused the net effects of the buried sediments. Therefore, quantifying the trapped sediment amount plays a critical role in defining the magnitude of reservoirs in sequestrating carbon.

During the design and construction of most reservoirs, little attention has been given to maintaining reservoir functions as the original storage capacity is progressively lost to sedimentation, for example the Sanmenxia Reservoir in the Yellow River basin

(Wang et al., 2005). As reservoirs are usually constructed at the most viable sites, loss of the completed storage capacity due to sedimentation is difficult to offset by building new storage capacity (Morris and Fan, 1998). Maintaining existing reservoir storage capacity is substantially important, which requires accurate estimates of the volume of deposited sediments in reservoirs for providing guidance for future reservoir management.

Previous reservoir sedimentation studies were mainly based on bathymetric surveys, which were usually confined to individuals or at a small spatial scale (White et al., 1997; de Vente et al., 2005; Wang et al., 2005), while process-based models were not able to predict reservoir sedimentation at large spatial and/or temporal scales, primarily due to high data requirements and a general lack of system knowledge (White et al., 1997; Tarela and Menéndez, 1999; Verstraeten et al., 2003; Minear and Kondolf, 2009). Reservoir sedimentation estimation in the Yellow River basin has been mainly concerned with the largest dams on the major tributary or the mainstem channels (e.g., Xu 2003; Hu, 2005; Wang et al., 2005). Although the largest dams have been found to play a fundamental role, the smaller ones located much closer to sediment production zones could also intercept substantial amounts of sediment (Gong, 1987). Ignoring these smaller, but large in number, reservoirs would cause underestimates of the total trapped sediment, thus bringing about biases when evaluating human impacts on sediment load transport and carbon cycle. From another perspective, taking into account the contributions of the smaller reservoirs will definitely help understand the impacts of reservoirs on the observed reductions in

seaward sediment and carbon export (Wang et al., 2007b; Miao et al., 2011). As such, accurately estimating basin-wide sediment trapping by all reservoirs is central to studies on reservoir management, sediment budget, and carbon sequestration. This is particularly true for the Yellow River basin with large quantities of sediment being trapped within reservoirs.

To estimate basin-wide sediment trapping, detailed information for multiple reservoirs, such as their respective spatial location, storage capacity, and completion date, is a prerequisite. This is usually absent for most large river basins, however. Another difficulty is the shortage of long hydrological observations accompanying reservoir construction history. With more than 60 years of hydrological records across the river basin and detailed reservoir information derived from a remote sensing dataset, the Yellow River basin provides an excellent example for estimating basin-wide reservoir sedimentation and its impact on carbon budget.

This study was based on the delineated reservoirs from Landsat images presented in Chapter 5, in which the completed reservoirs in the Yellow River basin up to the period of 2006-2009 were delineated, and each reservoir's storage capacity was estimated through an empirical relation. In addition, their potential impacts on flow regulation were also evaluated using reconstructed natural annual water discharge and recent observations based on hydrological gauge stations. The objectives of the present study are: (1) to evaluate the potential sediment trapping efficiency (*TE*) of the reservoirs extracted from the satellite images; (2) to investigate the total trapped

sediment amount over the past decades and their contribution to basin-wide sediment load reduction; and (3) to elucidate its inherent implications for reservoir operation and sediment-related delivery processes. The estimated total sedimentation during the past decades is used in the next chapter to assess the basin-wide organic carbon budget.

6.2 Sediment yield and transport in the Yellow River

As described in Chapter 2, the Yellow River is characterized by high sediment yield due to strong soil erosion in its middle reaches (mainly the Loess Plateau). Prior to large-scale human activities that have significantly reduced the sediment flux into the ocean, the Yellow River used to be the second largest river of the world in terms of seaward sediment load over millennial-scale historical time, next only to the Ganges-Brahmaputra river system (Milliman and Meade, 1983). For the Loess Plateau with large amounts of highly erodible soil material, the suspended sediment concentration (SSC) could be in excess of 1000 kg/m^3 in some hyperconcentrated flow events, and the mean annual SSC was 35 kg/m^3 before the 1970s (Zhao, 1996; Xu, 2002). These concentrations are far greater than those for any other large river in the world. Prior to the 1970s, annually about 1.6 Gt of sediment was discharged through the Sanmenxia station, and about 1.21 Gt into the Bohai Sea based on measurements at Lijin station (see their locations in Figure 2.1).

However, both the water and sediment transport are characterized by significant spatial variability. As has been clearly stated in earlier chapters, while about 57% of

the water originates from the upper reaches above Toudaoguai, nearly 90% of the sediment load originates from the middle reaches extending from Toudaoguai to Huayuankou, where the river drains the extensive wind-deposited Loess Plateau. Composed of loosely compacted silt that is very prone to erosion, the Loess Plateau has been acknowledged as the most easily erodible region in the world to moving water (Milliman and Meade, 1983; Huang and Zhang, 2004). In contrast, the upper reaches contribute only about 10% sediment, whereas the middle reaches provide about 40% water discharge. For the lower reaches, due to gentle channel slope and reduced sediment carrying capacity, large amounts of sediment are deposited on the intervening alluvial plains each year, causing the lower mainstem channel to form a unique 'suspended river' whose riverbed is highly raised over the surrounding grounds for several meters (Wang et al., 2007b).

Spatial variations in the average SSC during 1950-2010 along the Yellow River is presented in Figure 6.1. Similar to the annual sediment load shown in Figure 2.4, the SSC in the upper reaches is substantially low, usually below 5 kg/m^3. In the middle reaches between Toudaoguai and Huayuankou stations, the SSC increases sharply to >25 kg/m^3 when huge amounts of sediment is delivered into the Yellow River through numerous tributaries. The maximum annual average SSC at Longmen and Tongguan stations are 61.3 kg/m^3 and 67 kg/m^3, respectively. While for the lower reaches, the SSC decreases gradually along the channel course towards the river mouth as a result of sediment trapping by reservoirs and channel sedimentation (Figure 6.1).

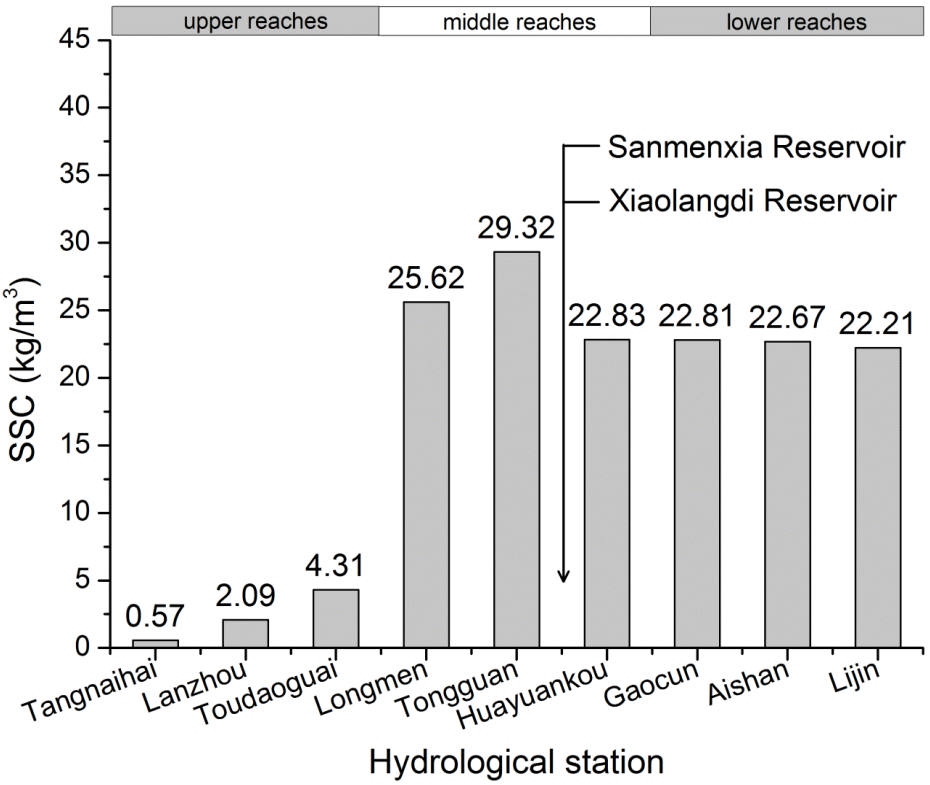

Figure 6.1 Changes of annual suspended sediment concentration (SSC) averaged from 1950 to 2010 at nine hydrological stations along the Yellow River. Due to sediment trapping and sediment deposition, the SSC decreased gradually in the lower reaches. Data from Ministry of Water Resources of China (2010a).

To develop river water resources for various purposes, such as hydroelectricity generation and flood control, and to alleviate the serious channel sedimentation in its lower reaches, massive dam construction activities were carried out in the river basin over the past decades. Particularly, the construction speed has been greatly accelerated during the last 30 years driven by economic development. By 2007, 3147 registered dams have been completed with a total storage capacity of 72 km^3 (see Chapter 5), amounting to 116% of the annual natural water discharge or 415% of the annual water discharge measured in recent years. Given the severity of soil erosion in the middle reaches, quite a number of reservoirs were built on the Loess Plateau to

trap sediment, and the trapping effects are enormous (Zhao, 1996). In addition, widespread soil conservation measures were carried out on sloping lands to control soil erosion, and the benefits are also gigantic (Ran et al., 2013b). In recent years, increasingly improved vegetation cover has also helped reduce the magnitude of soil erosion and sediment transport. As a result, the sediment load discharged into the ocean has declined to 0.12 Gt per year during 2006-2010. From another perspective, sedimentation and the resulting loss of storage capacity have badly affected water availability and the reservoirs' operating schedules, which have further triggered a cascade of geomorphological, ecological, and biogeochemical problems.

6.3 Data sources

Out of the registered 3147 reservoirs completed in the Yellow River basin, 2816 were successfully delineated from remote sensing images through supervised classification after several corrections (see Chapter 5). The Yellow River Conservancy Commission (YRCC), the official organization in charge of hydrological investigation in the basin, conducts regular hydrometric measurements based on national standards (Xu, 2002; Hassan et al., 2008). Annual sediment load and water discharge data used in this study were extracted from the Yellow River Hydrological Yearbooks yearly published by the YRCC, which summarize measurements from a network of hydrological stations throughout the whole basin. The original records for each station provide detailed information on the station's coordinates (latitude and longitude), control area, and mean monthly and annual water discharge and sediment loads (Hassan et al., 2008; 2010; 2011). The use of historical records raises the

question of data quality (Lu and Higgitt, 1998). The annual water discharge and sediment loads are based on discrete rather than continuous measurements. Therefore, the sampling frequency does not ensure that all ranges of flow were measured. As such, only the stations with temporal records longer than 5 years were used in this study to minimize the errors caused by sampling intervals.

It should be pointed out that the exclusion of bedload may have resulted in underestimation of sediment load. As the bedload component usually contributes less than 10% to the total sediment load (Wu et al., 2008a), the exclusion would not significantly affect the subsequent analyses. Furthermore, large-scale soil conservation work in the river basin started in the 1970s, and since then a large quantity of sediment has been retained and thus has not reached the channel. That makes a precise reservoir sediment assessment difficult to achieve, because without detailed records it is hard to identify where the reduced sediment observed at outlet stations is retained. To minimize these external human-induced impacts and to avoid confounding the effect of reservoirs in trapping sediment, the data after 1970 which were substantially affected by various soil conservation projects were therefore excluded (Hassan et al., 2008).

Representative reservoir sedimentation data were extracted from the Yellow River Sediment Bulletins published also by the YRCC. In particular, for the two most important large reservoirs, the Sanmenxia and Xiaolangdi (see their locations in Figure 2.1), the YRCC frequently monitors the water level changes and storage

capacity losses. Annual sediment budget and water volume for both reservoirs are regularly reported. Data for the two reservoirs started respectively from 1960 and 2002 when they were immediately completed.

6.4 Methods

6.4.1 Sediment yield mapping

Among the 225 stations with at least 5-year-long sediment sampling records over the period of 1950s-1970, 35 are located on the Yellow River mainstem channel or on the major tributaries which cross various hydrological, geomorphoglocial, and geological boundaries. Consequently, the measured sediment loads at these stations cannot reflect the actual sediment transport processes as a result of sediment storage; they were thus removed from the analysis. In addition, although no massive dam construction activity was carried out within the basin before 1970, there still had been a few dam completions. Because the stations located immediately downstream of these dams cannot reveal the actual sediment transport process, they were also removed. After the selection process, 179 potentially useful stations were identified (Figure 6.2). There are huge variations in their catchment areas. Approximately, 42% of the stations serve catchment areas <1000 km^2, while 3% cover areas >10,000 km^2.

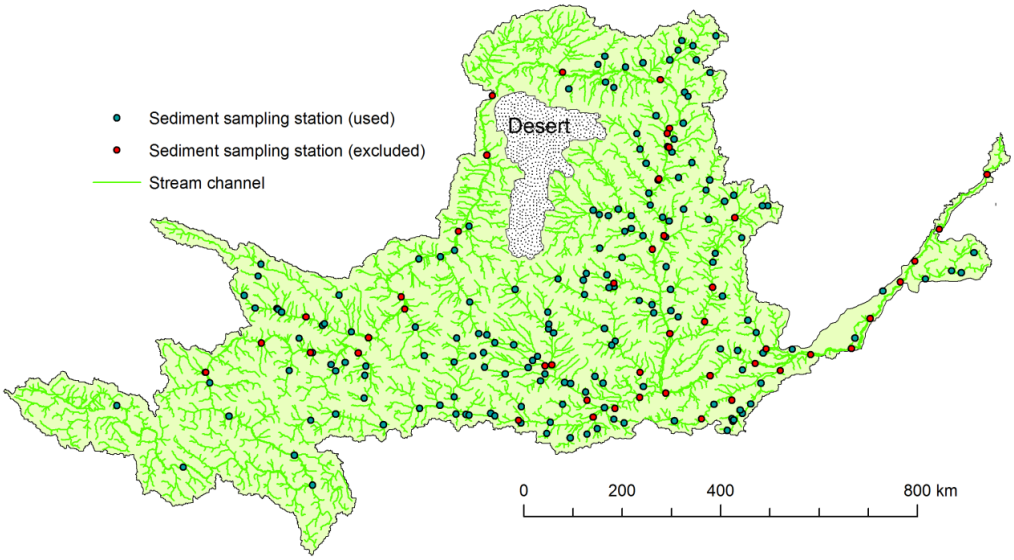

Figure 6.2 Spatial distribution of sediment sampling stations considered in this study. Also shown is the river network extracted from the SRTM DEM dataset.

With the sediment records of the selected stations, a basin-wide sediment yield map was generated through interpolation using the universal Kriging method in ESRI ArcGIS 9.3 (Lu et al., 2003; Hassan et al., 2008). The specific sediment yield for the basin that each station controls was first calculated by dividing the sediment load by the corresponding drainage area. If there are several stations along a river channel with the sub-basins that the upstream stations control contained in the sub-basins that the downstream stations control, the nested sub-basins the upstream stations control were first deducted to remove spatial scaling effects. The specific sediment yield of the remaining basin was calculated by dividing the sediment load difference between the downstream and upstream stations by their drainage area difference. Finally, the obtained specific sediment yields at the 179 stations were interpolated to the whole Yellow River basin to estimate the total basin-wide sediment yield. The pixel size was set as 1×1 km^2, and the value for each pixel was in units of t/km^2/yr. Due to the

aforementioned sediment production characteristics, the river basin was divided into 12 sub-basins (Figure 6.3). In particular, in view of the high soil erosion intensity, the Loess Plateau was divided into 8 sub-basins. In addition, the mainstem reaches were divided into 4 segments with each ending at a hydrological gauge station. Particularly, the Toudaoguai and Huayuankou stations are respectively near the boundary between the upper and middle, and between the middle and lower reaches. The sub-basin boundaries were generated from the SRTM-DEM dataset with a spatial resolution of 90 m (from USGS: http://srtm.csi.cgiar.org). The produced sediment load by erosion for each sub-basin can then be calculated for further analysis after accuracy evaluation. The sediment load data for the period of 1950s-1970 were used to generate a sediment yield map. It is commonly believed that the sediment yield before 1970 was only slightly affected by reservoirs and thus could be used to estimate the maximum sediment trapping (Xu, 2003; 2004; Hassan et al., 2008).

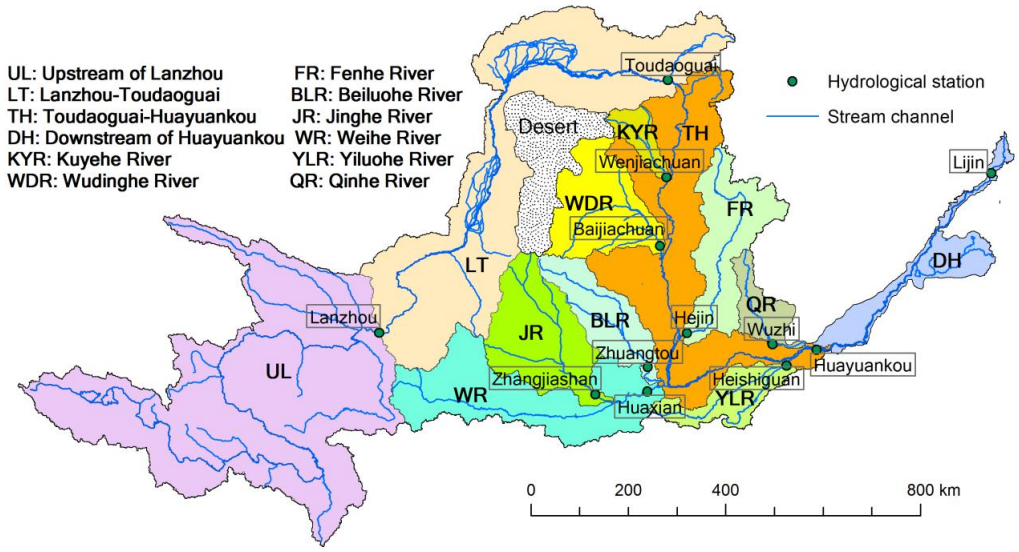

Figure 6.3 Division of the sub-basins of the Yellow River basin. In particular, based on the sub-basin division in Figure 5.13, Kuyehe (KYR) and Jinghe (JR) rivers were also delineated as they represent the highest sediment yielding tributaries.

6.4.2 Calculation of trapping efficiency

For a single reservoir, the theoretical amount of trapped sediment can be calculated through the empirical sediment retention function originally developed by Brune (1953). The same calculation method could also be employed for estimating the total trapped sediment amount of a group of reservoirs in a basin (Vörösmarty et al., 2003; Kummu et al., 2010). Although the original empirical relationship was based on reservoirs in the United States, it has been widely tested and used in other countries as it can provide reasonable estimates of long-term mean sediment *TE* (Morris and Fan, 1998; Syvitski et al., 2003; Kummu and Varis, 2007).

In the Yellow River basin, the improved method by Vörösmarty et al (2003) was adopted, which divided a drainage basin into several sub-basins with each sub-basin being gauged at its outlet. At first, the residence time change for each sub-basin ($\Delta\tau_{reg,j}$) was determined through an aggregate-impounded storage volume and discharge. Then, the aggregate *TE* for each sub-basin ($TE_{reg,j}$) was calculated and the whole basin sediment *TE* (TE_{bas}) was adjusted by a discharge weighting associated with unimpounded interfluvial areas. The detailed computation formulas are as follows:

$$\Delta\tau_{reg,j} = \frac{\sum_{i=1}^{n_j} V_i}{Q_j} \qquad \text{(Equation 6.1)}$$

$$TE_{reg,j} = 1 - \frac{0.05}{\sqrt{\Delta\tau_{reg,j}}} \qquad \text{(Equation 6.2)}$$

$$TE_{bas} = \frac{\sum_{j=1}^{m} TE_{reg,j} Q_j}{Q_m} \quad \text{(Equation 6.3)}$$

where, V_i is the estimated storage of reservoir i (km^3), Q_j is the annual discharge at the mouth of each regulated sub-basin j (km^3/a), Q_m is the annual discharge at basin mouth (km^3/a), n_j is the number of reservoirs in each regulated sub-basin j, and m is the number of regulated sub-basins.

6.4.3 Calibration of sediment trapping

Most reservoirs on the Loess Plateau were constructed during the period of 1970-2000 (Figure 6.4). In contrast to the reservoirs located in the upper reaches where sediment supply is limited, these reservoirs have played an unparalleled role in retaining sediment. However, since reservoir construction is not a consecutive process, it is difficult to precisely estimate how much sediment has been trapped by each reservoir. Therefore, the sedimentation amount cannot be simply computed by using the sediment *TE* and the generated sediment yield map, as only a very small number of reservoirs were completed during the period of 1950-1970 (Figure 6.4). Given the spatial characteristics of sediment production and the reservoir construction history, the obtained sediment load from the 1950-1970 scenario was applied to the period of 1971-1999 in which most reservoirs were completed. Assuming the in-channel sediment delivery process - the ratio of the sediment load measured at the outlet to that entering the upstream channels - remained constant over the two periods, the annual sediment load entering channels during 1971-1999 could then be converted from the 1950-1970 scenario through a sediment load conversion coefficient (C_s):

$C_s = Q_{s,\,1971\text{-}1999} / Q_{s,\,1950\text{-}1970}$ (Equation 6.4)

where, Q_s is the mean annual sediment load recorded at the outlet for each sub-basin. That is, $Q_{s,\,1950\text{-}1970}$ and $Q_{s,\,1971\text{-}1999}$ represent the mean annual sediment load during the periods of 1950-1970 and 1971-1999, respectively.

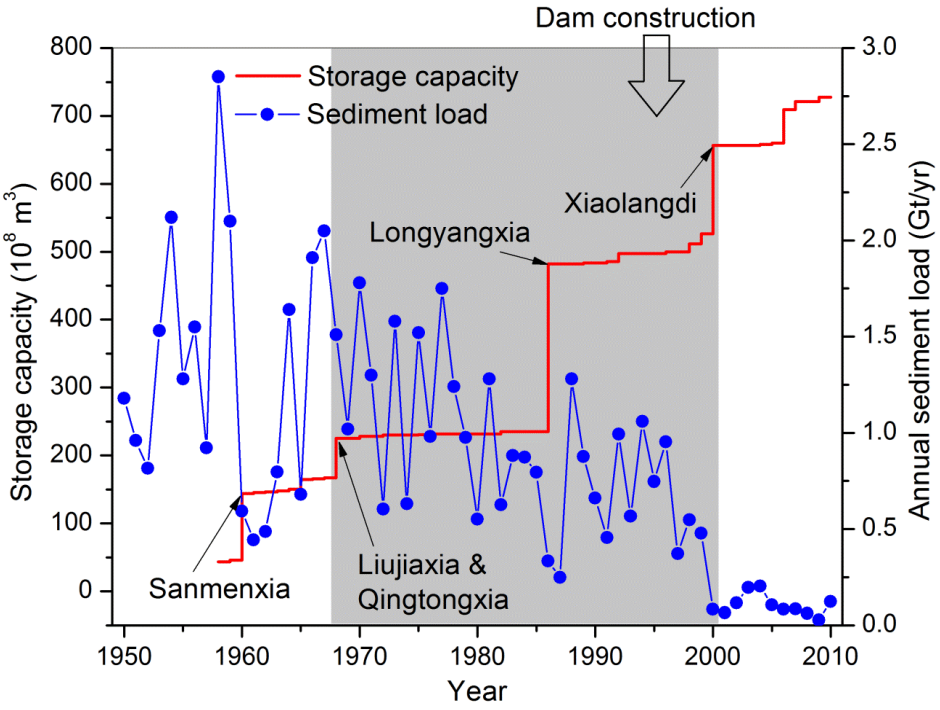

Figure 6.4 Temporal variations of reservoir storage capacity for the Yellow River basin and sediment load at the Huayuankou station. The gray background denotes the period of large-scale dam construction. Also shown are the key reservoirs constructed on the Yellow River mainstem channel (refer to Figures 2.1 and 2.8 for location).

With the conversion coefficient, the actual sediment load during the large-scale reservoir construction period could then be estimated, which will be used to assess the sediment trapping caused by the reservoirs. In addition, it is clear that no reservoir is constructed exclusively for sediment trapping. But rather, it has to be regulated

properly to maintain operation safety and to meet other needs as mentioned earlier. Most often, to effectively control floods, a reservoir will be deliberately emptied by the end of dry season to ensure it has enough storage space for inflowing flood runoff during the flood season (Morris and Fan, 1998). Furthermore, maintaining a reservoir at the highest level where the stored water volume is close to its storage capacity is dangerous and impractical for the Yellow River with relatively low water supply (Zhao, 1996; Hu et al., 2005b).

As a result, most reservoirs in the Yellow River basin are operating at a lower water stage, particularly for these located in the loess region where precipitation is quite low (<500 mm/yr). For the Yellow River basin with high SSC, as the sediment amount transported into reservoirs for deposition correlates closely with the incoming water (Zhao, 1996), the deposited sediment amount is expected to be approximately proportional to the regularly stored water volume. Using 11-year-long monitoring data of water storage changes at seven typical reservoirs in the river basin, their water storage ratios were calculated by dividing the stored water volume over their respective storage capacity (Figure 6.5). On average, the stored waters accounted for about 43.9% of the storage capacity, indicating that less than half of the storage capacity was actually utilized. This ratio will be used to validate the actually trapped sediment amount.

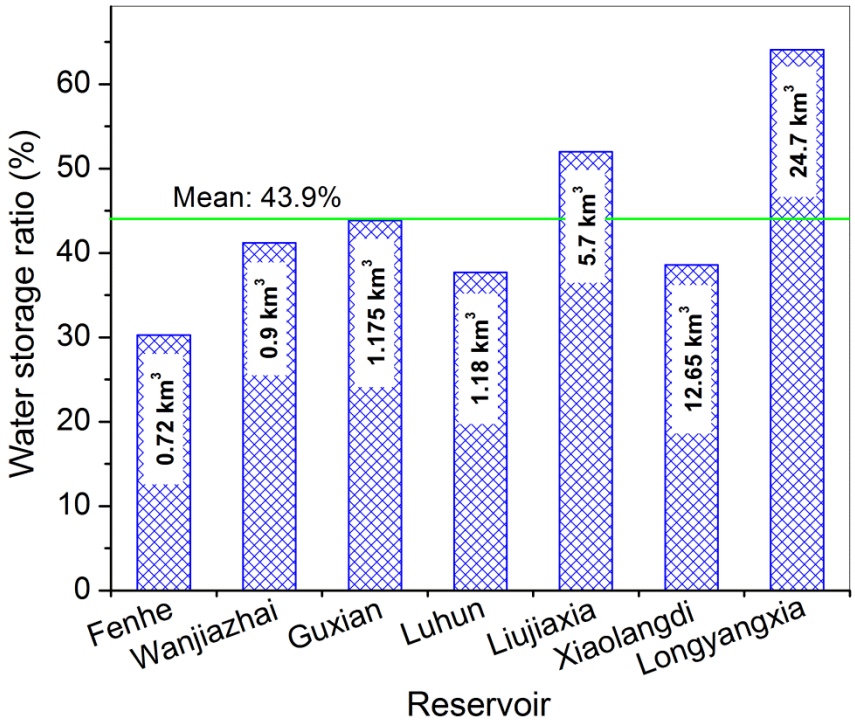

Figure 6.5 Water storage ratio of typical reservoirs during the period of 2000-2010. The figure in each bar denotes the reservoir's storage capacity.

6.5 Results

6.5.1 Sediment trapping efficiency of individual sub-basins

In addition to regulation of the reservoirs, the hydrological regime in the Yellow River has also been significantly affected by other anthropogenic activities, such as irrigation diversion for agricultural production (Chen et al., 2005; Wu et al., 2008a). Together with other irretrievable losses like evaporation, the mainstem water discharge shows a descending trend, especially for the reaches in arid regions with huge tracts of cropland to irrigate. For example, the annual mean water discharge (1950-2009) at the Lanzhou station (basin area: 222,550 km^2) is 308.7×10^8 m^3, while it is only 215.4×10^8 m^3 at the downstream Toudaoguai station (basin area: 367,572 km^2) over the same period. Similar downstream reductions can also be found between

the Huayuankou (basin area: 730,000 km^2) and Lijin (basin area: 752,146 km^2) stations. In this sense, it is unreasonable to apply the water discharge data measured at gauge stations to calculate the residence time change ($\Delta\tau_{reg,j}$) and the potential sediment *TE*. But rather, the natural water discharge reconstructed by Li and Yang (2004) was used to assess the residence time and the subsequent sediment trapping. They first divided the river basin into several small sub-basins based on hydrological characteristics, and then reconstructed their natural water discharge by summing the measured water discharge at the outlet and the water volumes of agricultural consumption, domestic use, and reservoir storage (see Chapter 5).

The calculated results are presented in Table 6.1. The discharge-weighted mean $\Delta\tau_{reg}$ varies substantially among the sub-basins, which is highly correlated to the scale of reservoir construction, including reservoir size and number. With several gigantic reservoirs, the mainstem stretches usually have higher residence time. For example, water in the sub-basin upstream of Lanzhou and in the Toudaoguai-Huayuankou stretch has a residence time of around 1.05 and 4.8 yr, respectively. In contrast, except for the Wudinghe River, the residence time for the other tributaries is mostly short, usually in the range of 0.1-0.34 yr.

Table 6.1 Summary of sub-basin sediment trapping efficiency (*TE*).

Sub-basin	Controlling station	Reservoir number	Storage	Natural annual discharge	$\Delta\tau(yr)$	*TE* (%)
			km^3	km^3/yr		
Mainstem stretch:						
Lanzhou-Toudaoguai (LT)	Toudaoguai	301	0.605	1.527	0.396	92.1
Toudaoguai-Huayuankou (TH)	Huayuankou	723	25.151	5.258	4.783	97.7
Downstream of Huayuankou (DH)	Lijin	113	0.881	2.649	0.333	91.3
Tributary:						
Kuyehe River (KYR)	Wenjiachuan	20	0.073	0.753*	0.097	83.9
Wudinghe River (WDR)	Baijiachuan	196	1.196	1.541*	0.776	94.3
Beiluohe River (BLR)	Zhuangtou	345	0.103	0.89	0.116	85.3
Weihe River (WHR)	Huaxian	359	0.595	6.976	0.085	82.9
Jinghe River (JR)	Zhangjiashan	204	0.447	1.953	0.229	89.6
Yiluohe River (YLR)	Heishiguan	59	1.058	3.153	0.336	91.4
Qinhe River (QR)	Wuzhi	38	0.129	1.186	0.109	84.9
Fenhe River (FR)	Hejin	223	0.56	2.103	0.266	90.3
Mainstem accumulative basin:						
Upstream of Lanzhou (UL)	Lanzhou	235	35.912	34.244	1.049	95.1
Upstream of Toudaoguai	Toudaoguai	536	36.517	35.771	1.021	95.1
Upstream of Sanmenxia	Sanmenxia	2581	53.825	54.13	0.994	95
Upstream of Huayuankou	Huayuankou	2703	65.108	59.584	1.093	95.2
Upstream of Lijin (whole basin)	Lijin	2816	66.71	62.233	1.072	95.2

* Averaged based on measured data during 1950s-1970 retrieved from the Yellow River Sediment Bulletins, this time period is usually assumed without strong human interventions and flow varied under "natural" conditions (Xu, 2004). $\Delta\tau$ is water residence time, and *TE* represents sediment trapping efficiency.

As shown in Table 6.1, the sediment *TE* in the river basin is generally high. For the tributary basins, the *TE* ranges from 82.9% to 94.3%, depending on the reservoir size and the natural water discharge. The lowest sediment *TE* occurs in the Weihe River basin, while the highest *TE* is in the Wudinghe River basin. As for the mainstem accumulative basins, the sediment *TE* is highly similar (Table 6.1), ranging from 95% to 95.2%. In view of the river basin as a whole, potentially 95.2% of the sediment could be trapped by reservoirs, if other factors like reservoir operating schedule are not taken into account.

6.5.2 Estimation of the trapped sediment amount

Using the 20-year-long sediment records of the selected 179 stations located throughout the Yellow River basin, the basin-wide sediment yield map was generated (Figure 6.6). Before the implementation of soil conservation practices, sediment yield in the basin was very high. The Loess Plateau is the major sediment source, in particular the upper segment of the middle reaches near the desert. Coupled with hyperconcentrated flows that have the ability to carry almost all the eroded sediment downstream to the mainstem channel, the specific sediment yield can be greater than 20,000 $t/km^2/yr$, which is consistent with the region's strong soil erosion characteristics (Jing et al., 1993). The specific sediment yield in the upper Yellow River is mostly lower than 1000 $t/km^2/yr$, except in the tributaries close to Lanzhou which originate in the loess regions (see Figure 2.1). In contrast, the lower Yellow River basin produces little sediment owing to its good vegetation cover and strong soil resistance to erosion.

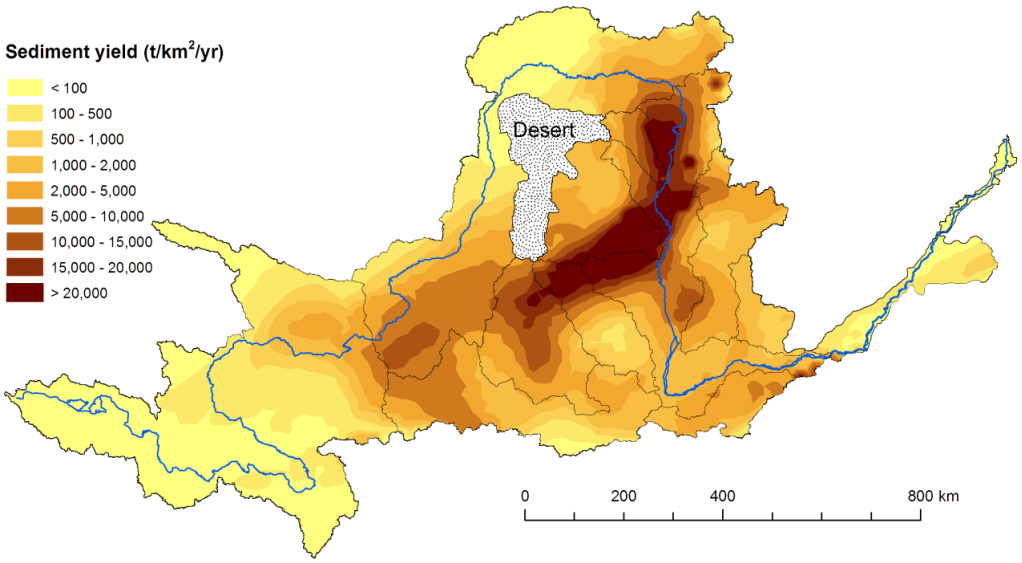

Figure 6.6 Spatial variation of the sediment yield in the Yellow River basin during 1950-1970 through universal Kriging interpolation.

Based on the interpolated sediment yield map, annual sediment load reaching channels during the period of 1950-1970 was about 2.483 Gt (Table 6.2). The measured sediment load at hydrological stations represents upstream sediment dynamics of both production on sloping lands and transport in stream channels. Although the adopted interpolation method has significantly removed the scaling effect by dividing the basin into small and separate patches, it could not remove the potential impacts of channel erosion or storage before sediment is measured at the hydrological stations. For all the sub-basins (or patches) that each hydrological station controls, the sediment yield by interpolation is slightly higher than that measured at the stations (Figure 6.7).

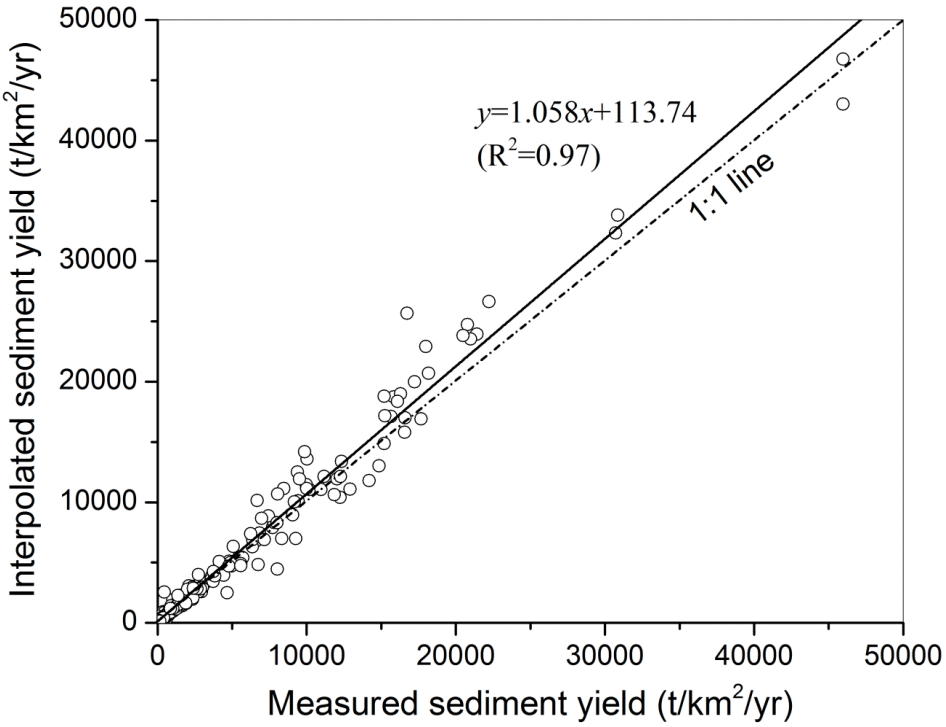

Figure 6.7 Differences in sediment yield between the interpolated using universal Kriging and the measured at the hydrological stations.

It is clear that a certain amount of sediment should have been deposited within the channels, but the proportion is small as compared to the total sediment quantity. Furthermore, considering the fact that some small reservoirs were situated immediately downstream of the sediment production areas, a portion of the sediment would have been trapped before channel deposition. Therefore, the effect of channel storage on sediment trapping is likely small, and correcting the estimated sediment trapping is not necessary. Approximately, 91.9% of the sediment came from the Loess Plateau, while the sub-basin above Lanzhou and the lower Yellow River reaches (downstream of the Huayuankou station) contributed around 7.8% and 0.3%, respectively.

If all the reservoirs were completed in 1970 and started impounding sediment immediately, the sediment trapping for each sub-basin can be determined by combining the generated sediment load with the potential *TE* of the reservoirs listed in Table 6.2. Nevertheless, it must be pointed out that these results are based on the assumption that all reservoirs had been put into full operation since 1970, and no other measures causing the sediment reaching channels to decrease were conducted. Under this assumption these reservoirs can collectively trap sediment of about 2.36 Gt per year. As the obtained sediment trapping amount was based on the storage capacity, it is therefore the maximum sediment amount the impoundments could retain in theory.

Taking into account the operation conditions of each reservoir, the potentially trapped sediment amount can be estimated by multiplying the mean water storage ratio (C_w) by the maximum sediment trapping (Table 6.2). For the whole river basin, roughly 1.04 Gt of sediment would be intercepted by reservoirs each year. That is, under the assumption of the absence of other strong human activities like soil conservation programmes (i.e., for the period 1950-1970), these reservoirs are able to intercept around 41.8% of the sediments reaching the channels from sloping lands.

Table 6.2 Summary of sediment yield and corrected reservoir sediment trapping amount.

Sub-basin	Sediment load	Maximum sediment trapping	Corrected Sediment trapping (C_w)	C_S	Actual sediment trapping (2000-2010)
	Gt/yr	Gt/yr	Gt/yr		Gt/yr
Upstream of Lanzhou (UL)	0.1941	0.1846	0.0810	0.429	0.0347
Lanzhou-Toudaoguai (LT)	0.3651	0.3363	0.1476	0.580	0.0856
Kuyehe River (KYR)	0.0968	0.0812	0.0357	0.672	0.0240
Wudinghe River (WDR)	0.2533	0.2389	0.1049	0.355	0.0372
Beiluohe River (BLR)	0.1644	0.1402	0.0616	0.741	0.0456
Weihe River (WHR)	0.1866	0.1672	0.0734	0.448	0.0329
Jinghe River (JR)	0.2966	0.2459	0.1079	0.796	0.0859
Yiluohe River (YLR)	0.0527	0.0482	0.0211	0.169	0.0036
Qinhe River (QR)	0.0134	0.0114	0.0050	0.250	0.0013
Fenhe River (FR)	0.1063	0.096	0.0421	0.210	0.0088
Toudaoguai-Huayuankou (TH)	0.7478	0.8075*	0.3545*	0.645	0.2287*
Downstream of Huayuankou (DH)	0.0060	0.0055	0.0024	0.519	0.0012
Total	2.4831	2.3628	1.0372		0.59

* Sediment subject to deposition into the reservoirs of the TH stretch was also supplied from the tributaries and upstream reaches.

The sediment load conversion coefficient C_s varies significantly among the sub-basins (Table 6.2), ranging from 0.169 to 0.796. With the determined C_s for each sub-basin, the sediment load reaching channels during 1971-1999 was quantified, upon which the trapped sediment load after 1999 was estimated (Table 6.2). For a given basin, reservoir sediment trapping is highly dependent on reservoir number and storage capacity with large storage capacity usually trapping more sediment, such as the Toudaoguai-Huayuankou stretch that has two large reservoirs (the Sanmenxia and Xiaolangdi, Figures 2.1 and 6.3). While reservoirs in the high sediment yield areas could retain more sediment due to sufficient sediment supply, the reservoirs in the sub-basin below Huayuankou (the DH stretch) intercepted the least resulting from limited sediment sources (Table 6.2). In total, annually about 0.59 Gt of sediment has been retained during 2000-2010. Over the same period, the mean sediment load at the Huayuankou station has decreased to 0.1 Gt/yr from 1.34 Gt/yr during the period of 1950-1970, indicating the sediment load reduction caused by reservoir trapping contributes around 47.6% to the total reduction.

6.5.3 Total trapped sediments in the Yellow River basin

Although reservoir construction in the Yellow River basin started in the late 1950s, most of these reservoirs are situated in tributary channels and are small. In the 1960s, great advantages of reservoir trapping sediment and reducing in-channel sedimentation for the lower Yellow River were recognized. Several large dams, including the Sanmenxia and Liujiaxia, were completed during this period. Since the 1970s, driven by accelerated soil erosion and favorable vegetation restoration policies,

massive reservoir construction has been carried out throughout the basin. In particular, a number of medium and small reservoirs were completed on the Loess Plateau.

During 1990-1992, a basin-wide reservoir sedimentation investigation in the Yellow River basin was conducted. For the 601 reservoirs with storage capacity larger than 1 million m^3, the deposited sediment in the backwater zones was estimated at 10.9 billion m^3 by 1989, which accounts for 21% of the total storage capacity at the time (Han and Yang, 2003). Sedimentation amount up to 2000 in the major reservoirs of the Yellow River basin is tabulated in Table 6.3. Totally, 13.42 Gt of sediment had been trapped by 2000. In particular, it showed that most of the sedimentation occurred in the largest reservoirs, such as the Sanmenxia, Liujiaxia, and Qingtongxia.

Table 6.3 Major reservoir sedimentation in the river basin before 2000.

Reservoir name	Initial storage capacity	Filled sediment	Time period
	km^3	Gt	
Sanmenxia	9.75	8.908	1960 - 1997
Liujiaxia	5.7	1.833	1968 - 2000
Longyangxia	24.7	0.277	1986 - 2000
Qingtongxia	0.62	0.736	1967 - 2000
Yanguoxia	0.22	0.24	1962 - 2000
Tianqiao	0.068	0.076	1977 - 2000
Wangyao	0.203	0.134	1978 - 2000
Wanjiazhai	0.898	0.078	1997 - 2000
Bapanxia	0.049	0.038	1970 - 1999
Bajiazhui	0.525	0.42	1961 - 2000
Fengjiashan	0.389	0.11	1974 - 2000
Fenhe	0.7	0.472	1961 - 2000
Sanshenggong	0.08	0.056	1960 - 1999
Taoqupo	0.057	0.019	1979 - 1995
Yangmaowan	0.12	0.023	1973 - 1995
Total	44.08	13.42	

Among the numerous reservoirs in the basin, the Sanmenxia Reservoir represents a milestone of watershed management (Figure 2.1). As a multipurpose project, it is the first large water control project ever built on the Yellow River mainstem channel. The drainage area above the dam supplies 89% of the runoff and 98% of the sediment to the lower Yellow River (Wang et al., 2005). With a storage capacity of 9.75 billion m^3 below the elevation of 335 m, the reservoir was originally expected to impound inflowing sediment and control flood flows entering the downstream reaches. However, due to underestimation of the importance of soil erosion and sediment transport at the design stage, sedimentation behind the dam occurred soon after the completion in 1960 (Figure 6.8). During the first 18 months after the river was closed, approximately 1.8 Gt of sediment accumulated in the reservoir. Although immediate measures were taken to control the rapid sedimentation, about 8.9 Gt of sediment has been impounded by 1997 (Table 6.3). Since then, the total sedimentation amount has remained roughly stable (e.g., ~9 Gt by 2006, Zhang et al., 2008).

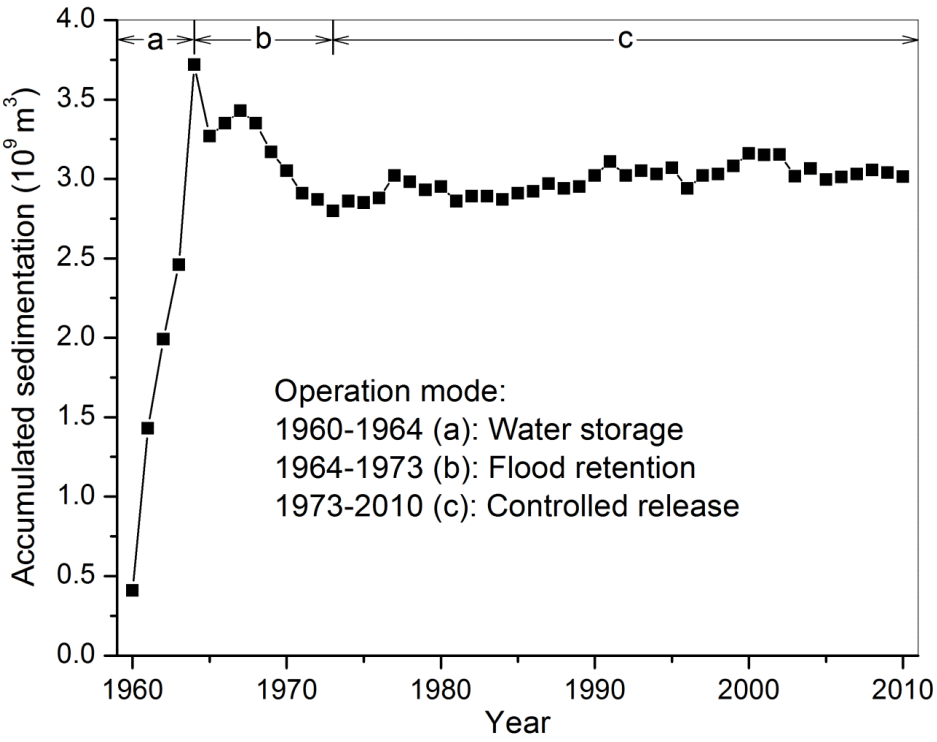

Figure 6.8 Temporal variation of the accumulated sedimentation volume in the Sanmenxia Reservoir below the Tongguan station (adapted from Wang et al., 2005).

For the latest decade, the largest sediment control project constructed in the river basin is the Xiaolangdi Reservoir (see location in Figure 2.1). With a dam height of 154 m and a sediment trapping storage of 7.55 billion m^3, one major purpose of the reservoir is to intercept sediment coming from the Loess Plateau and thus alleviate channel sedimentation problems in the lower Yellow River. Consequently, a huge amount of sediment has been trapped since its operation in 1999. With continued sedimentation behind the dam, the storage capacity has shrunk sharply to 99.2×10^8 m^3 (or 9.92 billion m^3) in 2010 (Figure 6.9a).

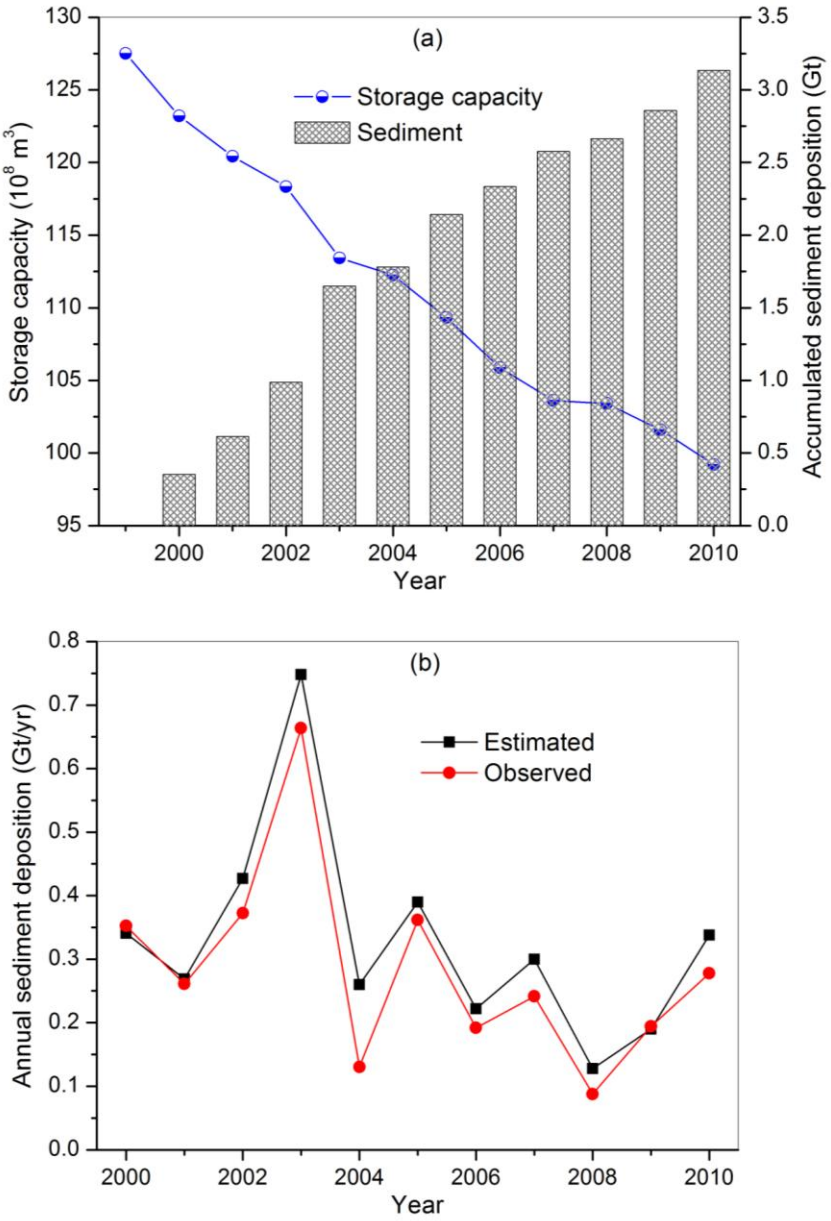

Figure 6.9 Sediment deposition in the Xiaolangdi Reservoir since its completion. (a), continued storage capacity loss due to sediment deposition; (b), comparison of sediment deposition between *TE* based estimation and bathymetric survey made by the YRCC.

Using the estimated 0.59 Gt per year as the mean sedimentation rate, the deposited sediment amount in the recent decade is 5.9 Gt. In total, the sediment amount trapped by reservoirs up to 2010 is 19.32 Gt, which is close to the estimate by Chu et al (2009) of 17.52 Gt. In addition to the reservoirs analyzed in this study, various soil

conservation practices conducted in the drainage basin have also played important roles in reducing seaward sediment load (Wang et al., 2007). Among these practices, the widely constructed silt check dams in the highly erodible Loess Plateau valleys have made the biggest contribution to the measured sediment reduction (Zhao, 1996). Supported by the authority since the 1950s, substantial money and labor have been invested into developing silt check dams. As a result, about 110,000 silt check dams have been completed on the Loess Plateau by 2010 to retain sediment (Chang, 2011). It is estimated that more than 21 Gt of sediment has been intercepted with a mean sedimentation rate of about 0.35-0.45 Gt per year (Chang, 2011; Xin et al., 2012). Summing all the trapped sediments together, approximately 40.32 Gt of sediment has already been trapped behind human-made dams in the river basin.

6.6 Discussion

6.6.1 Error analysis and reliability

Given the complexity of sediment production in the basin with high spatial heterogeneities and the long duration of reservoir construction, the obtained estimate should be considered with caution. Other factors that could affect the sedimentation amount were not accounted for here.

Reservoir operating schedules are diverse and could significantly affect sediment deposition (Morris and Fan, 1998). One example is the Sanmenxia Reservoir (Figure 6.8). Since its completion in 1960, the reservoir has undergone three different operation modes to maintain a sediment balance. During the first few years, the

reservoir was operated at a high-head operation mode to retain sediment according to the original design. As a result, about 93% of the incoming sediment was trapped, with only 7% released downstream (Wang et al., 2005). The accumulated sediment deposition below the elevation of 335 m reached 4.05 billion m^3 by 1964, amounting to a 41.5% loss of the corresponding storage capacity. To mitigate the deposition problems, the reservoir was renovated twice and its operating schedule was adjusted in 1964 and 1973. Since then, reservoir sedimentation has been greatly reduced and a relatively stable sediment balance has been reached. In some years, the reservoir has even been reverted to scouring from deposition due to human-made floods. It is therefore clear that different operating schedules influence the trapped sediment amount, and necessary care is needed in applying the method for sedimentation estimation.

The Xiaolangdi Reservoir provides another excellent example of substantial sedimentation variations resulting from changing operating schedules (Figure 6.9b). During the first two years, as the reservoir was mainly operated to trap sediment, the estimated sedimentation was very close to the investigation values. While in the following years, with human-made density currents to reduce sedimentation in the reservoir and to scour the lower Yellow River mainstem channel, the annual sedimentation rate decreased accordingly. In particular, two large density currents made in 2004 resulted in about 56.4% of the input sediment being discharged into the downstream channel (Zhang et al., 2008), causing a considerable difference between estimated and observed values. Comparison of the deposited sediment between the

TE based estimation and the bathymetric survey made by YRCC suggests that the empirical sediment retention function can be used to estimate the trapped sediment amount (Figure 6.9b).

Furthermore, due to delineation failure from the satellite images, about 300 'missing' small reservoirs were not taken into account (see Chapter 5). These small reservoirs are mostly located on the first-order river channels where sediment is directly supplied from sloping lands. In such cases, the incoming sediment usually has a higher coarse particle component and a higher concentration in contrast to the sediments already transported for a certain distance within the channels. Thus, the missing small reservoirs are able to trap sediment more efficiently. However, given their small storage size and the decreased water and sediment supply, the total retained sediment by all reservoirs would not be substantially changed. In addition, as no large reservoirs were reportedly completed during the period 2006-2009, the recently completed small reservoirs in this interval period would not significantly underestimate the sedimentation amount estimated in this study.

Other potential influencing factors include climate change and ecological recovery. Decreased precipitation resulting from climate change has been suggested to account for 20% or even more of the total sediment load reduction (Wang et al., 2007; Peng et al., 2010). Recent ecological restoration efforts made in the basin have also started to pay off, which have helped to reduce the soil erosion intensity (Fu et al., 2011). With

decreasing precipitation and increasing vegetation cover, the available sediments subject to deposition in reservoirs will be reduced.

It seems that changes in the operating schedules, precipitation, and vegetation cover tend to facilitate overestimation of the actual sediment deposition amount, while ignoring small reservoirs would then result in underestimation. Considering that large reservoirs on the mainstem channel, such as the Sanmenxia and Xiaolangdi, can intercept far more sediment than the small ones (Wang et al., 2006), it is expected that neglecting the missing small reservoirs would not significantly affect the total deposited sediment amount. Therefore, the recent annual sedimentation rate of 0.59 Gt is reliable. Comparing the calculated total trapped sediments with the estimate of Chu et al (2009) also suggests that the adopted methods are applicable. Obviously, the above arguments only make the estimation results more believable, but not free from errors. These errors, which are too complex to be defined definitely, may be introduced by data accuracy problems or by assumptions made in the calculations. Further amendments to the results can be achieved through more comprehensive field investigations and corrections.

6.6.2 Implications for basin-wide sediment and carbon delivery

Length of the residence time reveals a reservoir's potential ability to regulate the flow and sediment dynamics (Chapter 5). A longer residence time suggests that the sediment is more likely to be deposited within the reservoir. Likewise, high sediment *TE* suggests the strong regulation effects of artificial impoundments on sediment

delivery process. With the sediment *TE* for all the sub-basins greater than 80%, the sediment *TE* of reservoirs in the Yellow River basin is much higher than the global mean value (28%), and is comparable to that in other large rivers, such as the Nile, Indus, and Colorado rivers (Vörösmarty et al., 2003). The high sediment *TE* is the result of massive reservoir construction with an attempt to mitigate the serious channel sedimentation in the lower Yellow River (Wang et al., 2007b; Wu et al., 2008a). Currently, extensive reservoir construction in the Yellow River basin is underway. In particular, several large reservoirs are located on the mainstem channel near the sediment production source area. Upon completion, the *TE* will be further increased and, as a result, more sediment deposition will occur in the reservoirs.

The obtained sediment yield through spatial interpolation is close to the estimates made by using statistical tools or numerical models (Shi, 1990; Fu et al., 2011). The slight deviation of the fitted line from the 1:1 line suggests that the sediment delivery ratio at small scale is about 0.95 (Figure 6.7), which is consistent with the Yellow River's high sediment delivery characteristics in the sediment source areas (Zhao, 1996; Jing et al., 1993; Walling and Fang, 2003). In contrast, at the basin scale, the sediment delivery ratio is only 0.49 determined by dividing the mean annual seaward sediment load recorded at Lijin station by the total annual sediment load (refer to Figure 2.1 for location). The lower sediment delivery ratio reflects strong sediment storage and associated buffering capacity of the drainage basin. Substantial fluvial sedimentation must have occurred during the sediment delivery process, particularly in the lower mainstem channel which acts as a net sediment sink (Wang et al., 2007b).

Accordingly, large amounts of organic carbon, in particular the particulate fraction (POC) that is transported with sediment, must have also been sequestered.

The highly variable conversion coefficient C_s reflects the magnitude of sediment reduction over the two periods. Generally, C_s variability demonstrates the effects of human activities on sediment production and delivery. For example, in the Wudinghe River basin, large-scale soil conservation programmes have been carried out to control soil erosion since the 1970s and as a result, the annual sediment load has decreased sharply (Xu, 2004), resulting in a comparatively lower C_s. Although widespread soil conservation and reservoir construction efforts have been conducted throughout the whole river basin, the lowest C_s occurred only in the sub-basins with an initially low sediment yield, such as the Fenhe, Yiluohe, and Qinghe tributaries (Table 6.1; Figure 6.6). In comparison, the C_s for the major sediment production regions, such as the Kuyehe, Beiluohe, and Jinghe tributaries, remained high, although far more soil conservation efforts have been devoted to these sub-basins.

Construction of reservoirs plays a predominant role in sediment load reduction for most large Asian rivers (cf. Lu and Siew, 2006; Chu et al., 2009; Wang et al, 2011a). However, it is not straightforward to assess the cumulative impact of all the reservoirs on the seaward sediment load reduction. As for the reservoirs constructed in the Yellow River basin, Wang et al (2007) concluded that only 30% sediment load reduction was caused by reservoirs. However, it seems this is an underestimate, because the sediment retention in the Xiaolangdi Reservoir alone has represented 23%

of the total decrease (from YRCC data), while with the Sanmenxia Reservoir they have collectively accounted for 30% (Peng et al., 2010). If all the other reservoirs were taken into account, their contribution to the total reduction should be higher, on the order of 47.6% as obtained in this study. Based on global reservoir inventory, Vörösmarty et al (2003) found that the global annual sedimentation rate of all registered reservoirs was estimated to be on the order of 4-5 Gt/yr. That is, sedimentation in the Yellow River basin contributes around 12%-15% to the global mean sedimentation rate. Similarly, with organic carbon burial associated with the deposited sediment within the reservoirs in the Yellow River basin, its contribution to the global carbon budget will be considerable. In view of the importance of the Yellow River in global sediment transport and the continuing sediment retention efforts, the estimated annual sedimentation amount of 0.59 Gt is consistent with its contribution to global annual sedimentation rate.

Assuming the sediment density to be 1.3 t/m^3 (Chu et al., 2009), the recent annual sedimentation rate corresponds to an annual storage capacity loss of about 0.454×10^9 m^3, thus annually the river basin is losing approximately 0.6% of its total water storage capacity to sedimentation. As for the total trapped sediment amount by reservoirs, the corresponding storage capacity loss is 14.86×10^9 m^3. That means a large reservoir with storage larger than the Xiaolangdi (12.65×10^9 m^3) has been lost to sedimentation. On the other hand, the seaward sediment load reduction has negatively brought about a multitude of morphological, ecological, and biogeochemical responses in the downstream channels, estuary, and the delta regions

(Wang et al., 2007b; Syvitski et al., 2009). Reduced sediment load due to retention by reservoir cascades has caused a continuous channel scouring and bank collapse in the lower Yellow River channel (Xia et al., 2008). Because the greatly decreased sediment delivery could not resist coastal erosion, some preliminary studies have suggested that the Yellow delta size has greatly shrunken, which further triggered a series of problems, such as ecological degradation and biodiversity loss in the delta wetlands and loss of productive land for farming (Cui et al., 2009; Peng et al., 2010) .

However, although these complex responses have become recognized, they have yet to be fully investigated. In particular, as has been stated earlier, because particulate carbon is intimately tied to sediment transport, burial of sediment has significant implications for the global carbon budget (Syvitski et al., 2005), and should thus be given more attention in the context of impending global warming. In view of the high sediment yield and high sediment *TE* of the reservoirs, sedimentation in the Yellow River basin may have global significance in carbon sequestration studies.

6.7 Summary and conclusions

Sediment deposition in reservoirs can not only influence reservoir operation and affect the downstream fluvial system negatively; it can also play a significant role in affecting the carbon cycle at the watershed or global scale. Necessary and accurate estimate of the deposited sediment is therefore important for better reservoir management and for understanding the closely correlated carbon cycle. Using remote sensing images capturing the reservoirs constructed in the Yellow River basin and

sediment records collected from hydrological gauge stations scattered throughout the basin, the cumulative reservoir sediment trapping in the Yellow River basin was fully evaluated.

With the sediment *TE* larger than 80% for all the sub-basins, theoretically reservoirs in the river basin are able to trap most of the sediment reaching the channels. For the Yellow River basin as a whole, the sediment *TE* of 95.2% is comparable to other large river basins, which suggests that the reservoirs can collectively make a significant anthropogenic signature on basin-wide sediment delivery. The sediment yield interpolation results summarized that the annual sediment load reaching observable channels during 1950-1970 was about 2.483 Gt. Taking into account the water storage changes and the reservoir construction history, the total trapped sediment amount was corrected. In the recent decade, the reservoir sedimentation rate was estimated at 0.59 Gt per year, which approximately accounted for 47.6% of the total annual sediment load reduction. In total, 19.32 Gt of sediment has been trapped by reservoirs by 2010, of which 5.9 Gt was impounded in the past decade and the remaining 13.42 Gt was intercepted prior to 2000 by major reservoirs. Summing up the trapped sediments by silt check dams showed that about 40.32 Gt of sediment has been artificially fixed in valleys or channels, revealing the tremendous effects of human-made dams on reducing seaward sediment load.

Sedimentation has posed a great risk for reservoirs of the Yellow River basin. Recent annual sedimentation rate demonstrates that the total storage capacity has been losing

at a rate of 0.6% per year, and accumulatively a giant reservoir larger than the Xiaolangdi has been lost to sedimentation. From a global perspective, reservoir sedimentation in the Yellow River basin represents about 12%-15% of the global mean sedimentation rate. Driven by rapid economic development and growing energy shortages, the Yellow River basin has been listed as a key area for water resources development. Numerous reservoirs are under construction or being planned. With new reservoirs, particularly these located on the Loess Plateau or immediately downstream of it, are commissioned, the magnitude of sediment retention by reservoirs will be further enhanced. Accordingly, the sediment load reaching the lower Yellow mainstem channel and the ocean will be further reduced. The resultant changes in downstream channel morphology and ecological system near the estuary require more efforts to elucidate. With the estimated sediment trapping by dams during the past few decades and the associated organic carbon content, the buried organic carbon due to sediment trapping will be investigated in the next chapter. In addition, the impact of dam trapping on the basin-wide organic cycle will be discussed through budgetary calculations by taking into account the erosion, transport, and deposition processes of organic carbon within the Yellow River basin.

Chapter 7 Erosion-induced organic carbon budget within the basin

7.1 Introduction

As one of the most active mechanisms controlling soil formation and evolution, soil erosion affects not only the translocation of soil materials, but also the dynamics of organic carbon (OC) and nutrients, such as nitrogen and phosphorus. The 2300 Gt of carbon stored in the soil globally is 3 times the size of the atmospheric carbon pool and 4.1 times the biotic carbon pool (Lal, 2003). Soil erosion in terrestrial ecosystems is therefore capable of influencing global carbon redistribution among the five strongly interrelated carbon pools, with the other two being the oceanic and geologic carbon pools. Quantifying carbon transport within each pool or exchange between different pools is of key importance for refining the understanding of the carbon cycle at watershed, regional, and global scales.

Owing to the difficulty of constraining the carbon source/sink strength at erosional and depositional sites, the impact of soil erosion on associated carbon cycling has not been well documented. Prior estimates of the portion of soil organic carbon (SOC) oxidized during soil erosion and sediment transport range from 0% to almost 100% (e.g., Schlesinger, 1995; Smith et al., 2001; Cole and Caraco, 2001; Van Hemelryck et al., 2011; Lal, 2003; Mchunu and Chaplot, 2012). With varying carbon oxidation rates, the global soil erosion process has been described both as a net carbon source of around 1 Gt/yr (Lal, 2003) and a net carbon sink of up to 1.5 Gt/yr (Stallard, 1998). It

is clear that the fate of SOC mobilized by erosional processes remains largely unknown.

For the Yellow River basin, although a number of studies have attempted to analyze its sediment dynamics at a sub-basin scale, systematic assessment of its basin-wide sediment budget taking into account both natural transport and anthropogenic impact is lacking. Furthermore, despite the fact that preliminary studies on the transport of OC in worldwide rivers have been documented, Asian rivers, which alone contribute about 40% of global sediment flux, have not received sufficient attention in terms of OC transport (Schlünz and Schneider, 2000). Given such high sediment fluxes, it is expected that the OC fluxes for Asian rivers is substantial. With respect to the Yellow River, there is currently a great gap in knowledge regarding its sediment and OC cycles. Understanding these cycles may also have global implications, given its extremely intense land use and high sediment transport. Several investigations concerning OC transport in the Yellow River basin show that most of the OC is transported in the particulate form, while the dissolved fraction accounts for less than 10% of the total, due to its high sediment load and relatively low water discharge (Gan et al., 1983; Zhang et al., 1992; Cauwet and Mackenzie, 1993). Analyzing the fate of OC could provide insights into understanding the basin-wide OC cycling.

With the estimated reservoir sediment trapping in Chapter 6, this chapter investigated the sediment and organic redistribution across the landscape and the amount of carbon decomposed through soil erosion and sediment transport within the Yellow

River basin during the period 1950-2010. Compared with conventional methods by using models with many assumptions, the fates of eroded OC were analyzed by constructing a bulk sediment budget (Smith et al., 2001). The obtained results would provide new insights into understanding the role soil erosion plays in carbon cycling and the impacts of large-scale human activities on the watershed carbon budget.

7.2 Data and methods

7.2.1 Data sources

Sediment flux and water diversion data were extracted from the Yellow River Sediment Bulletins produced by the Yellow River Conservancy Commission (YRCC). The basin-wide soil map to estimate SOC was provided by the Environmental and Ecological Science Data Center for West China (http://westdc.westgis.ac.cn). The map is based on the second national soil survey results conducted since 1979, which was compiled by the Institute of Soil Science, Chinese Academy of Sciences. The spatial resolution for each raster grid cell is 1×1 km^2. The SOC content for each soil profile was compiled in two depth classes, including the topsoil (0-30 cm) and the subsoil (30-100 cm). The Yellow River basin is covered by 9123 polygons with each including a soil profile. The soil map provides an important measure for assessing the spatial variations of SOC throughout the basin. Given that the SOC content decreases with depth in soil horizon, only the SOC content in the topsoil is considered in this study, because it is the topsoil horizon that closely correlates with soil erosion processes. However, it is important to note that, as the soil map is based on modern soil surveys, properties of the soil reflect human-induced changes, and thus are

primarily a function of long-term regional factors with an overprint of recent impacts of human activities.

In addition to these datasets, research results reported in the literature were used. Estimation of basin-wide water erosion has been made for the highly erodible Loess Plateau. In recent years, statistical approaches and established empirical models, such as the Universal Soil Loss Equation (USLE), have been tried to estimate the basin-wide soil erosion (e.g., Li and Liu, 2006; Fu et al., 2011). Generally, the model-based water erosion estimates are consistent with these extrapolated from field observations.

7.2.2 Conceptual framework

Processes of soil erosion by water in a drainage basin is usually composed of three phases, including production, transport, and deposition of soil particles. The production occurs in the uplands where soil is vulnerable to erosion, and the eroded soils and associated chemical elements are subject to transport and deposition along their course to the ocean (Figure 7.1). Understanding erosional effects on sediment and the carbon cycle requires consideration of all three phases. For the Yellow River basin, all the three phases have been affected by human activity mainly through soil conservation, dam construction, and irrigation withdrawal, as shown in Figure 7.1.

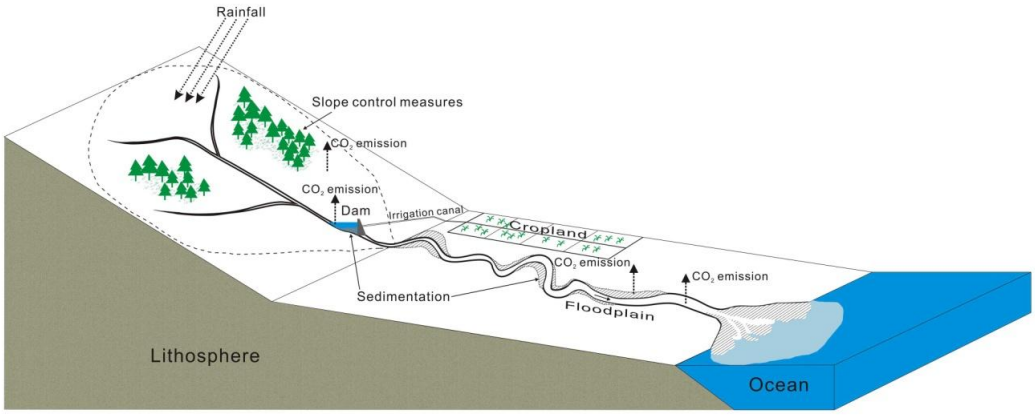

Figure 7.1 A sketch map showing production, transport, and deposition of bulk sediment and soil organic carbon within an eroding basin and the impact of human activity.

A simple transport model for production, transport, and sedimentation of bulk sediment through various transport pathways and depositional compartments can be expressed as follows:

$$E_S = T_S + H_S + W_S + O_S + P_S + R_S \qquad \text{(Equation 7.1)}$$

where, E represents soil erosion; T represents dam trapping; H represents channel deposition; W represents water diversion; and O, P, and R represent seaward transport, slope soil conservation, and hillslope redistribution, respectively. The subscript S represents bulk sediment. While E_S, T_S, H_S, W_S, O_S, and P_S can be directly estimated from existing data through empirical modeling or hydrometric measurement, R_S is determined as a residual. Therefore, R_S includes potential errors arising from other sedimentation processes not considered in the budgetary calculations. For a specific channel reach, H_S can be calculated as

$$H_S = \sum[input] - \sum[output] - \sum[damdiv] \qquad \text{(Equation 7.2)}$$

In the Yellow River basin, the $\sum[input]$ is the sum of sediment input measured at upstream gauge stations; the $\sum[output]$ is the sum of sediment output measured at downstream gauge stations; and the $\sum[damdiv]$ is the sum of sediment trapped by dams and diverted by canals.

As T_S, H_S, W_S, and P_S represent the sediment fraction deposited within the landscape, and O_S is the sediment amount delivered into the ocean, Equation 7.1 can be regarded as the balance among the three phases with respect to the soil erosion product of sediment. It also indicates that bulk sediments are conserved within the entire fluvial system.

With regard to the OC cycling, a similar budget equation can be obtained by taking into account its dynamics in the production, transport, and sedimentation phases within the basin.

$$E_C = T_C + H_C + W_C + O_C + P_C + R_C + D_C \qquad \text{(Equation 7.3)}$$

The subscript *C* represents OC. Unlike the sediment pathways, there is an additional flux for OC. A considerable portion of the eroded OC is labile and is therefore vulnerable to oxidation after erosion. The OC decomposed to CO_2 gas is represented by *D*. Similarly, the decomposed OC (D_C) can be determined as a residual between the eroded OC and the transported as well as the deposited OC. As the oxidation into the atmosphere (D_C) is not reflected in the bulk sediment cycle, OC within the basin may not be conserved in comparison with bulk sediments during the erosion and sedimentation processes (Smith et al., 2001).

The eroded OC (E_C) can be estimated through the total eroded soil materials and their SOC content. For the Yellow River basin, both were adequately known in literature. O_C can be determined through the seaward sediment flux and the associated OC content. Seaward sediment flux has been continuously recorded near the river mouth for more than 60 years, and the sediment's OC content has also been analyzed in recent years. Variables T_C, H_C, W_C, P_C, and R_C are not directly known but can be approximated from sediment flux data and the corresponding OC content. Assuming the OC content to be θ,

$$\theta_E = \left[\frac{C}{S}\right]_E ;\ \theta_T = \left[\frac{C}{S}\right]_T ;\ \theta_H = \left[\frac{C}{S}\right]_H ;\ \theta_W = \left[\frac{C}{S}\right]_W ;\ \theta_O = \left[\frac{C}{S}\right]_O ;\ \theta_P = \left[\frac{C}{S}\right]_P ;$$

$$\theta_R = \left[\frac{C}{S}\right]_R \qquad \text{(Equation 7.4)}$$

Rearranging Equations (7.1-7.3), the decomposed OC (D_C) can be solved as a function of the known quantities. It can be expressed as:

$$D_C = E_S * \theta_E - T_S * \theta_T - H_S * \theta_H - W_S * \theta_W - O_S * \theta_O - P_S * \theta_P - R_S * \theta_R \qquad \text{(Equation 7.5)}$$

It is clear that D_C depends on the total eroded OC amount available for delivery and the burial rates of the OC associated with sediments. With each category of the carbon cycle being quantified, a carbon budget that is similar to the bulk sediment budget can be delineated. The difference provides a measure of the eroded OC that is neither buried on land nor delivered into the ocean.

7.3 Results

7.3.1 Bulk sediment budget

Total soil erosion

Numerous attempts have been made to quantify the amount of soil erosion induced by water in the Yellow River basin over the past decades (Table 7.1). While these estimates vary by a factor of 1.5 from 1.7 Gt/yr to 2.5 Gt/yr; most fall in the range of 2.1-2.3 Gt/yr. In the present study, 1.7 Gt/yr as the minimum soil erosion intensity and 2.5 Gt/yr as the maximum, with a mean of 2.2 Gt/yr available for subsequent redistribution, sedimentation, and export, were adopted. The range is expressed as mean ±(maximum-minimum)/2. That is, the mean water erosion rate is about 2900 ±540 t/km^2/yr throughout the basin, which indicates the drainage basin is at a moderate soil erosion level in general, according to the latest national standards of soil erosion classification which defines the moderate level as soil erosion intensity in the range of 2500-5000 t/km^2/yr (Ministry of Water Resources of China, 2008). In comparison, the mean water erosion rate in the Yellow River basin is substantially higher than the global mean value (Reich et al., 2001), and is about tenfold that of the conterminous United States (317 t/km^2/yr, see Smith et al., 2001). In total, 134.2 ±24.7 Gt of soils have been eroded across the drainage basin for the studied 61 years.

Table 7.1 Previous estimates of soil erosion in the Yellow River basin.

Estimated scale	Soil erosion (Gt/yr)	Method	Source and notes
Yellow River basin	2.1-2.3	Statistical estimation	(Chen, 1983). Sum of hydrological measurements and human-induced reductions.
Yellow River basin	2.2	Statistical estimation	(Shi, 1990). Total soil erosion rate in the 1950s and took sediment trapping into account.
Yellow River basin	2.23	Sedimentological investigation	(Wang et al., 2003). Sum of observed erosion and human accelerated erosion.
Yellow River basin	2.2	Remote sensing survey and field observation	Ministry of Water Resources of China (http://www.mwr.gov.cn/ztbd/huihuang/hh50/chapter9.htm).
Yellow River basin	1.7	Statistical estimation	(Li and Liu, 2006). Reconstruction of the soil erosion rate in the 1950s.
Yellow River basin	1.97	Statistical estimation	(Wang et al., 2010a). Averaged for the period of 1950-1959 before large-scale soil conservation.
Loess Plateau	2.4-2.5		(Fu, 1989). The erosion rate ranged from 2000 to 20,000 t/km^2/yr for the period before 1970.
Loess Plateau	2.11	USLE model	(Fu et al., 2011). For the year of 2000.
Middle Yellow River basin	1.66	Sedimentological investigation and USLE model	(Jing et al., 1998). Reconstruction of the soil erosion in the 1970s by summing hydrological measurement and human-induced reductions.

Sediment deposition within dams and channels

Recent statistical reports indicate that globally around 70% of rivers are intercepted by large reservoirs (Ran and Lu, 2012). With a total storage capacity of 72 km^3 substantially exceeding the natural water, flow dynamics in the Yellow River basin have been significantly modified. In addition, reservoir sedimentation in the basin has directly altered the riverine sediment delivery process (Figure 7.2). Temporally, the sediment transport can be divided into 4 stages resulting from the combined operation of reservoirs. With the commission of each critical reservoir, such as the Liujiaxia Reservoir in 1969, the Longyangxia Reservoir in 1986, and the Xiaolangdi Reservoir

in 2000, the sediment load at the affected gauge stations decreased sharply. For instance, for the Sanmenxia Reservoir located immediately downstream of the Loess Plateau (see Figure 2.1), about 6.6 km^3 of sediment, or 8.6 Gt assuming a bulk density of 1.3 t/m^3, has been trapped over the period 1960-2010 (Ministry of Water Resources of China, 2010a). Another example is the Xiaolangdi Reservoir. During the first 10 years after its completion, approximately 2.83 km^3 of its storage capacity had been lost to sedimentation, which accounts for 22.4% of the initial storage capacity (Ministry of Water Resources of China, 2010a).

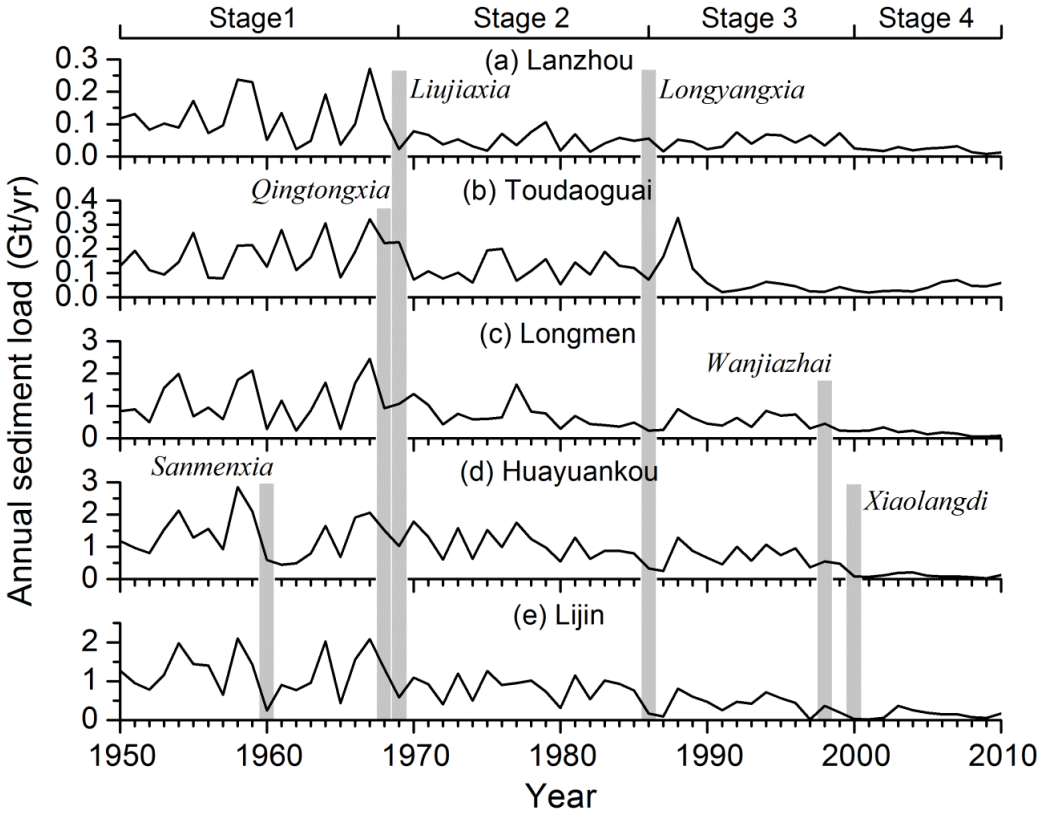

Figure 7.2 Temporal variations of annual sediment load at the five major hydrological gauge stations along the mainstem: (a) Lanzhou, (b) Toudaoguai, (c) Longmen, (d) Huayuankou, and (e) Lijin. Also shown are large reservoirs constructed on the mainstem channel, whose joint operation has resulted in stepwise reductions of sediment load over the past decades. Locations of the gauge stations and reservoirs are shown on Figures 2.1 and 2.8; Lanzhou is situated on the uppermost and Lijin on the lowermost.

The average reservoir sedimentation rate of all inventoried reservoirs in recent years was estimated at 0.59 Gt/yr, and totally 19.32 Gt of sediment has been retained by reservoirs during the study period (Chapters 5 and 6). Particularly, most of the sediment was trapped in the large mainstem reservoirs (Table 7.2), highlighting their disproportionate importance in trapping sediment and OC compared with the smaller ones. Adding up the contribution from the silt check dams constructed within the river basin leads to a total sediment trapping of 40.32 Gt (see Chapter 6).

Table 7.2 Sediment retention within the major mainstem reservoirs[†].

Reservoir	Year of completion	Storage capacity (km^3)	Sediment trapping (Gt)
Sanmenxia	1960	9.64	8.6
Qingtongxia	1968	0.62	0.78[*]
Liujiaxia	1969	5.7	2.2[*]
Longyangxia	1986	24.7	0.4[*]
Wanjiazhai	1998	0.9	0.31[*]
Xiaolangdi	2000	12.65	3.68

[†] Date are from Ministry of Water Resources of China, 2010a
[*] Sediment trapping is estimated to the year of 2005.

In addition to sediment trapping by dams, a huge quantity of sediment has been deposited in channels and on floodplains. Three major sediment sink zones in the Yellow River basin are the Ningxia-Inner Mongolian segment, the Fenwei graben, and the Lower Yellow River reaches (Xu, 2005), as shown in Figure 7.3. All three sediment sinks are situated in crustal subsidence regions of the mainstem channel, where their sedimentation history can be traced back to the Quaternary period. The stored sediment within each sediment sink zone is calculated using Equation 7.2. Based on the sedimentation rates in the three major sinks (Zhao, 1996; Xu, 2005), a total of 17.8 ± 3.5 Gt of sediment has been deposited in the mainstem channels or on the floodplains during the period 1950-2010.

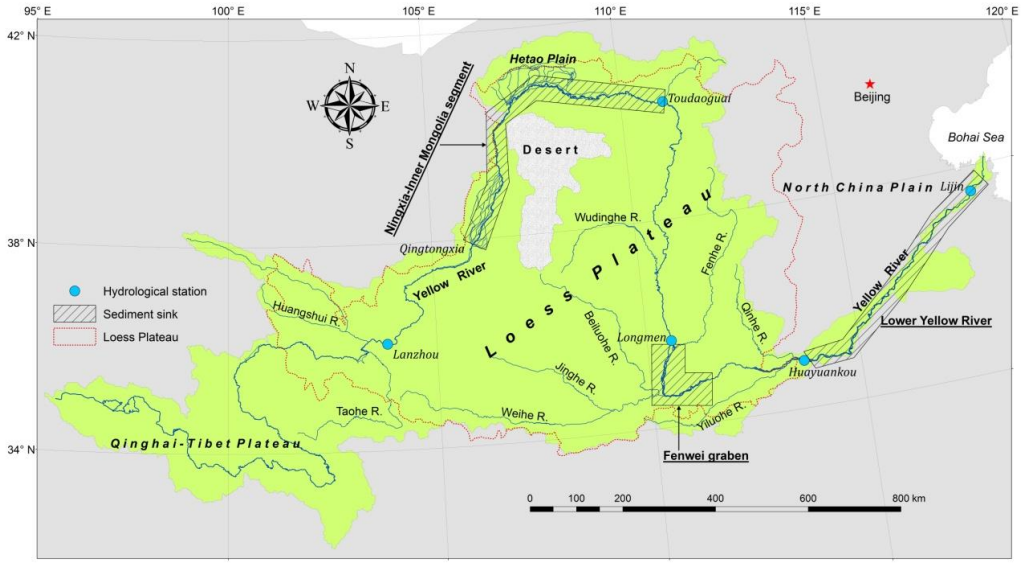

Figure 7.3 Location of the three major sediment sink zones along the mainstem channel. The Loess Plateau is mostly overlapped with the middle Yellow River basin. Toudaoguai and Huayuankou can be regarded as the mainstem boundary of the upper-middle and the middle-lower reaches, respectively.

Sediment reduction by soil control measures

Soil conservation efforts have been made on slopes since the late 1950s to reduce the erosive capacity of heavy rainfall and to maintain land productivity with an attempt to improve the deteriorated environment. In addition to silt check dams, the commonly adopted measures also include construction of terraces, reforestation, and grass planting (Ran et al., 2013b). However, the soil erosion intensity did not see significant reduction until the 1970s when massive soil conservation measures were implemented and since then, the sediment yield from the Loess Plateau has sharply decreased (Zhao, 1996).

By dividing the middle Yellow River basin into four subcatchments, Ran (2007) studied the effects of each soil conservation measure conducted during the period from 1970 to 1996 on soil erosion control and sediment reduction. The three slope

measures mentioned above have collectively retained 3±0.7 Gt of sediment by 1996. Starting from 1999, the Grain-for-Green Project, which returns cropland to forest or grassland by subsidizing farmers, was launched on the Loess Plateau. Huge areas of steep croplands have been converted into forest and grassland and as a result, the previously damaged vegetation has been greatly restored (Xin et al., 2008). With enhanced root protection for soil particles and ground surface resistance to erosion, soil erosion intensity on the Loess Plateau has been greatly retarded. By using the USLE model, the accumulatively controlled soil erosion due to vegetation recovery during the past decade was estimated at 1.3±0.4 Gt (Fu B.J., unpublished data).

In addition, as most adaptable slope lands, with a slope gradient usually less than 25°, have been converted into terraces before the 1990s, the total area of terraces has remained largely unchanged since (Ran et al., 2012). Hence, the soil erosion control rate of terraces can be assumed to be the same as that in the 1990s. As a consequence, approximately 0.8 Gt of soil has been intercepted after 1996 by terraces. Adding up the controlled soils before 1970 by slope conservation measures and that during 1997-2010 (Zhao, 1996; Kang et al., 2010), as well as the estimate for 1970-1996, the total reduced sediment by slope soil conservation measures is estimated at 6.0±1.1 Gt during the study period.

Water diversion

The annual water diversion has increased steadily over the period (Figure 7.4). For example, the mean annual water diversion has doubled to 27.5 km^3/yr for the period

2000-2008 from the level of 13.8 km^3/yr during 1952-1959. In particular, the withdrawn water volume from the Yellow River has exceeded the actual water discharge into the sea since 1986 (Figure 7.4). The excessive water diversion has caused the lower reaches near the river mouth to suffer from continuing periods of interrupted water flow since 1972, with a peak of 226 dry days in 1997 (Liu and Xia, 2004). This phenomenon did not end until recent years when the central government intervened to execute a stricter water diversion quota, which could partly explain the slightly reduced water diversion compared with the early 1990s (Figure 7.4).

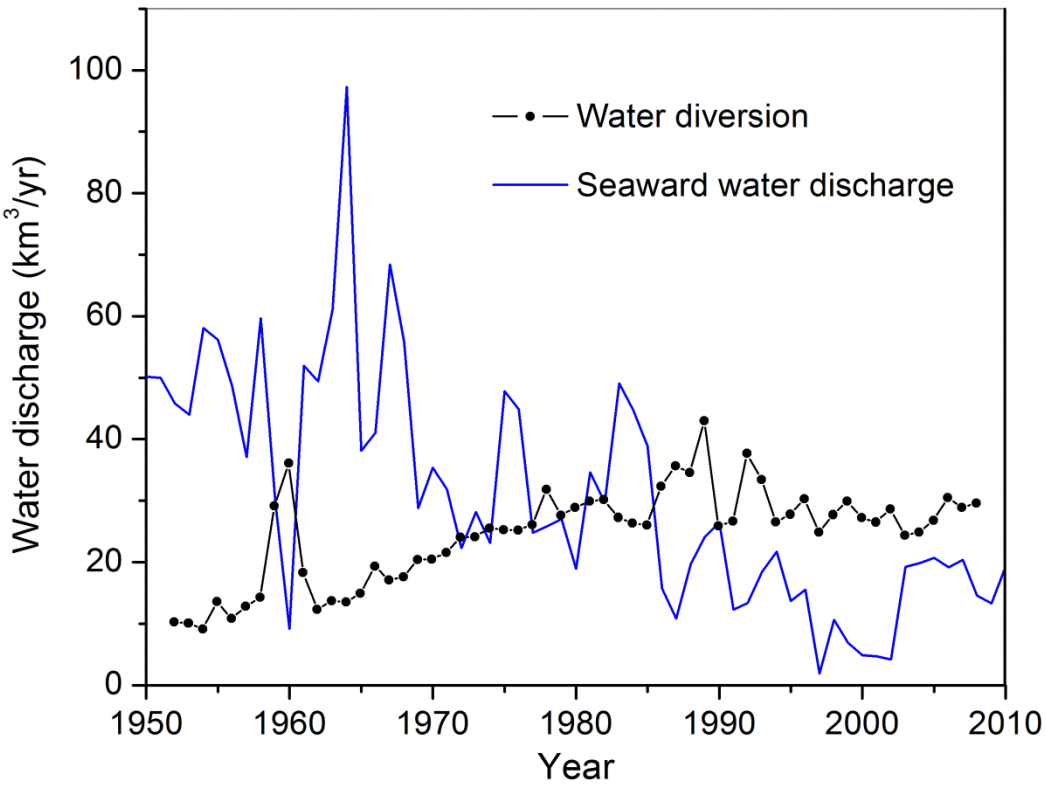

Figure 7.4 Time series of basin-wide water diversion and water discharge into the Bohai Sea. Data from YRCC (2007) and Jiongxin Xu (unpublished data).

Similar to the temporal variations of the withdrawn water, for the mainstem channel from Huayuankou to Lijin, the mean rate of diverted sediment increased from 0.055

Gt/yr during 1950-1959 to 0.131 Gt/yr during 1980-1990 (Hu et al., 2005a). It then gradually decreased to 0.056 Gt/yr during 2000-2010 (Hu et al., 2008; Ministry of Water Resources of China, 2010a). Overall, the diverted sediment from the Yellow River mainstem channel resulting from water consumption is estimated at 10.5 Gt over the 61 years. Of this amount, about 6 Gt was diverted from the channel between Huayuankou and Lijin; 2.6 Gt from the channel between Lanzhou and Toudaoguai; 1.7 Gt from the channel between Toudaoguai and Huayuankou; and the remaining 0.2 Gt from the channel above Lanzhou. The estimated rate is slightly larger than the rate made by Chu et al. (2009) if the total amount is divided by the number of years.

Seaward sediment flux

For the Yellow River, suspended sediment discharge to the ocean has been monitored at the Lijin gauge station since 1950 (Figure 7.2). Over the 61 years, the seaward sediment load has experienced a stepwise reduction in response to the combined effects of climate change and human activities (Wang et al., 2007b). For the period of 1950-1968, human acitivites in the basin were relatively limited. Except for the commission of Sanmenxia Reservoir in 1960, there was no other large-scale construction of dams and implementation of soil conservation measures. Furthermore, the magnitude of water withdrawal was significantly reduced as severe soil salinization in the irrigated cropland occurred after excessive flood irrigation during 1959-1961 (Figure 7.4). As a result, the sediment flux into the ocean averaged 1.24 Gt/yr in this period.

In the following decades, the annual sediment flux decreased gradually due to soil conservation measures on sloping lands and sediment trapping by dams, as well as the enhanced water diversion since the 1970s. The average sediment flux during 1969-1986 was 0.8 Gt/yr, which accounts for 64.5% of that of the period 1950-1968. After the joint operation of Longyangxia and Liujiaxia reservoirs since 1986, more sediment has been deposited within the landscape as a result of altered flow dynamics and reduced sediment carrying capacity. The mean sediment flux during the period 1987-2000 further declined to 0.39 Gt/yr. Starting from 2000, with the operation of the Xiaolangdi Reservoir, which has a storage capacity for sedimentation of 7.55 km^3, the mean sediment flux has plummeted to around 0.15 Gt/yr. Current sediment flux represents only 12.1% of that during 1950-1968, which is largely the result of anthopogenic impacts (Peng et al., 2010; Miao et al., 2011). The cumulative suspended sediment load into the ocean is 44.8 Gt over the 61 years, amounting to one third of the eroded soil amount.

Besides the suspended load, the river also carries bed load into the ocean simultaneously. However, obtaining the accurate bedload transport flux is very difficult although several methods have been proposed. In many cases, the bed load fraction is taken to be a fixed fraction of the suspended load (Turowski et al., 2010; Boateng et al., 2012). Assuming that the bed load accounts for 10% of the suspended load, then the total bed load into the ocean during the study period is 4.48 Gt. As this study is focused on the sediment budget over a long timescale, both the suspended

and bed loads are supposed to be derived from soil erosion. Together, the total sediment load into the ocean is around 49.3 Gt.

Slope redistribution

Unlike other sediment pathways where sediment destination could be clearly defined, it is hard to explicitly illustrate where the locally redeposited sediments are stored. They may have been retained on slope lands close to the eroding sites, or stored in colluvial deposits or valley bottoms. Here, all the locally redeposited sediments are referred to as slope redistribution for simplicity. When the values of the aforementioned categories are defined, the redistributed slope sediment can be quanfitied by rearranging Equation 7.1. The total of 10.3 ± 24.9 Gt over the 61 years indicates a mean annual redistribution rate of 0.17 ± 0.41 Gt, which is comparable to the mean seaward sediment flux during 2001-2010 (0.15 Gt/yr). Moreover, it demonstrates that the sediment delivery ratio (SDR) from slope lands to the Yellow River mainstem is about 0.9, which is in good agreement with the high SDR estimated previously, but significantly higher than the global mean of about 0.1 (Zhao, 1996; Walling and Fang, 2003).

7.3.2 Associated organic carbon budget

About 20 soil types have been detected in the Yellow River basin. Cultivated loessial soils, cinnamon soils, sierozems, and dark loessial soils are the dominant soil orders on the Loess Plateau, which together cover around 70% of its total surface area. In general, the SOC content in the loess soils is quite low, usually in the range of 0.4-

1.5%. With the vegetation rehabilitation efforts and widespread use of chemical fertilizers, the SOC pool has been found to increase gradually (Chen et al., 2007b).

Soil organic carbon content in the top 30-cm soil layer across the river basin is very low and shows strong spatial variability (Figure 7.5). Due to OC input from plant residues, mainly alpine meadow, the headwater areas have a relatively higher SOC content than the loess regions. In some places on the eastern edge of the Qinghai-Tibetan Plateau where the annual precipitation is 800 mm, the SOC content can reach up to 39%. In contrast, approximately 70% of the middle reaches show a SOC content of below 0.8%, in particular for the regions around the desert where the SOC content is mostly less than 0.5%. Taking into account the spatial variability of soil erosion intensity (see Figure 6.6), the basin-wide SOC content (θ_E) is averaged to $0.84 \pm 0.12\%$ based on the SOC map (Figure 7.5) using a sampling density of 1×1 km^2. In addition, because the light SOC fraction will be preferentially removed, the eroded soils will be enriched in SOC in comparison with the parent topsoils (Quinton et al., 2010). The enrichment ratio, defined as the ratio of the SOC content in the eroded soils to that in the parent topsoils, has been introduced as a means of quantifying the magnitude of SOC enrichment. It can vary significantly from less than 1 to larger than 5, depending on several factors, including erosion intensity, particle size of the eroded soils, and sediment concentration (Wang et al., 2010b).

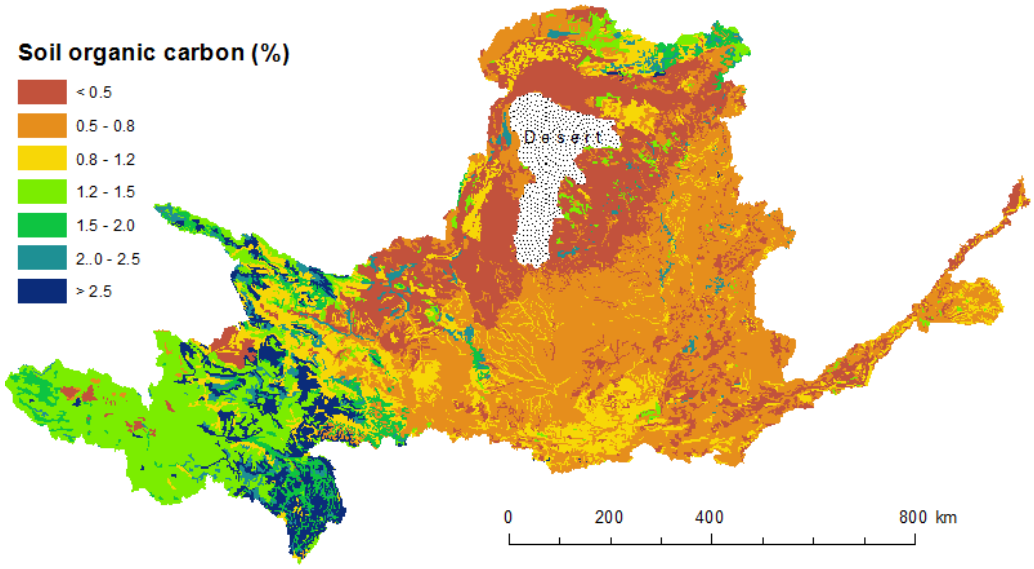

Figure 7.5 Map of soil organic carbon of the Yellow River basin showing strong spatial variability. The middle and lower reaches are characterized by low SOC.

For the Yellow River basin, as a result of high erosion intensity of heavy storms and rapid water transport, the OC enrichment ratio in the eroded soils is relatively low, usually less than 1.2 (Wang et al., 2008b). An enrichment ratio of 1.1 was used here to estimate the eroded OC amount from the topsoils. Because the sediments supplied by gully erosion are found to represent about 50% of the total with the remainder from sheet and rill erosion (Zhao, 1996; Jing et al., 1998; Xu, 1999) and the SOC content of the subsoils is lower than the topsoils (Liu et al., 2003; Wang et al., 2008), the enrichment ratio for half of the eroded soils from the subsoils was estimated at 0.8. Accordingly, the total eroded SOC over the period was estimated at 1.07 ±0.16 Gt.

By analyzing sediment samples collected near the estuary, at Lijin gauge station for example (Figure 7.3), the riverine transport of OC can be estimated. Numerous researchers have tried to estimate the OC transport from the Yellow River to the Bohai Sea (Cauwet and Mackenzie, 1993; Wang et al., 2012). Owing to its high

turbidity, the DOC flux in the Yellow River is very low (Zhang et al., 1992), which is in stark contrast to global river transport of OC that is roughly equally divided between dissolved and particulate fractions (Ludwig et al., 1998; Stallard, 1998). For the POC content, in comparison with the global average at 0.95% (Ludwig et al., 1996; Smith et al., 2001), it mostly falls into the range of 0.37-0.8% for the Yellow River (Table 7.3). In this study, the seaward sediment OC content (θ_O) is estimated to be $0.51 \pm 0.28\%$. The total transported OC into the ocean is therefore 0.251 ± 0.138 Gt over the 61 years.

Table 7.3 Summary of organic carbon content in the Yellow River seaward sediment.

Sampling location	POC content (%)	Source and notes
Lijin gauge station	0.4-0.6	(Zhang et al., 2009). Measurements for the fine sediments (<16μm in size), which concentrate >80% OC.
Lijin gauge station	0.37-0.79	(Wang et al., 2012). Based on a monthly sampling frequency.
Near the estuary	0.42-0.5	(Cauwet and Mackenzie, 1993). 0.42 in May (dry season) and 0.5 in August (wet season).
Near the estuary	0.15-0.75	(Cai, 1994). Calculated from 115 sediment samples.
Mainstem channel	0.44-0.85	(Liu and Zhang, 2010). For the mainstem channel downstream of Lanzhou.
Mainstem channel	0.4-0.8	(Wang et al., 2007c). Mainly the middle-lower reaches.

Liu and Zhang (2010) have explored the spatial and temporal variations of OC of the Yellow River mainstem by sampling from the headwater regions to the river mouth during the period of 2003-2009. For the reaches downstream of Lanzhou (see location in Figure 7.3), they discovered that the OC content in sediment remained fairly stable along the mainstem in the range of 0.44%-0.85%, in particular in the major water

diversion reaches. This demonstrates that the OC in the diverted sediments has an approximately equivalent OC content as that in the seaward sediment. Thus, the OC content of diverted sediment (θ_W) was assigned to be 0.51±0.28%. The total diverted OC was estimated at 0.054±0.03 Gt over the period. With the diverted sediment, this OC was largely deposited in irrigation canals or on croplands, where it was subject to further biogeochemical processes.

As stated earlier, soil erosion in the Yellow River basin is mainly controlled by several intense storms, and the resulting sediment transport process is characterized by hyperconcentrated flows with SSC exceeding 1000 kg/m^3. During intense storm events, the eroded soil materials can quickly reach the deposition sites after a short delivery. Except for the readily decomposable labile fraction, it is likely that the eroded recalcitrant OC has little chance to be mineralized and reworked (Quinton et al., 2010). For the Loess Plateau, this is highly possible, given the strong carrying capacity of flows generated from heavy storms. The OC content of sediments retained by silt check dams situated close to eroding sites is comparable to that of the eroded soils (Wang et al., 2008). While the OC content of the sediments buried in reservoirs is more likely to be similar to that of the mainstem channel sediments, because most of the sediments intercepted by dams are deposited in the mainstem reservoirs (Table 7.2). Therefore, the OC content of the sediments trapped by silt check dams (21 Gt) and intercepted by reservoirs (19.3 Gt) is 0.798±0.11% and 0.51±0.28%, respectively. The mean OC content for all the sediments trapped by all dams (θ_T) is weighted to be 0.66±0.19%. Likewise, the OC content for the sediment deposited in channels or on

floodplains (θ_H), mainly in the three mainstem sediment sink zones (Figure 7.3), is assumed equivalent to that of the mainstem sediments ($0.51 \pm 0.28\%$). As a result, the accumulated OC trapped by dams during 1950-2010 was estimated at 0.266 ± 0.077 Gt, and that deposited in channels or on floodplains was about 0.091 ± 0.053 Gt during the same period.

On the Loess Plateau, the soil materials controlled by slope control measures are mostly fixed by the restored vegetation. For the Toudaoguai-Longmen reaches (see location in Figure 7.3), which supply >75% of the sediment for the Yellow River, Ran et al (2013) analyzed the sediment reduction resulting from each measure. Due to widespread plantings within the basin, at least 70% of the stabilized soils by slope control measures are attributable to the restored vegetation, and the contribution would further increase given the continuing vegetation restoration efforts. The soils stabilized by vegetation are assumed to have the same OC content as the noneroded topsoils (Chen et al., 2007b). For the built terraces, crop planting, mainly potato, wheat, and maize, is pursued periodically. While tillage practices would accelerate OC decomposition, the planted crops are able to enhance soil OC input through decaying litter, crop residues, and root-related processes. Generally, agricultural activity represents an atmospheric CO_2 sink (Smith et al., 2005; Van Oost et al., 2007). Thus, with regard to the built terraces, the OC content of the controlled soils is at least similar to, if not higher than, that of the noneroded topsoils. As such, the OC content of the soils controlled by all slope soil conservation measures (θ_P) is assumed to be

0.84±0.12% as in the noneroded topsoils. The total stored OC is estimated to be 0.05±0.012 Gt.

Considering that the locally redistributed sediments are mostly stored on slope lands or valley bottoms, the associated OC content may be similar to that of the sediment trapped behind silt check dams. However, an important point is that the associated OC is more likely to be oxidized by enhanced exposure to atmosphere, compared with the sediments stored in anoxic environments as behind the silt check dams or in the reservoirs. On the other hand, these locally redistributed sediments transport over a relatively short distance and would soon be covered by subsequent sediments or protected by regrown plants, and are subject to next erosion events. Their OC content should thus be comparable to that in the eroding sites. In this case, the average of the OC content in the two components (θ_T and θ_E) is assumed to represent the OC content of the locally redistributed sediments, then θ_R is estimated at 0.75±0.16%. With the local redistribution of sediment amounting to 10.3±24.9 Gt, the corresponding OC redistributed is about 0.077±0.187 Gt.

Finally, when the associated OC of each sediment budget item is determined, the OC amount decomposed and lost to the atmosphere can be quantified. Substituting the estimated OC fluxes into Equation 7.5 produces an estimate of 0.281±0.299 Gt of OC decomposition over the 61 years. Uncertainties were propagated in quadrature assuming that individual errors were uncorrelated.

7.3.3 Summation of bulk sediment and organic carbon categories

For large river basins with complex geomorphological backgrounds and strong human impacts, soil erosion in the uplands and seaward transport of eroded materials measured at river mouth are usually not in balance. Some portion of the erosion products is deposited within landscapes as a result of natural processes and/or human activity. In modern times, the extent to which the eroded materials would be retained on land depends increasingly more on human activity. For the Yellow River basin which is home to 107 million people, all the three soil erosion phases are largely controlled by human activity.

Figure 7.6 shows the budget of soil erosion products of the Yellow River basin over the 61 years. Dam trapping is the largest single component for the eroded sediments across the landscape, and decomposition and release to the atmosphere is the largest single component for the eroded OC. While the sediment amount diverted with water from the mainstem is nearly twofold that stabilized by slope soil conservation measures, the OC amount of the two components is roughly equivalent. In all, the sediment and OC directly stabilized by human activities, including dam trapping, sediment diversion, and slope soil control measures, are 56.8 ± 1.1 Gt and 0.37 ± 0.08 Gt, respectively, both of which are larger than the seaward fluxes. Also, the vertical exchange between land and atmosphere (the decomposed OC) is slightly higher than the lateral export to the Bohai Sea. Particularly, the decomposed OC could be as high as 0.58 Gt, which is about 1.5 times the lateral export to the ocean in an extreme situation (Figure 7.6).

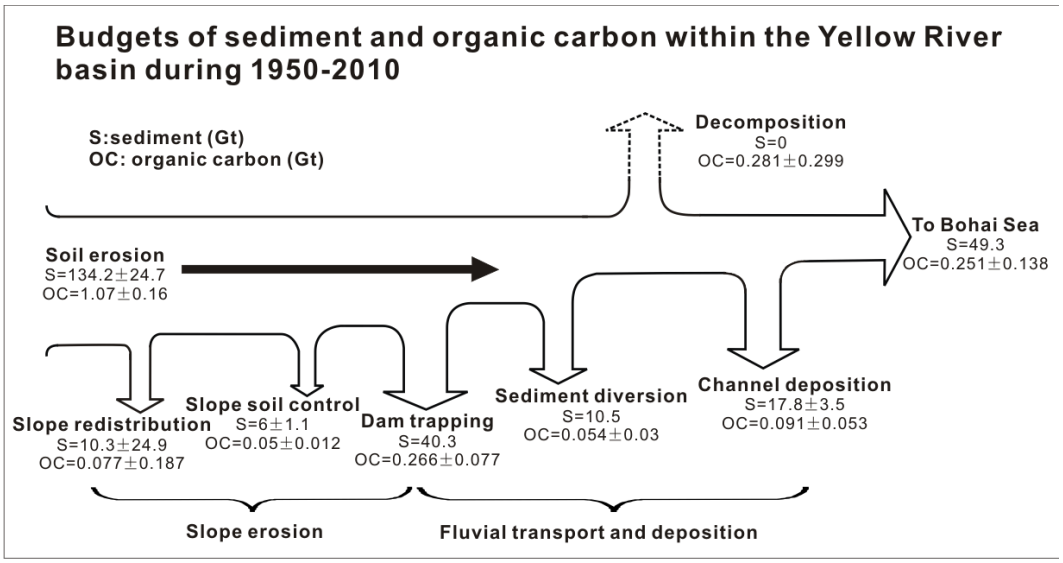

Figure 7.6 Fates of the eroded sediment and organic carbon in the Yellow River basin for the period 1950-2010 using an average soil erosion rate of 2.2 Gt/yr. The maximum of 2.5 Gt/yr and the minimum of 1.7 Gt/yr, expressed as mean±(maximum-minimum)/2, are considered to account for the uncertainties associated with erosion. Dam trapping includes trapping by silt check dams on slope lands and by reservoirs on river channels. The line widths of the arrows are approximately proportional to the sediment amounts.

7.4 Discussion

7.4.1 Assessing the bulk sediment budget

In the present study, a soil erosion rate range of 1.7-2.5 Gt/yr with a mean of 2.2 Gt/yr is used to represent the basin-wide erosion intensity induced by flowing water over the 61 years. Indeed, because of the coupled effects of climate change and human activity, the soil erosion rate in the basin has changed significantly over time. This can be seen from the temporally decreasing sediment load at the mainstem gauge stations presented in Figure 7.2. In view of the temporal variability and the difficulty to assess the soil erosion amount in each year, the reconstructed soil erosion rate was adopted and then applied to the study period to estimate the sediment and OC budgets (Table 7.1).

As mentioned earlier, it is clear that the obtained sediment amount of slope redistribution includes sediment deposition processes not accounted for in the sediment budget equation. One most possible 'deposition' process is the sediment loss due to sand mining. Although accurate information is lacking, sand mining in the Yellow River channel is limited (Chu et al., 2009). In addition, quantifying the channel sedimentation would have also brought about certain errors. Since 2000, after the completion of the Xiaolangdi Reservoir (see location in Figure 2.1), sediment flushing policy has been introduced to mitigate channel sedimentation in the lower Yellow River by generating density flows from a cascade of reservoirs (called "sediment regulation" in China). In each year, man-made turbid water is regularly released to flush downstream sediments deposited within the channel. As a result, the lower Yellow River channel has reversed from originally being a sediment sink to a net source (Wang et al., 2007). Therefore, the actual amount of channel sedimentation should be smaller than that estimated, and accordingly, the resulting amount of slope redistribution should be a larger fraction based on the budgetary equation.

Sediment transport induced by wind could increase the channel deposition amount. Input of windblown sands into the Yellow River occurs mainly in the desert channel in the Ningxia-Inner Mongolian segment (Figure 7.3). A recent investigation shows that the windblown sand transport in this area is 0.02 Gt/yr (Ta et al., 2008), which is small relative to the estimated soil erosion rate of 1.7-2.5 Gt/yr. Contributions of windblown sand input to the total eroded sediment are not significant in comparison with the erosion induced by water. This can also be validated from the high SDR that

is largely consistent with previous results. If the windblown sand input amount is quite high, the obtained SDR based on water erosion would be greatly reduced.

In addition to the categories determined with a range, the sediment amount trapped by dams may bring some degree of uncertainty, given the large number of dams and the difficulty in estimating their respective sediment trapping efficiency at a large spatial scale (see Chapter 6). As for sediment diversion and seaward transport, there may be some uncertainties related to measurement errors, because these estimates were based on hydrological measurements (water discharge × sediment concentration). In general, the greatest uncertainty associated with the bulk sediment budget is in the total eroded soil estimate (Figure 7.6), which determines the distribution pattern of sediment among the considered budgetary components. As a result, the slope redistribution item varies widely, depending on the used soil erosion rate, because the other budget categories have been relatively well constrained.

When the maximum soil erosion rate of 2.5 Gt/yr is considered, the accumulated sediment redistributed on the slope lands could be as high as 30 Gt (Figure 7.6). However, even with the used 2.5 Gt/yr, the actual erosion rate may have been underestimated. Because the eroded soils from stream bank collapse are difficult to determine through conventional techniques, they are usually excluded in the cited total erosion rates (Valentin et al., 2005). Based on the mean sediment load at Huayuankou (1.5 Gt/yr) and a global mean SDR of 0.1 (Walling and Fan, 2003), the extreme soil erosion rate is assumed to be 15 Gt/yr that includes the mobilized

sediments from gully erosion and bank collapse. If this soil erosion is used, the slope redistribution will be the largest single component for storing the eroded sediments.

7.4.2 Assessing the organic carbon budget

During the soil erosion processes, detachment of soil particles will expose SOC that is initially encapsulated within aggregates and clay domains to microbial degradation (Lal and Pimentel, 2008). Fine soil materials and light SOC are preferentially transported away from the eroding sites to low-lying depressional locations where they would be sequestered. As for the three phases of soil erosion, the first two, including production and transport, are likely to increase OC oxidation and release of CO_2. The depositional process could protect SOC from mineralization as the SOC eroded from soil surface is buried under a thick layer of fresh sediment. However, it is arbitrary to claim that the soil erosion would necessarily result in a net carbon source or sink. To answer this question, the strength of carbon source and sink must be comprehensively considered.

At eroding sites, removal of the topsoil will be dynamically replaced with subsurface soil that usually has lower SOC contents, thus likely reducing CO_2 emission (Liu et al., 2003). Although the lost OC at eroding sites can be partly replenished by enhanced carbon stabilization (Van Oost et al., 2008), this is likely difficult in the Loess Plateau (Li et al., 2007), unless improved land management practices, such as application of manures and chemical fertilizers, crop rotation, and reduced tillage, can be widely conducted. Widespread implementation of vegetation restoration programs

since the late 1990s has greatly increased plant residues, which can increase OC input to the newly exposed subsurface soil layer and reduce soil erosion. It is therefore expected that the net primary productivity at the eroding sites has increased.

Carbon that is protected physically by aggregation or buried in alluvial or colluvial sites is vulnerable to further human disturbances (Berhe et al., 2007). The floodplains along the Yellow River mainstem are usually used as croplands (Figure 7.7a). Particularly, more floodplains have been reclaimed in recent years due to reduced risk of overflowing. While the conventional tillage techniques and resultant enhanced exposure of deep sedimentary carbon to the surface would accelerate the decomposition rate of otherwise stabilized carbon, the residual plant litter is able to increase the carbon pool of the deposited sediments. With such opposing influences, it is difficult to precisely evaluate the carbon storage dynamics.

Figure 7.7 Secondary disturbances on sediments deposited on floodplains (a) or in irrigation canals (b). Both photos were taken in the Yellow River near the Toudaoguai gauge station.

To maintain water delivery efficiency, irrigation canals in the Yellow River basin are regularly dredged and the deposited sediments are excavated to adjacent banks

(Figure 7.7b). It is expected that some of the OC buried in the deposited sediments is likely to be oxidized under aerobic conditions after remobilization. If half of the calculated channel deposition is assumed to have been deposited on floodplains, then the buried OC in canals and on floodplains is about 0.1 Gt in total, or 8% of the eroded OC. Obviously, although unpractical, even complete oxidization of these remobilized OC could not substantially affect the evaluation on the fates of the total eroded OC.

Based on the soil erosion rate of 2.2 Gt/yr, decomposition (0.281 Gt or 0.005 Gt/yr) over the study period represents the largest single carbon fate (Figure 7.6). Nevertheless, the total decomposed OC would have been underestimated, given that a certain proportion of the OC diverted with water would also be decomposed due to dredging (Figure 7.7b). This figure could be much larger when taking into account the implementation of the sediment regulation policy. Owing to the great variability in soil erosion intensity and SOC content, the decomposed OC ranged from 0.08 to 0.482 Gt (Figure 7.6). Thus, the estimate of OC decomposition through water erosion is preliminary, and a better constraint on soil erosion rate in future will improve the OC budget. Particularly, if the extreme soil erosion rate of 15 Gt/yr is used, the decomposed OC is estimated to be 0.07 Gt/yr based on the budget calculations. Overall, in view of the low SOC content of the parent soils and the intense soil erosion character, it can be concluded that erosion-induced OC transport within the Yellow River basin likely represents a carbon source to the atmosphere, despite the uncertainties.

Compared with the SOC content, the seaward sediment POC content is lower, indicating a fraction of the eroded OC has been lost during the delivery process. On the other hand, the sediment POC content remains fairly stable along the mainstem from Lanzhou to Lijin (Liu and Zhang, 2010), demonstrating that decomposition is mainly confined to the initial transport stage before the OC reaches the mainstem. As the labile OC fraction is vulnerable to degradation, it would have been decomposed quickly following erosion. Considering the long distance allowing for the labile OC to be fully mineralized before reaching the mainstem, it is easy to understand the relatively stable but lower POC content. For the sediments deposited behind dams, although the aerobic decomposition rate may be low, prevalence of anaerobic conditions would accentuate methanogenesis, thereby leading to CH_4 evasion. Consequently, the deposited OC associated with sediment would not be totally stabilized. Some of it may have been mineralized instead, and the extent is dependent on ambient environmental conditions. Overall, the buried OC with sediments deposited behind dams or in channels may have been overestimated somewhat, which requires further studies regarding anaerobic carbon transformation.

As for the seaward sediment and OC fluxes, they are based on the measurements at the lowermost Lijin gauge station, which is about 110 km upstream of the river mouth. Indeed, huge amounts of sediment would have been deposited in the estuary and delta zones, and does not actually reach the Bohai Sea (Wang et al., 2007). The deposited OC with sediments would further be oxidized and released to the atmosphere in these zones due to strong flow turbidity (Chen et al., 2012). As a result, the amount of both

the sediment and OC that actually enter the ocean should be smaller than that determined.

Although several uncertainties remain with respect to the eroded OC in comparison to sediment, the obtained budget results provide a preliminary estimate of the fates of the eroded soils and OC. This estimate suggests most eroded soils and OC were redeposited on land, rather than in the ocean. During the period 1950-2010, water-induced erosion in the Yellow River basin has buried about 0.54 Gt of OC on average, corresponding to a burial rate of about 8.85 Mt per year. In particular, with a mean OC burial rate of 4.4 Mt/yr, the constructed reservoirs and silt check dams accounted for about 49.7% of the annual total burial rate.

7.4.3 Anthropogenic impact and future implications

Transport dynamics of the eroded materials in the Yellow River basin has been markedly altered by humans during the past decades (Wang et al., 2007). Large-scale dam construction and the implementation of numerous soil conservation projects on the Loess Plateau have greatly reduced soil erosion and fluvial sediment and OC fluxes (Figure 7.8). Over the 61 years, about 30% of the eroded soils was intercepted by dams and 4.5% stabilized by slope soil control measures. In addition, water diversion contributed 7.8%, which is larger than the effects of slope soil conservation practices. Summing up, these direct human activities account for 42.3% of the total eroded soils (Figure 7.8a). The higher percentage relative to the seaward sediment

flux illuminates the strong impact of human activities on sediment redistribution between terrestrial and ocean systems.

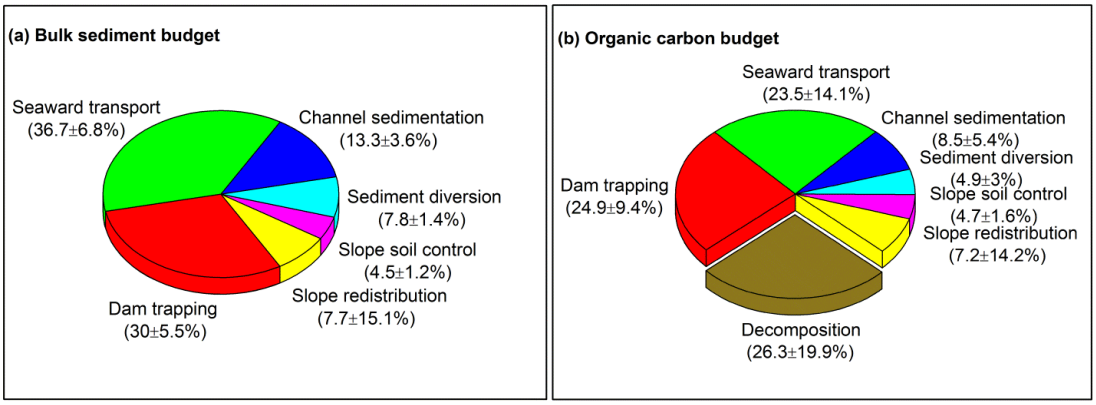

Figure 7.8 Pie chart summarizing the redistribution of the bulk sediment (a) and organic carbon (b) eroded during 1950-2010. The percentages are based on the soil erosion rate of 2.2 Gt/yr with 1.7-2.5 Gt/yr for the consideration of uncertainties.

From the carbon perspective, the decomposed OC represents about 26.3% of the total eroded OC on average (Figure 7.8b). In consideration of the fairly stable OC content along the long mainstem channel that allows for sufficient time for the labile OC to be fully decomposed, it indicates that the labile fraction has been largely oxidized before reaching the ocean. Hence, it can be concluded that approximately the labile fraction accounts for one-quarter of the total eroded OC, validating the commonly used assumption that about 20-40% of the displaced OC is emitted into the atmosphere (Davidson and Ackerman, 1993; Lal, 2003; Berhe et al., 2007; Quinton et al., 2010). Nevertheless, the decomposed fraction obtained through the budget equation shows great uncertainty (Figure 7.8b), indicating the complexity in estimating the magnitude of OC decomposition due to its multiple influencing factors. In contrast to the Yellow River characterized by low SOC content (0.84%), more OC is vulnerable to decomposition for river basins with high SOC content. In addition,

the human-induced OC redistribution on land, including dam trapping, sediment diversion, and slope soil control (Figure 7.8b), totally represents 34.5% of the eroded OC, which is slightly larger than the decomposed fraction. Without human activities, particularly silt check dams and slope soil control measures which are able to stabilize large amounts of sediment quickly after erosion, more OC would have been oxidized and not transported to the river. Furthermore, the seaward OC flux would have been larger if no sediment was stored on land by humans.

Currently, more dams are under construction or planned, and vegetation restoration and other soil conservation projects are also being carried out throughout the basin (Ran et al., 2013c). These activities, in conjunction with lower precipitation in response to climate change, are expected to further enhance the magnitude of burial of sediments and OC on land in future, thereby reducing their seaward fluxes. With continuous decrease of sediment and OC fluxes to the sea, the coupling influences on the biogeochemical cycle and aquatic ecosystems at the estuary, delta, and coastal ocean will be significant. Further work is undoubtedly needed to explore their responses. Similar studies are also required for other large Asian rivers where sediment and OC fluxes used to be very high (Bird et al., 2008; Lu et al., 2012).

7.5 Summary and conclusions

A basin-wide sediment budget of the Yellow River basin was constructed by considering the coupled processes of soil erosion on upland hillslopes, sediment deposition in low-lying sites and transport to the ocean. After the quantifiable

categories were defined, the sediment amount redistributed on slope lands was estimated. The obtained small slope redistribution corroborates the high SDR (>0.9), indicating that most of the eroded soil materials are transported away from the eroding sites. In addition, soil erosion and sediment dynamics within the Yellow River basin have been greatly affected by human activities during the period of 1950-2010. Particularly, dams and soil conservation measures have progressively stabilized 34.5% of the eroded soils on average. Overall, approximately 63% of the eroded soils were deposited on land, and only 37% were transported into the Bohai Sea.

In combination with the spatial variability of SOC and soil erosion intensity throughout the river basin, the total eroded OC during the study period was estimated at 1.07±0.16 Gt. Fates of the eroded OC were examined in relation to the sediment transport and deposition processes within the basin. Approximately, ~50% of the eroded OC (0.54±0.18 Gt) was buried on land, and 23.5% (0.25±0.14 Gt) was discharged into the ocean. On average, approximately 8.85 Mt of OC was buried on land per year. In particular, half of the terrestrially redeposited OC was buried behind dams, highlighting the importance of artificial dam sediment trapping in sequestering the mobilized OC resulted from soil erosion. Closure of the OC budget equation indicates that the decomposed OC after soil erosion was estimated at 0.281 Gt with an annual average of 4.61 Mt, accounting for 26.3% of the total eroded OC. This decomposition proportion validates the commonly used assumption that about 20-40% of the displaced OC will be oxidized.

Despite several uncertainties to be more explicitly constrained regarding the budgetary components, the budgetary estimates provide a means of assessing the potential fates of the eroded soils and OC within a watershed. As human activities in the Yellow River basin are becoming increasingly strong, the resulting responses and related implications warrant further research to increase our understanding of the sediment and carbon dynamics induced by soil erosion. This is especially important given the current context of global warming and increasing atmospheric CO_2 concentration.

Chapter 8 Recent organic carbon transport along the mainstem

8.1 Introduction

Rivers represent efficient conduits of carbon from terrestrial sources to the oceans and the atmosphere. Lateral fluxes of organic carbon from land to ocean are an especially important and sensitive component in the global carbon cycle (Schlünz and Schneider, 2000; Battin et al., 2009; Aufdenkampe et al., 2011). Globally, the total organic carbon flux transported into the ocean is estimated to vary between 400 and 900×10^{12} g/yr (Bird et al., 1994; Hope et al., 1994; Suchet et al., 2003; Cole et al., 2007). Whilst it is 1-2 orders of magnitude smaller than the annual exchange flux among the carbon pools of vegetation, atmosphere, and the oceans (Aitkenhead et al., 1999), this unidirectional flux has an important role in a number of biogeochemical processes within aquatic and coastal environments. Because most of the organic carbon is ultimately derived from terrestrial primary production (Tranvik et al., 2009; Bass et al., 2013), the riverine flux may therefore act as a means of regulating changes in the terrestrial carbon pool.

Asian rivers, particularly those originating from the Qinghai-Tibetan Plateau with abundant runoff, carry about 70% of the global suspended solids to the oceans (Milliman and Meade, 1983). It is therefore widely expected that the associated organic carbon transport represents an important component of the global carbon budget. Understanding its delivery dynamics is thus crucial for global carbon cycle studies. With respect to the Yellow River, numerous studies on dissolved inorganic

carbon (DIC) transport have been widely reported (e.g., Hu et al., 1982; Zhang et al., 1995a; Chen et al., 2005; Wu et al., 2005), as discussed in the preceding chapters. In contrast with the inorganic carbon transport, little attention has been given to the organic carbon fraction. Cauwet and Mackenzie (1993) measured the organic carbon concentrations in the river estuary, but with only two cruises conducted separately in May and August of 1985. Likewise, Zhang et al (1992) reported the transport pattern of organic carbon by collecting samples from the estuary. However, their results were also only based on two single expeditions (May and September in 1987). It is evident that these studies based on only two samplings could not fully reflect the organic carbon delivery dynamics. The obtained fluxes are likely misleading, because the hydrological regime, upon which organic carbon flux is calculated, is highly variable between different seasons. On the basis of monthly sampling, seasonal changes of organic carbon concentration in 2009 were investigated by Wang et al (2012). However, they restricted to only one station near the river mouth and, as a result, no information was available on spatial changes.

For a river basin, estimating the trajectory of carbon transport depends greatly on understanding how it is controlled by upstream natural processes and human activities within the watershed. For the first time, this study aimed to analyze the spatial and seasonal variations in organic carbon concentration and export in the Yellow River along its mainstem channel on the basis of weekly sampling over a hydrological year.

The objectives of this study are threefold: (1) to determine the seasonal variations in concentrations of dissolved and particulate organic carbon in the Yellow River; (2) to examine the spatial variability of organic carbon transport along the mainstem channel as a reference point for future studies on a river being increasingly affected by human activities and; (3) to assess the annual organic carbon export into the ocean and its implications for global carbon flux studies.

8.2 Materials and methods

8.2.1 Field sampling

Field sampling was carried out at three mainstem hydrological gauge stations between July 2011 and July 2012 for the upstream Toudaoguai and Tongguan stations, and from August 2008 to July 2012 for the Lijin station, respectively (Figure 8.1). The sampling work was conducted simultaneously with the inorganic carbon sampling presented in Chapter 3. The stations were selected to fully represent the spatial variation of the riverine system in the Yellow River drainage basin. Particularly, Toudaoguai and Tongguan stations are located near the boundaries of the upper-middle and the middle-lower reaches, respectively. Comparative analysis of the two stations could approximately reveal the dynamic nature of water, sediment, and associated organic carbon from the Loess Plateau. Located about 110 km upstream of the river mouth and free of tidal influences, Lijin measurements are able to represent organic carbon delivery to the Bohai Sea. A weekly sampling frequency was adopted throughout the study period, with more intensive sampling during flooding events. In total, 267 samples were collected from the three sites for this study.

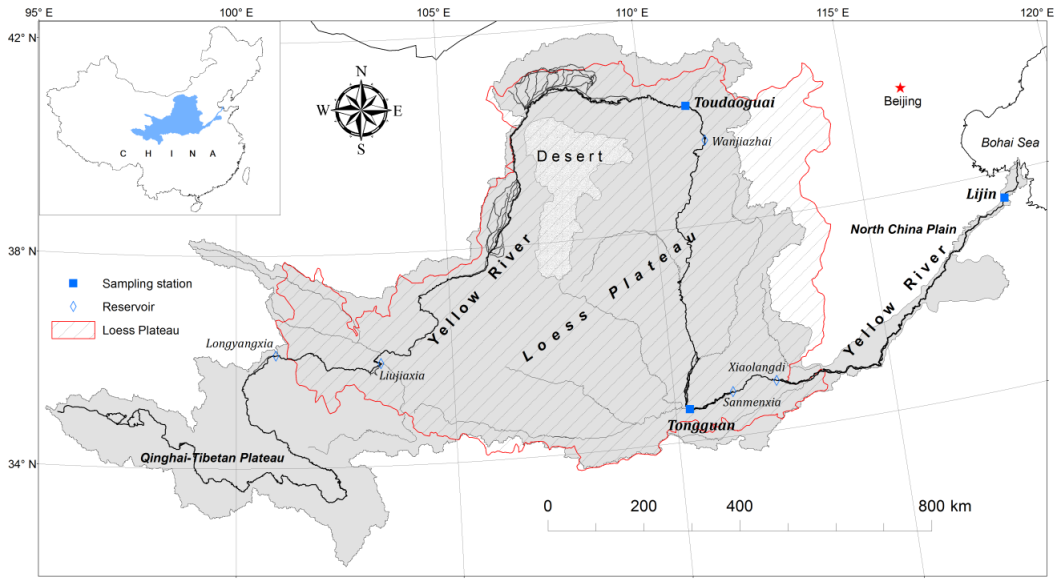

Figure 8.1 Location of the sampling stations on the mainstem channel.

Given that water depth of the mainstem channel was comparatively shallow (< 2 m) in most times during the year, water column samples were collected ~0.5 m below the surface water from 3-5 points across the cross-section using acid-washed but carefully neutralized 5-L high density polyethylene (HDPE) containers. The collected waters from different sampling points were then fully mixed to create one sample representing the organic carbon delivery through the entire cross-sectional profile as the same sampling strategy described in Chapter 3 (see Figure 3.1). On the sampling day, samples were filtered by vacuum filtration through two stacked Whatman GF/F (47 mm in diameter) filter papers that were precombusted at 450 ℃ for 6 h. The residues on the filter paper were dried at 50 ℃ for 24 h and then stored in sealed plastic bags for particulate organic carbon (POC) analysis. The filtrates for dissolved organic carbon (DOC) analysis were first acidified with concentrated HNO_3 to let the pH<2 for the removal of DIC, and were then stored in glass vials at 4 ℃ until analysis. In addition, daily records of water discharge and total suspended solids (TSS)

at the stations were provided courtesy of the Yellow River Conservancy Commission (YRCC). TSS concentration was calculated as the dry weight of suspended solids in 100 ml water sample after filtering through filter papers and being dried at 105 ℃ for 24 h (Xu, 1999).

8.2.2 Measurement of DOC, POC, and PN

DOC concentrations were determined by the high temperature combustion (HTC) method using an Elementar Vario TOC Select Analyzer at 850 ℃ in Beijing Normal University. DOC standard was prepared by diluting a stock solution of potassium hydrogen phthalate (KHP, 500 mg/l TOC) to 5 mg/l with deionized water. A DOC standard was inserted in every 10 water sample sequence for quality control. Results of triple injections suggested the analytical precision was <3%. Filter residues were analyzed for POC and particulate total nitrogen (PN) using a Perkin-Elmer 2400II CHNS/O Analyzer in the Institute of Geology and Geophysics, Chinese Academy of Sciences (Beijing). Sediment samples were first acidified using 10% HCl to remove inorganic carbon. Acetanilide with 71.09% C and 10.36% N was used as an analytical standard. The resultant POC and PN contents (POC% and PN%) were calibrated according to the measurements of the standard samples which were inserted in every five sediment sample sequence. The analytical errors based on replicate analysis were less than 0.3%. Further descriptions concerning the analytical procedures can be found in Sun et al. (2007). Molar C/N ratios were calculated based on the corrected POC and PN contents.

8.3 Results

8.3.1 Hydrological characteristics of water and TSS

Water discharge and TSS are characterized by strong seasonal variations (Figure 8.2 and Table 8.1). The highest water discharge occurred usually in September and the lowest in April-May just before the onset of the flooding season. The maximum/minimum water discharge ratios for Toudaoguai, Tongguan, and Lijin were 2.6, 5.7, and 4.1, respectively. While the highest TSS concentrations coincided with peak water discharge, the lowest TSS concentrations were recorded in February except Tongguan that showed the lowest in June. The maximum/minimum TSS concentration ratios at all the three stations are significantly larger than that of the water discharge, suggesting that disproportionately more TSS was delivered during the high water discharge periods. Due to the intensive rainfall characteristics in the middle reaches (the Loess Plateau), ratios of both water and TSS at Tongguan are higher than that of the upstream Toudaoguai and the downstream Lijin. In addition, compared with Toudaoguai and Tongguan, water discharge and TSS at Lijin showed different seasonal patterns (Figure 8.2). Its highest TSS concentration was in June-July when man-made turbid flows were released downstream from reservoir cascades (Figure 8.1) to mitigate in-channel sedimentation in the lower reaches.

Both the water and TSS fluxes showed downriver changes, increasing from Toudaoguai to Tongguan, as related to the contribution of the Loess Plateau to water and TSS in the Yellow River. Particularly, although the drainage area above Toudaoguai represents nearly half (49%) of the whole river basin, its contribution to

TSS is small. This can be seen from the low concentration in most time of the year (Figure 8.2b). In contrast, the fluxes decreased gradually during the stretch downstream of Tongguan until Lijin (Figure 8.2), because no large tributaries join the mainstem channel, but considerable water withdrawal and in-channel sedimentation occur in the lower Yellow River (see Section 2.4.1).

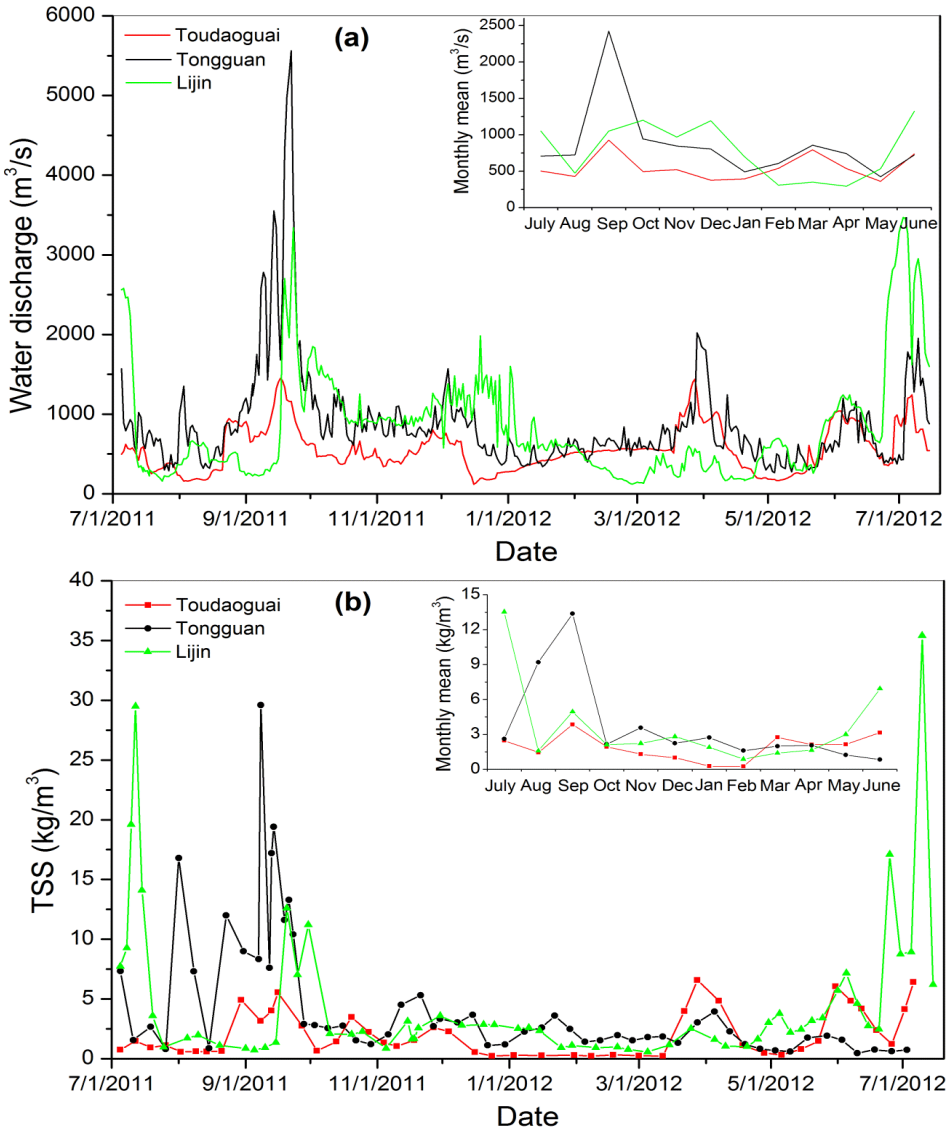

Figure 8.2 Temporal changes in water discharge (a) and TSS (b) at the three sampling stations during the study period. Inserted were the calculated monthly averages showing seasonal variations. Time series for Lijin station during July 2011-July 2012 only was presented for comparison with the other two stations. For TSS, only the weekly values for the sampled days were presented to highlight its trend (see Appendix).

Table 8.1 Monthly average water discharge, TSS, DOC, POC, and PN concentrations measured at the three sampling stations during the study period[a].

Month	Water discharge	TSS	DOC	POC	PN	C/N
	m^3/s	kg/m^3	mg/l	%	%	ratio
		Toudaoguai				
July	502	2.47	2.93	0.45	0.14	3.4
August	429	1.46	3.27	0.47	0.13	3.7
September	928	3.86	2.74	0.30	0.10	3.0
October	496	1.94	3.09	0.41	0.18	2.3
November	521	1.31	2.74	0.40	0.16	2.5
December	375	1.00	2.51	0.49	0.21	2.4
January	395	0.28	2.99	0.40	0.24	1.7
February	541	0.27	2.97	0.51	0.16	3.4
March	793	2.76	6.73	0.45	0.10	4.3
April	536	2.14	6.60	0.89	0.15	5.4
May	360	2.16	2.72	0.67	0.12	5.4
June	739	3.16	3.89	0.42	0.15	2.8
		Tongguan				
July	708	2.61	3.45	0.66	0.13	5.2
August	723	9.18	2.52	0.36	0.14	2.7
September	2425	13.37	2.98	0.27	0.10	2.7
October	945	2.17	3.57	0.44	0.12	3.7
November	845	3.58	2.57	0.37	0.10	3.7
December	807	2.25	3.63	0.43	0.10	4.3
January	491	2.74	4.39	0.42	0.08	5.5
February	606	1.61	6.18	0.34	0.09	4.0
March	859	2.00	5.71	0.61	0.11	5.4
April	744	2.07	5.87	0.73	0.10	7.5
May	424	1.24	6.32	0.70	0.08	8.5
June	723	0.85	4.18	0.64	0.08	8.6
		Lijin				
July	1052	13.53	3.73	0.42	0.09	5.7
August	475	1.60	3.24	0.36	0.06	6.5
September	1052	4.96	3.17	0.33	0.05	6.5
October	1202	2.13	2.83	0.27	0.05	5.6
November	968	2.24	2.92	0.31	0.04	7.2
December	1195	2.83	2.91	0.37	0.05	7.4
January	697	1.90	3.22	0.43	0.07	5.5
February	308	0.89	3.31	0.43	0.10	4.8
March	349	1.41	3.34	0.41	0.10	4.6
April	295	1.66	3.31	0.36	0.06	6.0
May	535	3.01	2.91	0.49	0.09	6.2
June	1323	6.94	3.85	0.38	0.08	4.8

[a] The monthly water discharge and TSS were averaged based on daily measurements. Mean DOC, POC, and PN concentrations and molar C/N ratios were calculated from the sampling results in each month (see Appendix).

8.3.2 Spatial and seasonal changes of DOC and POC

The dissolved organic carbon concentration at the three stations showed seasonal variability. At Toudaoguai station, the DOC concentrations were mostly in the range of 2-4 mg/l (Figure 8.3a). However, from early March when spring floods started, it increased sharply and could be as high as 9.3 mg/l. The high DOC concentrations lasted for about two months before decreasing to a low level. At Tongguan station, the DOC export dynamics was characterized by two distinct periods (Figure 8.3b). The DOC concentration in the dry season is approximately twofold that in the wet season. While for Lijin station, the DOC concentration showed more complex seasonal variations. In general, high DOC concentrations were measured in two periods (Figure 8.3c). One occurred from early March to April, coinciding with the melting period of ice and snow. The other occurred in the period when man-made turbid flows were released downstream. These seasonal variations could also be found from the monthly averages summarized in Table 8.1. Based on all sampling results, the mean DOC concentration at Toudaoguai, Tongguan, and Lijin is 3.6 mg/l, 4.1 mg/l, and 3.3 mg/l, respectively.

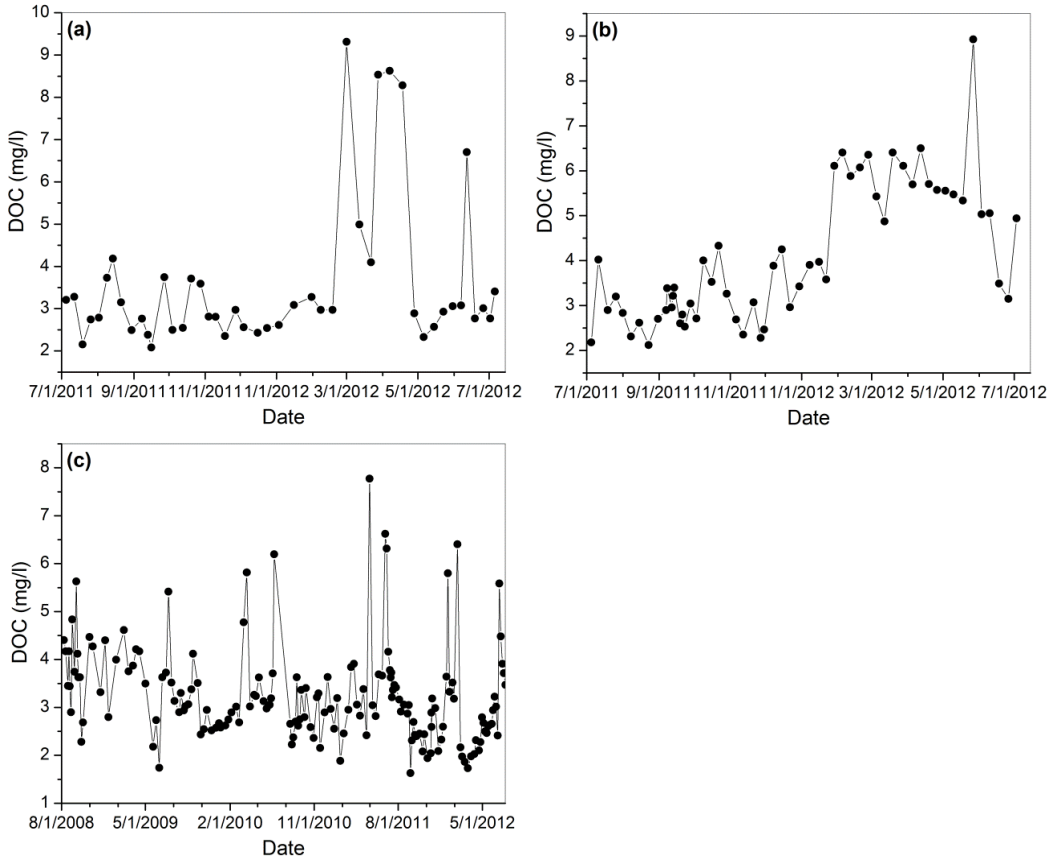

Figure 8.3 Weekly DOC concentration variability during the sampling period at (a) Toudaoguai, (b) Tongguan, and (c) Lijin stations.

Transport of DOC is generally highly dependent on flow dynamics. However, the DOC concentration at Toudaoguai did not show a significant relationship with water discharge (Figure 8.4a). High DOC concentration values (i.e., >6 mg/l) were mostly measured during the spring flood period, in which the water discharge increased as a result of melting of ice and snow. For Tongguan and Lijin stations, the DOC concentrations correlated negatively with water discharge (Figures 8.4b and 8.4c). With increasing water discharge in the wet season, the DOC concentrations decreased rapidly. At Lijin station, however, the DOC concentration showed an upward trend when the water discharge was larger than 2500 m^3/s, which is different from the leveling off observed at Tongguan station. Because the flow dynamics in the lower

Yellow River has been significantly regulated by reservoir cascades, high water transport events are usually due to man-made turbid flows released from reservoirs.

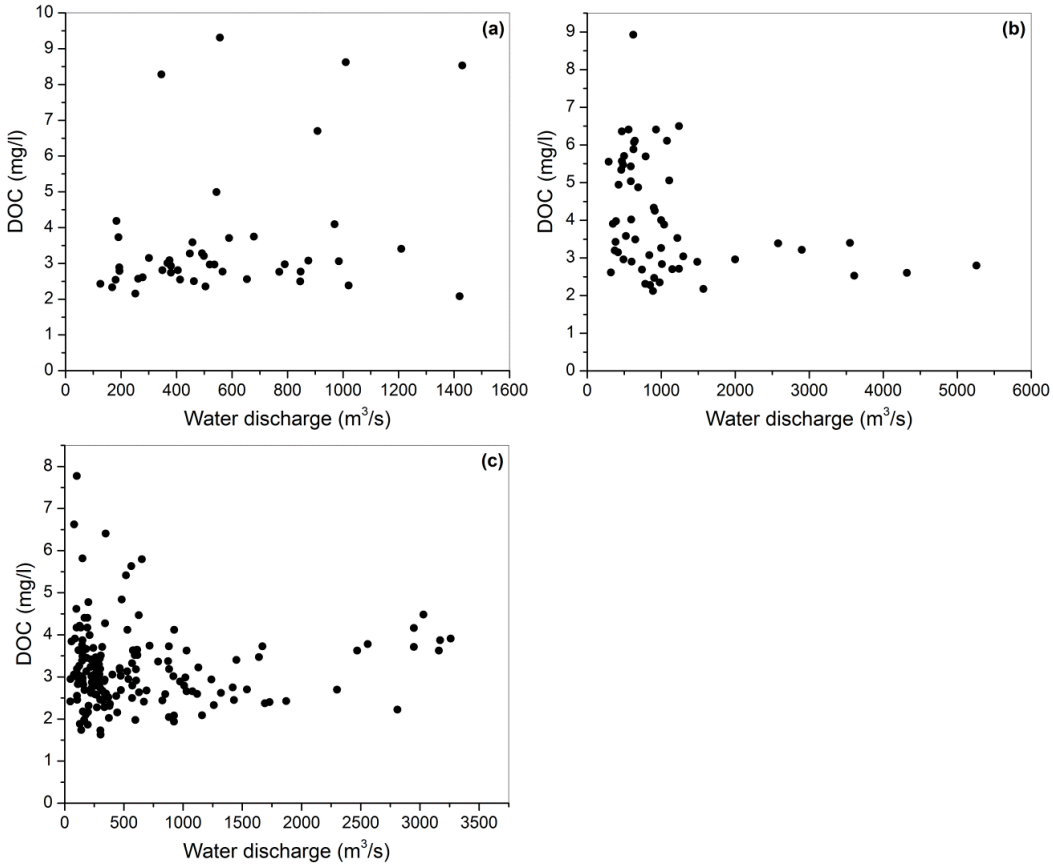

Figure 8.4 Relationship between DOC concentration and water discharge at (a) Toudaoguai, (b) Tongguan, and (c) Lijin stations.

Due to the low carbon content in the parent soils of the Loess Plateau, the Yellow River sediments are characteristic of low POC%, mostly ranging from 0.11% to 0.89% with very few cases exceeding 1% (Table 8.1). The average POC% at Toudaoguai, Tongguan, and Lijin stations was 0.48%, 0.47%, and 0.37%, respectively, which is substantially lower than the global mean (0.95%, calculated from Ludwig et al., 1996). Similarly, the PN% in the Yellow River sediments is also very low, with most falling into the range of 0.05-0.24% (Table 8.1). The average PN% at the three stations was 0.15%, 0.1%, and 0.07%, respectively. Both POC and PN presented weak seasonal

changes, with a slight increase in the dry season, in particular the months before the start of the wet season. When relating to the corresponding TSS changes, the POC% generally showed a negative relationship with increasing TSS concentrations, in spite of large scatter (Figure 8.5). Similar negative correlations could also be found between PN% and TSS. With a narrower magnitude of seasonal variation in comparison with POC%, the PN% showed a relatively small decreasing rate with TSS. The decreasing trends of POC% and PN% with increasing TSS are more significant at Toudaoguai and Tongguan stations than at the downstream Lijin station.

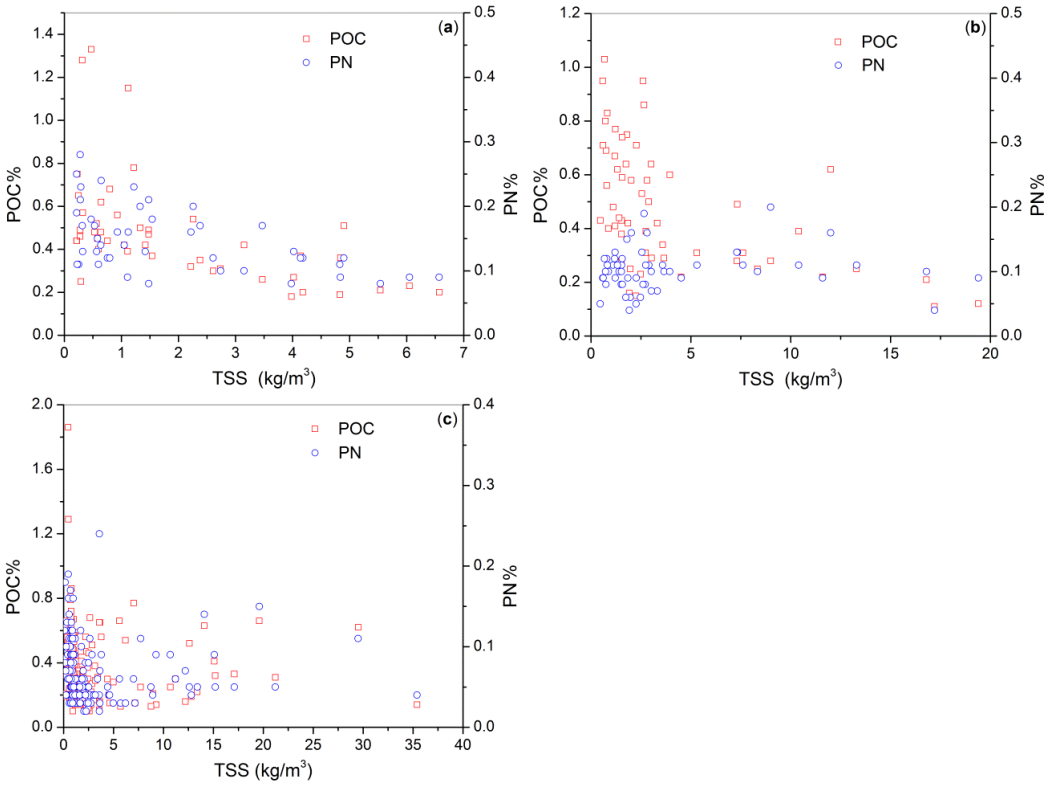

Figure 8.5 Relationship between POC and PN contents and TSS at (a) Toudaoguai, (b) Tongguan, and (c) Lijin stations.

The molar C/N ratio of the TSS transported by rivers is generally indicative of the source of riverine organic matter and to what extent organic matter has been degraded. Terrestrial organic matter usually has significantly higher C/N ratios (>10) in

comparison with those of aquatic origin (<8), such as phytoplankton (Hedges et al., 1997; Balakrishna and Probst, 2005; Leithold et al., 2006). Compared with other rivers with high C/N ratios (i.e., 8.6-10.9 for the Yangtze, Wang et al., 2012), the Yellow River TSS was characterized by low C/N ratios as a result of low POC% (Table 8.1). Spatially, the mean C/N ratios increased from upstream Toudaoguai (3.4) through Tongguan (4.8) to downstream Lijin (5.9). In addition, the C/N ratios showed strong temporal changes (Figure 8.6). For Toudaoguai and Tongguan stations, high C/N ratios were observed in the period from early March to May, in which the C/N ratios were 5.3 and 8.4, respectively. In contrast, the C/N ratios in the wet season were obviously lower, with 2.8 for Toudaoguai and 3.7 for Tongguan. While for Lijin station, the C/N ratios showed larger temporal fluctuations. High C/N ratios were usually measured in high flow periods, such as the man-made turbid flows from mid June to early July and the high natural runoff in September (Figure 8.2). These variations were in good agreement with that found by Wang et al (2012) for the same station. Evidently, the spatial and temporal differences in C/N ratios are the combined results of natural and human factors.

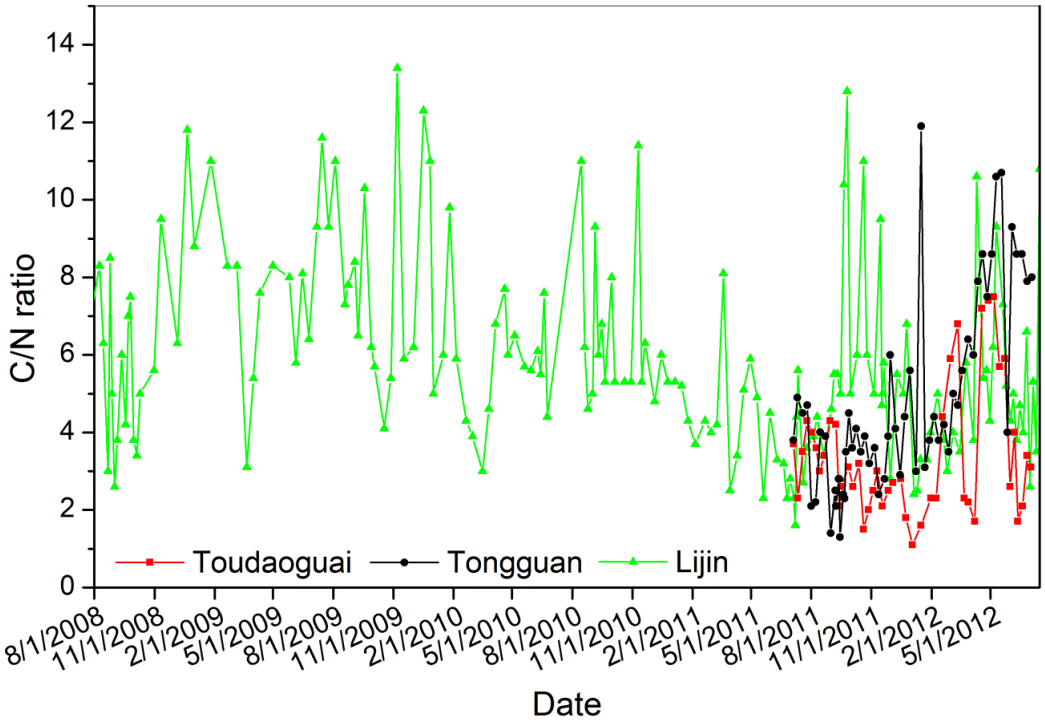

Figure 8.6 Molar C/N ratios of particulate organic matter at the three sampling stations.

8.3.3 Fluxes of DOC and POC

Considering that organic carbon was measured with "sparse" sampling frequency while water discharge and TSS had a continuous daily measurement, Beale's stratified ratio estimator was used to calculate the loading (Beale, 1962 in Dolan et al., 1981). This method could greatly reduce the bias introduced by relatively low sampling frequency, in particular the high flow events that are often undersampled (Parks and Baker, 1997).

Regarding the annual DOC and POC loadings, the formula can be expressed as follows:

$$\mu_y = \mu_x \frac{m_y}{m_x}\left(\frac{1+\frac{1}{n}\frac{S_{xy}}{m_x m_y}}{1+\frac{1}{n}\frac{S_x^2}{m_x^2}}\right) \quad \text{(Equation 8.1)}$$

where, μ_y is the estimated load, μ_x is the mean daily water discharge for the year measured, m_y is the mean daily loading for the days on which the DOC concentration and POC% were determined, m_x is the mean daily water discharge for the days on which the DOC concentration and POC% were determined, and n is the number of days on which the DOC concentration and POC% were determined. Furthermore,

$$S_{xy} = \frac{1}{(n-1)}\sum_{i=1}^{n} x_i y_i - n m_x m_y \quad \text{(Equation 8.2)}$$

$$S_x^2 = \frac{1}{(n-1)}\sum_{i=1}^{n} x_i^2 - n m_x^2 \quad \text{(Equation 8.3)}$$

where, x_i is the individual measured flow, y_i is the daily loading for each day on which the DOC concentration and POC% were measured. It is evident that the DOC or POC load estimate is derived from a ratio, m_y/m_x, which is defined as the ratio of the mean of measured loads to the mean of water discharge of the days when loads were quantified. Finally, this ratio is used with the overall mean water discharge, μ_x, to estimate the annual DOC or POC loading.

The DOC and POC fluxes at Toudaoguai were 0.06×10^{12} g/yr and 0.16×10^{12} g/yr, respectively. At Tongguan, they were 0.11×10^{12} g/yr and 0.59×10^{12} g/yr, respectively. It is clear that the OC flux at Tongguan (0.7×10^{12} g/yr) is more than 3 times that at Toudaoguai (0.22×10^{12} g/yr). Taking Lijin as the control station for seaward export, the mean seaward DOC and POC fluxes of the Yellow River during the period 2008-

2012 were 0.06×10^{12} g/yr and 0.41×10^{12} g/yr, respectively. Unlike the world average of organic carbon transport which is equally distributed between the dissolved and the particulate fractions (Stallard, 1998), the seaward POC flux in the Yellow River is about 7 times higher than the DOC flux, highlighting the importance of sediment delivery in carrying associated carbon into the ocean. The total amount of organic carbon delivered by the Yellow River was 0.47×10^{12} g/yr during the period. In conjunction with the DIC flux of 1.09×10^{12} g/yr computed in Chapter 4, annually, about 1.56×10^{12} g carbon is transported into the Bohai Sea.

8.4 Discussion

8.4.1 Factors controlling organic carbon delivery

Based on the temporal changes of water and DOC in the entire study period (Figures 8.2 and 8.3), the DOC concentrations did not follow the flushing effect that indicates it increases with increasing water discharge found in most other rivers (e.g., Ludwig et al., 1996; Worrall and Burt, 2004). In contrast, in the Yellow River, the seasonal variability of the hydrograph played a significant role in determining the DOC export. The highest DOC concentration at Toudaoguai and Tongguan stations occurred in spring floods induced by melting of ice and snow. During the winter months with less rainfall, the groundwater table decreases, allowing for the production of DOC via leaching from litter and live vegetation, or from soils via microbial metabolism and erosion of soil organic matter (Hope et al., 1994). In addition, the lowered groundwater table could also cause DOC production by triggering the enzymic latch mechanisms (Freeman et al., 2001). During the spring melting period, DOC stored

within upper soil horizons was flushed out into the river, causing a sharp increase in DOC concentration (Table 8.1), similar to that observed in boreal watersheds (Neff et al., 2006). Although the water discharge of spring floods was significantly lower than that in the wet season (Table 8.1 and Figure 8.2), a considerable proportion of the annual DOC flux was transported during this period. For example, the DOC flux transported by the spring floods at Toudaoguai station accounted for about 41% of the annual flux. The percentage decreased gradually towards the downstream Lijin station with increasing proportion of rainfall-supplied drainage area.

It is worth noting that the duration of high DOC concentration at Tongguan is longer than at Toudaoguai, but the absolute values of the latter are higher than that of the former (Figures 8.3a and 8.3b). Such contrasts are indicative of the differences in climate and DOC pool available for leaching and transport. First, Toudaoguai controls the upper Yellow River, half of which is located on the Qinghai-Tibetan Plateau with high altitudes and the other half on the northernmost part of the basin. These characteristics determine the later beginning of the melting of ice and snow compared with the Loess Plateau that Tongguan controls. In addition, soil pool of DOC is significantly higher in the upper Yellow River basin than on the Loess Plateau (see Chapter 7, Figure 7.5 in particular), causing higher DOC concentration at Toudaoguai through flood flushing. In the following wet season, the DOC concentration decreased rapidly to a low level (Figure 8.3), which is probably because most of the leachable DOC in surface soils had already been released into the river with the spring floods. It may also be due to dilution effects of the sharply increased

water discharge (Figure 8.2). Higher DOC concentrations at Lijin in June-July were likely the result of extended water residence time due to reservoir trapping which promotes *in situ* production, resulting in increased concentration under high water discharge scenarios (i.e., >2500 m^3/s). Furthermore, flow regulation has also reduced the seasonal differences. Based on the mean monthly DOC concentration, the maximum over minimum ratio at Lijin is 1.4, which is substantially lower than Toudaoguai (2.7) and Tongguan (2.5).

Instantaneous TSS concentrations showed seasonal variations similar to the water discharge (Figure 8.2), indicating its dependence on hydrological regime (Lu et al., 2012). The POC% in the riverine suspended solids generally decreased exponentially with increasing TSS concentration. This is the case for all the three stations with different magnitudes of TSS, which suggests that this relationship is fundamentally similar at both the seasonal and spatial scales. This inverse relationship observed in the Yellow River may be due to the dilution of riverine POC with more mineral matter in highly turbid waters (Ludwig et al., 1996; Gao et al., 2002). Gully erosion on the Loess Plateau could contribute >50% to the total eroded suspended solids during heavy storm events (Xu, 1999; Valentin et al., 2005), by which more coarse sediments are transported into the river. Compared with the finer sediment particles, the coarser fraction has a higher percentage of mineral matter and a lower POC percentage (Zhang et al., 2009a). Therefore, increased TSS concentration indicated higher gully erosion contribution, resulting in reduced POC% for the analyzed TSS samples. Another process that would also lead to the inverse relationship is the

decrease in the phytoplankton material with increasing TSS concentration (Balakrishna and Probst, 2005). Higher TSS concentration can inhibit the growth of phytoplankton due to reduced availability of light. Considering that the lowest TSS concentration in the Yellow River waters is already very high, growth of phytoplankton is greatly restricted and its effect on POC% changes is therefore insignificant. This is particularly true for the Toudaoguai and Tongguan stations that are not significantly affected by reservoir regulation which is likely to promote aquatic production.

Although the DOC concentration and POC percentage showed a negative relationship with water discharge and TSS concentration, respectively, the DOC and POC fluxes correlated positively with water and TSS with statistical significance (e.g., at Tongguan, DOC flux-water discharge: R^2=0.84, p<0.01, n=57; POC flux-TSS: R^2=0.65, p<0.01, n=57). In view of the heavy storm character, this indicated that a large amount of the terrestrially-derived organic carbon was delivered into the rivers by runoff during high flow periods. In comparison, despite with higher DOC concentration and POC%, the low flow period transported less organic carbon, accounting for only 28% of the annual total flux.

8.4.2 Sources of organic carbon

For rivers with low TSS concentration, possible sources of riverine POC include *in situ* productivity, litterfall, soils, and sedimentary rocks (Leithold et al., 2006), while for highly turbid rivers, POC is usually allochthonous. Radioactive carbon isotope

studies suggested that the ^{14}C ages of the POC in the Yellow River are considerably old, ranging from 4110 to 8040 years, which are much older than the ^{14}C ages of the transported DOC (Wang et al., 2012). The old POC age indicated that the POC was not supplied by recently-fixed organic matter through biological processes. Instead, it was largely derived from clay-sized minerals, loess materials, and chemical weathering products of old rocks and ancient kerogens (Wang et al., 2012). Based on a relationship between POC and TSS of several highly turbid rivers, Meybeck (1993a) assumed that riverine suspended loads have an ancient sedimentary OC origin of about 0.5% on average. However, he did not take into account net oxidation of rock organic carbon (Ludwig et al., 1996). As most of the POC% values in the Yellow River are above 0.2% irrespective of the magnitude of the TSS concentration (Figure 8.5), it seems that the POC% of sedimentary rock origin is smaller than previously assumed. This low POC% is determined by the widespread carbonates that are characterized by low organic carbon content (Di-Giovanni et al., 2002; Chen et al., 2005).

Given the characteristics of high sediment yield and low POC% in the Yellow River, a considerable portion of the riverine POC was probably derived from the eroded loess deposits as supported by the old ^{14}C age. On the other hand, under the circumstances of lower TSS concentrations, the POC% could be 0.6% or above (Figure 8.5), indicating that a portion of the organic carbon may originate from soil horizons, which is usually the case for less turbid waters (Meybeck, 1993b). Soil erosion at the preliminary stage occurring mainly at the uppermost soil horizon will

first carry the solids with high POC% into river. With enhanced soil erosion rates, solids from deeper horizons, in which the organic carbon is highly degraded and refractory and the POC% is thus low, are transported into the river water, resulting in lower POC% in TSS as a whole. This may also explain the decreasing POC% with increasing TSS concentration. Therefore, the riverine POC is a mixture of the loess deposit origin with organic carbon from upper soil horizons when the TSS concentration is relatively low; while it is mainly from the loess deposits and the deeper soils when the TSS concentration is high.

With respect to the DOC, its sources include decomposition of terrestrial organic matter and autochthonous production by aquatic plants and microbes. The younger age reported by Wang et al (2012) demonstrated that it was primarily derived from recently decomposed litterfall and belowground production (Ludwig et al., 1996; Raymond and Bauer, 2001a; Lu et al., 2012). Similarly, owing to the high TSS concentration and the reduced availability of light in river waters, autochthonous aquatic biological activity is substantially restrained and its contribution to riverine DOC is thus negligible. The argument that the DOC is principally of terrestrial origin could also be supported by the significant correlation between the DOC flux and water discharge as indicated by the high R^2 shown above (see Section 8.4.1).

Previous studies have demonstrated that a low C/N ratio is indicative of an aquatic origin for POC, because phytoplankton on average has a C/N ratio of about 6 while terrestrial inputs of POC have higher C/N ratios of usually larger than 8 (Gupta et al.,

1997). Compared with the arguments on the POC sources discussed above, the low C/N ratios of the suspended solids in the Yellow River (Table 8.1 and Figure 8.6) appeared to be contradictory to the common knowledge. A possible explanation for this is the low organic carbon content in the sedimentary rocks and parent soils. Except in the high flow periods in which the C/N ratios could exceed 8 and be up to 13.4 at Lijin, they are below 8 in most part of the investigation period at the three stations. As described earlier, at Toudaoguai and Tongguan, higher C/N ratios occurred in the period of March-May, indicating the flushing of POC-rich suspended materials by spring floods. With increasing temperature in spring, ice and snow begin to melt and as a result, the decomposed litterfall in winter is flushed downslope into the river by floods. Although the water discharge and TSS concentration are not very large as compared with that in the wet season (Figure 8.2), the flushed suspended materials are relatively rich in organic carbon after long chemical and biological processes in winter, resulting in higher C/N ratios. Downstream of the Tongguan station, operation of a reservoir cascade has greatly increased the water residence time as indicated in Chapter 5, thereby allowing for *in situ* phytoplankton production because of increased light availability and reduced flow turbulence. Coupled with terrestrial inputs, the C/N ratio at Lijin increased during the high flow periods (Figure 8.6).

The seasonal differences in C/N ratio indicated the source variations of suspended materials. While sedimentary loess deposits are the major source for the riverine suspended materials during the high flow period, decomposition of litterfall and

erosion of surface soil horizons contribute substantially in the low flow periods. Furthermore, downstream increase of the mean annual C/N ratio along the mainstem channel revealed their increasingly important contribution. Phytoplankton production may have also affected the C/N ratio at the Lijin station. More importantly, in combination with the low C/N ratios and the old ages of POC suggested by isotopic evidence (Wang et al., 2012), the method using C/N ratio=8 to identify POC source is challengeable. This may only hold true when the POC% is significantly higher than 0.5%, which enables other terrestrial inputs except from sedimentary rocks.

8.4.3 Spatial and temporal variations of organic carbon fluxes

Downstream variations of the organic carbon fluxes reflect the impacts of human activities and basin characteristics on organic carbon export. Great flux differences between Toudaoguai and Tongguan suggested the significance of the Loess Plateau in providing organic matter. Compared with Toudaoguai, while the DOC flux at Tongguan nearly doubled, the POC flux showed a 3.7-fold increase, which is consistent with the Loess Plateau's contribution to sediment supply (Zhao, 1996; Chen et al., 2005). Due to long-term agricultural production and vegetation restoration (Ran et al., 2013b), most of the Loess Plateau, in particular the southeastern part, has a relatively high soil organic carbon content (see Chapter 7). This unique soil property, coupled with the most serious soil erosion that also occurred in the southeastern catchments, caused the organic carbon flux to increase sharply. On the contrary, decrease in the organic carbon flux from Tongguan to Lijin was primarily caused by reduced water discharge and sediment load. Water diversion

for agriculture and sediment trapping by reservoirs in the lower Yellow River have collectively resulted in progressive reductions of water and sediment along the river course (Wang et al., 2007). For example, during the past decade since impoundment of the Xiaolangdi Reservoir in 2002 (Figure 8.1), water discharge and sediment load at Lijin accounted for only 72% and 48%, respectively, of that measured at Tongguan. It is evident that human-induced reductions of water and sediment are the major reason for the net decreases of organic carbon loadings.

Furthermore, according to calculation results presented in Chapter 4, riverine partial pressure of CO_2 (pCO_2) at the three stations was well above the atmospheric equilibrium during the sampling period, indicating a net emission of CO_2 to the atmosphere. Specifically, the pCO_2 at Tongguan is significantly higher than that at the upstream Toudaoguai and the downstream Lijin. In association with the Loess Plateau's importance, tremendous input of organic carbon from the Loess Plateau and its rapid decomposition is an important reason for the highest pCO_2 at Tongguan. For the lower Yellow River with limited tributary inputs, continuous degradation of organic carbon in river waters caused the DOC concentration and POC% to decrease gradually towards the river mouth, resulting in reduced fluxes of DOC, POC, and the total organic carbon at Lijin. In particular, compared with Tongguan, whereas the DOC flux at Lijin decreased by about 50% to be equivalent to Toudaoguai, its POC flux decreased by 30%. Slower POC decomposition is probably the result of enhanced preservation efficiency of increasingly finer sediments downstream (Robert, 2008; Zhang et al., 2009a). It has been widely found that the finer sediment particles

(i.e., < 38 μm) could better protect riverine POC from oxidation during the delivery stage (Bergamaschi et al., 1997; Keil et al., 1997).

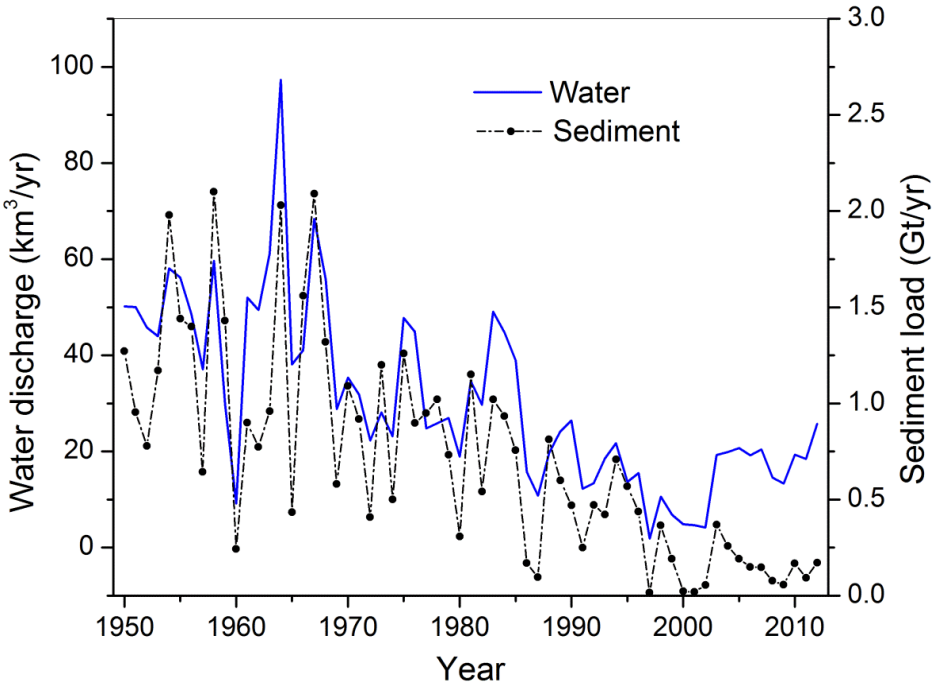

Figure 8.7 Long-term annual water discharge and suspended sediment load at Lijin station showing stepwise reductions.

Over the past six decades, the annual export of water and sediment from the Yellow River into the ocean has decreased markedly in response to climate change and human activity (Figure 8.7). Transport dynamics of water and sediment have been systematically analyzed with respect to the spatial and temporal variations and possible reasons (Wang et al., 2007b; Peng et al., 2010). These studies have explicitly indicated that human activities are the major reason for the rapid reductions, because climate variables, such as precipitation, did not significantly change during the period (Lu et al., 2013). In contrast, less work has been done to estimate the organic carbon flux (Table 8.2). Due to continuously decreasing water and TSS discharges, both the

DOC and POC fluxes are substantially lower than the historical records based on samplings in 1980s while comparable to recent estimates.

Table 8.2 Estimated organic carbon fluxes of the Yellow River.

Year	Monitoring site	DOC $\times 10^{12}$ g/yr	POC $\times 10^{12}$ g/yr	Sampling frequency	Source
1983	Jinan	0.54	0.35	n/a	Gan et al., 1983
1985	Estuary	0.06	4.5	May/Aug.	Cauwet and Mackenzie, 1993
1987	Estuary	0.2	6.1	May/Sept.	Zhang et al., 1992
2009	Lijin	0.032	0.389	Monthly	Wang et al., 2012
2008-2012	Lijin	0.06	0.41	Weekly	This study

Worldwide, the organic carbon inputs into the ocean have experienced a significant temporal change (Worrall and Burt, 2004; Bianchi et al., 2007). As for the Yellow River, reasons for the discrepancies between the present estimate and the historical records are multiple. Although greatly reduced water and sediment fluxes over the period are the major reason, a limited number of sampling, in particular for the campaigns conducted in the 1980s (Table 8.2), would introduce significant biases to annual export calculation. This can be clearly seen from the huge differences in both the DOC and POC fluxes over a short period of four years from 1983 to 1987. With respect to the POC flux, the estimate obtained in this study is approximately equivalent to that estimated by Wang et al (2012). That is because the POC% was very low and showed little seasonal variation. Indeed, there is no significant difference in the POC% even at a decadal timescale. For example, the average POC% in 1985 based on two samplings in May and August is 0.46% (Cauwet and Mackenzie, 1993), which is very close to the present POC% value. If the POC% is assumed to remain stable over the period, the POC flux from the Yellow River to the Bohai Sea has decreased by 90% from 4.5×10^{12} g/yr prior to 1970, due to the rapid

reduction of TSS (Figure 8.7). For the DOC flux, the present estimate is nearly twice that calculated by Wang et al (2012). It seems that their DOC flux estimate has been underestimated. The reasons are twofold. The first is that the year 2009, when their sampling campaign was carried out, showed exceptionally low water discharge as illustrated in Figure 8.7, which is about 27% lower than the multi-annual average of the recent decade. The other is its low sampling frequency. A monthly sampling is not able to account for the storm events, which have been identified to play an important role in controlling DOC export (Boyer et al., 1997; Hood et al., 2006). Based on a 4-year-long weekly sampling taken from several points across the cross-section, the obtained estimates of the organic carbon fluxes from this study are more accurate and are thus representative of the actual delivery.

Through a conceptual model involving production, transport, and deposition of organic carbon, the fates of bulk organic carbon in the Yellow River basin were assessed in Chapter 7. In the budgetary assessment, the total amount of organic carbon decomposed during the transport processes from the uplands into the ocean was quantified by closing the budget equation. Approximately, 4.61 Mt of organic carbon is released into the atmosphere per year on average. In addition, based on widespread hydrological gauge stations located on the mainstem and major tributary channels, CO_2 outgassing flux from surface water of the Yellow River network was estimated at 4.19 Mt/yr in Chapter 4 (the maximum was adopted here). While all the used gauge stations are located on higher order streams, the lower order streams are not effectively represented. Before being measured at the gauge stations, a

considerable portion of labile organic carbon may have been rapidly decomposed before or after reaching the lower order streams. In fact, the CO_2 outgassing rates from small streams were found to be 2-3 times higher than those observed in larger rivers (Aufdenkampe et al., 2011), and the labile fraction of organic carbon would be oxidized in a very short distance and evaded into the atmosphere (Johnson et al., 2008). The difference between the two estimates highlights the significance of lower order streams in affecting organic carbon transport assessments. Small streams must be taken into account when evaluating organic carbon cycle at the watershed scale, the resulting carbon loss would otherwise be considerably underestimated.

8.4.4 Implications for global organic carbon export

The average DOC concentration for the Yellow River waters is 3.3 mg/l, which is comparable to the neighbouring Yangtze River (Wang et al., 2012), while slightly lower than the global mean of 4.9 mg/l (Ludwig et al., 1998). Due to its low water discharge, however, the DOC flux of the Yellow River is very small. On the other hand, despite its extremely high sediment load, the POC flux in the Yellow River is relatively low as a result of the low POC% that is significantly lower than the global mean of 0.95% (calculated from Ludwig et al., 1996). Accordingly, the seaward organic carbon delivery through the Yellow River is small in comparison with other large rivers of the world (Table 8.3). Contribution of the Yellow River to global carbon export to the ocean is quite small, accounting for approximately 0.19% of the total flux via rivers, which is in stark contrast to its role in global sediment delivery (5%). Furthermore, it should be pointed out that the fate of the riverine organic

carbon in the estuary was not followed in this study. A substantial portion of the organic carbon that enters the estuary would be buried there or decomposed and released into the atmosphere (Galy et al., 2007; Chen et al., 2012). Therefore, the actual flux reaching the ocean would be smaller than the value calculated here.

Table 8.3 Comparison of carbon fluxes of world large rivers.

River	Water	DOC	POC	DIC	Total	Source
	km^3/yr	$\times10^{12}$ g/yr	$\times10^{12}$ g/yr	$\times10^{12}$ g/yr	$\times10^{12}$ g/yr	
Yellow	25.2	0.06	0.41	1.09	1.56	This study
Amazon	5500	18.6	13.2	26	57.8	Probst et al., 1994
Yangze	971	0.9	2.2	14.6	17.7	Wu et al., 2007
Xijiang (Pearl)	230	0.66	2.93	5.8[a]	9.4	Gao et al., 2002
Mekong	470	4.2	4.7	8.9	17.8	Li and Lu, 2012
Ganges	459	1.7	18	7.9	27.6	Degens et al., 1991
Mississippi	547	3.1	0.93	13.5	17.53	Bianchi et al., 2007
Godavari	105	0.76	0.76	2.52	4.04	Balakrishna and Probst, 2005
Congo	1300	8.9	1.1	3.3	13.3	Probst et al., 1994
St Lawrence	413	1.55	0.31	7.02	8.88	Degens et al., 1991
Niger	152	0.53	0.66	1.24	2.43	Degens et al., 1991
Yukon	210	0.9	0.3	4	5.2	Degens et al., 1991
Columbia	249	0.52	0.06	3.77[b]	4.35	Ludwig et al., 1996
Indus	104	2.67	1.64	2.1[b]	6.41	Ludwig et al., 1996
World	41800	206	188	327	721	Ludwig et al., 1998
World	38600[c]	200	200	400-500	800-900	Aufdenkampe et al., 2011

[a]Degens et al., 1991; [b]Cai et al., 2008; [c]Schlünz and Schneider, 2000.

Both fluvial water and TSS discharges have been greatly reduced in worldwide rivers, and a major reason is the regulation of numerous dams constructed within the watersheds (Syvitski et al., 2005). The resultant water retention and burial of sediment have significant implications for not only the organic carbon budget but also the closely related biogeochemical processes occurring in riverine and coastal ecosystems. For example, reduced sediment load in the Mississippi River has resulted

in changes in mass accumulation rates of organic carbon on the Louisiana shelf and an increase in phytoplankton biomass (Allison et al., 2007; Bianchi et al., 2007). More work is strongly needed in future to investigate these responses related to organic carbon transport in the Yellow River.

The DOC/POC ratio indicates the partition of organic carbon between the dissolved and particulate fractions. Global average DOC/POC ratio is about 1-1.2 (Ludwig et al., 1998; Aufdenkampe et al., 2011). When plotted against sediment yield, it decreases exponentially from a high of about 8.7 for the Columbia River to an asymptotic value of approximately 0.08-0.16 for the Yellow and Lanyang Hsi rivers (Figure 8.8). It is important to emphasize that, when the sediment yield exceeds 1000 $t/km^2/yr$, the DOC/POC ratio remains roughly stable. In such cases, the POC constitutes about 90% of the total organic carbon transported. Owing to high sediment concentration, photochemical degradation of POC is restricted and the delivered POC could be refractory along the flow path to the ocean. This can be validated by the stable POC% along the Yellow River mainstem channel (Liu et al., 2006). In contrast, in the rivers with lower sediment yield, rapid decomposition of labile POC would increase the DOC pool (Keil et al., 1997; Wang et al., 2012b).

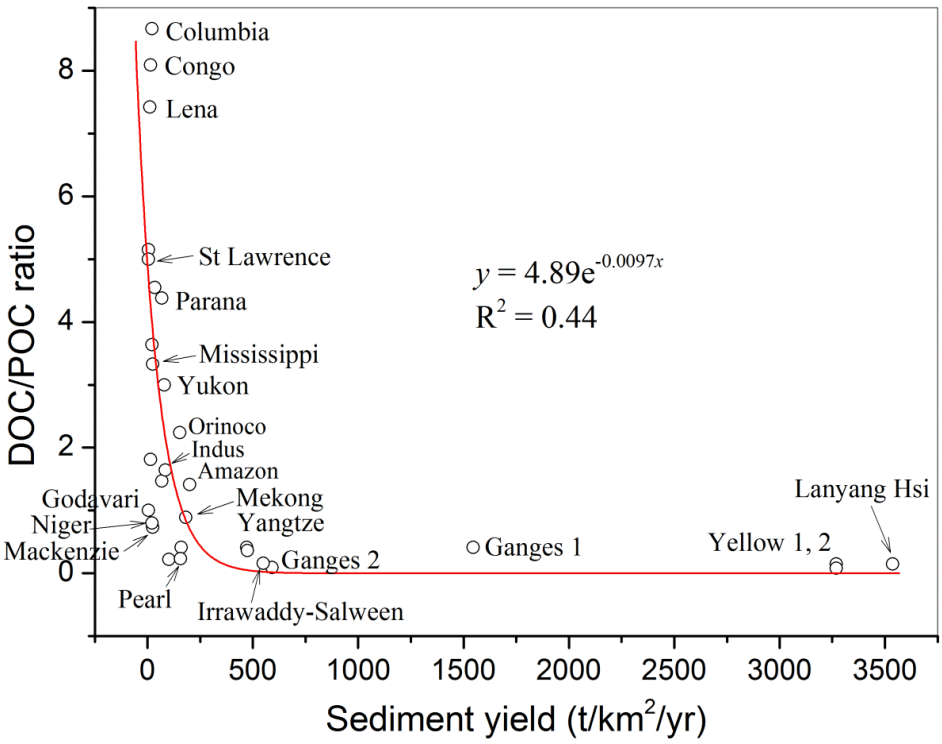

Figure 8.8 Correlation between DOC/POC ratio and sediment yield in typical rivers of the world. In addition to rivers presented in Table 2, data were from Wang et al (2012) for Yellow 1, Kao and Liu (1997) for Lanyang Hsi (Taiwan), Bird et al (2008) for Irrawaddy-Salween, and Wu et al (2007) for the remaining rivers (including Ganges 1). Yellow 2 was from this study.

Tropical monsoon rivers, such as the Ganges, Yangtze, and Mekong rivers originating from the Himalayan highlands, are characterized by high sediment yields (Lu et al., 2010). They usually have lower DOC/POC ratios in spite of the considerable DOC fluxes (Table 8.3). In contrast, non-monsoon rivers, such as these in northern America, have higher DOC/POC ratios (>2) and lower sediment yield, which result from a number of physical, biological, and chemical processes (Ludwig et al., 1996; Wu et al., 2007). Nonetheless, once the sediment yield is significantly high, the DOC/POC ratio will be very low independent of the climate. For instance, with tremendous sediment supply from landslides triggered by tropical cyclones, the coastal mountainous river of Lanyang Hsi in Taiwan has a DOC/POC ratio of only 0.16

(Figure 8.8). With a similar low DOC/POC ratio, approximately 90% of the organic carbon transport in the Yellow River is in the particulate form, which is definitely different from the neighbouring Asian rivers. With decreasing sediment loading due to vegetation protection and dam trapping over the past decades, the relative proportion of DOC in the total organic carbon transport has increased sharply as compared to the historical fluxes in Table 8.2.

8.5 Summary and conclusions

Behaviour of organic carbon delivery in the Yellow River was investigated in detail and its possible sources and implications were discussed. Both the concentrations of DOC and POC showed significant spatial and seasonal variations, which are the combined results of natural hydrological processes and anthropogenic activities. Organic carbon transport showed different seasonality among the three investigated stations. Whereas the DOC export at the upstream Toudaoguai and Tongguan stations was mainly controlled by hydrological regime such as melting of ice and snow in spring, it was more affected by reservoir regulation at the lowermost Lijin station. POC% in the Yellow River sediments is quite low as compared to other large rivers, which is most likely due to the low soil organic carbon content. Riverine POC is mostly terrestrial origin, including sedimentary loess deposits and soil horizons, while autochthonous contribution is small as a result of low light availability.

Based on daily records of water discharge and TSS concentration, the total DOC and POC fluxes into the Bohai Sea during the study period were estimated at 0.06×10^{12}

g/yr and 0.41×10^{12} g/yr, respectively. If the DIC flux (1.09×10^{12} g/yr) calculated in Chapter 4 is included, the total riverine carbon flux transported by the Yellow River into the ocean was 1.56×10^{12} g/yr. This accounts for about 0.19% of the total carbon flux discharged into the oceans by world rivers. The extremely low DOC/POC ratio represents the lowest level among major world rivers, which is consistent with its intense soil erosion. Over the past decades, the POC flux has decreased by 90%. Such rapid reduction can be explained by the decrease in the TSS load, because the POC% remained largely unchanged over the period. In addition, significant reductions in water discharge may have resulted in a decrease in the DOC flux of the same amplitude, although historical DOC concentrations were not available. Changes in the fluxes of different carbon species over space and time have far-reaching effects on the biogeochemical processes in the estuary and coastal ecosystems. Full understanding of the resulting effects warrants further research in future.

Chapter 9 Conclusion

9.1 A brief overview of the study

Based on retrieved historical records measured at a hydrological gauge network and recent sampling along the mainstem channel as well as remote sensing data, this thesis for the first time fully examined the lateral delivery and vertical exchange of riverine carbon in the Yellow River and investigated their respective responses to various natural factors and human modifications. Given the Yellow River's role in global sediment transport (Milliman and Meade, 1983), three forms of carbon that have implications for global climate change studies, including dissolved inorganic carbon (DIC) and dissolved and particulate organic carbon (DOC and POC) were studied. Transport of particulate inorganic carbon (PIC) was not taken into account as it is not involved in climate change. In the following sections, the major findings of this thesis and their implications are summarized, as are the limitations and corresponding recommendations for future research.

9.2 Summary and implications of the major findings

9.2.1 Atmospheric CO_2 drawdown and inorganic carbon transport

With weekly sampling results at three mainstem stations, this study investigated the spatial and seasonal variability of chemical weathering and the associated atmospheric carbon consumption. Owing to rock weathering occurring widely in the basin, about 0.628 Mt of atmospheric CO_2 is consumed per year, of which 74% is caused by carbonate weathering and 26% by silicate weathering. With a drainage area

of ~752,000 km^2, the mean atmospheric CO_2 uptake rate was estimated at 0.7×10^5 $mol/km^2/yr$, which is significantly low compared with most other river basins. Overall, the annual CO_2 uptake in the Yellow River plays a significant role in global carbon cycling and is comparable to other large rivers, such as the Amazon (Richey et al., 2002), Mekong (Alin et al., 2011), and Yangtze river basins (Zhai et al., 2007). Weathering-induced CO_2 uptake in the Yellow River basin represents 0.22-0.32% of the global total uptake rate through rock weathering.

Seaward DIC transport flux from the Yellow River has decreased significantly over the past few decades. One major reason for the sharp reduction in the seaward flux is flow reduction due to large-scale water diversion for irrigation within the basin. In addition, precipitation changes and implementation of continuous soil conservation programmes have also resulted in the decreased water, thus reducing the DIC flux. Human activities have probably played a far more important role than climate change in reducing the seaward DIC delivery. This is particularly true in the recent decade since 2000 with the completion of Xiaolangdi Reservoir on the lower mainstem channel. Flow regulation has significantly altered the seasonal patterns of DIC delivery and other major solutes, and has changed the internal dynamics of riverine carbon. The obtained conclusions could contribute to a better understanding of how human activities affect riverine inorganic carbon delivery.

9.2.2 pCO_2 and CO_2 outgassing

The pCO_2 in the Yellow River network showed strong spatial and temporal variations during the survey period, which is the result of differences in a myriad of factors, including terrestrial ecosystem, soil properties, hydrology regime, and human activity. The distinct spatial and temporal changing patterns indicate the importance of investigating the differences in various driving forces at high spatial and temporal resolution. Impacts of extreme events of precipitation and temperature need to be identified in the future.

Downstream changes along the mainstem channel suggest the significance of the Loess Plateau in affecting the pCO_2 level. The waters from the Loess Plateau have higher pCO_2 values than the upper and the lower Yellow River waters. The Loess Plateau is characterized by severe physical erosion. Physical erosion could accelerate chemical weathering by increasing the exposure surface of fresh minerals to the atmosphere. In addition, the dry climate of the plateau allows the soil horizons to interact with the atmosphere. Consequently, chemical weathering of loess deposits, which are abundant in carbonates, is considerably strong, generating the release of high quantities of HCO_3^- into the stream and river waters, and therefore creating high pCO_2. In the lower Yellow River, owing to artificial regulation of water and suspended solids through reservoirs, the river-borne carbon dynamics have been significantly altered. Starting from late June in every year, when man-made floods are released from the reservoir sluice gates, the deep water with supersaturated CO_2 is first discharged downstream, resulting in high riverine pCO_2 values at Lijin station in

the flooding season. This high pCO_2 in the flooding season differs from the upstream stations where high pCO_2 usually occurs in the dry season. Other human activities, such as irrigation, have also contributed to pCO_2 changes at both inter-annual and seasonal scales. For example, the return waters washed from irrigated farmlands were characterized by high pH, resulting in increased riverine pH and thus reduced riverine pCO_2.

Like most other rivers in the world, the Yellow River waters are a net source for atmospheric CO_2 despite the strong spatial and seasonal variations similar to the pCO_2. Every year, $0.98\text{-}3.49\times10^{11}$ mol of CO_2 is emitted into the atmosphere. The estimated outgassing fluxes are considerable for global total carbon efflux from rivers. If existing uncertainties in estimating the gas transfer velocity could be better constrained, the total CO_2 outgassing fluxes from the Yellow River channel network would be higher. Accordingly, the Yellow River would play a more important role in global carbon emissions from inland waters.

Just as in the widely acknowledged tropical rivers such as the Amazon and Mekong (Richey et al., 2002; Alin et al., 2011), these results suggest that some temperate rivers are also important carbon sources for the atmosphere, although with different magnitudes of outgassing. Future studies of global riverine CO_2 evasion must put more emphasis on temperate river basins. Indeed, their contribution to global total riverine CO_2 evasion could be significantly elevated with climate warming. For instance, for the rivers originating from the Tibetan Plateau, growing temperature will

thaw permafrost, releasing the initially trapped carbon from high-latitude sinks into rivers and thus further exacerbating riverine carbon emission. Given the drainage development of temperate rivers and the permafrost distribution in the world, CO_2 outgassing fluxes of temperate river waters would be substantially increased. In a warmer climate, CO_2 evasion from temperate rivers is thus likely to become part of more actively carbon cycling pathways.

9.2.3 Role of soil erosion in carbon cycle

Through budgetary calculations of the carbon amount allocated to various sedimentation components, erosion-induced organic carbon cycle in the Yellow River basin was analyzed. This study found that erosion-induced organic carbon transport represented a carbon source for the atmosphere. On average, about 26.3% of the eroded organic carbon is decomposed during its delivery processes, which validates previous assumptions that 20-40% of the mobilized organic carbon is mineralized during its transport towards the catchment outlet or the ocean. As the obtained decomposition proportion was based on several simplifications, it is acknowledged that this study is only a tentative analysis.

However, with respect to the whole soil erosion process, this study could not yet answer the question if soil erosion represents a carbon sink or a carbon source for the atmosphere (Lal, 2003; Van Oost et al., 2008). Other important biological processes that will increase the soil carbon pool were not investigated in this work. Apart from carbon burial with sediment that reduces decomposition of erosion-induced soil

organic carbon and could lead to long-term carbon storage, sediment deposition is also likely to stabilize soil nutrients, thereby increasing primary productivity and carbon uptake. Furthermore, subsoils at eroding sites are generally enriched with less reactive carbon substrates and contain nutrients. Exposure of the subsoils by erosion would enhance plant growth and thus increase the soil organic carbon pool. For example, the proportion of eroded carbon replaced at the eroding sites as a result of plant regrowth has been found to range from 0.11 to 0.55 (Van Oost et al., 2007). It should be noted that this replacement proportion rate was mostly based on studies in Europe and North America where soils are enriched with organic matter and erosion is slight. It needs further research in China as the exposed fresh soils are very poor and could not sustain vegetation growth, causing soil degradation instead. As a result, the replacement proportion would be low. Overall, the question about the role of soil erosion as a whole in changing atmospheric carbon concentration can be resolved only if the two carbon stabilizations are incorporated.

As an effective tool to intercept flow and trap sediment, large-scale dam construction in the Yellow River basin started from the late 1950s. Although the POC content of the Yellow River sediment is generally low, the buried POC amount with sediment trapping is considerable due to the large amount of reservoir sedimentation. Approximately, 0.27 Gt of POC has been buried behind dams during the period 1950-2010, accounting for one quarter of the total organic carbon amount mobilized by soil erosion. Except for the fraction that was decomposed, burial behind dams was the single largest carbon destination once eroded. When other terrestrial carbon burial or

stabilization components were included, about half of the eroded organic carbon appears to have been sequestered or stabilized on land, with dam trapping being the largest contributor. The magnitude of sediment trapping by dams in the future will be enhanced with the commissioning of new dams. Therefore, the proportion of the eroded POC subject to burial with sediment behind dams will surely increase, though the total eroded organic carbon amount will decrease over time with gradually reduced soil erosion.

This study quantitatively estimated the amount of the buried carbon within the Yellow River basin and assessed its implications for erosion-induced organic carbon cycle. As the trapped sediment is settled under anoxic environments, the associated organic carbon could be effectively protected from further decomposition, thus constituting an important carbon sequestration process. Moreover, when more POC is buried in future, the decomposition fraction, 26.3% on average for the period 1950-2000, should decrease accordingly. If the sediment trapping estimated from individual river basins is extended to the globe, the amount of carbon sequestration will be considerable. However, this additional carbon burial has rarely been incorporated into analyses of the global carbon budget in previous assessments. The obtained results based on the Yellow River illustrated that the amount will be of considerable importance, in particular at the global scale, thus providing a new perspective on studies on global carbon cycle. A preliminary estimate has indicated that as much as 1-3 Gt of carbon has been sequestered due to global reservoir trapping within the past 50 years (Syvitski et al., 2005).

9.2.4 Organic carbon transport

As for the DOC transport, this study showed that significant seasonal changes existed during the transport processes, with higher DOC concentration in the dry season and lower DOC concentration in the wet season. Relatively low DOC concentration in the Yellow River waters was probably caused by the dilution effect of flood waters in the wet season. However, although the DOC concentration in the wet season was lower than that in the dry season, the total DOC flux in the former was significantly higher than in the latter due to higher water discharge. Among the three studied stations, the DOC transport dynamics also showed different seasonality. These seasonal changes reflected the differences in controlling factors. Whereas the DOC export at the upstream Toudaoguai and Tongguan stations was mainly controlled by hydrological events such as melting of ice and snow in spring, it was more affected by flow regulation at Lijin station as a result of reservoir operation in June-July. The obtained relationships between DOC flux/concentration with controlling factors could be extended to other river basins with similar environmental characteristics. This study may provide insights into riverine carbon studies for rivers with obvious seasonal variations in hydrology.

The flux of POC was tightly dependent on suspended sediment delivery. The POC content in the Yellow River was mostly lower than that in other large rivers and the global average, suggesting the lower soil organic carbon content and the effects of severe soil erosion on POC formation. Comparing the POC flux calculated from historical records with that derived from recent sampling shows that it has decreased

by about 90% in the past decades. Similar to the changes of DOC flux, the biggest reason for the reduction is sediment trapping by reservoirs that have been widely constructed in the basin. High proportion of the POC trapped by reservoirs indicates the strong impacts of human activities on basin-wide carbon cycle. Currently, dam construction in the world, particularly in developing countries, is being carried out at an unprecedented pace. Reservoir-induced POC burial would result in further seaward POC flux reductions and thus affect global carbon budget assessments.

Taking DOC and POC together, the DOC/POC ratio in the Yellow River is completely different from other rivers, such as the Amazon, Mississippi, Indus, and Mekong rivers. The extremely low DOC/POC ratio in the Yellow River is the lowest among major world rivers. This pattern is consistent with intense soil erosion in the catchment. Further, although riverine organic carbon fluxes are largely equally distributed between DOC and POC for the global total, great variations in the DOC/POC ratio for individual rivers indicate significant differences in controlling factors that determine DOC and POC export.

9.2.5 Riverine carbon cycling within the Yellow River basin

Through systematic study of inorganic and organic carbon dynamics within the Yellow River basin, basin-wide carbon cycling involving both lateral delivery into the ocean and vertical exchange with the atmosphere and geosphere was preliminarily investigated (Figure 9.1). Compared with the carbon fluxes into the river network, the seaward carbon export, including both inorganic and organic, showed a considerable

reduction, accounting for only 41% for the inorganic fraction and even less for the organic fraction (Figure 9.1a). One major reason is rapid decreases in water discharge and sediment load along the channel course towards the ocean, in particular in the lower Yellow River. Due to water withdrawal from the mainstem and sediment trapping by reservoir cascades, both the water and sediment fluxes have showed stepwise decreases along the mainstem channel. As a result, the closely correlated dissolved and particulate carbon fluxes have experienced similar reductions. In comparison with natural factors, human activities are the primary reasons for such rapid reductions. Particularly, as more than 90% of the eroded sediment has been stabilized on land, mainly behind dams, the amount of the POC reaching the ocean is negligible relative to the total mobilized.

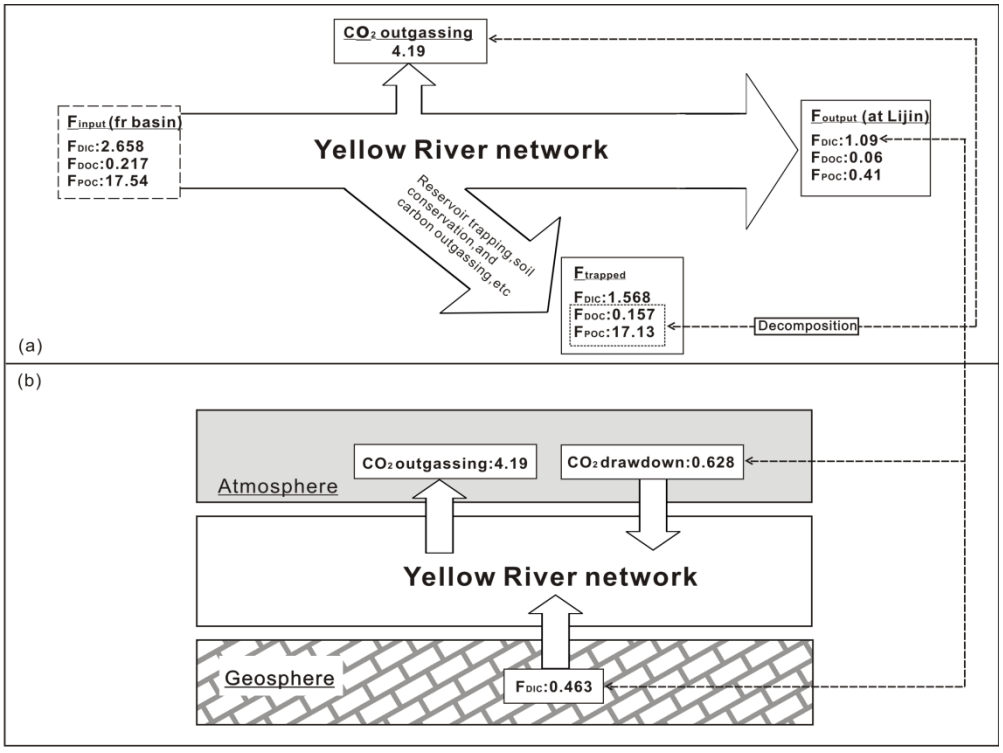

Figure 9.1 Delivery dynamics of inorganic and organic carbon (F_{DIC}, F_{DOC}, and F_{POC}, in units of Mt/yr) in the Yellow River (a) and vertical exchange of inorganic carbon with the atmosphere and the geosphere (b). F_{input} represented the fluxes into the river network from the entire drainage basin, F_{output}

represented the fluxes delivered into the Bohai Sea as measured at Lijin station, and $F_{trapped}$ was calculated as the sum of the fluxes trapped within the basin and losses en route into the atmosphere through the network. The fluxes in the dashed square were computed based on the estimates of 1950-2010 by assuming that the concentrations of DIC and POC did not change significantly, except the F_{DOC} that was based on the DOC concentration measured during 2011-2012. Magnitude of atmospheric CO_2 drawdown and rock weathering contribution to riverine DIC, as shown in (b), was determined using the seaward DIC export shown in (a).

In spite of the uncertainties inherent in the estimation method, the CO_2 outgassing fluxes from the water surface of the river channel network system appeared to be significantly higher than the CO_2 drawdown via chemical weathering within the basin (Figure 9.1b). Chemical weathering associated atmospheric CO_2 drawdown could only partly balance the outgassing flux of CO_2 injected into the atmosphere, suggesting the Yellow River network's role as a net carbon source for the atmosphere. Furthermore, the mineralized organic carbon loss rate after erosion was estimated at 4.61 Mt/yr. Difference between the estimated CO_2 outgassing (4.19 Mt/yr) and the organic carbon oxidation indicated that a considerable amount of the organic carbon was quickly decomposed after erosion before reaching the river network. Supporting this idea is that some fraction of the eroded organic carbon is readily degradable. Both estimates however have uncertainties and need to be further constrained. In addition, while annually about 8.82 Mt of the eroded POC by erosion is buried in the basin with sediment (see Figure 7.6), the DIC released into the Yellow River waters from geosphere through weathering is only 0.463 Mt per year. It is clear that the amount of the POC sequestered in the geosphere is larger than that of the DIC derived from the geosphere via weathering. This is because the total POC flux into the river (17.54 Mt/yr) is significantly higher than the DIC flux (2.658 Mt/yr) (Figure 9.1a).

As a typical drainage basin located in diverse climatic regions with strong human impacts, a holistic assessment of riverine carbon in the Yellow River highlights the importance of taking into account riverine carbon dynamics in catchment carbon cycle studies. Along with the delivery from land to ocean, carbon outgassing into the atmosphere and carbon burial with sediments have become the major destinations for the transported carbon (Figure 9.1). In contrast, the carbon fluxes reaching the Bohai Sea accounted for only a small proportion of the total generated. This striking contrast reflects the long-term impacts of anthropogenic perturbations in redistributing terrestrially-derived carbon between the land and the ocean. Such contrast will be more significant in future with increasingly stronger human impacts. In addition, the resulting reallocation of riverine carbon among different carbon reservoirs will further affect the accuracy and precision of carbon budget assessments. Overlooking riverine carbon outgassing and carbon burial en route to the ocean would cause unexpected errors and biases. This is particularly possible for studies focusing on continental and global scales in which both outgassing and burial are substantial.

9.3 Limitations of the current study

Being an exploratory study, this work made a preliminary study of riverine carbon delivery in the Yellow River basin. There are several limitations in this thesis and additional efforts are needed in future to obtain a more comprehensive understanding of riverine carbon delivery and its biogeochemical impacts on the drainage basin and the sea into which the river discharges.

9.3.1 Field sampling only on the mainstem channel

Due to logistic constraints and difficulty of field accessibility, high-frequency sampling was only conducted at three hydrological stations on the mainstem channel. In contrast, sampling based on tributary channels was not carried out. While the sampling results could largely reveal the carbon delivery dynamics along the mainstem, detailed information on tributary export was lacking, which makes spatial analysis of riverine carbon transport dynamics incomplete. Some large tributaries, such as the Wudinghe and Weihe rivers, flow through regions with high sediment yields or dense population. To what extent the riverine carbon delivery processes have been affected remain largely unknown. Furthermore, the mainstem channel in the headwater region was not effectively sampled. Located under a completely different climate, riverine carbon delivery in the headwater region would significantly differ from that in the middle and lower Yellow River.

In addition, the field sampling lasted for only one hydrological year (i.e., July 2011-July 2012). The relatively short sampling duration may have not revealed the actual long-term sediment and carbon transport processes, because these processes are heavily dependent on precipitation regime which is highly variable. If longer duration sampling covering temporal variations was conducted, the observation results could be more convincing in analyzing the actual changes under different hydrological regimes.

9.3.2 Gas transfer velocity of CO_2 across the water-air interface

The estimated CO_2 outgassing fluxes should be regarded as preliminary as no direct outgassing measurement from the water surface was conducted due to the difficulty in instrument installation and logistical accessibility. But rather, the gas transfer velocity was estimated on the basis of previously established empirical functions involving wind speed and water current velocity. As has often been mentioned, gas transfer velocity is also controlled by other factors except the two variables considered here, and is thus highly variable. Therefore, accurate quantification of gas transfer velocity over space and time is critical for assessing CO_2 outgassing. The estimated gas transfer velocities using empirical relationships are comparable to that of other world large rivers with similar geographical characteristics.

9.3.3 Identification of sources and age of organic carbon

Molar C/N ratio was calculated in this study to determine the sources of riverine organic carbon. In freshwater environments, the C/N ratio is commonly used to determine the relative proportions of allochthonous and autochthonous organic carbon. Terrestrially derived organic matter usually has higher C/N ratios of >8, while the C/N ratio of aquatic end member is mostly less than 8. As such, sources of riverine organic carbon could largely be determined by comparing the calculated ratios against the C/N end members. However, due to the complexity and diversity of organic carbon sources, particularly in large river basins, using C/N ratios alone could not precisely identify its sources. In addition, quantifying the age of riverine carbon is of critical importance, because it can help eludicate the turnover time of carbon cycle

and the interactions between different forms of carbon (i.e., DIC, PIC, DOC, and POC).

This study did not explore the age of the transported carbon due to the difficulty in field sampling. With respect to the Yellow River waters, the extremely high suspended sediment concentration has inhibited the growth of autochthonous organisms, such as phytoplankton, as a result of reduced availability of light. Contribution of autochthonous species to riverine organic matter was believed to be small, and most of the riverine organic carbon was of terrestrial orgin.

9.4 Recommendations for future work

Based on the experimental results obtained, the discussion presented and the conclusions drawn from this research work, there are several important and interesting directions for future work on riverine carbon transport. Four major research subjects that should be targeted to address existing limitations were shortly summarized below.

9.4.1 Longer duration sampling at larger spatial scale

In this study, spatial and temporal variations of chemical weathering and atmospheric CO_2 consumption were analyzed based on the collected samples at three mainstem stations during 2011-2012. To further broaden the generalisability of the obtained spatial and temporal patterns, one recommendation for future research is to conduct widespread spatial sampling throughout the river basin. For example, future sampling

at major tributary channels and in the highest sediment yielding areas could better explore the spatial variability of chemical weathering and its responses to physical denudation. With such spatial differences, changes in the associated CO_2 uptake could be further analyzed.

Another possible avenue for future work is to extend the sampling duration. The delivery dynamics of different forms of carbon would be considerably different under different hydrological regimes. For example, concentrations of dissolved solutes, such as DIC and DOC, would increase sharply in the beginning period of floods as a result of flushing effect in soil horizons, and the concentrations would then decrease slightly in the following high flow periods due to dilution effect. If a sampling campaign is conducted solely in low-flow hydrological year, the obtained DIC and DOC concentrations would be significantly different from that measured in high-flow years. Accordingly, the annual DIC and DOC fluxes would be quite different. As such, the obtained results based on longer sampling duration will be more representative. This is particularly true for rivers with significant inter-annual variations in precipitation.

9.4.2 Field measurement of gas transfer velocity

Understanding the relationship between gas transfer velocity and its influencing factors, such as boundary layer stability, surface films, wind speed, and slope, is one of the most important and challenging research focuses in evaluating the role of river systems play in carbon cycle. This study focused primarily on the effects of wind speed and flow velocity, while the potential impacts of other factors were not

explored. Based on this work, it is highly recommended that future studies conduct field measurement of gas transfer velocity under different conditions of stream turbulence, channel slope, and wind speed. Moreover, comparing the obtained gas transfer velocities through field direct measurements with the empirically estimated values is able to shed light on better parameterization. Great geomorphological and climatic differences in the Yellow River basin provide an example for studying the possibility of applying the established empirical relationships to other unmeasured rivers.

Due to extended residence time, reservoir waters are different from river waters in terms of physical and biogeochemical properties. In a reservoir, growth of aquatic plants as a result of increased light availability and reduced turbulence will increase its organic carbon pool. Decomposition of this organic carbon would increase the pCO_2 level and thus the outgassing flux. In addition, reduced flow turbulence is likely to decrease the gas transfer velocity, which further restrains CO_2 evasion. Consequently, the magnitude of CO_2 outgassing from reservoir waters would be significantly different from rivers. Large-scale reservoir construction in the Yellow River basin has formed a considerable water surface (~2381 km^2 by 2009). It is expected that the CO_2 outgassing flux from such a huge surface area will also be considerable. Future research should attempt to measure such CO_2 outgassing, upon which a more comprehensive CO_2 emission from the Yellow River could be achieved. With more reservoirs under construction or being planned, assessing CO_2 outgassing from reservoir waters is urgently needed.

9.4.3 Application of tracer techniques

Abundances of carbon isotopes, including stable carbon isotope ($\delta^{13}C$) and radiocarbon isotope ($\Delta^{14}C$), are powerful tools for identifying the sources, ages, and residence times of riverine carbon. Combined use of ^{13}C and ^{14}C can often overcome problems associated with source overlap. In particular, compared with using either isotope separately, use of paired ^{13}C and ^{14}C can provide a more robust interpretation (Raymond and Bauer, 2001b). Another direct extension of the current work would be using carbon isotopic techniques to identify the riverine carbon sources and to determine its residence times. In addition, although ^{13}C and ^{14}C measurements have been extensively used in riverine organic carbon studies, until recently there has been little application to the inorganic carbon fraction. For Asian rivers, there are only sporadic studies of ^{13}C (e.g., Zhang et al., 1995a; Wu et al., 2007; Gao et al, 2007; Zhang et al., 2009), or ^{14}C (e.g., Gao et al., 2007; Wei et al., 2010) of riverine carbon. Systematic analyses of carbon isotope in Asian rivers, including both ^{13}C and ^{14}C in particular, have never been conducted.

Furthermore, sediment tracers, such as Caesium-137, can be used to determine the sediment sources within the basin. With the determined sources, it is expected that the sediment and therefore the OC budget could be better improved. Overall, future research is required to employ tracer techniques to analyze the spatial and temporal variability of riverine carbon delivery and outgassing within the river system.

9.4.4 Responses of carbon transport to human activities

Human activities can profoundly affect (in)organic carbon transport within a drainage basin by changing the basin's physical and biogeochemical characteristics. For example, extensive land use/cover change converting croplands to forests is likely to increase biomass and the soil organic carbon pool (Pacala et al., 2001; Post and Kwon, 2008). Compared with agricultural fields, organic carbon dynamics in forest lands respond differently to drainage features, such as rainfall and soil moisture. Large-scale soil conservation in the Yellow River basin in the past decades has substantially changed its land cover. Future research needs to evaluate the relative contributions of direct and indirect effects of land use/cover change on (in)organic carbon delivery.

Dam construction is another important human impact in the Yellow River basin that affects (in)organic carbon dynamics. Extended water residence time allows for aerobic and anaerobic decomposition of organic matter in aquatic environments. The magnitude and rate of decomposition are spatially and temporally variable, depending on drainage characteristics of water, sediment, and carbon export as well as reservoir operation schemes. Reservoir trapping of sediment and water has been a major reason for the decreased water and sediment fluxes. Mechanistic understanding of its impacts on carbon cycle remains largely elusive. To unravel these problems, further studies should attempt to investigate the complex carbon transformation processes, from organic to inorganic due to oxidation for example. A possible strategy to explore is to install instruments in reservoir waters and identify the transformation processes between different forms of carbon. Conducting laboratory simulation experiments would also be helpful for modeling carbon dynamics.

Bibliography

Abril, G., Etcheber, H., Borges, A.V. and Frankignoulle, M., 2000. Excess atmospheric carbon dioxide transported by rivers into the Scheldt estuary. Comptes Rendus de l'Académie des Sciences - Series IIA - Earth and Planetary Science, 330(11): 761-768.

Aitkenhead, J., Hope, D. and Billett, M., 1999. The relationship between dissolved organic carbon in stream water and soil organic carbon pools at different spatial scales. Hydrological Processes, 13(8): 1289-1302.

Alekin, O.A., Semenov, A.D. and Skopintsev, B.A., 1973. Handbook of Chemical Analysis of Land Waters. Gidrometeoizdat, St. Petersburg, Russia.

Alin, S.R. et al., 2011. Physical controls on carbon dioxide transfer velocity and flux in low-gradient river systems and implications for regional carbon budgets. Journal of Geophysical Research, 116(G1): G01009.

Allègre, C.J. and Lewin, E., 1989. Chemical structure and history of the Earth: evidence from global non-linear inversion of isotopic data in a three-box model. Earth and Planetary Science Letters, 96(1): 61-88.

Allison, M.A., Bianchi, T.S., McKee, B.A. and Sampere, T.P., 2007. Carbon burial on river-dominated continental shelves: Impact of historical changes in sediment loading adjacent to the Mississippi River. Geophysical Research Letters, 34(1): L01606.

American Public Health Association (APHA), 1985. Standard Methods for the Examination of Water and Wastewater, 16th edition. American Public Health Association, Washington, DC.

Amiotte-Suchet, P. and Probst, J.L., 1993. Modelling of atmospheric CO_2 consumption by chemical weathering of rocks: Application to the Garonne, Congo and Amazon basins. Chemical Geology(3-4): 205-210.

Amiotte-Suchet, P., Probst, J.L. and Ludwig, W., 2003. Worldwide distribution of continental rock lithology: Implications for the atmospheric/soil CO2 uptake by continental weathering and alkalinity river transport to the oceans. Global Biogeochemical Cycles, 17(2).

An, M., 1992. Analysis of scouring and silting of Youhe Reservoir in Weinan. Journal of Water Resources and Water Engineering 4: 83-88(in Chinese).

Annor, F. et al., 2009. Delineation of small reservoirs using radar imagery in a semi-arid environment: A case study in the upper east region of Ghana. Physics and Chemistry of the Earth, Parts A/B/C, 34(4): 309-315.

Aucour, A.M., Sheppard, S.M.F., Guyomar, O. and Wattelet, J., 1999. Use of ^{13}C to trace origin and cycling of inorganic carbon in the Rhone river system. Chemical Geology, 159(1-4): 87-105.

Aufdenkampe, A.K. et al., 2011. Riverine coupling of biogeochemical cycles between land, oceans, and atmosphere. Frontiers in Ecology and the Environment, 9(1): 53-60.

Balakrishna, K. and Probst, J.L., 2005. Organic carbon transport and C/N ratio variations in a large tropical river: Godavari as a case study, India. Biogeochemistry, 73(3): 457-473.

Baron, J., 1990. Chemical weathering in the Loch Vale watershed, Rocky Mountain National Park, Colorado. Water Resources Research, 26: 2971.

Basak, C. and Martin, E.E., 2013. Antarctic weathering and carbonate compensation at the Eocene-Oligocene transition. Nature Geoscience, 6(2): 121-124.

Bass, A.M., Bird, M.I., Liddell, M.J. and Nelson, P.N., 2011. Fluvial dynamics of dissolved and particulate organic carbon during periodic discharge events in a steep tropical rainforest catchment. Limnology and Oceanography, 56(6): 2282-2292.

Bass, A.M., Munksgaard, N., LeBlanc, M., Tweed, S. and Bird, M., 2013. Contrasting carbon export dynamics of human impacted and pristine tropical catchments in response to a short-lived discharge event. Hydrological Processes.

Battin, T.J. et al., 2009. The boundless carbon cycle. Nature Geosci, 2(9): 598-600.

Benedetti, M.F. et al., 2003. Chemical weathering of basaltic lava flows undergoing extreme climatic conditions: the water geochemistry record. Chemical Geology, 201(1): 1-17.

Benstead, J.P. and Leigh, D.S., 2012. An expanded role for river networks. Nature Geosci, 5(10): 678-679.

Bergamaschi, B.A. et al., 1997. The effect of grain size and surface area on organic matter, lignin and carbohydrate concentration, and molecular compositions in Peru Margin sediments. Geochimica Et Cosmochimica Acta, 61(6): 1247-1260.

Berhe, A.A., Harte, J., Harden, J.W. and Torn, M.S., 2007. The significance of the erosion-induced terrestrial carbon sink. Bioscience, 57(4): 337-346.

Berner, E.K. and Berner, R.A., 2012. Global environment: water, air, and geochemical cycles. Princeton University Press.

Berner, R.A., 1995. Chemical weathering and its effect on atmospheric CO2 and climate. Chemical Weathering Rates of Silicate Minerals, 31: 565-583.

Berner, R.A., Lasaga, A.C. and Garrels, B.M., 1983. The carbonate-silicate geochemical cycle and its effect on atmospheric carbon dioxide over the past 100 million years American Journal of Science(283): 43.

Beusen, A., Dekkers, A., Bouwman, A., Ludwig, W. and Harrison, J., 2005. Estimation of global river transport of sediments and associated particulate C, N, and P. Global Biogeochemical Cycles, 19(4).

Bianchi, T.S., 2011. The role of terrestrially derived organic carbon in the coastal ocean: A changing paradigm and the priming effect. Proceedings of the National Academy of Sciences, 108(49): 19473-19481.

Bianchi, T.S., Wysocki, L.A., Stewart, M., Filley, T.R. and Mckee, B.A., 2007. Temporal variability in terrestrially-derived sources of particulate organic carbon in the lower Mississippi River and its upper tributaries. Geochimica et Cosmochimica Acta, 71(18): 4425-4437.

Bird, M.I., Lloyd, J. and Farquhar, G.D., 1994. Terrestrial carbon storage at the LGM. Nature, 371(6498): 566-566.

Bird, M.I. et al., 2008. A preliminary estimate of organic carbon transport by the Ayeyarwady (Irrawaddy) and Thanlwin (Salween) Rivers of Myanmar. Quaternary International, 186(1): 113-122.

Boateng, I., Bray, M. and Hooke, J., 2012. Estimating the fluvial sediment input to the coastal sediment budget: A case study of Ghana. Geomorphology, 138(1): 100-110.

Borges, A.V. et al., 2004. Gas transfer velocities of CO2 in three European estuaries (Randers Fjord, Scheldt, and Thames). Limnology and Oceanography, 49(5): 1630-1641.

Boyer, E.W., Hornberger, G.M., Bencala, K.E. and McKnight, D.M., 1997. Response characteristics of DOC flushing in an alpine catchment. Hydrological Processes, 11(12): 1635-1647.

Brady, P.V. and Carroll, S.A., 1994. Direct effects of CO_2 and temperature on silicate weathering: Possible implications for climate control. Geochimica Et Cosmochimica Acta, 58(7): 1853-1856.

Brune, G.M., 1953. Trap efficiency of reservoirs. Transactions of the American Geophysical Union, 34: 407-418.

Butcher, D., Labadz, J., Potter, A. and White, P., 1993. Reservoir sedimentation rates in the southern Pennine region, UK. In: J. McManus and R.W. Duck (Editors), Geomorphology and sedimentology of Lakes and Reservoirs. John Wiley & Sons, New York, pp. 73-92.

Butman, D. and Raymond, P.A., 2011. Significant efflux of carbon dioxide from streams and rivers in the United States. Nature Geoscience, 4(12): 839-842.

Cai, D., 1994. Geochemical studies on organic carbon isotope of the Huanghe River (Yellow River) estuary. Science in China Series B: Chemistry, 37: 1001-1015.

Cai, W.-J. et al., 2004. The biogeochemistry of inorganic carbon and nutrients in the Pearl River estuary and the adjacent Northern South China Sea. Continental Shelf Research, 24(12): 1301-1319.

Cai, W.-J. et al., 2008. A comparative overview of weathering intensity and HCO_3^- flux in the world's major rivers with emphasis on the Changjiang, Huanghe, Zhujiang (Pearl) and Mississippi Rivers. Continental Shelf Research, 28(12): 1538-1549.

Canadell, J.G. et al., 2007. Contributions to accelerating atmospheric CO_2 growth from economic activity, carbon intensity, and efficiency of natural sinks. Proceedings of the National Academy of Sciences, 104(47): 18866-18870.

Cauwet, G. and Mackenzie, F.T., 1993. Carbon inputs and distribution in estuaries of turbid rivers: the Yang Tze and Yellow rivers (China). Marine Chemistry, 43(1–4): 235-246.

Chang, C.H., 2011. A perspective on the construction of silt check dams on the Loess Plateau. Soil and Water Conservation Science and Technology in Shanxi, 1: 31-33 (in Chinese).

Chao, B.F., Wu, Y.H. and Li, Y.S., 2008. Impact of artificial reservoir water impoundment on global sea level. Science, 320(5873): 212-214.

Chen, C.-T.A., Huang, T.-H., Fu, Y.-H., Bai, Y. and He, X., 2012. Strong sources of CO_2 in upper estuaries become sinks of CO_2 in large river plumes. Current Opinion in Environmental Sustainability, 4(2): 179-185.

Chen, J., He, D. and Cui, S., 2003. The response of river water quality and quantity to the development of irrigated agriculture in the last 4 decades in the Yellow River Basin, China. Water Resources Research, 39(3): 1047.

Chen, J. et al., 2005. Spatial and temporal analysis of water chemistry records (1958-2000) in the Huanghe (Yellow River) basin. Global Biogeochemical Cycles, 19(3): GB3016.

Chen, J.C., Tang, C.T., Sakura, Y.S., Kondoh, A.K. and Shen, Y.S., 2002a. Groundwater flow and geochemistry in the lower reaches of the Yellow River: a case study in Shandang Province, China. Hydrogeology Journal, 10(5): 587-599.

Chen, J.S., Wang, F.Y., Xia, X.H. and Zhang, L.T., 2002b. Major element chemistry of the Changjiang (Yangtze River). Chemical Geology, 187(3-4): 231-255.

Chen, L., Wei, W., Fu, B. and Lü, Y., 2007a. Soil and water conservation on the Loess Plateau in China: review and perspective. Progress in Physical Geography, 31(4): 389-403.

Chen, L.D. et al., 2007b. Effect of land use conversion on soil organic carbon sequestration in the loess hilly area, loess plateau of China. Ecological Research, 22(4): 641-648.

Chen, X. et al., 2007c. An 8.1 Ma calcite record of Asian summer monsoon evolution on the Chinese central Loess Plateau. Science in China Series D: Earth Sciences, 50(3): 392-403.

Chen, Y., 1983. A preliminary analysis of the processes of sediment yield in small catchment on the Loess Plateau. Geographical Research, 2(1): 35-47 (in Chinese).

Chen, Y. and Brantley, S.L., 1997. Temperature-and pH-dependence of albite dissolution rate at acid pH. Chemical Geology, 135(3): 275-290.

Chetelat, B. et al., 2008. Geochemistry of the dissolved load of the Changjiang Basin rivers: anthropogenic impacts and chemical weathering. Geochimica Et Cosmochimica Acta, 72(17): 4254-4277.

Chu, Z.X. et al., 2009. A quantitative assessment of human impacts on decrease in sediment flux from major Chinese rivers entering the western Pacific Ocean. Geophysical Research Letters, 36: DOI: 10.1029/2009GL039513.

Clow, D.W. and Drever, J.I., 1996. Weathering rates as a function of flow through an alpine soil. Chemical Geology, 132(1-4): 131-141.

Cole, J.J. and Caraco, N.F., 2001. Carbon in catchments: connecting terrestrial carbon losses with aquatic metabolism. Marine and Freshwater Research, 52(1): 101-110.

Cole, J.J. et al., 2007. Plumbing the global carbon cycle: Integrating inland waters into the terrestrial carbon budget. Ecosystems, 10(1): 171-184.

Cui, B., Tang, N., Zhao, X. and Bai, J., 2009. A management-oriented valuation method to determine ecological water requirement for wetlands in the Yellow River Delta of China. Journal for Nature Conservation, 17(3): 129-141.

Dalai, T.K., Krishnaswami, S. and Sarin, M.M., 2002. Major ion chemistry in the headwaters of the Yamuna river system: Chemical weathering, its temperature dependence and CO2 consumption in the Himalaya. Geochimica Et Cosmochimica Acta, 66(19): 3397-3416.

Davidson, E.A. and Ackerman, I.L., 1993. Changes in Soil Carbon Inventories Following Cultivation of Previously Untilled Soils. Biogeochemistry, 20(3): 161-193.

Davidson, E.A., Figueiredo, R.O., Markewitz, D. and Aufdenkampe, A.K., 2010. Dissolved CO_2 in small catchment streams of eastern Amazonia: A minor pathway of terrestrial carbon loss. J. Geophys. Res., 115(G4): G04005.

de Vente, J., Poesen, J. and Verstraeten, G., 2005. The application of semi-quantitative methods and reservoir sedimentation rates for the prediction of basin sediment yield in Spain. Journal of Hydrology, 305(1-4): 63-86.

Dean, W.E. and Gorham, E., 1998. Magnitude and significance of carbon burial in lakes, reservoirs, and peatlands. Geology, 26(6): 535-538.

DeConto, R.M. and Pollard, D., 2003. Rapid Cenozoic glaciation of Antarctica induced by declining atmospheric CO_2. Nature, 421(6920): 245-249.

Degens, E.T., Kempe, S. and Richey J.E., 1991. Chapter 15, summary: biogeochemistry of major world rivers. In: E.T. Degens, S. Kempe and Richey J.E. (Editors), Biogeochemistry of major world rivers. Scope 42. Wiley, New York, pp. 323-344.

Di-Giovanni, C., Disnar, J.R. and Macaire, J.J., 2002. Estimation of the annual yield of organic carbon released from carbonates and shales by chemical weathering. Global and Planetary Change, 32(2): 195-210.

Dolan, D.M., Yui, A.K. and Geist, R.D., 1981. Evaluation of river load estimation methods for total phosphorus. Journal of Great Lakes Research, 7(3): 207-214.

Duane Nellis, M., Harrington Jr, J.A. and Wu, J., 1998. Remote sensing of temporal and spatial variations in pool size, suspended sediment, turbidity, and Secchi depth in Tuttle Creek Reservoir, Kansas: 1993. Geomorphology, 21(3): 281-293.

Dürr, H., Meybeck, M., Hartmann, J., Laruelle, G.G. and Roubeix, V., 2011. Global spatial distribution of natural riverine silica inputs to the coastal zone. Biogeosciences, 8: 597-620.

Edmond, J. and Huh, Y., 1997. A critique of geochemical models of the Cenozoic/Phanerozoic evolution of atmospheric pCO_2. Rev Geophys.

Edwards, A., 1973. The variation of dissolved constituents with discharge in some Norfolk rivers. Journal of Hydrology, 18(3): 219-242.

Epron, D., Farque, L., Lucot, E. and Badot, P.M., 1999. Soil CO_2 efflux in a beech forest: dependence on soil temperature and soil water content. Annals of Forest Science, 56(3): 221-226.

Feth, J. and Gibbs, R., 1971. Mechanisms controlling world water chemistry: evaporation-crystallization process. Science, 172(3985): 870.

Feth, J.H., 1981. Chloride in natural continental water: a review. U.S. Geological Survey Water-Supply Paper 2176.

Finlay, J.C., 2003. Controls of streamwater dissolved inorganic carbon dynamics in a forested watershed. Biogeochemistry, 62(3): 231-252.

Foody, G., 1998. Sharpening fuzzy classification output to refine the representation of sub-pixel land cover distribution. International Journal of Remote Sensing, 19(13): 2593-2599.

Frankignoulle, M. et al., 1998. Carbon dioxide emission from European estuaries. Science, 282(5388): 434-436.

Freeman, C., Ostle, N. and Kang, H., 2001. An enzymic 'latch'on a global carbon store. Nature, 409(6817): 149.

Fu, B. et al., 2011. Assessing the soil erosion control service of ecosystems change in the Loess Plateau of China. Ecological Complexity, 8(4): 284-293.

Fu, G., Chen, S., Liu, C. and Shepard, D., 2004. Hydro-climatic trends of the Yellow River basin for the last 50 years. Climatic Change, 65(1-2): 149-178.

Fu, K.D., He, D.M. and Lu, X.X., 2008. Sedimentation in the Manwan reservoir in the Upper Mekong and its downstream impacts. Quaternary International, 186(1): 91-99.

Gabet, E.J. and Mudd, S.M., 2009. A theoretical model coupling chemical weathering rates with denudation rates. Geology, 37(2): 151-154.

Gabet, E.J., Wolff-Boenisch, D., Langner, H., Burbank, D.W. and Putkonen, J., 2010. Geomorphic and climatic controls on chemical weathering in the High Himalayas of Nepal. Geomorphology, 122(1-2): 205-210.

Gaillardet, J., Dupre, B., Louvat, P. and Allegre, C.J., 1999. Global silicate weathering and CO_2 consumption rates deduced from the chemistry of large rivers. Chemical Geology, 159(1-4): 3-30.

Galy, A. and France-Lanord, C., 1999. Weathering processes in the Ganges–Brahmaputra basin and the riverine alkalinity budget. Chemical Geology, 159(1): 31-60.

Galy, V. et al., 2007. Efficient organic carbon burial in the Bengal fan sustained by the Himalayan erosional system. Nature, 450(7168): 407-410.

Gan, W.B., Chen, H.M. and Hart, Y.F., 1983. Carbon transport by the Yangtze (at Nanjing) and Huanghe (at Jinan) Rivers, People's Republic of China. In: E.T. Degens, S.K. and and H. Soliman (Editors), Transport of Carbon and Minerals in Major World Rivers, Part 2. Mitt. Geol. Palaöntol. Inst. Univ. Hamburg, SCOPE/UNEP Sonderbd., pp. 459-470.

Gao, Q. et al., 2009. Chemical weathering and CO_2 consumption in the Xijiang River basin, South China. Geomorphology, 106(3): 324-332.

Gao, Q. et al., 2002. Riverine organic carbon in the Xijiang River (South China): seasonal variation in content and flux budget. Environmental Geology, 41(7): 826-832.

Gao, Q. et al., 2007. Elemental and isotopic signatures of particulate organic carbon in the Zengjiang River, southern China. Hydrological Processes, 21(10): 1318-1327.

Gao, X. and Feng, L., 2002. Estimation of the sediment in Longyangxia Reservoir. Journal of Sediment Research, 1: 78-80(in Chinese).

Garrels, R.M. and Mackenzie, F.T., 1967. Origin of the chemical compositions of some springs and lakes. Equilibrium concepts in natural water systems, 67: 222-242.

Gibbs, R.J., 1970. Mechanisms controlling world water chemistry. Science, 170(3962): 1088.

Goel, M., Jain, S.K. and Agarwal, P., 2002. Assessment of sediment deposition rate in Bargi Reservoir using digital image processing. Hydrological sciences journal, 47(S1): S81-S92.

Goldsmith, S.T. et al., 2010. Stream geochemistry, chemical weathering and CO_2 consumption potential of andesitic terrains, Dominica, Lesser Antilles. Geochimica Et Cosmochimica Acta, 74(1): 85-103.

Gong, S.Y., 1987. The Role of Reservoirs and Silt-Trap Dams in Reducing Sediment Delivery into the Yellow-River. Geografiska Annaler Series a-Physical Geography, 69(1): 173-179.

Grafton, R.Q. et al., 2013. Global insights into water resources, climate change and governance. Nature Climate Change, 3: 315-321.

Guo, J.H. et al., 2010. Significant acidification in major Chinese croplands. Science, 327(5968): 1008-1010.

Gupta, L.P., Subramanian, V. and Ittekkot, V., 1997. Biogeochemistry of particulate organic matter transported by the Godavari River, India. Biogeochemistry, 38(2): 103-128.

Gupta, R. and Bodechtel, J., 1982. Geotechnical applications of landsat image analysis of Bhakra Dam Reservoir, India. Remote Sensing of Environment, 12(1): 3-13.

Han, Q.W. and Yang, X.Q., 2003. A review of the research work of reservoir sedimentation in China. Journal of China Institue of Water Resources and Hydropower Research, 1: 169-178 (in Chinese).

Hartmann, J., Jansen, N., Dürr, H.H., Kempe, S. and Köhler, P., 2009. Global CO_2-consumption by chemical weathering: What is the contribution of highly active weathering regions? Global and Planetary Change, 69(4): 185-194.

Hartmann, J. et al., 2013. Enhanced chemical weathering as a geoengineering strategy to reduce atmospheric carbon dioxide, a nutrient source and to mitigate ocean acidification. Reviews of Geophysics: doi:10.1002/rog.20004.

Hassan, M.A., Church, M., Xu, J. and Yan, Y., 2008. Spatial and temporal variation of sediment yield in the landscape: Example of Huanghe (Yellow River). Geophysical Research Letters, 35(6): L06401.

Hassan, M.A., Church, M., Yan, Y. and Slaymaker, O., 2010. Spatial and temporal variation of in-reach suspended sediment dynamics along the mainstem of Changjiang (Yangtze River), China. Water Resour. Res., 46(11): W11551.

Hassan, M.A., Church, M., Yan, Y., Slaymaker, O. and Xu, J., 2011. Suspended sediment balance for the mainstem of Changjiang (Yangtze River) in the period 1964–1985. Hydrological Processes, 25(15): 2339-2353.

Hedges, J., Keil, R. and Benner, R., 1997. What happens to terrestrial organic matter in the ocean? Organic Geochemistry, 27(5-6): 195-212.

Hedges, J.I. and Keil, R.G., 1995. Sedimentary organic matter preservation: an assessment and speculative synthesis. Marine Chemistry, 49(2): 81-115.

Hoffmann, T. et al., 2010. Human impact on fluvial regimes and sediment flux during the Holocene: Review and future research agenda. Global and Planetary Change, 72(3): 87-98.

Hood, E., Gooseff, M.N. and Johnson, S.L., 2006. Changes in the character of stream water dissolved organic carbon during flushing in three small watersheds, Oregon. Journal of Geophysical Research, 111(G1): G01007.

Hope, D., Billett, M. and Cresser, M., 1994. A review of the export of carbon in river water: fluxes and processes. Environmental Pollution, 84(3): 301-324.

Hope, D., Billett, M.F., Milne, R. and Brown, T.A., 1997. Exports of organic carbon in British rivers. Hydrological Processes, 11(3): 325-344.

Hope, D., Palmer, S.M., Billett, M.F. and Dawson, J.J.C., 2004. Variations in dissolved CO_2 and CH_4 in a first-order stream and catchment: an investigation of soil－stream linkages. Hydrological Processes, 18(17): 3255-3275.

Horton, R.E., 1945. Erosional development of streams and their drainage basins: hydrophysical approach to quantitative morphology. Bulletin of the Geological Society of America, 56: 275-370.

Hren, M.T., Chamberlain, C.P., Hilley, G.E., Blisniuk, P.M. and Bookhagen, B., 2007. Major ion chemistry of the Yarlung Tsangpo–Brahmaputra river: Chemical weathering, erosion, and CO_2 consumption in the southern Tibetan plateau and eastern syntaxis of the Himalaya. Geochimica Et Cosmochimica Acta, 71(12): 2907-2935.

Hu, C., Chen, X. and Chen, J., 2008. Spatial distribution and its variation process of sedimentation in Yellow River. Journal of Hydraulic Engineering, 39(5): 518-527 (in Chinese).

Hu, C. et al., 2005a. Case Study on The Yellow River Sedimentation, International Research and Training Center on Erosion and Sedimentation, Beijing, China.

Hu, J., Song, H. and Yang, Z., 2005b. Study on the Longyangxia Reservoir operation. Yellow River, 10: 65-67(in Chinese).

Hu, M., Stallard, R.F. and Edmond, J.M., 1982. Major ion chemistry of some large Chinese rivers. Nature, 298(5874): 550-553.

Huang, M. and Zhang, L., 2004. Hydrological responses to conservation practices in a catchment of the Loess Plateau, China. Hydrological Processes, 18(10): 1885-1898.

Huh, Y., Tsoi, M.-Y., Zaitsev, A. and Edmond, J.M., 1998. The fluvial geochemistry of the rivers of Eastern Siberia: I. Tributaries of the Lena River draining the sedimentary platform of the Siberian Craton. Geochimica et Cosmochimica Acta, 62(10): 1657-1676.

Humborg, C. et al., 2000. Silicon retention in river basins: far-reaching effects on biogeochemistry and aquatic food webs in coastal marine environments. AMBIO: A Journal of the Human Environment, 29(1): 45-50.

IPCC (Intergovernmental Panel on Climate Change), 2007. Climate Change 2007: The Physical Science Basis, Contribution of Working Group I to the Fourth Assessment Report of the Intergovernmental Panel on Climate Change. In: Solomon et al (Editor). Cambridge University Press, Cambridge, U. K.

Jacinthe, P.A., Filippelli, G.M., Tedesco, L.P. and Raftis, R., 2012. Carbon storage and greenhouse gases emission from a fluvial reservoir in an agricultural landscape. CATENA, 94: 53-63.

Jacobson, A.D., Blum, J.D., Chamberlain, C.P., Craw, D. and Koons, P.O., 2003. Climatic and tectonic controls on chemical weathering in the New Zealand Southern Alps. Geochimica Et Cosmochimica Acta, 67(1): 29-46.

Jarvie, H.P. et al., 1997. Major ion concentrations and the inorganic carbon chemistry of the Humber rivers. Science of the Total Environment, 194: 285-302.

Jha, P.K., Tiwari, J., Singh, U.K., Kumar, M. and Subramanian, V., 2009. Chemical weathering and associated CO_2 consumption in the Godavari river basin, India. Chemical Geology, 264(1): 364-374.

Jing, K., Chen, Y. and Li, F., 1993. Sediment and Environment of the Yellow River. Science Press, Beijing.

Jing, K., Li, J. and Li, F., 1998. Erosion yield from the middle Yellow River basin and tendency prediction. Acta Geographica Sinica, 53: 107-115 (in Chinese).

Johnson, M.S. et al., 2008. CO_2 efflux from Amazonian headwater streams represents a significant fate for deep soil respiration. Geophysical Research Letters, 35.

Jones, J.B., Jr., Stanley, E.H. and Mulholland, P.J., 2003. Long-term decline in carbon dioxide supersaturation in rivers across the contiguous United States. Geophys. Res. Lett., 30(10): 1495.

Kang, L., Zhang, S., Wei, Y. and Liu, X., 2010. Review of the effects researches of soil and water conservation on sediment reduction in the middle reaches of the Yellow River. Science of Soil and Water Conservation, 8(2): 111-116 (in Chinese).

Kao, S. and Liu, K., 1997. Fluxes of dissolved and nonfossil particulate organic carbon from an Oceania small river (Lanyang Hsi) in Taiwan. Biogeochemistry, 39(3): 255-269.

Kato, T. et al., 2004. Carbon dioxide exchange between the atmosphere and an alpine meadow ecosystem on the Qinghai-Tibetan Plateau, China. Agricultural and Forest Meteorology, 124(1–2): 121-134.

Keil, R.G., Mayer, L.M., Quay, P.D., Richey, J.E. and Hedges, J.I., 1997. Loss of organic matter from riverine particles in deltas. Geochimica Et Cosmochimica Acta, 61(7): 1507-1511.

Kempe, S., 1979. Carbon in the rock cycle. In: B. Bolin, E.T. Degens, S. Kempe and P. Ketner (Editors), The Global Carbon Cycle-Scope 13. Scientific Committee on Problems on the Environment (SCOPE) Old working, pp. 343-375.

Kempe, S., 1982. Long-term records of CO_2 pressure fluctuations in fresh water. In: E.T. Degens (Editor), Transport of Carbon and Minerals in Major World Rivers, Pt. 1. Mitt. Geol.-Palaönt. Inst. Univ. Hamburg, SCOPE/UNEP Sonderbd, pp. 91-332.

Kuhn, N.J., Hoffmann, T., Schwanghart, W. and Dotterweich, M., 2009. Agricultural soil erosion and global carbon cycle: controversy over? Earth Surface Processes and Landforms, 34(7): 1033-1038.

Kummu, M., Lu, X.X., Wang, J.J. and Varis, O., 2010. Basin-wide sediment trapping efficiency of emerging reservoirs along the Mekong. Geomorphology, 119(3-4): 181-197.

Kummu, M. and Varis, O., 2007. Sediment-related impacts due to upstream reservoir trapping, the Lower Mekong River. Geomorphology, 85(3-4): 275-293.

Kump, L.R. and Arthur, M.A., 1999. Interpreting carbon-isotope excursions: carbonates and organic matter. Chemical Geology, 161(1): 181-198.

Kump, L.R., Brantley, S.L. and Arthur, M.A., 2000. Chemical, weathering, atmospheric CO2, and climate. Annual Review of Earth and Planetary Sciences, 28: 611-667.

Lal, R., 2003. Soil erosion and the global carbon budget. Environment International, 29(4): 437-450.

Lal, R., 2004. Soil carbon sequestration impacts on global climate change and food security. Science, 304(5677): 1623-1627.

Lal, R., Griffin, M., Apt, J., Lave, L. and Morgan, M.G., 2004. Managing soil carbon. Science, 304(5669): 393.

Lal, R. and Pimentel, D., 2008. Soil erosion: a carbon sink or source? Science, 319(5866): 1040-1042.

Lehner, B. and Döll, P., 2004. Development and validation of a global database of lakes, reservoirs and wetlands. Journal of Hydrology, 296(1-4): 1-22.

Leithold, E.L., Blair, N.E. and Perkey, D.W., 2006. Geomorphologic controls on the age of particulate organic carbon from small mountainous and upland rivers. Global Biogeochemical Cycles, 20(3).

Lenton, T.M. and Britton, C., 2006. Enhanced carbonate and silicate weathering accelerates recovery from fossil fuel CO2 perturbations. Global Biogeochemical Cycles, 20(3): GB3009.

Leopold, L. and Maddock, T., 1953. The hydraulic geometry of stream channels and some physiographic implications. USGS Professional Paper 252.

Lerman, A., Wu, L. and Mackenzie, F.T., 2007. CO_2 and H_2SO_4 consumption in weathering and material transport to the ocean, and their role in the global carbon balance. Marine Chemistry, 106(1): 326-350.

Lewis, E. and Wallace, D.W.R., 1998. Program developed for CO_2 system calculations. ORNL/CDIAC-105, Carbon Dioxide Information Analysis Center, Oak Ridge National Laboratory, U.S.

Li, C.H. and Yang, Z.F., 2004. Division assessment of natural runoff in the Yellow River basin. Journal of Beijing Normal University (Natural Science), 40: 548-553 (in Chinese).

Li, D., Jiang, X., Wang, Y. and Li, H., 2001. Analysis of calculation of natural runoff in the Yellow River Basin. Yellow River 23(2): 35-38(in Chinese).

Li, J. and Zhang, J., 2005. Chemical weathering processes and atmospheric CO_2 consumption of Huanghe River and Changjiang River basins. Chinese Geographical Science, 15(1): 16-21.

Li, S. and Lu, X.X., 2012. Water-air interface CO_2 outgassing and chemical loads in the Lower Mekong River, Workshop on Sediment Flux and Carbon Emission from Large Asian Rivers, National University of Singapore, Singapore.

Li, S. et al., 2012. Daily CO_2 partial pressure and CO_2 outgassing in the upper Yangtze River basin: A case study of the Longchuan River, China. Journal of Hydrology, 466-467: 141-150.

Li, X.D., Fu, H., Guo, D., Li, X.D. and Wan, C.G., 2010. Partitioning soil respiration and assessing the carbon balance in a Setaria italica (L.) Beauv. Cropland on the Loess Plateau, Northern China. Soil Biology & Biochemistry, 42(2): 337-346.

Li, Y. et al., 2007. Changes in soil organic carbon induced by tillage and water erosion on a steep cultivated hillslope in the Chinese Loess Plateau from 1898-1954 and 1954-1998. Journal of Geophysical Research-Biogeosciences, 112(G1).

Li, Z. and Liu, B., 2006. Calculation on soil erosion amount of main river basins in China. Science of Soil and Water Conservation, 4(2): 1-6 (in Chinese).

Liebe, J., van de Giesen, N. and Andreini, M., 2003. Region-wide Estimation of small Reservoir Storage Capacities and Evaporation Losses in a semi-arid Environment. A case study in the Upper East Region of Ghana, EGS-AGU-EUG Joint Assembly, pp. 6946.

Liebe, J., Van De Giesen, N. and Andreini, M., 2005. Estimation of small reservoir storage capacities in a semi-arid environment: A case study in the Upper East Region of Ghana. Physics and Chemistry of the Earth, Parts A/B/C, 30(6): 448-454.

Liu, C.M. and Xia, J., 2004. Water problems and hydrological research in the Yellow River and the Huai and Hai River basins of China. Hydrological Processes, 18(12): 2197-2210.

Liu, D., Ding, Z. and Guo, Z., 1991. Loess, environment, and global change. Science Pr.

Liu, D. and Zhang, L., 2010. Temporal and spatial distributions of organic carbon in the Huanghe (Yellow) River. Periodical of Ocean Univeristy of China, 40(12): 105-110 (in Chinese).

Liu, D. and Zhang, Z., 1988. Loess in China. China Ocean Press.

Liu, J. and Dai, C., 1996. The application of TM image in reservoir situation monitoring. Chinese Remote Sensing Environment 11(1): 54-58(in Chinese).

Liu, L., Zhang, L. and Zhang, X., 2006. Particulate organic carbon content in size-fractioned total suspended soilids at Lijin hydrographic station of the Huanghe River. Periodical of Ocean Univeristy of China, 36: 126-130(in Chinese).

Liu, S., Bliss, N., Sundquist, E. and Huntington, T.G., 2003. Modeling carbon dynamics in vegetation and soil under the impact of soil erosion and deposition. Global Biogeochem. Cycles, 17(2): 1074.

Liu, Z., Dreybrodt, W. and Liu, H., 2011. Atmospheric CO_2 sink: Silicate weathering or carbonate weathering? Applied Geochemistry, 26: S292-S294.

Liu, Z., Dreybrodt, W. and Wang, H., 2010. A new direction in effective accounting for the atmospheric CO_2 budget: Considering the combined action of carbonate dissolution, the global water cycle and photosynthetic uptake of DIC by aquatic organisms. Earth-Science Reviews, 99(3): 162-172.

Loughnan, F., 1969. Chemical Weathering of the Silicate Minerals. Elsevier, New York

Lu, X., 2004. Vulnerability of water discharge of large Chinese rivers to environmental changes: an overview. Regional Environmental Change, 4(4): 182-191.

Lu, X., Zhang, S. and Xu, J., 2010. Climate change and sediment flux from the Roof of the World. Earth Surface Processes and Landforms, 35(6): 732-735.

Lu, X.X., Ashmore, P. and Wang, J., 2003. Sediment yield mapping in a large river basin: the Upper Yangtze, China. Environmental Modelling & Software, 18(4): 339-353.

Lu, X.X. and Higgitt, D.L., 1998. Recent changes of sediment yield in the Upper Yangtze, China. Environmental Management, 22(5): 697-709.

Lu, X.X. et al., 2012. Organic carbon fluxes from the upper Yangtze basin: an example of the Longchuanjiang River, China. Hydrological Processes, 26: 1604-1616.

Lu, X.X. et al., 2013. Sediment loads response to climate change: A preliminary study of eight large Chinese rivers. International Journal of Sediment Research, 28(1): 1-14.

Lu, X.X. and Siew, R.Y., 2006. Water discharge and sediment flux changes over the past decades in the Lower Mekong River: possible impacts of the Chinese dams. Hydrology and Earth System Sciences, 10(2): 181-195.

Ludwig, W., Amiotte-Suchet, P., Munhoven, G. and Probst, J.L., 1998. Atmospheric CO_2 consumption by continental erosion: present-day controls and implications for the last glacial maximum. Global and Planetary Change, 17: 107-120.

Ludwig, W., Probst, J.L. and Kempe, S., 1996. Predicting the oceanic input of organic carbon by continental erosion. Global Biogeochemical Cycles, 10(1): 23-41.

Luo, W., Taylor, M.C. and Parker, S.R., 2008. A comparison of spatial interpolation methods to estimate continuous wind speed surfaces using irregularly distributed data from England and Wales. International Journal of Climatology, 28(7): 947-959.

Luo, X.-L., Zeng, E.Y., Ji, R.-Y. and Wang, C.-P., 2007. Effects of in-channel sand excavation on the hydrology of the Pearl River Delta, China. Journal of Hydrology, 343(3–4): 230-239.

Magome, J., Takeuchi, K. and Ishidaira, H., 2002. Estimating water storage in reservoirs by satellite observations and digital elevation model-a case study of the Yagisawa reservoir Journal of Hydroscience and Hydraulic Engineering, 20(1): 49-58.

Marcus, W.A. and Fonstad, M.A., 2008. Optical remote mapping of rivers at sub‐meter resolutions and watershed extents. Earth Surface Processes and Landforms, 33(1): 4-24.

Mazvimazvi, D., Kusangaya, S. and Williams, H., 2004. Assessment of surface water resources of Zimbabwe and guidelines for planning. In: T. Sawunyama (Editor), Estimation of Small Reservoir Storage Capacitiesin Limpopo River Basin Using Geographical Information Systems (GIS) and Remotely Sensed Surface Areas: A Case of Mzingwane Catchment, Master thesis, University of Zimbabwe; 24-26.

McCarty, G.W. and Ritchie, J.C., 2002. Impact of soil movement on carbon sequestration in agricultural ecosystems. Environmental Pollution, 116(3): 423-430.

Mchunu, C. and Chaplot, V., 2012. Land degradation impact on soil carbon losses through water erosion and CO2 emissions. Geoderma, 177–178(0): 72-79.

McLaughlin, C., Smith, C., Buddemeier, R., Bartley, J. and Maxwell, B., 2003. Rivers, runoff, and reefs. Global and Planetary Change, 39(1): 191-199.

McNally, A., Magee, D. and Wolf, A.T., 2009. Hydropower and sustainability: Resilience and vulnerability in China's powersheds. Journal of Environmental Management, 90: S286-S293.

Meigh, J., 1995. The impact of small farm reservoirs on urban water supplies in Botswana, Natural Resources Forum. Wiley Online Library, pp. 71-83.

Melack, J., 2011a. Biogeochemistry: Riverine carbon dioxide release. Nature Geosci, 4(12): 821-822.

Melack, J., 2011b. Riverine carbon dioxide release. Nature Geoscience, 4(12): 821-822.

Meybeck, M., 1987. Global chemical weathering of surficial rocks estimated from river dissolved loads. American Journal of Science, 287(5): 401-428.

Meybeck, M., 1993a. C, N, P and S in rivers: from sources to global inputs. In: R. Wollast, F.T. Mackenzie and L. Chou (Editors), Interactions of C, N, P and S Biogeochemical Cycles and Global Change. Springer-Verlag, Berlin, pp. 163-193.

Meybeck, M., 1993b. Riverine transport of atmospheric carbon: sources, global typology and budget. Water, Air, & Soil Pollution, 70(1): 443-463.

Meybeck, M., 2004. Global occurrence of major elements in rivers. In: J.I. Drever (Editor), Treatise On Geochemistry. Elsevier, New York, pp. 202-233.

Meybeck, M. and Ragu, A., 1997. River Discharges to the Oceans: An Assessment of Suspended Solids, Major Ions and Nutrients. UNEP.

Mialhe, F., Gunnell, Y. and Mering, C., 2008. Synoptic assessment of water resource variability in reservoirs by remote sensing: General approach and application to the runoff harvesting systems of south India. Water Resources Research, 44(5).

Miao, C., Ni, J., Borthwick, A.G.L. and Yang, L., 2011. A preliminary estimate of human and natural contributions to the changes in water discharge and sediment load in the Yellow River. Global and Planetary Change, 76(3-4): 196-205.

Milliman, J.D. and Meade, R.H., 1983. World-wide delivery of river sediment to the oceans. The Journal of Geology, 91(1): 1-21.

Millot, R., Gaillardet, J., Dupre, B. and Allegre, C.J., 2002. The global control of silicate weathering rates and the coupling with physical erosion: new insights from rivers of the Canadian Shield. Earth and Planetary Science Letters, 196(1-2): 83-98.

Minear, J.T. and Kondolf, G.M., 2009. Estimating reservoir sedimentation rates at large spatial and temporal scales: A case study of California. Water Resources Research, 45.

Ministry of Water Resources of China, 2008. Standard for Classification and Gradation of Soil Erosion SL 190-2007. China Waterpower Press, Beijing, China.

Ministry of Water Resources of China, 2010a. China River Sediment Bulletin. China Waterpower Press, Beijing, China.

Mitchell, T., 1976. The yield of an average dam in Rhodesia. Rhodesian Engineer 14(4): 37-41.

Moon, S., Huh, Y., Qin, J. and van Pho, N., 2007. Chemical weathering in the Hong (Red) River basin: rates of silicate weathering and their controlling factors. Geochimica Et Cosmochimica Acta, 71(6): 1411-1430.

Morris, G.L. and Fan, J., 1998. Reservoir Sedimentation Handbook. McGraw-Hill Book Co., New York: 848.

Mortatti, J. and Probst, J.L., 2003. Silicate rock weathering and atmospheric/soil CO_2 uptake in the Amazon basin estimated from river water geochemistry: seasonal and spatial variations. Chemical Geology, 197(1): 177-196.

Mu, X., Li, J., Wang, F. and Xu, X., 2003. Analysis on the annual natural runoff variety process of the Yellow River. Journal of Arid Land Resources and Environment 17: 1-5(in Chinese).

Munhoven, G., 2002. Glacial–interglacial changes of continental weathering: estimates of the related CO_2 and HCO_3^- flux variations and their uncertainties. Global and Planetary Change, 33(1): 155-176.

Neal, C. et al., 1990. Hydrogeochemical variations in Hafren forest stream waters, Mid-Wales. Journal of Hydrology, 116(1–4): 185-200.

Neff, J. et al., 2006. Seasonal changes in the age and structure of dissolved organic carbon in Siberian rivers and streams. Geophysical Research Letters, 33(23): L23401.

Negrel, P., Allègre, C.J., Dupré, B. and Lewin, E., 1993. Erosion sources determined by inversion of major and trace element ratios and strontium isotopic ratios in river water: The Congo Basin case. Earth and Planetary Science Letters, 120(1): 59-76.

Nilsson, C., Reidy, C.A., Dynesius, M. and Revenga, C., 2005. Fragmentation and flow regulation of the world's large river systems. Science, 308(5720): 405-408.

Oliva, P., Viers, J. and Dupré, B., 2003. Chemical weathering in granitic environments. Chemical Geology, 202(3): 225-256.

Onikienko, T., 1995. Corrected correlations between the capacity and levels of the Ust'-Khantaika hydroelectric power plant. Hydrotechnical Construction, 29(3): 157-163.

Pacala, S.W. et al., 2001. Consistent land-and atmosphere-based US carbon sink estimates. Science, 292(5525): 2316-2320.

Pang, J. and Jiang, M., 2003. On the evolution of the Yellow River Estuary (II). Transactions of Oceanology and Limnology, 4: 1-13 (in Chinese).

Parks, S.J. and Baker, L.A., 1997. Sources and transport of organic carbon in an Arizona river-reservoir system. Water Research, 31(7): 1751-1759.

Peng, D.Z., Guo, S.L., Liu, P. and Liu, T., 2006. Reservoir storage curve estimation based on remote sensing data. Journal of Hydrologic Engineering, 11(2): 165-172.

Peng, J., Chen, S. and Dong, P., 2010. Temporal variation of sediment load in the Yellow River basin, China, and its impacts on the lower reaches and the river delta. CATENA, 83(2-3): 135-147.

Petit, C. and Lambin, E., 2001. Integration of multi-source remote sensing data for land cover change detection. International Journal of Geographical Information Science, 15(8): 785-803.

Piňol, J. and Avila, A., 1992. Streamwater Ph, Alkalinity, Pco2 and Discharge Relationships in Some Forested Mediterranean Catchments. Journal of Hydrology, 131(1-4): 205-225.

Piper, A., 1953. A graphic procedure in the geochemical interpretation of water analyses: in US Geological Survey Ground Water Notes. Geochemistry(12): 5.

Post, W.M. and Kwon, K.C., 2008. Soil carbon sequestration and land‐use change: processes and potential. Global Change Biology, 6(3): 317-327.

Probst, J.L., Mortatti, J. and Tardy, Y., 1994. Carbon river fluxes and weathering CO_2 consumption in the Congo and Amazon river basins. Applied Geochemistry, 9(1): 1-13.

Probst, J.L. et al., 1992. Dissolved major elements exported by the Congo and the Ubangi rivers during the period 1987–1989. Journal of Hydrology, 135(1): 237-257.

Propastin, P.A., 2008. Simple model for monitoring Balkhash Lake water levels and Ili River discharges: Application of remote sensing. Lakes & Reservoirs: Research & Management, 13(1): 77-81.

Quinton, J.N., Govers, G., Van Oost, K. and Bardgett, R.D., 2010. The impact of agricultural soil erosion on biogeochemical cycling. Nature Geosci, 3(5): 311-314.

Ran, D., 2007. Water and sediment variation and ecological protection measures in the Middle Reach of the Yellow River. Resources Science, 28(1): 93-100 (in Chinese).

Ran, D., Wu, Y., Li, X., Wang, F. and Shen, Z., 2012. Analysis on contribution rate of water and sediment reduction by human activities at Hekouzhen-Longmen section in last years. Yellow River, 34(2): 84-86 (in Chinese).

Ran, L. and Lu, X.X., 2012. Delineation of reservoirs using remote sensing and their storage estimate: an example of the Yellow River basin, China. Hydrological Processes, 26(8): 1215-1229.

Ran, L. and Lu, X.X., 2013. Redressing China's strategy of water resource exploitation. Environmental Management, 51(3): 503-510.

Ran, L., Lu, X.X. and Xu, J.C., 2013a. Effects of vegetation restoration on soil conservation and sediment loads in China: A critical review. Critical Reviews in Environmental Science and Technology, 43: 1-32.

Ran, L., Lu., X.X., Xin, Z.B. and Yang, X., 2013b. Cumulative sediment trapping by reservoirs in large river basins: A case study of the Yellow River basin. Global and Planetary Change, 100: 308-319.

Rasera, M.d.F.F.L. et al., 2008. Estimating the surface area of small rivers in the southwestern Amazon and their role in CO_2 outgassing. Earth Interactions, 12: 1-16.

Raymo, M., 1991. Geochemical evidence supporting TC Chamberlin's theory of glaciation. Geology, 19(4): 344-347.

Raymo, M. and Ruddiman, W.F., 1992. Tectonic forcing of late Cenozoic climate. Nature, 359(6391): 117-122.

Raymond, P.A. and Bauer, J.E., 2001a. Riverine export of aged terrestrial organic matter to the North Atlantic Ocean. Nature, 409(6819): 497-500.

Raymond, P.A. and Bauer, J.E., 2001b. Use of ^{14}C and ^{13}C natural abundances for evaluating riverine, estuarine, and coastal DOC and POC sources and cycling: a review and synthesis. Organic Geochemistry, 32(4): 469-485.

Raymond, P.A., Bauer, J.E. and Cole, J.J., 2000. Atmospheric CO_2 evasion, dissolved inorganic carbon production, and net heterotrophy in the York River estuary. Limnology and Oceanography, 45(8): 1707-1717.

Raymond, P.A., Caraco, N.F. and Cole, J.J., 1997. Carbon dioxide concentration and atmospheric flux in the Hudson River. Estuaries, 20(2): 381-390.

Raymond, P.A. and Cole, J.J., 2001. Gas exchange in rivers and estuaries: choosing a gastransfervelocity. Estuaries, 24(2): 312-317.

Raymond, P.A. and Cole, J.J., 2003. Increase in the export of alkalinity from North America's largest river. Science, 301(5629): 88-91.

Regnier, P. et al., 2013. Anthropogenic perturbation of the carbon fluxes from land to ocean. Nature Geoscience: doi:10.1038/ngeo1830.

Reich, P., Eswaran, H. and Beinroth, F., 2001. Global dimensions of vulnerability to wind and water erosion. In: D.E. Stott, R.H. Mohtar and G.C. Steinhardt (Editors), Sustaining the Global Farm. Selected papers from the 10th International Soil Conservation Organization Meeting, May 24-29, 1999. Perdue University and USDA-ARS National Soil Erosion Research Laboratory, pp. 838-846.

Renwick, W., Smith, S., Sleezer, R. and Buddemeier, R.W., 2004. Comment on" managing soil carbon"(ii). Science, 305(5690): 1567-1567.

Richey, J.E., 2003. Pathways of atmospheric CO_2 through fluvial systems. In: Field C.B. and Raupach M. (Editors), Scientific Committee on Problems of the Environment (SCOPE) / United Nations Environment Programme (UNEP)-The Global Carbon Cycle: Integrating Humans, Climate, and the Natural World. USA: Island Press, pp. 329-340.

Richey, J.E., Brock, J.T., Naiman, R.J., Wissmar, R.C. and Stallard, R.F., 1980. Organic Carbon: Oxidation and Transport in the Amazon River. Science, 207, Issue 4437, pp. 1348-1351(4437): 4.

Richey, J.E., Melack, J.M., Aufdenkampe, A.K., Ballester, V.M. and Hess, L.L., 2002. Outgassing from Amazonian rivers and wetlands as a large tropical source of atmospheric CO_2. Nature, 416(6881): 617-620.

Richey, J.E., Victoria, R.L., Salati, E. and Forsberg, B.R., 1991. The biogeochemistry of a major river system: The Amazon case study. In: E.T. Degens, S. Kempe and Richey J.E. (Editors), Biogeochemistry of major world rivers. Wiley, New York, pp. 57-74.

Riebe, C.S., Kirchner, J.W., Granger, D.E. and Finkel, R.C., 2001. Strong tectonic and weak climatic control of long-term chemical weathering rates. Geology, 29(6): 511-514.

Ritchie, J.C., 1989. Carbon content of sediments of small reservoirs. JAWRA Journal of the American Water Resources Association, 25(2): 301-308.

Robert, C.M., 2008. Chapter Twelve Organic Sediments. In: M.R. Christian (Editor), Developments in Marine Geology. Elsevier, pp. 415-450.

Rodrigues, L.N. and Liebe, J., 2013. Small reservoirs depth-area-volume relationships in Savannah Regions of Brazil and Ghana. Water Resources and Irrigation Management, 2(1): 1-10.

Roy, S., Gaillardet, J. and Allegre, C., 1999. Geochemistry of dissolved and suspended loads of the Seine river, France: anthropogenic impact, carbonate and silicate weathering. Geochimica Et Cosmochimica Acta, 63(9): 1277-1292.

Rueda, F., Moreno-Ostos, E. and Armengol, J., 2006. The residence time of river water in reservoirs. Ecological Modelling, 191(2): 260-274.

Ryu, J.-S., Lee, K.-S., Chang, H.-W. and Shin, H.S., 2008. Chemical weathering of carbonates and silicates in the Han River basin, South Korea. Chemical Geology, 247(1): 66-80.

Sarma, V.V.S.S. et al., 2011. High CO_2 emissions from the tropical Godavari estuary (India) associated with monsoon river discharges. Geophysical Research Letters, 38.

Sawunyama, T., Senzanje, A. and Mhizha, A., 2006. Estimation of small reservoir storage capacities in Limpopo River Basin using geographical information systems (GIS) and remotely sensed surface areas: Case of Mzingwane catchment. Physics and Chemistry of the Earth, Parts A/B/C, 31(15): 935-943.

Schlesinger, W.H., 1995. Soil respiration and changes in soil carbon stocks. In: G.M. Woodwell and F.T. Mackenzie (Editors), Biotic Feedback in the Global Climatic System: Will the Warming Feed the Warming? Oxford University Press, New York, USA, pp. 159-168.

Schlünz, B. and Schneider, R.R., 2000. Transport of terrestrial organic carbon to the oceans by rivers: re-estimating flux- and burial rates. International Journal of Earth Sciences, 88(4): 599-606.

Schmidt, J.C. and Wilcock, P.R., 2008. Metrics for assessing the downstream effects of dams. Water Resources Research, 44: W04404, doi:10.1029/2006WR005092.

Sebastian, M. et al., 1995. Reservoir storage loss assessment and sedimentation modeling through remote sensing techniques. In: C. Varma and A. Rao (Editors), Management of sediment-Philosophy, Aims and Techniques, New Delhi, India, pp. 629-634.

Seitzinger, S. et al., 2010. Global river nutrient export: A scenario analysis of past and future trends. Global Biogeochemical Cycles, 24(4).

Shi, C., Dian, Z. and You, L., 2002. Changes in sediment yield of the Yellow River basin of China during the Holocene. Geomorphology, 46(3-4): 267-283.

Shi, D., 1990. Effects of soil erosion on ecological environment and natural disasters. Advances in Earth Science, 4: 41-44 (in Chinese).

Singh, S.K., Sarin, M. and France-Lanord, C., 2005. Chemical erosion in the eastern Himalaya: Major ion composition of the Brahmaputra and $\delta^{13}C$ of dissolved inorganic carbon. Geochimica et Cosmochimica Acta, 69(14): 3573-3588.

Smith, S.V., Renwick, W.H., Buddemeier, R.W. and Crossland, C.J., 2001. Budgets of soil erosion and deposition for sediments and sedimentary organic carbon across the conterminous United States. Global Biogeochemical Cycles, 15(3): 697-707.

Smith, S.V., Sleezer, R.O., Renwick, W.H. and Buddemeier, R., 2005. Fates of eroded soil organic carbon: Mississippi basin case study. Ecological Applications, 15(6): 1929-1940.

Stallard, R. and Edmond, J., 1983. Geochemistry of the Amazon 2. The influence of geology and weathering environment on the dissolved load. Journal of Geophysical Research, 88(C14): 9671-9688.

Stallard, R.F., 1980. Major element geochemistry of the Amazon River system, Massachusetts Institute of Technology.

Stallard, R.F., 1998. Terrestrial sedimentation and the carbon cycle: Coupling weathering and erosion to carbon burial. Global Biogeochemical Cycles, 12(2): 231-257.

Strebelle, S. and Journel, A., 2001. Reservoir modeling using multiple-point statistics, SPE Annual Technical Conference and Exhibition, New Orleans, LA.

Stumm, W. and Morgan, J.J., 1970. Aquatic Chemistry; An Introduction Emphasizing Chemical Equilibria in Natural Waters. New York, Wiley-Interscience.

Suchet, P.A., Probst, J.L. and Ludwig, W., 2003. Worldwide distribution of continental rock lithology: Implications for the atmospheric/soil CO_2 uptake by continental weathering and alkalinity river transport to the oceans. Global Biogeochemical Cycles, 17(2).

Sugunan, V.V., 1997. Fisheries management of small water bodies in seven countries in Africa, Asia and Latin America, 149. FAO.

Summerfield, M. and Hulton, N., 1994. Natural controls of fluvial denudation rates in major world drainage basins. Journal of Geophysical Research, 99: 13871-13883.

Sun, H., Han, J., Zhang, S. and Lu, X., 2011. Transformation of dissolved inorganic carbon (DIC) into particulate organic carbon (POC) in the lower Xijiang River, SE China: an isotopic approach. Biogeosciences Discussions, 8(5): 9471-9501.

Sun, H.G., Han, J.T., Zhang, S.R. and Lu, X.X., 2007. The impacts of '05.6' extreme flood event on riverine carbon fluxes in Xijiang River. Chinese Science Bulletin, 52(6): 805-812.

Syvitski, J.P.M. et al., 2009. Sinking deltas due to human activities. Nature Geosci, 2(10): 681-686.

Syvitski, J.P.M., Peckham, S.D., Hilberman, R. and Mulder, T., 2003. Predicting the terrestrial flux of sediment to the global ocean: a planetary perspective. Sedimentary Geology, 162(1-2): 5-24.

Syvitski, J.P.M., Vorosmarty, C.J., Kettner, A.J. and Green, P., 2005. Impact of humans on the flux of terrestrial sediment to the global coastal ocean. Science, 308(5720): 376-380.

Ta, W., Xiao, H. and Dong, Z., 2008. Long-term morphodynamic changes of a desert reach of the Yellow River following upstream large reservoirs' operation. Geomorphology, 97(3–4): 249-259.

Tarela, P.A. and Menéndez, A.N., 1999. A model to predict reservoir sedimentation. Lakes & Reservoirs: Research & Management, 4(3-4): 121-133.

Telmer, K. and Veizer, J., 1999. Carbon fluxes, pCO_2 and substrate weathering in a large northern river basin, Canada: carbon isotope perspectives. Chemical Geology, 159(1-4): 61-86.

Teodoru, C.R., Del Giorgio, P.A., Prairie, Y.T. and Camire, M., 2009. Patterns in pCO_2 in boreal streams and rivers of northern Quebec, Canada. Global Biogeochemical Cycles, 23.

Terada, H., Ueda, H. and Wang, Z., 2002. Trend of acid rain and neutralization by yellow sand in east Asia—a numerical study. Atmospheric Environment, 36(3): 503-509.

Töyrä, J., Pietroniro, A., Martz, L.W. and Prowse, T.D., 2002. A multi - sensor approach to wetland flood monitoring. Hydrological Processes, 16(8): 1569-1581.

Tranvik, L.J. et al., 2009. Lakes and reservoirs as regulators of carbon cycling and climate. Limnology and Oceanography, 54(6): 2298-2314.

Turner, B.F., White, A.F. and Brantley, S.L., 2010. Effects of temperature on silicate weathering: Solute fluxes and chemical weathering in a temperate rain forest watershed, Jamieson Creek, British Columbia. Chemical Geology, 269(1): 62-78.

Turowski, J.M., Rickenmann, D. and Dadson, S.J., 2010. The partitioning of the total sediment load of a river into suspended load and bedload: a review of empirical data. Sedimentology, 57(4): 1126-1146.

Valentin, C., Poesen, J. and Li, Y., 2005. Gully erosion: Impacts, factors and control. CATENA, 63(2–3): 132-153.

Van Hemelryck, H., Govers, G., Van Oost, K. and Merckx, R., 2011. Evaluating the impact of soil redistribution on the in situ mineralization of soil organic carbon. Earth Surface Processes and Landforms, 36(4): 427-438.

Van Oost, K. et al., 2007. The impact of agricultural soil erosion on the global carbon cycle. Science, 318(5850): 626-629.

Van Oost, K., Six, J., Govers, G., Quine, T. and Gryze, S.D., 2008. Response to 'Soil erosion: a carbon sink or source ?'. Science, 319(5866): 1042-1042.

Van Oost, K. et al., 2012. Legacy of human-induced C erosion and burial on soil-atmosphere C exchange. Proc Natl Acad Sci U S A, 109(47): 19492-7.

Vance, D., Teagle, D.A.H. and Foster, G.L., 2009. Variable Quaternary chemical weathering fluxes and imbalances in marine geochemical budgets. Nature, 458(7237): 493-496.

Verdin, J.P., 1985. Monitoring water quality conditions in a large western reservoir with Landsat imagery. Photogrammetric Engineering and Remote Sensing, 51(3): 343-353.

Verstraeten, G., Poesen, J., de Vente, J. and Koninckx, X., 2003. Sediment yield variability in Spain: a quantitative and semiqualitative analysis using reservoir sedimentation rates. Geomorphology, 50(4): 327-348.

Viers, J., Oliva, P., Dandurand, J.L., Dupré, B. and Gaillardet, J., 2007. 5.20 - Chemical weathering rates, CO_2 consumption, and control parameters deduced from the chemical composition of rivers. In: D.H. Editors-in-Chief: Heinrich and K.T. Karl (Editors), Treatise On Geochemistry. Pergamon, Oxford, pp. 1-25.

Vörösmarty, C.J. et al., 2003. Anthropogenic sediment retention: major global impact from registered river impoundments. Global and Planetary Change, 39(1-2): 169-190.

Vörösmarty, C.J. and Sahagian, D., 2000. Anthropogenic disturbance of the terrestrial water cycle. Bioscience, 50(9): 753-765.

Vörösmarty, C.J. et al., 1997. The storage and ageing of continental runoff in large reservoir systems of the world. Ambio, 26(4): 210-219.

Walling, D., 2006. Human impact on land–ocean sediment transfer by the world's rivers. Geomorphology, 79(3): 192-216.

Walling, D. and Webb, B., 1986. Solutes in river systems. Solute processes: 251-327.

Walling, D.E., 2012. The role of dams in the global sediment budget. In: A.L. Collins et al. (Editors), Erosion and Sediment Yields in the Changing Environment. IAHS Publication, Oxfordshire, UK, pp. 3-11.

Walling, D.E. and Fang, D., 2003. Recent trends in the suspended sediment loads of the world's rivers. Global and Planetary Change, 39: 111-126.

Wang, B., Clemens, S.C. and Liu, P., 2003a. Contrasting the Indian and East Asian monsoons: implications on geologic timescales. Marine Geology, 201(1): 5-21.

Wang, F., Li, R. and Yang, Q., 2003b. Review on effects of human activities on the soil erosion in the Loess Plateau. Journal of Sediment Research, 5: 74-80 (in Chinese).

Wang, F.S. et al., 2011a. Carbon dioxide emission from surface water in cascade reservoirs-river system on the Maotiao River, southwest of China. Atmospheric Environment, 45(23): 3827-3834.

Wang, F.S., Wang, Y.C., Zhang, J., Xu, H. and Wei, X.G., 2007a. Human impact on the historical change of CO_2 degassing flux in River Changjiang. Geochemical Transactions, 8.

Wang, G. and Li, S., 1998. Application of remote sensing data to extraction of underwater topography of reservoir. Journal of Hohai University 26(6): 91-94(in Chinese).

Wang, G., Wu, B. and Wang, Z.-Y., 2005. Sedimentation problems and management strategies of Sanmenxia Reservoir, Yellow River, China. Water Resour. Res., 41(9): W09417.

Wang, H., Yang, Z., Saito, Y., Liu, J.P. and Sun, X., 2006. Interannual and seasonal variation of the Huanghe (Yellow River) water discharge over the past 50 years: Connections to impacts from ENSO events and dams. Global and Planetary Change, 50(3-4): 212-225.

Wang, H.J. et al., 2007b. Stepwise decreases of the Huanghe (Yellow River) sediment load (1950-2005): Impacts of climate change and human activities. Global and Planetary Change, 57(3-4): 331-354.

Wang, J.J., Lu, X.X. and Kummu, M., 2011b. Sediment load estimates and variations in the Lower Mekong River. River Research and Applications, 27(1): 33-46.

Wang, P., Qiu, G., Yin, J., Xiong, Y. and Xie, F., 2008a. Spatial distribution and temporal trend of temperature and pan evaporation in Jinghe River Basin. Arid Meteorology, 26: 17-22 (in Chinese).

Wang, S., Jin, H., Li, S. and Zhao, L., 2000. Permafrost degradation on the Qinghai-Tibet Plateau and its environmental impacts. Permafrost and Periglacial Processes, 11(1): 43-53.

Wang, X., Ma, H., Li, R., Song, Z. and Wu, J., 2012. Seasonal fluxes and source variation of organic carbon transported by two major Chinese Rivers: The Yellow River and Changjiang (Yangtze) River. Global Biogeochem. Cycles, 26(2): GB2025.

Wang, Y., Hu, C. and Shi, H., 2010a. Allocation and utilization of sediment resource in the Yellow River Basin. Science of Soil and Water Conservation, 8(4): 20-26 (in Chinese).

Wang, Y., Huang, Q., Zhu, J. and Ran, B., 2003c. Analysis on the operation of Longyangxia Reservoir under long-term lower water level and its countermeasures. Water Resources and Hydropower Engineering, 34: 53-56(in Chinese).

Wang, Y., Xia, H., Fu, J. and Sheng, G., 2004. Water quality change in reservoirs of Shenzhen, China: detection using LANDSAT/TM data. Science of the Total Environment, 328(1): 195-206.

Wang, Y., Zhang, X. and Han, F., 2008b. Profile variability of soil properities in check dams on the Loess Plateau and its functions. Environmental Science, 29: 1020-1026 (in Chinese).

Wang, Z. et al., 2010b. Catchment-scale carbon redistribution and delivery by water erosion in an intensively cultivated area. Geomorphology, 124(1–2): 65-74.

Wang, Z., Wang, W. and Tian, S., 2007c. Mineral composition and distribution of the sediment in the Yellow River basin. Journal of Sediment Research, 5: 1-8 (in Chinese).

Wang, Z. et al., 2011c. Sedimentation management assessment of Sanmenxia Reservoir based on RESCON model. Yellow River, 33: 25-28 (in Chinese).

Wanninkhof, R., 1992. Relationship between wind speed and gas exchange. Journal of Geophysical Research, 97(25): 7373-7382.

Waterpub, 2007. China Water Power Press (http://www.waterpub.com.cn/).

Wei, J., Zhou, J., Tian, J., He, X. and Tang, K., 2006. Decoupling soil erosion and human activities on the Chinese Loess Plateau in the 20th century. CATENA, 68(1): 10-15.

Wei, X. et al., 2010. ^{14}C as a tool for evaluating riverine POC sources and erosion of the Zhujiang (Pearl River) drainage basin, South China. Nuclear Instruments and Methods in Physics Research Section B: Beam Interactions with Materials and Atoms, 268(7): 1094-1097.

Weiss, R.F., 1974. Carbon dioxide in water and seawater: the solubility of a non-ideal gas. Marine Chemistry, 2(3): 203-215.

West, A.J., Galy, A. and Bickle, M., 2005. Tectonic and climatic controls on silicate weathering. Earth and Planetary Science Letters, 235(1–2): 211-228.

White, A.F. and Blum, A.E., 1995. Effects of climate on chemical weathering in watersheds. Geochimica Et Cosmochimica Acta, 59(9): 1729-1747.

White, A.F. and Brantley, S.L., 1995. Chemical weathering rates of silicate minerals: an overview. Chemical Weathering Rates of Silicate Minerals, 31: 1-22.

White, P., Butcher, D.P. and Labadz, J.C., 1997. Reservoir sedimentation and catchment sediment yield in the Strines catchment, U.K. Physics and Chemistry of The Earth, 22(3-4): 321-328.

Wisser, D., Fekete, B., Vörösmarty, C. and Schumann, A., 2010. Reconstructing 20th century global hydrography: a contribution to the Global Terrestrial Network-Hydrology (GTN-H). Hydrology and Earth System Sciences, 14(1): 1.

World Commission on Dams, 2000. Dams and Development: A New Framework for Decision-making. Earthscan Publications Ltd, London, 356 pp.

Worrall, F. and Burt, T., 2004. Time series analysis of long-term river dissolved organic carbon records. Hydrological Processes, 18(5): 893-911.

Wu, B., Wang, G., Xia, J., Fu, X. and Zhang, Y., 2008a. Response of bankfull discharge to discharge and sediment load in the Lower Yellow River. Geomorphology, 100(3-4): 366-376.

Wu, L.L., Huh, Y., Qin, J.H., Du, G. and van der Lee, S., 2005. Chemical weathering in the Upper Huang He (Yellow River) draining the eastern Qinghai-Tibet Plateau. Geochimica Et Cosmochimica Acta, 69(22): 5279-5294.

Wu, W., Xu, S., Yang, J. and Yin, H., 2008b. Silicate weathering and CO_2 consumption deduced from the seven Chinese rivers originating in the Qinghai-Tibet Plateau. Chemical Geology, 249(3): 307-320.

Wu, Y. et al., 2007. Sources and distribution of carbon within the Yangtze River system. Estuarine Coastal and Shelf Science, 71(1-2): 13-25.

Xia, J.Q., Wu, B.S., Wang, Y.P. and Zhao, S.G., 2008. An analysis of soil composition and mechanical properties of riverbanks in a braided reach of the Lower Yellow River. Chinese Science Bulletin, 53(15): 2400-2409.

Xin, Z., Yu, X. and Lu, X., 2011. Factors controlling sediment yield in China's Loess Plateau. Earth Surface Processes and Landforms, 36(6): 816-826.

Xin, Z.B., Ran, L. and Lu, X.X., 2012. Soil erosion control and sediment load reduction in the Loess Plateau: Policy perspectives. International Journal of Water Resources Development, 28(2): 325-341.

Xin, Z.B., Xu, J.X. and Zheng, W., 2008. Spatiotemporal variations of vegetation cover on the Chinese Loess Plateau (1981-2006): Impacts of climate changes and human activities. Science in China Series D: Earth Sciences, 51(1): 67-78.

Xu, J., 1999. Erosion caused by hyperconcentrated flow on the Loess Plateau of China. CATENA, 36(1–2): 1-19.

Xu, J., 2002. Implication of relationships among suspended sediment size, water discharge and suspended sediment concentration: the Yellow River basin, China. CATENA, 49(4): 289-307.

Xu, J., 2003. Sediment flux to the sea as influenced by changing human activities and precipitation: Example of the Yellow River, China. Environmental Management, 31(3): 328-341.

Xu, J., 2004. Response of erosion and sediment producing processes to soil and water conservation measures in the Wudinghe River Basin. Acta Geographica Sinica 59: 972-981(in Chinese).

Xu, J., 2005. Effect of sediment sink of lower Yellow River on grain size of sediment flux to the sea. Journal of Sediment Research, 6: 21-28 (in Chinese).

Xu, J. and Yan, Y., 2005. Scale effects on specific sediment yield in the Yellow River basin and geomorphological explanations. Journal of Hydrology, 307(1): 219-232.

Xu, Z., Li, Y., Tang, Y. and Han, G., 2009. Chemical and strontium isotope characterization of rainwater at an urban site in Loess Plateau, Northwest China. Atmospheric Research, 94(3): 481-490.

Yamagishi, Y. et al., 2006. Integration of geophysical and geochemical data, AGU Fall Meeting Abstracts, pp. 1142.

Yang, C., Telmer, K. and Veizer, J., 1996. Chemical dynamics of the "St. Lawrence" riverine system: δD_{H2O}, $\delta^{18}O_{H2O}$, $\delta^{13}C_{DIC}$, $\delta^{34}S_{sulfate}$, and dissolved $^{87}Sr/^{86}Sr$. Geochimica Et Cosmochimica Acta, 60(5): 851-866.

Yang, D. et al., 2004a. Analysis of water resources variability in the Yellow River of China during the last half century using historical data. Water Resources Research, 40(6): W06502.

Yang, Q.Y. and Yuan, B.Y., 1991. Natural Environment of Loess Plateau and Its Evolution. Science Press, Beijing (in Chinese).

Yang, S.L. et al., 2006. Drastic decrease in sediment supply from the Yangtze River and its challenge to coastal wetland management. Geophys. Res. Lett., 33(6): L06408.

Yang, S.L., Zhang, J., Dai, S.B., Li, M. and Xu, X.J., 2007. Effect of deposition and erosion within the main river channel and large lakes on sediment delivery to the estuary of the Yangtze River. J. Geophys. Res., 112(F2): F02005.

Yang, S.Y., Jung, H.S. and Li, C.X., 2004b. Two unique weathering regimes in the Changjiang and Huanghe drainage basins: geochemical evidence from river sediments. Sedimentary Geology, 164(1-2): 19-34.

Yang, Z., Cheng, Y. and Wang, H., 1986. The geology of China. Clarendon Press Oxford.

Yao, G.R. et al., 2007. Dynamics of CO_2 partial pressure and CO_2 outgassing in the lower reaches of the Xijiang River, a subtropical monsoon river in China. Science of the Total Environment, 376(1-3): 255-266.

Yellow River Conservancy Committee, 2000-2007. Yellow River Sediment Bulletin. China Waterpower Press, Beijing, China (in Chinese).

Yellow River Sediment Bulletin, 1950-2009. The Ministry of Water Resources of the People's Republic of China (http://www.mwr.gov.cn/).

YRCC (Yellow River Conservancy Commission), 2007. Bulletin of Water Resources in the Yellow River Basin, The Ministry of Water Resources of the People's Republic of China, Beijing, China.

Zhai, W.D., Dai, M.H. and Guo, X.G., 2007. Carbonate system and CO2 degassing fluxes in the inner estuary of Changjiang (Yangtze) River, China. Marine Chemistry, 107(3): 342-356.

Zhang, J., Huang, W.W., Létolle, R. and Jusserand, C., 1995a. Major element chemistry of the Huanghe (Yellow River), China: weathering processes and chemical fluxes. Journal of Hydrology, 168(1-4): 173-203.

Zhang, J., Huang, W.W., Liu, M.G. and Zhou, Q., 1990. Drainage basin weathering and major element transport of two large Chinese rivers (Huanghe and Changjiang). Journal of Geophysical Research, 95(C8): 13277-13,288.

Zhang, J. et al., 1995b. Water geochemistry of the rivers around the Taklimakan Desert (NW China): Crustal weathering and evaporation processes in arid land. Chemical Geology, 119(1): 225-237.

Zhang, L.J., Zhang, J. and Gong, M., 2009a. Size distributions of hydrocarbons in suspended particles from the Yellow River. Applied Geochemistry, 24(7): 1168-1174.

Zhang, S., Gan, W.-B. and Ittekkot, V., 1992. Organic matter in large turbid rivers: the Huanghe and its estuary. Marine Chemistry, 38(1–2): 53-68.

Zhang, S., Lu, X., Sun, H., Han, J. and Higgitt, D.L., 2009b. Geochemical characteristics and fluxes of organic carbon in a human-disturbed mountainous river (the Luodingjiang River) of the Zhujiang (Pearl River), China. Science of the Total Environment, 407(2): 815-825.

Zhang, S. et al., 2008a. Recent changes of water discharge and sediment load in the Zhujiang (Pearl River) Basin, China. Global and Planetary Change, 60(3–4): 365-380.

Zhang, S.R., 2008. Sediment and Carbon Transport in a Meso-scale Mountainous Tributary of the Zhujiang (Pearl River), China, National University of Singapore, Singapore, 319 pp.

Zhang, S.R. et al., 2007. Water chemistry of the Zhujiang (Pearl River): Natural processes and anthropogenic influences. Journal of Geophysical Research-Earth Surface, 112(F1).

Zhang, X.H., Shang, H.X., Zheng, Y.S., Li, Y. and Li, G.X., 2008b. Fluvial Process After Large Dam Construction on The Yellow River Main Stem. Yellow River Conservancy Press, Zhengzhou, 168-188 pp.

Zhang, Z. et al., 2008c. Calculation of reservoir-retained sediment and characteristics of sediment distribution of the Yellow River basin. Soil and Water Conservation in China, 4: 20-23(in Chinese).

Zhang, Z., Wang, W., Zhang, Y. and Lu, G., 1999. Application of GPS in surveying reservoir capacity. Journal of Hohai University 27: 29-33(in Chinese).

Zhao, M.X., Zhou, J.B. and Kalbitz, K., 2008. Carbon mineralization and properties of water-extractable organic carbon in soils of the south Loess Plateau in China. European Journal of Soil Biology, 44(2): 158-165.

Zhao, W., 1996. The Yellow River's Sediment. Yellow River Conservancy Press, Zhengzhou, China, 807 pp.

Zheng, M., 1997. An introduction to saline lakes on the Qinghai-Tibet Plateau, 76. Kluwer Academic Pub.

Zheng, Z., 1984. History of Water Conservancy in China. Shanghai Bookstore Press, Shanghai, China (in Chinese).

Zhou, J., Civco, D. and Silander, J., 1998. A wavelet transform method to merge Landsat TM and SPOT panchromatic data. International Journal of Remote Sensing, 19(4): 743-757.

Appendix

The collected data used in this study are compiled in a CD-ROM attached with the thesis.